NUI MAYNOOTH

Ollscoil na hÉireann Má Nuad

Electrocoagulation for Water Treatment: the Removal of Pollutants using Aluminium Alloys, Stainless Steels and Iron Anodes

Adelaide Dura, M.Sc.

Thesis Submitted to the National University of Ireland in Fulfillment of the requirements for the Degree of Doctor of Philosophy

Department of Chemistry
National University of Ireland Maynooth

August 2013

Head of Department: Dr. John C. Stephens
Supervisor: Prof. Carmel B. Breslin

Table of Contents

Declaration

I hereby certify that this thesis, which I now submit for assessment on the programme of study leading to the award of PhD has not been submitted, in whole or part, to this or any other University for any degree and is, except where otherwise stated the original work of the author.

Date: _____ Signed: _____

To Francesco and my parents, with love.

I am a clown...and I collect moments.

— Heinrich Böll, *The Clown*

Some things will always be stronger
than time and distance.
Deeper than languages and ways.
Like following your dreams,
and learning to be yourself.
Sharing with others
the magic you have found…

— Sergio Bambarén, *The Dolphin: Story of a Dreamer*

Acknowledgments

I would like to express my sincere gratitude to my supervisor Prof. Carmel B. Breslin for her guidance over the course of this research. She was always helpful, understanding and provided a positive support. Particular thanks to Dr. John Colleran for his help over the past years.

I wish to acknowledge the Irish Research Council's EMBARK Initiative for funding this study.

I am extremely indebted to all the technical staff, in particular Ria Collery-Walsh, Orla Fenelon, Anne Clearly, Dr. Ken Maddock, and the Executive Assistant Niamh Kelly, who have always been available and willing to help whenever I needed it. A special mention is for Noel Williams for his help, support and inspiring discussions.

A number of people have made my stay in Ireland an enjoyable experience. My friends from the ESL course, Esteban and Sohrab, thanks for all the laughter, Wenbai, Maryam and Buket, you are the sweetest people I have ever met, and the 'Italians' Giorgio, Martina, Daniela and Francesco. I thank all my current and former colleagues in the Department of Chemistry who provided such an enjoyable and great research environment. A special word of thanks to Paul, Foxy, Conor, Richard, Niall (Joey), Orla, Wayne, Emer, Gama, Sam, Dave, Declan, Niamh, Carol, Trish, Ken, my 'fellow' Owen and Rob.

I am forever indebted to Valeria and Sinéad. Thanks for your friendship, your support and your being there whenever I needed it. I was unbelievably lucky for having you as friends and lab mates. I am also particularly grateful to Enrico for his remarkable knowledge and expertise, and Susan for her sincere friendship and all the good times we had together.

To my parents, my sister Gabriella and the little Iris, thank you for your support, encouragements and love. Finally, I am deeply grateful to Francesco, for his love and understanding. He has always stood by me and given support even during the hardest periods.

Abstract

The development of effective and sustainable wastewater treatments is becoming increasingly important. Electrocoagulation is one of the more promising approaches as it is simple and efficient and, compared with traditional processes, has the advantages of short treatment times and low sludge production.

The objective of this research was to determine the feasibility of the electrocoagulation technique as a method to remove pollutants from wastewater. Electrocoagulation tests were first carried out in phosphate-containing solutions with an aluminium-magnesium and a stainless steel electrode. Several operating conditions, such as the initial concentration of phosphates, current density, initial pH and sodium chloride concentration, were varied and the corresponding effects were investigated. Removal efficiencies of 95.9% and 79.7% were observed after 60 min with the aluminium-magnesium and the stainless steel electrodes, respectively, using an initial phosphate concentration of 150 mg L^{-1}, an initial pH of 5.0, a current density of 11.0 mA cm^{-2} and a ratio of the surface area of the electrode to the volume of the solution of 11.7 m^{-1} and 10.5 m^{-1} for the aluminium-magnesium and the stainless steel electrodes, respectively.

The electrochemical behaviour of several electrode materials was then correlated with the removal and energy performance of these electrodes in the treatment of phosphates, an azo dye and zinc ions dissolved in synthetic wastewaters. The synthetic wastewaters were designed to contain a mixture of ions with different conductivity values. Pure iron and an aluminium-indium-zinc electrode were identified as the most promising materials, giving low corrosion potentials and active dissolution. Excellent removal efficiencies for the three pollutants were observed using the pure iron electrode (96%, 99% and 100% for phosphates, azo dye and zinc ions, respectively) with an energy consumption of 0.52 Wh. The aluminium-indium-zinc alloy required the lowest energy supply of 0.26 Wh, gave excellent removal for both the phosphates and zinc ions (95% and 100%, respectively). However, only a moderate efficiency, 78%, was observed for the removal of the azo dye.

A screening design of experiment, DoE, was carried out to determine the most significant factors affecting the electrocoagulation removal process. These factors were identified as the current density and the ratio of the surface area of the electrode to the volume of the solution, SA/V.

List of Figures

List of Tables

List of Symbols

ROMAN SYMBOLS

Symbol	Meaning
A	absorbance
b	path length
C	concentration of a species
D	diffusion coefficient of a species
E	(a) potential of an electrode versus a reference
	(b) flocculation rate correction factor or collision efficiency factor
E^0	standard potential of an electrode
E_{br}	breakdown potential
E_{cell}	potential of the cell
E_{corr}	corrosion potential
E_{eq}	equilibrium potential of an electrode
E_{pass}	passivation potential
F	the Faraday constant; charge on one mole of electrons
ΔG	Gibbs free energy change in a chemical process
I	current
I_L	limiting current
j	current density
j_0	exchange current density
j_{corr}	corrosion current density
j_{lim}	limiting current density
k	rate constant for a reaction
K	equilibrium constant
m	mass of substance deposited or dissolved
n	stoichiometric number of electrons involved in a reaction
R	(a) gas constant
	(b) resistance
t	time
T	absolute temperature

Symbol	Meaning
V	volume
W	gram atomic weight
z	stoichiometric number of electrons involved in a reaction

GREEK SYMBOLS

Symbol	Meaning
α	transfer coefficient
β	Tafel slope
δ	diffusion layer thickness for a species at an electrode fed by convective transfer
ε_λ	molar absorbtivity at a specific wavelength, λ
ζ	zeta potential
η	(a) overpotential, E-E_{eq} (b) removal efficiency
θ	fractional surface coverage
κ	conductivity of a solution
ν	kinematic viscosity
Ψ	potential at the electrical interface
ω	angular frequency of rotation

1 Introduction and Literature Review

1.1 Research topic

One of the more pressing challenges in the 21st century is the provision of an adequate clean water supply that is free from pollutants. At the beginning of 2000, one-sixth of the global population was without access to a clean water supply, leaving over 1 billion people in Asia and Africa alone with a polluted water system [1]. In addition, legislative regulations concerning the discharge of wastewater are drastically increasing and becoming more stringent. Therefore, it is not surprising that there is a growing interest in developing new technologies that are simple, cheap and highly efficient in the removal of pollutants from water.

Existing treatments involve biological and chemical approaches. The biological treatments are effective, but require long treatment times, large treatment facilities and are expensive. The chemical approaches, which involve adding chemicals to extract or precipitate the pollutant, are very effective in removing the target pollutant, but the anion of the salt added can cause secondary pollution and large amounts of sludge. Electrochemical techniques are, in this case, promising because of their versatility, safety, selectivity, amenability to automation and environmental compatibility [2]. Electrocoagulation appears to be one of the most effective approaches.

Electrocoagulation has been suggested as an alternative to chemical coagulation in the treatment of waters and wastewaters. In this technology, metal cations are released into the water by dissolving metal electrodes. Electrochemistry, coagulation, and flotation are identified as the key elements in the electrocoagulation process [3]. Indeed, the performance and energy efficiency of the electrocoagulation processes are directly related to the choice of the electrode material (electrochemistry), the reactions occurring in the bulk solution involving the coagulant species and the pollutants (coagulation), and the separation of the pollutants either by flotation or settling.

The electrocoagulation treatment of wastewater has been extensively reported in the literature, however the mechanisms are not yet clearly understood mainly because electrocoagulation is a very complex chemical and physical system [4]. Although recently more attention has been paid to identify the key underlying mechanisms of pollutant removal, few researchers have addressed the problem of the electrode materials employed in electrocoagulation [5]. Indeed, the electrocoagulation process takes place in an electrochemical cell. Consequently, its efficiency performance is directly related to the operational state of the electrodes. In addition, the choice of the material has an important impact on the energy utilised in the process.

1.2 Water treatment technologies

Water and wastewater treatments can be defined as the processes used to achieve a water quality that meets specific goals or standards [6]. In Ireland wastewater discharge quality is governed by the S.I. no. 254/2001 and S.I. no. 684/2007 regulations. Water treatment technologies can be broadly divided into three general methods: mechanical/physical, chemical and biological [7]. More rigorous treatments can include the removal of specific contaminants using advanced technologies. In order to achieve different levels of contaminant removal, these methods are usually combined into a variety of systems, classified as primary, secondary and tertiary wastewater treatments. Figure 1.1 shows a schematic diagram used for typical treatment of surface water.

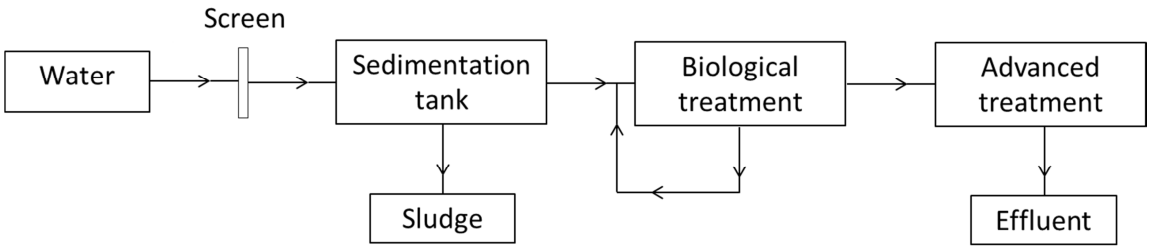

Figure 1.1: Typical water treatment process flow diagram.

The removal of sand and large solid particles is brought about during the preliminary treatment, which consists of screens, scrubbers or filters. A large fraction of the total suspended solids and of the organic matter is removed by gravity in a primary sedimentation tank. The screened water is held in the tank for several hours to allow solid particles to settle to the bottom of the tank, while oil, grease and lighter solid particles float to the surface. Both the settled and the floating materials are then removed from the water. Moreover, settling can be enhanced using chemical precipitation or coagulation. The secondary treatment process can remove up to 90% of the organic matter in wastewater by using biological treatment processes [8]. For example in an activated sludge process, which is the most commonly used biological method, bacteria and other microorganisms use the organic matter for their growth in the aeration tanks. A tertiary treatment is sometimes required for removal of residual suspended solids and disinfection for pathogen reduction [9]. Eventually, advanced treatment can be employed to further increase the quality of the effluent, for example for potential water reuse applications or for removal of toxic compounds [9]. A list of the processes used in water treatment is presented in Table 1.1.

Table 1.1: Levels and methods of water and wastewater treatments.

Treatment Level	Treatment Method	
1. Preliminary	Mechanical/physical	Screening
		Sedimentation
2. Primary	Mechanical/physical	Sedimentation
		Flotation
	Chemical	Coagulation
		Chemical precipitation
3. Secondary	Biological	Activated sludge
		Aerated lagoon
		Trickling filters
		Rotating biological contactors
		Pond stabilisation
		Anaerobic digestion
		Biological nutrient removal
4. Tertiary or advanced	Physical	Activated carbon adsorption
		Ion exchange
		Reverse osmosis
		Membrane filtration
		Gas stripping
	Chemical	Advanced oxidation
		Chlorination
		Ozonation
		UV irradiation

Recently, with the increasing standards and the stringent environmental regulation regarding wastewater discharge, electrochemical technologies have received particular attention in water treatment [10]. Indeed, it has been suggested that they can potentially replace some of the treatments discussed above, such as the preliminary, primary and secondary treatments in a typical wastewater treatment plant presented in Figure 1.1 [11]. Electrochemical techniques include electrocoagulation [2], electroflotation [2], electrodecantation [4] and others [12]. They offer distinctive major benefits in comparison to the conventional technique. For example, Rajeshwar [13] listed several advantages such as environmental compatibility, versatility, energy efficiency, amenability to automation and cost effectiveness. Among the electrochemical techniques, electrocoagulation has received particular interest as a very promising water treatment technology [4].

1.2.1 The removal of phosphates

Phosphorus is a commonly occurring element which is essential to the growth of algae and most other biological organisms [8]. However, an excess of phosphorus can have adverse effects on a water system, such as the phenomenon of eutrophication, which is responsible for the proliferation of algal growth [14]. Nitrogen and phosphorus are the main contributing nutrients to this process and the rate of enrichment of natural waters has tended to be accelerated by particular anthropogenic activities. Eutrophication can cause many problems including the extinction of some species of fish due to reduction in the dissolved oxygen levels, unpleasant odours and discolouration of the water.

The phosphorus that enters a wastewater treatment facility comes from three main sources: industrial, municipal and agricultural activities. The municipal contribution is divided between cleaning products and species of human origin;, industrial contribution is mainly from chemicals, and the agricultural component is from fertiliser drainage and from animals [15]. Municipal wastewaters may contain from 4 to 16 mg L^{-1} of elemental phosphorus as P [8].

Phosphorus typically exists in domestic wastewater in three forms: organic, condensed inorganic (polyphosphates) and simple inorganic (orthophosphates) species [16]. The first form typically accounts for 10% or less of the total phosphorus present. The remaining is approximately divided equally between the other two forms. However, most authors agree that the orthophosphates are the main compounds in natural water and domestic wastewater [17, 18]. In solution, the orthophosphate speciation is pH dependent, as displayed in Figure 1.2. The $H_2PO_4^-$ and HPO_4^{2-} are the main species at pH values between 6.0 and 8.0.

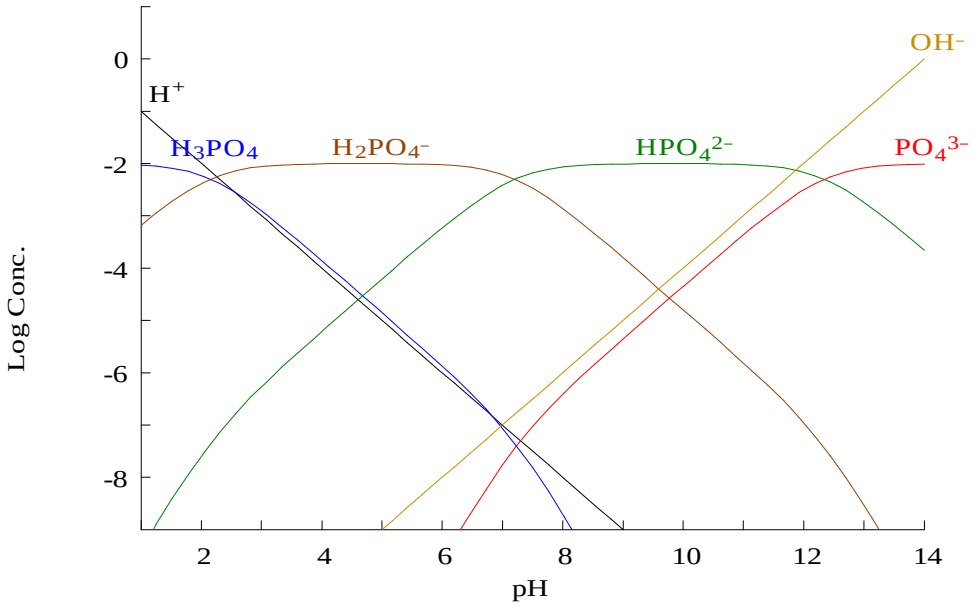

Figure 1.2: Distribution of major species of orthophosphates in water. The diagram was realised with the MEDUSA software developed by Puigdomenech [19] at the KTH Royal Institute of Technology, Sweden, and based on the SOLGASWATER algorithm [20].

Two processes are mainly employed for removing phosphorus from wastewater, chemical precipitation and enhanced biological removal [21]. Chemical precipitation, the most commonly applied process, can remove up to 90% of all phosphate species [22]. Maurer and Boller [23] suggested that the principle of chemical phosphorus removal from wastewater is to transfer dissolved orthophosphates into a particulate form by producing chemical precipitates of low solubility from the addition of metal salts. Standard treatment processes such as sedimentation, flotation and filtration can then remove the solids. Phosphate precipitation is achieved by the addition of metal salts that form sparingly soluble phosphates such as calcium, ferric iron, ferrous iron, and aluminium [24]. However, the addition of metal salts gives rise to an increase in the volume of sludge. Sludges that are produced are then treated by a sludge treatment processes. The increasing costs involved in the disposal of the large volumes of sludge and in the chemicals required for the precipitation and for the control of the solution pH represent the main disadvantages for this process [21].

Phosphorus can also be removed biologically from wastewater by incorporation into cells, which are then removed as sludge. Conventional biological treatments typically remove only 20% of the phosphates species present [25]. However, the establishment of

bacteria that can take up and store more phosphates than they need for their normal metabolic requirements can increase this to 90%. This process is termed enhanced biological phosphorus removal, EBPR, and relies on establishing a community of phosphorus-accumulating organisms, PAO, that take up 20 to 30% of their dry weight as phosphorous compared to 2% for conventional organisms [26]. Critical factors for a successful treatment are the presence of sufficient quantities of readily biodegradable matter, specifically volatile fatty acids, VFAs, and the integrity of an anaerobic zone free from nitrate to avoid the competition of PAOs with other bacterial populations [25].

1.2.2 The removal of dyes

Dyes are substances that possess a high degree of colouration and are used in several industries, such as textile, pharmaceutical, plastics, photography, paper and food [27]. The classification of dyes is based on the Colour Index, where each dye or pigment is given two numbers referring to the basis of the colouristic and the chemical classification. One number refers to the dye classification and its hue or shade, and it is called C.I. Generic Name. The other number is called C.I. Constitution Number and consists of five figures. Dyes are classified into two types based on their mode of application on the fibres and on their chemical structure [27]. The azo compounds are among the largest group of dyes and account for more than 50% of the dyes produced annually [28]. Their chromophoric system consists of an azo group (-N=N-) associated with aromatic systems and auxochromes (-OH, $-SO_3$, etc.,) [27].

It has been estimated that over 700,000 tons of approximately 10,000 types of dyes and pigments are produced annually worldwide and about 20% of these are discharged as industrial effluent [29]. Several dyes, especially the ones containing the azo group, can cause harmful effects to an organism [30]. Consequently, these wastewaters need to be treated before they are discharged into the environment. However, wastewater containing dyes is very difficult to treat, since the dyes are organic molecules, which are resistant to aerobic digestion and are stable to light, heat and oxidising agents. The most common method used for the treatment of dye-containing wastewaters is the combination of biological oxidation and physical-chemical treatment. However, these techniques are not completely effective since most dyes are toxic to the organism used in the biological process, while the physical-chemical treatments provide only a phase

transfer of the dyes, generating high volumes of hazardous sludge [29]. Recently, other emerging techniques, known as advanced oxidation processes, have been applied with success for pollutant degradation [31]. Although these methods are efficient for the treatment of waters contaminated with pollutants, they are very costly and commercially unattractive.

1.2.3 The removal of zinc ions

Heavy metals is a general term applied to the group of metals and metalloids with an atomic density greater than 5 g cm^{-3} or with a molecular weight above 40 g mol^{-1} [32]. Although the term heavy metal has been considered meaningless by IUPAC [33], it is still widely used and is commonly associated with pollution and toxic properties. Unlike organic contaminants, heavy metals are not biodegradable and tend to accumulate in living organisms. Many heavy metal ions are known to be toxic or carcinogenic [34]. The toxic heavy metals of particular concern in the treatment of industrial wastewaters include zinc, copper, nickel, mercury, cadmium, lead and chromium.

Zinc is a trace element that is essential for human health. Indeed, it is important for the physiological functions of living tissue and regulates many biochemical processes. However, too much zinc can cause health problems [32]. Its uses are quite variable ranging from galvanisation of steel, to the manufacture of the plates in electrical batteries, and the preparation of some alloys, such as brass. As a pigment, zinc is used in plastics, cosmetics, photocopier paper, wallpaper, printing inks etc., whereas in rubber production its role is to act as a catalyst during manufacture and as a heat disperser in the final product [35]. Since zinc is widely used in many industries, it should be removed from the wastewater to protect people and the environment.

Many methods are used to remove heavy metal ions including chemical precipitation, ion-exchange, adsorption, membrane filtration and electrochemical treatment technologies. Chemical precipitation is effective and by far the most widely used process in industry [34] because it is relatively simple and inexpensive to operate. In precipitation processes, chemicals react with heavy metal ions to form insoluble precipitates. The precipitates can then be separated from the water by sedimentation or filtration. Although widely used, chemical precipitation has some limitations [34]. It

generates large volumes of relatively low density sludge, which can present dewatering and disposal problems. In addition, some metal hydroxides are amphoteric and thus the pH plays an important role. Furthermore, if complexing agents are present in the wastewater, they inhibit the precipitation of the metal ions. Physico-chemical treatments, such as membrane filtration, adsorption, ion exchange, reverse osmosis or solvent extraction commonly achieve incomplete metal removal and require high reagent costs and energy requirements. Better efficiencies and more advantages are offered from using biological methods, such as the actions of microorganisms and microalgae. Indeed, they require reduced use of chemicals, low operating costs, are more environmentally acceptable (as no toxic sludge results) and exhibit high efficiency at low levels of contamination. They also offer possibilities for metal recovery and the regeneration of the biosorbent [36]. However, these studies are still in the experimental phase [34] and have not yet been employed in any real applications.

1.3 Electrocoagulation

Electrocoagulation consists of delivering metallic hydroxide flocs to the water by electrodissolution of the electrodes. Using electricity to treat water was first proposed in the UK in 1889 [37] and later electrocoagulation with aluminium and iron electrodes was patented in the US in 1909 [10]. During this period, several water treatment plants were operating in the UK [38, 39] using electrochemical techniques, for example in Salford, England, a plant was commissioned to use iron electrodes with seawater as the source for chlorine disinfection [39]. However, because of the relatively large capital investment and the expensive electricity supply, coupled with the ready availability of mass-produced alternatives for chemical coagulant dosing, electrochemical treatment of water did not find widespread applications worldwide [40]. Later, during the 1970s and 1980s significant and growing interest was generated by Russian scientists on the use of electrocoagulation for a variety of water treatment processes [41-50].

Today electrochemical technologies have reached such a state of consideration that they are considered a reliable and effective technology. In specific situations, they may be the indispensable step in treating wastewaters containing recalcitrant pollutants [12]. Electrocoagulation has been shown to remove a wide range of pollutants. For example, it has been efficiently applied for the treatment of various wastewaters containing heavy

metals [51-53], foodstuffs [54, 55], oil wastes [56, 57], textile dyes [58-63], fluoride [64], polymeric waste [65], organic matter from landfill leachate [66], suspended particles [67-70], chemical and mechanical polishing wastes [71], aqueous suspensions of ultrafine particles [38], nutrients [72], phenolic waste [73], arsenic [74] and refractory organic pollutants including lignin and EDTA [75]. Some authors have used electrocoagulation for drinking water treatment [10, 39, 76]. This ability to remove a wide range of contaminants accounts for the increasing interest from the industrial sector in investigating the feasibility of the electrocoagulation process.

1.3.1 Advantages and disadvantages of the electrocoagulation technique

Mollah *et al.* [4] reported various advantages of the electrocoagulation process compared to the traditional coagulation process. For example, the equipment required for the electrocoagulation process is simple and easy to operate. As a consequence, it can be carried out in small and compact treatment facilities, resulting in a relatively low cost and gives the possibility of complete automation. In addition, the process has no moving parts and most of the process is controlled electrically and, therefore, requires less maintenance. It has also been claimed that the electrocoagulation technique can be used in rural areas where electricity is not available. The energy required for the process can be provided by solar panels [77]. Furthermore, the electrocoagulation process represents a suitable choice where small, localised treatment technologies are preferable over centralised treatments [3].

In the electrocoagulation process there is no need to use chemical coagulants. Consequently, the occurrence of secondary pollution is minimised. Moreover, it produces lower amounts of sludge, which tends to be readily settable and easy to dewater. In addition, the flocs tend to be much larger, contain less bound water, are acid resistant and more stable and, therefore, can be easily separated by filtration. The electrocoagulation process has the advantage of removing small colloidal particles because the applied electric field sets them in faster motion, thereby facilitating their agglomeration. As a consequence, the produced effluent contains less total dissolved solids compared to other chemical treatments, resulting in lower water recovery costs. The generation of gas bubbles, produced during electrolysis, is considered another

advantage. Indeed, the bubbles can carry the flocs to the top of the reactor where they can be more easily collected and removed.

However, disadvantages are well known for the electrocoagulation process. For example, the use of electricity is considered one of the main limitations, because of the increase in the energy costs. The occurrence of an oxide or passive film on the surface of the electrodes can lead to a loss in the efficiency of the process. Moreover, high conductivity of the solutions is required and in some cases the gelatinous hydroxide may tend to solubilise.

1.3.2 Principles of electrocoagulation

The electrocoagulation technique uses an electrochemical cell to treat the water. In the simplest form, an electrochemical cell consists of two electrodes, the anode and the cathode, immersed in a conducting solution or the electrolyte and connected together *via* an electrical circuit which includes a current source and control device, as shown in Figure 1.3. The chemical processes occurring in the cell are oxidation and reduction reactions, which take place at the electrode/electrolyte interface. The electrode at which reduction occurs is referred as the cathode, whereas the anode is the electrode at which oxidation processes occur. The anode, also called the sacrificial electrode, corrodes to release active coagulant cations, usually aluminium or iron, to the solution [38, 39, 64, 78]. Consequently, electrocoagulation introduces metal cations *in situ*, rather than by external dosing. Simultaneously, electrolytic gases are generated, typically hydrogen at the cathode.

The current flow in the electrocoagulation cell is maintained by the flow of electrons resulting from the driving force of the electrical source. The solution electrolyte allows the current to flow by the motion of its ionic charged species. High conductivity is an advantage for the process, since it reduces the electrical resistance of the solution and the electrical consumption.

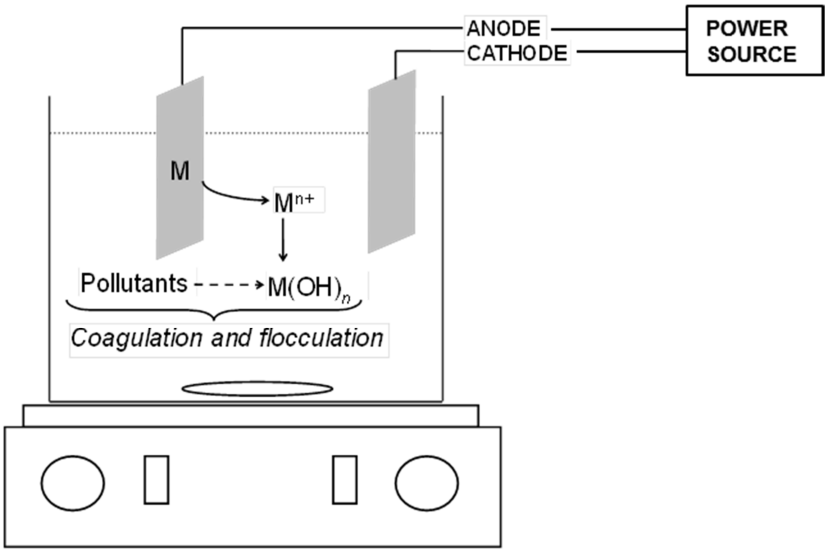

Figure 1.3: Simplified scheme of an electrocoagulation cell.

The metallic cations generated from the anode hydrolyse to form hydroxides, polyhydroxides and polyhydroxymetallic compounds with a strong affinity for dispersed particles and counter ions, thus causing coagulation [79]. Indeed, they can reduce the net surface charge of colloidal particles that are in suspension due to the reduction of the repulsive potential of the electrical double layer. As a result, the repulsive forces between the colloidal particles decrease and this brings the particles sufficiently close so that the van der Waals forces predominate and agglomeration of the particles occurs. In summary, the electrocoagulation process involves three successive stages [4, 11]. The first stage consists in the formation of coagulants by electrolytic oxidation of the sacrificial anode electrodes (Section 1.3.2.1). Then the destabilisation of the contaminants and particulate suspension takes place and finally the aggregation of the destabilised phases to form flocs occurs. The destabilisation of the suspension involves the occurrence of the coagulation process and can be brought about by several mechanisms, as discussed in Section 1.3.2.2. On the other hand, the formation of flocs is determined by flocculation models, as shown in Section 1.3.2.3. It is worth noting that in electrocoagulation the processes of coagulation and flocculation occur simultaneously and it is not possible to distinguish between the two stages as in chemical coagulation. Indeed, when metal salts are used in water treatment facilities, the two stages, coagulation and flocculation, are physically separated or differentiated on the basis of the time required for each of the processes.

1.3.2.1 Reactions at the electrodes

The electrodes that are commonly used for the electrocoagulation process are aluminium and iron, in the form of plates [39, 64]. The electrode materials used determine the type of coagulant. The nature of the coagulant, in turn, influences the coagulation and the efficiency processes. When a potential or a current is applied across the electrodes in the electrochemical cell displayed in Figure 1.3, the anode undergoes oxidation while the cathode is subject to reduction. At the cathode the evolution of hydrogen usually occurs and this gives rise to an increase in the pH of the solution at the cathode (Eq. 1.1 and Eq. 1.2).

$$2H^+ + 2e^- \rightarrow H_2 \qquad \text{acid} \qquad \textbf{Eq. 1.1}$$

$$2H_2O + 2e^- \rightarrow H_2 + 2OH^- \qquad \text{neutral/alkaline} \qquad \textbf{Eq. 1.2}$$

When iron or iron alloys are used as the anode, they produce iron hydroxide, $Fe(OH)_n$, with n = 2 or 3. Two mechanisms have been proposed for the production of $Fe(OH)_n$ and these are summarised as follows [4]:

Mechanism 1

$$Fe \rightarrow Fe^{2+} + 2e^- \qquad \textbf{Eq. 1.3}$$

$$Fe^{2+} + 2OH^- \rightarrow Fe(OH)_2 \qquad \textbf{Eq. 1.4}$$

Mechanism 2

$$4Fe \rightarrow 4Fe^{2+} + 8e^- \qquad \textbf{Eq. 1.5}$$

$$4Fe^{2+} + 10H_2O + O_2 \rightarrow Fe(OH)_3 + 8H^+ \qquad \textbf{Eq. 1.6}$$

In both cases, Fe^{2+} is generated from the oxidation of iron. The $Fe(OH)_2$ is produced by the reaction between Fe^{2+} and OH^-, while in the presence of dissolved oxygen $Fe(OH)_3$ is formed, containing the Fe^{3+} species.

For aluminium and aluminium alloy anodes, the chemical reactions taking place at the electrode and in the bulk for the production of $Al(OH)_3$ are given as follows:

$$Al \rightarrow Al^{3+} + 3e^- \quad \textbf{Eq. 1.7}$$

$$Al^{3+} + 3OH^- \rightarrow Al(OH)_3 \quad \textbf{Eq. 1.8}$$

Oxygen evolution, Eq. 1.9, is also possible at the anode [64], although it is not always detected or observed [80, 81].

$$2H_2O \rightarrow O_2 + 4H^+ + 4e^- \quad \textbf{Eq. 1.9}$$

On the other hand, at the anode hydrogen evolution can also occur by the mechanism concerned with the negative-difference effect, NDE [82]. The negative-difference effect is a phenomenon well-known for magnesium and its alloys. However, it may occur at other metals such as aluminium [83-85], aluminium alloys [86] and ferrous materials [87]. It results in strong hydrogen evolution and the rate of this reaction has been found to increase with the increase in the anodic polarization [82]. In the case of materials like aluminium or ferrous alloys, it has been reported that hydrogen evolution is related to occurrence of pitting corrosion, with conditions inside the pits that differ from those outside with respect to potential and electrolyte composition [85].

Faraday's laws of electrolysis provide a theoretical estimate of the amount of Fe^{2+} and Al^{3+} ions dissolved from the anodes. They relates the current passed, *I*, to the mass, *m*, of the electrolytically generated material in the electrochemical cell, as shown in Eq. 1.10. Here, *m* is the mass in g, *I* is the current in A, *t* is the time in seconds, *W* is the gram atomic weight in g mol^{-1}, *n* is the valence of dissolution and *F* is Faraday's constant (96,485 C mol^{-1}). However, dissolution efficiencies higher than 100% for both Fe and Al electrodes have been reported [11]. Donini *et al.* [68] and Cañizares *et al.* [88] identified the chemical dissolution as the likely source of the observed efficiency beyond that computed by Faraday's laws.

$$m = \frac{ItW}{nF} \quad \textbf{Eq. 1.10}$$

The electrogenerated Fe^{2+} and Al^{3+} ions (Eq. 1.3, Eq. 1.5 and Eq. 1.7) immediately undergo further spontaneous reactions to produce the corresponding hydroxides, as shown in Eq. 1.4, Eq. 1.6 and Eq. 1.8. In addition to these hydroxide species, Fe^{2+} and Al^{3+} ions also form monomeric, hydroxo complexes with hydroxide ions and polymeric species, depending on the pH range [11, 40, 89].

1.3.2.2 Coagulation

The coagulation step consists of destabilising the particle surface charge that keeps the particles in suspension. As a result, the suspended particles can stick to each other forming microflocs that are not visible to the naked eye [90]. Electrocoagulation adds the coagulant directly into the solution as a metal cation, therefore it could be considered similar to a salt induced aggregation process in terms of the mechanisms occurring in the solution. Consequently, the theory and the mechanisms reported for the electrocoagulation process concern the studies carried out on the chemical coagulation. However, it is worth noting that the time-dependent evolution of the chemical environment may differ in the two systems [91].

The interaction between the hydrolysed species and the contaminants present in the solution is described by coagulation theory. As already outlined in Section 1.3.2, the coagulant destabilises the colloidal suspension by reducing the energy barrier, thus allowing particles to aggregate. The stability of a colloidal particle is determined by the double layer repulsion forces and van der Waals forces of attraction [92]. Most particles in water are characterised by a surface charge, which can arise by different means, i.e., isomorphous substitution, ion dissolution, chemical reactions at the surface or adsorption of ions onto the particle surface [93]. Because of the overall electrical neutrality, the surface charge of a particle is counterbalances by ions of opposite charge (counter ions) in water. The charged surface of the particle and the oppositely charged layer of counter ions constitute the electrical double layer, which was first described by Helmholtz in 1879 [94]. This theory was then extended by Gouy and Chapman and later by Stern in 1924. The currently accepted model, based on the Bockris, Devanathan and Muller, BDM, model is shown in the schematic presented in Figure 1.4(a) and Figure 1.4(b) illustrates the corresponding variation of the potential versus distance from the surface.

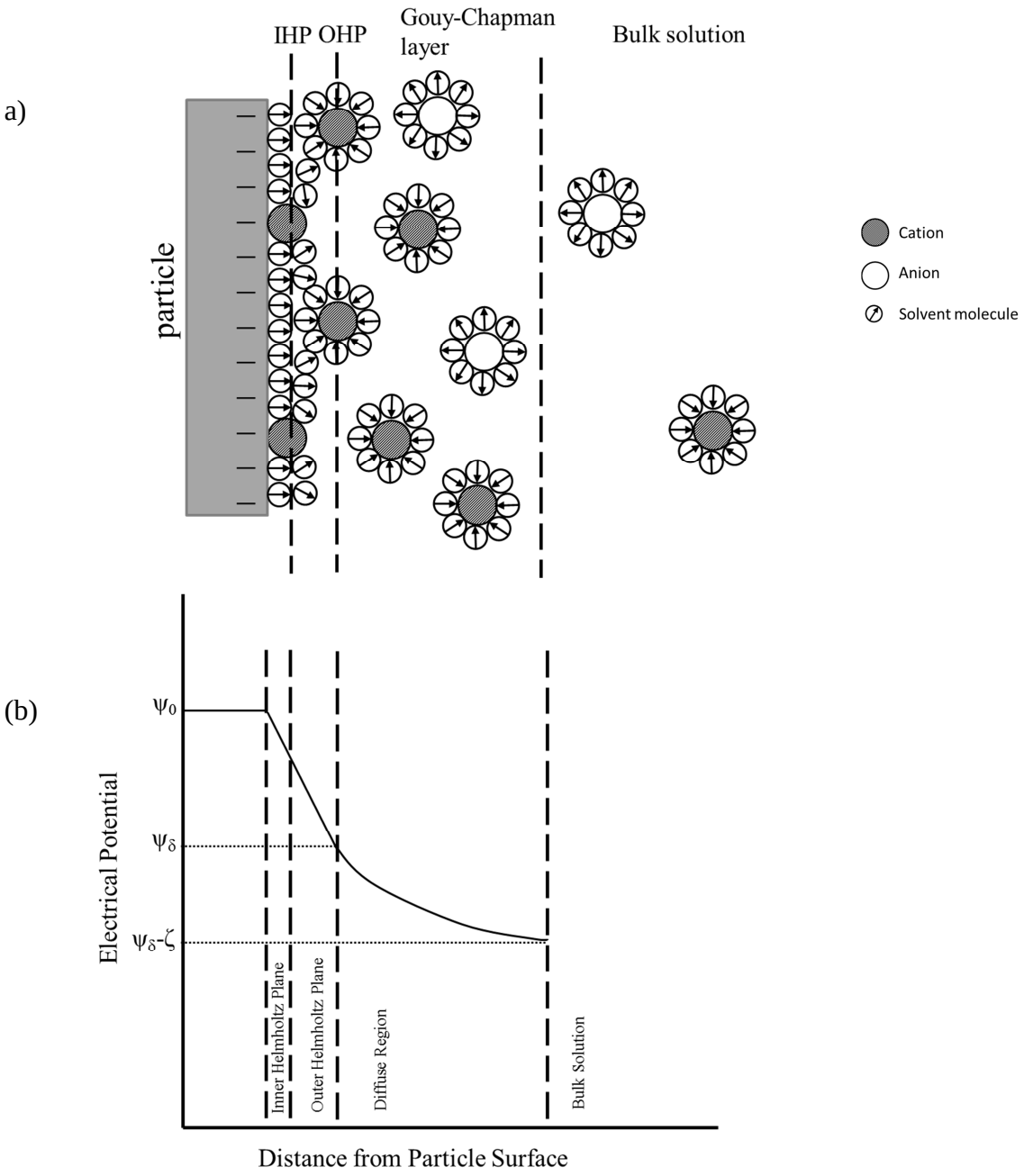

Figure 1.4: (a) Schematic of the different regions of the electrical double layer based on the BDM model and (b) variation of the potential versus distance from the surface.

The first part is a layer of ions specifically adsorbed to the interface and it is called Stern layer. According to a model proposed by Grahame in 1947, the Stern layer can be subdivided into the inner and outer Helmholtz regions [95]. The inner region, IHP, is immediately adjacent to the interface and contains specifically adsorbed ions, which no longer contain their hydration shells. In the outer Helmholtz region, OHP, hydrated counter ions can be found. Across this layer, the potential falls from the surface value, Ψ_0, to a value Ψ_δ. Beyond the Stern layer, is the so-called diffuse or Gouy-Chapman

layer where the potential decreases exponentially with increasing distance from the interface. The boundary of this layer is called shear plane. In this region the ions subject to normal thermal motion [93]. In 1963 Bockris, Devanathan and Muller proposed a model that included the influence of the solvent near the interface [96]. The model suggests that a layer of water is present within the inner Helmholtz plane. The dipoles of these molecules have a fixed alignment because of the charge in the electrode. On the other hand, some of the water molecules are displaced by specifically adsorbed ions as shown in Figure 1.4(a). Other layers of water follow the first, however the dipoles in these layers are not as fixed as those in the first layer.

The stability of the colloidal suspension is influenced by the potential of the Stern layer, Ψ_{δ}. This potential cannot be measured directly, however it is approximated by the zeta potential, ζ, representing the electrical potential between the shear plane and the bulk solution [97]. The particles coalesce if the kinetic energy of the particle is sufficiently large to overcome the potential created by the formation of the double layer, otherwise they remain as a stable suspension [97, 98]. This theory was developed by Derjaguin and Landau, and Verwey and Overbeek independently and is popularly known as the DLVO theory [99]. The combined effect of electrostatic repulsion and van der Waals attraction between two particles is described by the DLVO theory (Deryaguin and Landau, 1941; Verwey and Overbeek, 1948). It assumes that the effect of the attraction forces (London-van der Waals) and the repulsion forces (overlapping of electrical double layer) is additive and the results can be displayed in the form of a potential energy diagram shown in Figure 1.5. This figure suggests that, although it is energetically favourable for particles to come into close contact, a large energy barrier must first be overcome. The role of the coagulant is to destabilise the colloidal suspension by reducing the repulsive forces and consequently lowering the energy barrier and enabling particles to aggregate [100].

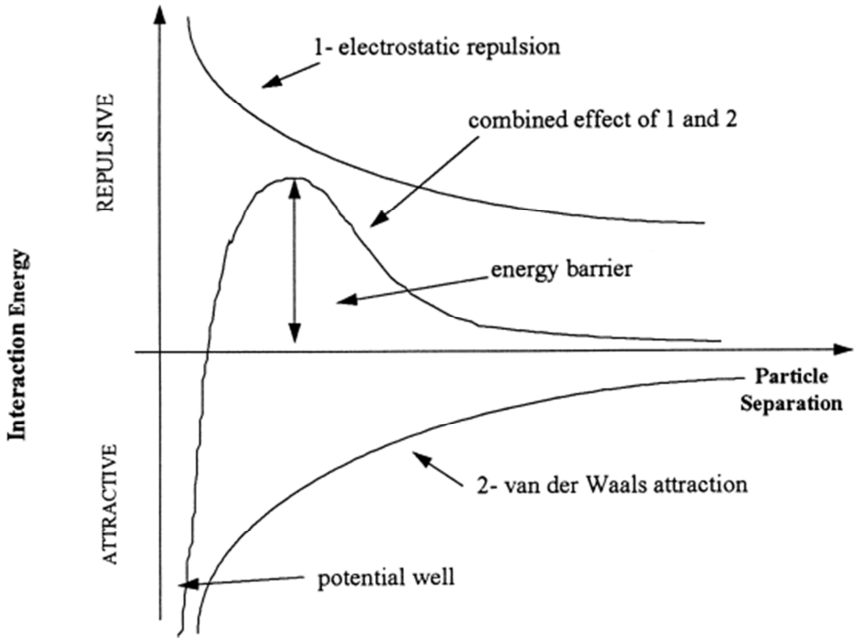

Figure 1.5: Representation of the DLVO theory.

It has been postulated that a number of coagulation mechanisms, which depend on the physical and chemical properties of the solution, pollutants and coagulant, are involved in the destabilisation of a solution [101]. They include double layer compression, charge neutralisation and bridging and sweep processes [102]. The compression of the diffuse double layer is due to the reduction of the net surface charge [98]. Ions with opposite charge to the net charge on the surface of the particles can reduce the repulsive potential of the electric double layer. On the other hand, destabilisation can also be brought about by charge neutralisation, which involves reducing the net surface charge of the particles. Coagulants, such as hydrolysis products formed from the dissolution of iron and aluminium electrodes, carrying a charge opposite in sign to the net surface charge of the particle are adsorbed onto the particle surface [98]. The formation of flocs, instead, forms a sludge blanket that entraps and removes the suspended particles when settling down, as a result of an enmeshment process.

For a given electrocoagulation cell, the dominant coagulation mechanism will vary according to the operating conditions of the reactor, the type and concentration of the pollutant, and the type and concentration of the coagulant. Consequently, the speciation of the cation generated by electrodissolution of the electrode in electrocoagulation is extremely important. Indeed, depending on the predominant hydrolysis species in solution, the coagulation mechanism can vary. The hydrolysed metal species can be

adsorbed on the colloid surface to create bridges between the particles or, alternatively, the amorphous solid hydroxide flocs that form may settle down causing the so-called sweep flocculation.

As outlined in Section 1.3.2.1, electrogenerated Fe^{3+} and Al^{3+} ions undergo hydrolysis. Indeed, all metal cations are hydrated in water. In the case of Fe^{3+} and Al^{3+}, it is known that the primary hydration shell consists of six molecules of water arranged in octahedral co-ordination [103]. Depending on the solution pH, water molecules in the primary hydration shell are polarised owing to a loss of one or more protons, according to Eq. 1.11. The metal hydroxides considered in the coagulation process are the amorphous precipitates, since the crystalline forms are usually formed very slowly. In this context polynuclear hydrolysis species are not considered.

$$M^{3+} + OH^- \rightarrow M(OH)^{2+} \xrightarrow{+OH^-} M(OH)_2^+ \xrightarrow{+OH^-} M(OH)_3 \xrightarrow{+OH^-} M(OH)_4^- \qquad \textbf{Eq. 1.11}$$

The amorphous hydroxides have a minimum solubility at a certain pH value. For example, it has been estimated that for aluminium this is approximately pH 6.0 at which the solubility is of the order of 1.0 μM [104], while for iron the solubility is much lower, approximately 0.01 μM and the region is broader than for aluminium, ranging from pH values of 7.0 up to 10.0 [105]. However, the predominant species at these pH values might not be an amorphous solid but a soluble hydrolysis species. If these soluble species have a charge of the same sign as the contaminant, then the efficiency of the coagulation process is reduced considerably.

The speciation of metal cations, such as Al^{3+} and Fe^{3+}, present in solution at a given pH can be calculated using thermodynamic data and displayed as speciation or distribution diagrams. These diagrams provide a deeper understanding of the aqueous solution chemistry of the Al^{3+} and Fe^{3+} ions and of their hydrolysis products, which depend on the total metal concentration and solution pH. **Figure 1.6** shows the speciation diagrams for Al^{3+} and Fe^{3+}. It is apparent from such diagrams that there is a significant difference in the hydrolysis behaviour of Al^{3+} and Fe^{3+} cations. Indeed, all the ferric hydrolysis species attain significant concentrations at different pH values, while in the aluminium diagram two species are predominant, Al^{3+} and $Al(OH)_4^-$, at low and high pH,

respectively. The other species, i.e., $Al(OH)^{2+}$, $Al(OH)_2^+$ and $Al(OH)_3$, are stable over a narrow pH region from approximately 5.0 to 6.0 [102]. According to **Figure 1.6**, a small amount of $Al(OH)_3$ forms between pH 5.5 and 8.0, which covers the pH range where the hydroxide has the minimum solubility. However, in this range $Al(OH)_2^+$ and $Al(OH)_4^-$ are the main hydrolysis products, representing almost 80% of the total Al^{3+} in the system. On increasing the total concentration of Al^{3+}, the hydroxide precipitate becomes more predominant in the system.

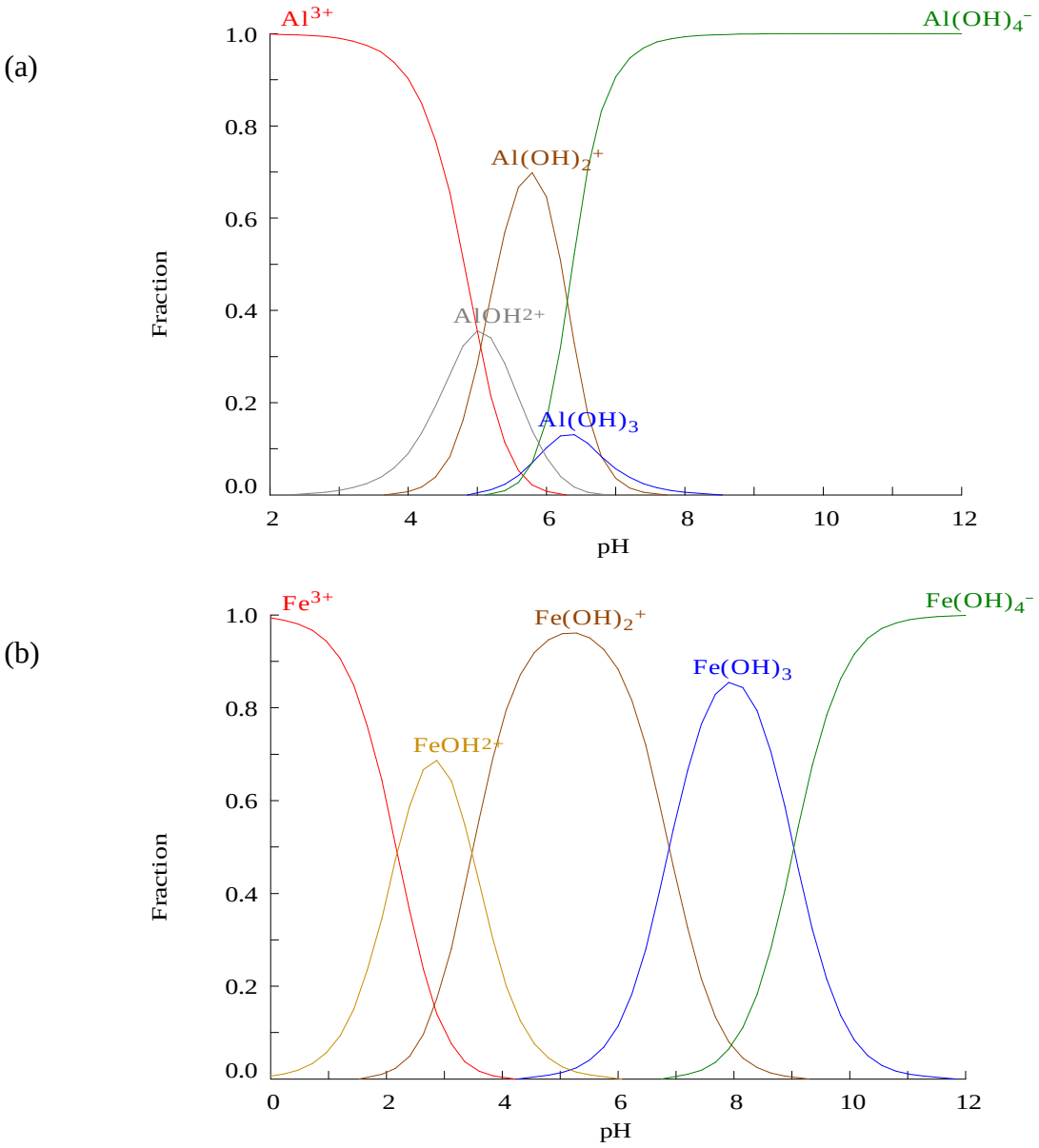

Figure 1.6: Speciation diagrams of the mononuclear hydrolysis products for (a) Al^{3+} and (b) Fe^{3+} ions at a concentration of 1.0 μM. The diagrams were realised with the MEDUSA software developed by Puigdomenech [19] at the KTH Royal Institute of Technology, Sweden and based on the SOLGASWATER algorithm [20].

1.3.2.3 Flocculation

Flocculation refers to the physical process of bringing particles together, once they have been destabilised by the coagulation process. In the flocculation process, the collisions of the microflocs formed during the coagulation step cause them to bond to produce larger, visible flocs. The size of the flocs continues to increase because of the collisions and interactions with the coagulant. The collisions between particles in a destabilised suspension are influenced by several processes [98]. Three mechanisms are usually adopted to explain the motion and collision of the particles and these include Brownian diffusion, fluid shear and differential sedimentation models. Brownian diffusion, or perikinetic flocculation, is due to the continuous bombardment by surrounding water molecules, while fluid shear or orthokinetic flocculation is caused by differences in the velocity gradients in either the laminar or turbulent fields. Differential sedimentation is related to the gravity of the particles, where particles that settle faster overtake and collide with slower settling particles [106].

Flocculation rate equations have been derived for each of these aforementioned mechanisms by assuming that the aggregation is a process where the rate of collision (f_{ij}) between *i*-and *j*-size particles is proportional to the product of the concentrations of the two colliding units (C_i and C_j) [98]. The general form of this relationship is:

$$f_{ij} = E_{ij} k_{ij} C_i C_j \qquad \textbf{Eq. 1.12}$$

where k_{ij} is a second-order rate constant that depends on the transport mechanism and a number of other factors, including particle size, and E_{ij} is a flocculation rate correction factor, or a collision efficiency factor.

1.3.3 Factors affecting electrocoagulation

1.3.3.1 Electrode materials

The electrode material determines the electrochemical reactions that take place in the electrocoagulation process. Aluminium and iron electrodes are mostly used as the electrode material in electrocoagulation systems [4]. Aluminium dissolves as Al^{3+}. However there is no general agreement on the nature of the iron species, with both Fe^{2+}

and Fe^{3+} proposed as the dissolved species [80, 107]. Indeed in some studies [5, 107, 108], the presence of Fe^{3+} is explained by the initial dissolution of iron to give Fe^{2+} species which are subsequently oxidised in the presence of dissolved oxygen at alkaline pH. It has been pointed out that Fe^{2+} is a poor coagulant compared to Fe^{3+} due to the higher solubility of the hydroxides and the lower positive charge of the ion [22].

The selection of the electrode materials depends on the pollutants to be removed and the chemical properties of the electrolyte. In general, aluminium seems to be superior compared to iron in most cases when only the efficiency of the treatment is considered. However, aluminium is more expensive than iron. Inert electrodes, such as stainless steel, are recommended as the cathode when significant amounts of calcium or magnesium ions are present in the solution [10]. Linares-Hernández *et al.* [5] obtained high removal of colour with aluminium electrodes, while iron was more effective than aluminium in reducing COD from industrial wastewater. A combination of iron and aluminium gave good efficiencies for the removal of the colour, 71%, and COD, 69%. Similar results were obtained for the treatment of paper mill wastewaters using various aluminium and iron electrode combinations [109]. Combined electrode systems have been used for arsenic removal from groundwater [110]. Iron electrodes and a combination of iron and aluminium electrodes gave the highest arsenic removal efficiencies [110]. Similar results were obtained for copper, chromium and nickel removal from metal plating wastewater [111] and for the removal of indium [112].

In some studies aluminium alloys have been employed as the anode material and they resulted in better removal performances than those observed with the pure metal. Vasudevan *et al.* used an aluminium-zinc alloy to treat successfully water containing phosphates [113], iron [114], arsenate [115], chromium [116] and copper [117]. In all cases, high removal efficiencies were obtained. For example, for the removal of phosphates the aluminium alloy gave an efficiency of 99% after 30 min compared to the efficiencies of 87% and 85% obtained with mild steel and pure aluminium electrodes under the same conditions. An aluminium-copper alloy was used by Khemis *et al.* [118] for the treatment of concentrated oil suspensions and again good removal efficiencies for both COD and TOC were achieved.

Studies were also carried out on electrocoagulation using iron-based alloys as the anode materials. For example, stainless steel has been found as an effective colour removal electrode. Arslan-Alaton *et al.* [119] reported complete decolorisation of reactive dye bath effluents using stainless steel within the first 5 min of electrocoagulation at all the studied pH values and applied current densities. Similar results were observed for the treatment of dyes [120, 121]. Stainless steel was also used for the treatment of total suspended solids and turbidity [67, 122], phthalic acid esters [123], nitrite [124] and strontium [125] with excellent removal efficiencies. However, the stainless steel electrodes were less efficient for the removal of COD and BOD. For example, Arslan-Alaton *et al.* [119] observed that the performance of the stainless steel electrodes was dependent on the initial pH of the dye bath solution. With pH values higher than 3.0, the COD removal was 80% and 90% after 25 and 60 min, respectively, with the removal efficiency decreasing with an increase of the initial pH. However, Kabdasli *et al.* [126] did not observe an improvement in the removal efficiency of TOC from metal plating wastewaters containing complexed metals with low initial pH values. They reported the highest TOC abatement as 66%, with a current density of 9 mA cm^{-2} and an initial pH of 6.0 after 3 h.

1.3.3.2 Electrode arrangements

A typical electrocoagulation cell consists of plate electrodes and the water flows through the space between the plates [10]. The electrodes can be arranged in several ways. For example they can be connected in monopolar or bipolar modes, as shown in Figure 1.7, and in series or parallel. In monopolar systems, displayed in Figure 1.7(a), all the anodes are electrically connected and similarly all cathodes are also connected. In bipolar systems, shown in Figure 1.7(b), only the outer electrodes are connected to a power source and the current passes through the other electrodes. In the bipolar systems, the side of the electrode facing the anode is negatively polarised and vice versa on the other side facing the cathode. The different electrode connections, which affect the pollutant removal efficiencies and operating costs, have been compared in several studies [127-132]. For example, on studying the removal of Cr^{3+} using mild steel electrodes, Golder *et al.* [127] found better removal efficiency when the electrodes were in the bipolar arrangement. However, the treatment costs were lower with a monopolar arrangement. Similar results were observed for the removal of fluoride from drinking

water [57]. In general, the monopolar configuration shows lower operating costs, however higher removal of the pollutants is usually achieved with the bipolar configuration.

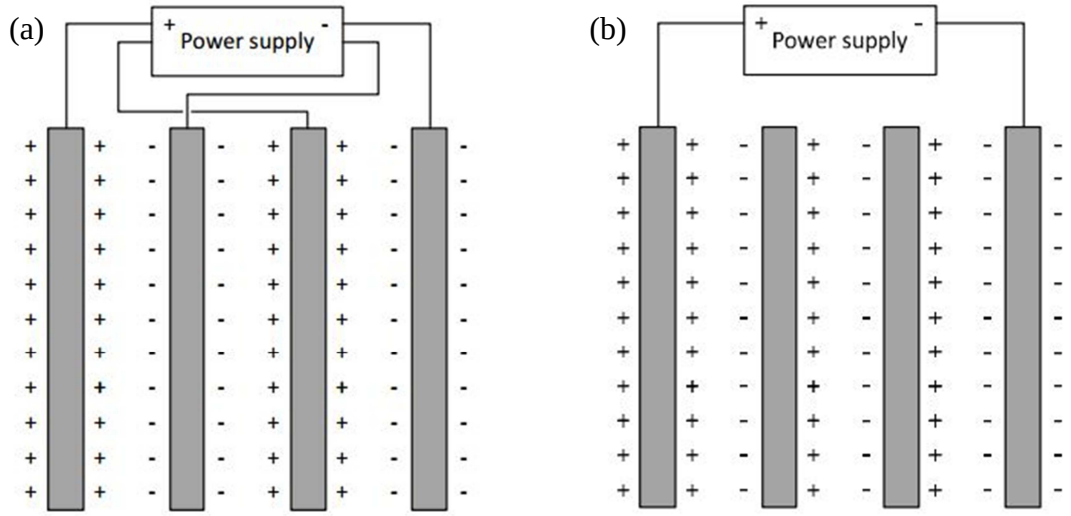

Figure 1.7: Schematic diagrams of (a) monopolar and (b) bipolar electrode connections.

1.3.3.3 Current density

In electrocoagulation, the applied current density affects the rate of the electrochemical reactions that generate the coagulant and the size and the number of hydrogen bubbles. In addition, it has an influence on the electrode potential, which determines the reactions taking place on the electrode surface. Indeed, it has been reported that the dissolution rate of the anode can be lower than the theoretical value computed by Faraday's law, indicating the occurrence of other reactions at the anode [107] and/or the occurrence of the negative-difference effect, presented in Section 1.3.2.1.

The concentration of Al^{3+} and Fe^{2+} ions produced from the anodes is usually calculated according to Faraday's law (Eq. 1.10), provided that the current and electrocoagulation times are known. However, current efficiencies higher than 100% have been observed in both the Al and Fe systems. Cañizares *et al*. [88] explained this difference in terms of the chemical dissolution of the electrode surface at alkaline pH for the Al system and at acidic pH for the Fe system. This certainly has an effect when the same material is used as the anode and the cathode. Indeed, the evolution of hydrogen at the cathode increases the local pH, as shown in Eq. 1.2, causing the chemical dissolution of an aluminium

cathode. This was confirmed by a study carried out by Mouedhen *et al.* [133] on the dissolution of aluminium from the cathodes using a platinised titanium anode. The concentration of Al(III) generated from the chemical dissolution of the aluminium cathodes increased with the electrocoagulation period. Indeed higher concentrations were observed with lower current densities and longer electrocoagulation times.

1.3.3.4 Supporting electrolyte

In the electrocoagulation process, the electrolyte plays an important role and the concentration and nature of the ions have a significant effect on the efficiency of the process. For example, Chen [55] reported that the presence of NaCl in the supporting electrolyte significantly reduced the adverse effects of anions, such as HCO_3^- and SO_4^{2-}. Indeed, in the presence of carbonate or sulfate ions the precipitation of Ca^{2+} or Mg^{2+} containing species forms an insulating layer on the surface of the electrodes, thus increasing the potential between the electrodes.

The presence of anions can also influence the electrode behaviour. Indeed, sulfate ions are well-known passivating agents, while chloride ions induce the breakdown of the passive layer [134]. Trompette and Vergnes [135] studied the effect of the supporting electrolyte on the electrocoagulation efficiency of unskimmed milk samples. They used aluminium electrodes and NaCl, Na_2SO_4, NH_4Cl and $(NH_4)_2SO_4$ as supporting electrolytes. An increase in electrical power consumption and lower efficiencies were observed with sulfate anions. In addition, a ratio of $[Cl^-]/[SO_4^{2-}]$ higher than 0.1 was necessary to ensure the breakdown of the passive film.

It has been reported that the supporting electrolyte can compete with the contaminants [136]. For example, on studying the removal of fluoride in the presence of chloride, nitrate and sulfate anions, Hu *et al.* [137] obtained the best results in the absence of these anions. In particular, they found that the sulfate ions have a significant effect on the removal efficiency of the fluoride, probably because they compete with fluoride ions to form precipitates with Al^{3+} species. Similar results were obtained by Vasudevan *et al.* [113] on studying the removal of phosphate ions where fluoride and arsenate acted as competitors.

1.3.3.5 Solution pH

The efficiency of electrocoagulation depends on the pH of the solution, which increases during the electrocoagulation process [10]. Indeed, it affects the current efficiency, the dissolution of the electrodes and the speciation of the hydrolysis products. Chemical dissolution occurs at acidic and alkaline pH for iron and aluminium electrodes, respectively, as discussed in Section 1.3.3.3. As outlined in Section 1.3.2.2, the predominant hydrolysed species that forms upon electrodissolution of the anode depends on the solution pH. It has been shown that in alkaline pH, $Al(OH)_4^-$ forms and this species has poor coagulation performance. On the other hand, Fe^{3+} is effective in a wider pH range as apparent from Figure 1.6.

It has been shown by Chen [10] that the solution pH increases for acidic solutions and decreases for alkaline solutions during the electrocoagulation process. The increase of pH under acidic conditions was attributed to the hydrogen evolution reaction which occurs at the cathode and to the release of CO_2 from hydrogen bubbling [39]. On the other hand, the pH decrease from alkaline conditions was attributed to the amphoteric character of aluminium hydroxide [138], according to Eq. 1.13.

$$Al(OH)_3 + OH^- \rightarrow Al(OH)_4^- \qquad \textbf{Eq. 1.13}$$

As with aluminium and iron, other metal cations can also form hydroxides in water that have low solubility and, consequently, can be removed by precipitation and co-precipitation with the electrocoagulation process. For example, Adhoum *et al.* [139] studied the removal of Cu(II), Zn(II) and Cr(VI) by aluminium electrodes and found an increase in the removal efficiency when the solution pH of the electroplating wastewater was increased. Similar results have been obtained for the removal of Co(II) [140], As(V) [74, 141], Cu(II), Cr(VI) and Ni(II) [111], Cu(II), Pb(II) and Cd(II) [142], Cu(II), Ni(II), Zn(II) and Mn(II) [143], In(III) [112] and Cr(III) [144, 145].

1.3.4 Removal of pollutants by electrocoagulation

A wide range of pollutants can be removed by electrocoagulation. Indeed an extensive literature exists on the use of the electrocoagulation technique for the treatment of water and wastewater. Most of the applications have been discussed in a review article by

Emamjomeh and Sivakumar [146]. Numerous researchers have investigated the decolourisation of dye solutions, since dyeing represents an important process applied in almost all the textile-manufacturing industries and produces large volumes of wastewater. These wastewaters are usually treated with traditional biological methods. However, due to the toxicity of most commercial dyes towards the organism used, the growth of the organisms is inhibited [147]. Electrocoagulation offers a potential and effective method for the treatment of textile wastewaters. A study carried out by Can *et al.* [148] showed that electrocoagulation is an efficient process for removing dyes from the solution. Indeed, an efficiency of 85% was observed for a reactive textile dye, Remazol Red RB 133, after 10 min at an initial pH of 6.0 and current density of 10 mA cm^{-2} using aluminium electrodes. The removal was attributed to the precipitation of aluminium hydroxopolymeric species formed during the earlier stage of the process and of $Al(OH)_3$ flocs in a subsequent stage. The authors also showed that the efficiency of the process depends on several factors, such as the initial pH, conductivity and dye concentration. A similar investigation was carried out by Daneshvar *et al.* [149] on the operational parameters affecting the removal of two dyes used in the wool and blanket industries. Using iron electrodes, the optimal removal efficiency was achieved with a current density between 7 and 8 mA cm^{-2}, a pH from 5.5 to 8.5 and a conductivity value of 8 mS cm^{-1}. Kobya *et al.* [40] compared the performance of iron and aluminium electrodes for the treatment of textile wastewaters. They observed that iron was superior to aluminium in terms of decolourisation, COD and energy consumption.

Several studies have been reported in the literature on the treatment of oily wastewaters. These studies indicate that electrocoagulation is a feasible technique to destabilise oil-in-water emulsions. Although several anode materials were proven effective, aluminium electrodes showed the best removal performance. For example, Ogutveren and Koparal [150] used iron or aluminium electrodes to treat solutions containing oil concentrations of 50, 200 and 500 mg L^{-1}. The removal efficiency was as high as 100% for all experiments when aluminium electrodes were used, probably because of high adsorption capacity of hydrous aluminium oxides. Chen *et al.* [138] presented an extensive study on the treatment of wastewater from restaurants in Hong Kong, containing high levels of oil and grease. Aluminium electrodes were used and the effect of several parameters was investigated. The loading charge and the electrocoagulation time were identified as the most important factors for an efficient treatment. On the

other hand, the conductivity of the solution had no significant effect on the removal efficiency when the solution pH was between 6.0 and 7.0. Removal efficiencies higher than 94% were achieved, indicating that the electrocoagulation process can be successfully used to remove oil and grease.

Electrocoagulation has also been used for the removal of heavy metals. Kumar *et al.* [151] treated arsenite and arsenate containing water by electrocoagulation. Laboratory scale experiments were conducted with three electrode materials, iron, aluminium and titanium to assess their efficiency for arsenic removal. The highest removal, 99%, was obtained using iron electrodes within a pH range of 6.0 to 8.0. The suggested mechanism involved the oxidation of As(III) to As(V) and its subsequent adsorption/complexation on ferric hydroxides. Other studies concerned the removal of combinations of metals. For example, Merzouk *et al.* [152] investigated the removal of some heavy metal ions, such as iron, nickel, copper, zinc, lead and cadmium, with different initial concentrations in the range of 50 to 600 mg L^{-1} and an initial pH of 7.8 from a synthetic wastewater. Using aluminium electrodes, the results showed a fast removal with efficiencies ranging between 70% and 99%. These values were observed for all the metal ions except for iron and copper, which required 15 min to attain the same removal efficiency. High removal efficiencies with aluminium electrodes were also reported by Heidmann and Calmano [153] for the removal of zinc, copper, nickel, silver and chromium ions. The removal rate of chromium appeared to depend on the initial concentration, with high concentrations facilitating the removal. According to the authors, zinc, copper, nickel and silver ions were removed following the same mechanism, which involved hydrolysis and then co-precipitation as hydroxides. On the other hand, Cr(VI) was reduced to Cr(III) at the cathode before precipitating as hydroxides.

Electrocoagulation has been shown to be an efficient method to reduce fluoride concentrations from potable water. Mameri *et al*. [64] studied the defluoridation of Sahara water using bipolar aluminium electrodes. The effects of several parameters and the kinetics of the process were investigated. The results showed that the removal of fluoride was more efficient for pH values between 5.0 and 7.6, where the formation of fluoro-aluminium complexes, such as AlF_3, $AlOHF_3^-$ and $Al(OH)_2F_2^-$, were favoured.

Koparal and Ogutveren [154] compared electrocoagulation and electroreduction for removing nitrate from water. A good efficiency was obtained in the electrocoagulation process within a pH range of 9.0 to 11.0 using iron rings as electrodes. Similar efficiencies with iron and aluminium electrodes were reported by Lacasa *et al.* [155]. The electrocoagulation process was identified as an effective technology for nitrate removal because nitrate anions preferentially adsorb onto the surfaces of growing metal-hydroxide precipitates. The removal of phosphate ions by iron and aluminium electrodes was investigated by Irdemez *et al.* [156-158] and parameters such as the initial pH, current density and initial phosphate concentration were studied. The pH was identified as a key parameter, with a pH of 3.0 being the optimal value for obtaining high removal efficiencies. Complete removal was achieved using aluminium electrodes, while the iron electrodes were less effective in the treatment and removal of phosphates.

1.4 Electrochemistry and corrosion properties of materials

As outlined in Section 1.1, the performance of the electrocoagulation process is strictly dependent on the electrode materials which are employed. For example, the electrode material determines the type and the concentration of the coagulant delivered to the solution. In addition, each material exhibits a different rate of dissolution, thus affecting the energy consumption of the system. In this section, the electrochemistry and corrosion properties of iron and aluminium and some of their alloys are briefly presented and discussed.

1.4.1 Corrosion and passivity

Corrosion is the change of metallic materials as a result of exposure to environment. Corrosion is normally referred as having a negative effect on materials of construction in various systems [134], however it can be beneficial or desirable in some cases, such as etching of metal surfaces, electropolishing, cathodic protection (galvanising), passive film formation and battery operation).

Corrosion can take different forms in aqueous environments, ranging from uniform corrosion to localised corrosion, such as pitting, or stress corrosion cracking. However, all metals and alloys, except for gold, develop an oxide-containing film due to the

reactions with the environment [159]. Some of these films are passive and protective and these provide more corrosion resistant metal or alloy surfaces. These protective surface films are responsible for the phenomenon of passivity, which reduces or limits the corrosion of a metal or alloy [134]. The phenomenon of passivity was first noted by Keir in 1790 and subsequently discussed by Schonbein and Faraday in 1836. In his famous iron-in-nitric acid experiments Faraday showed that the sample changed from the passive to the active state [160].

The nature and the composition of the passive films depend on the surface characteristics of the metal surface. Sato and Okamoto proposed three main mechanisms to account for the formation of passive films [161]. These models were based on direct film formation, a dissolution precipitation process and anodic oxidation. The direct film formation model involves the reaction of a metal surface with an aqueous solution to form either a chemisorbed oxygen film or a compact three-dimensional film, usually an oxide or oxyhydroxide film. It can be represented by Eq. 1.14 and Eq. 1.15:

$$M + H_2O \rightarrow MO_{ads} + 2H^+ + 2e^- \quad \textbf{Eq. 1.14}$$

$$M + H_2O \rightarrow MO(oxide) + 2H^+ + 2e^- \quad \textbf{Eq. 1.15}$$

The dissolution precipitation process produces a passive layer by the formation of an oxide, oxyhydroxide, or hydroxide film by the precipitation of dissolved metal ions as described by the two-step process:

$$M \rightarrow M^{n+} + ne^- \quad \textbf{Eq. 1.16}$$

$$M^{n+} + nH_2O \rightarrow M(OH)_n + nH^+ \quad \textbf{Eq. 1.17}$$

Lastly, the anodic oxidation of the metal in solution forms an oxide film containing the metal ion in a higher oxidation state as shown by:

$$M \rightarrow M^{n+} + ne^- \quad \textbf{Eq. 1.18}$$

$$2M^{n+} + (n+z)H_2O \rightarrow M_2O_{(n+z)} + 2(n+z)H^+ + 2ze^- \quad \textbf{Eq. 1.19}$$

The phenomenon of passivity has a central position in corrosion processes and corrosion control. Indeed, it is the breakdown of the passive film that results in several

forms of localised corrosion. This, in turn, may lead to failure in some engineering applications. In the electrocoagulation process, the existence of a passive layer on the metal surface causes an increase in the potential required to dissolve the metal cations from the electrodes. This leads to a corresponding increase in the energy demand of the system. Consequently, materials exhibiting poor passivity and active dissolution are preferred. Alloying elements play an important role in determining the properties of the passive film. As a result, if the alloying elements can be used to limit the formation of passive films, then the use of iron or aluminium alloys may be beneficial in electrocoagulation applications.

1.4.1.1 Basic concepts of corrosion

Corrosion is a process created by the reaction between a material, often a metal or alloy, and its environment that results in destruction or deterioration of that material [134]. Corrosion can be classified as wet or dry corrosion. The wet corrosion process involves liquid solutions, such as the corrosion of steel by water containing dissolved salts, whereas dry corrosion is associated with high temperatures and occurs in the absence of a liquid phase, by mechanisms such as carburisation or metal dusting and sulphidation [160]. Corrosion in aqueous environments occurs as a consequence of electrochemical reactions. This involves two partial reactions, anodic and cathodic. At the anodic sites an oxidation reaction occurs and simultaneously a reduction process takes place at the cathodic sites [162]. The anodic reaction of the metal is of the form:

$$\mathrm{M} \rightarrow \mathrm{M}^{n+} + n\mathrm{e}^{-} \qquad \textbf{Eq. 1.20}$$

The corresponding reduction reaction of the metal ions, generated from the oxidation reaction, can be represented as:

$$\mathrm{M}^{n+} + n\mathrm{e}^{-} \rightarrow \mathrm{M} \qquad \textbf{Eq. 1.21}$$

However, the reduction of dissolved oxygen and/or the release of hydrogen gas by the reduction of hydrogen ions are the most common reduction reactions during aqueous corrosion of metals or alloys [163]. The two reactions, anodic and cathodic, are complementary events and must proceed at the same rate. Anodic and cathodic sites can

form on the surface of the metal for many reasons: composition or grain size differences, discontinuities on the surface, presence of impurities or inclusions in the metal, local differences in the environment (e.g., temperature, oxygen, or salt concentration) and localised stresses. For electrochemical corrosion to take place, there are four fundamental requirements [162]: an anode, a cathode, a conducting environment for ionic movement (electrolyte) and an electrical connection between the anode and cathode for the flow of electrons. If any of these elements are missing or disabled, electrochemical corrosion cannot occur.

Thermodynamics and electrochemical kinetics are the foundations of corrosion studies. Thermodynamics gives an understanding of the energy changes involved in an electrochemical reaction and determines the spontaneous direction for the reaction. On the other hand, kinetics provides the basis of predicting the corrosion rate. In particular, thermodynamics predicts whether a metal will corrode in a specific environment and provides an understanding of the energy changes involved in the electrochemical reactions. These energy changes provide the driving force and control the direction for a chemical reaction. Each metal exhibits a potential with respect to its environment. This potential depends on several factors, such as the ionic strength and the composition of the electrolyte, the temperature, the metal or the alloy and other factors. The potential of the electrochemical cell is the sum of the potentials of the anodic and cathodic half cells, e_a and e_c, respectively. The potential of an electrochemical reaction can be related to the change in Gibbs energy, ΔG, as shown in Eq. 1.22, where n is the number of electrons participating in the reaction, F is Faraday's constant (96,485 C mol^{-1}) and E is the electrode potential [160]:

$$\Delta G = -nFE \qquad \textbf{Eq. 1.22}$$

The potential of the electrochemical cell, E, depends on the concentrations of the reactants and products of the respective partial reactions and on the pH of the aqueous solutions in contact with the metal. It is expressed by the Nernst equation:

$$E = E^0 + \frac{RT}{nF} \ln \frac{\{\mathrm{Ox}\}^n}{\{\mathrm{Red}\}^z} \qquad \textbf{Eq. 1.23}$$

Here, $E°$ is the standard electrode potential in V, R is the gas constant in J mol^{-1} K^{-1}, Ox is the activity of an oxidised species, Red is the activity of a reduced species and x and r are the stoichiometric coefficients involved in the respective half-cell reactions. Corrosion will occur if $\Delta G < 0$, indicating that the spontaneous direction of the reaction is the dissolution of the metal.

The application of thermodynamics to corrosion phenomena has been represented by potential-pH plots, or Pourbaix diagrams. These diagrams are constructed from calculations based on the Nernst equation and solubility data for various compounds. From these diagrams, it is possible to differentiate regions of potential as a function of pH in which the metal is either immune (no corrosion), passivated by a thin film or actively dissolved [164]. The Pourbaix diagram of iron in an aqueous solution is shown in Figure 1.8. In the region labelled as A, the iron is inert and stable, while in region B, the iron dissolves and an oxide or hydroxide layer is formed in the region labelled as C.

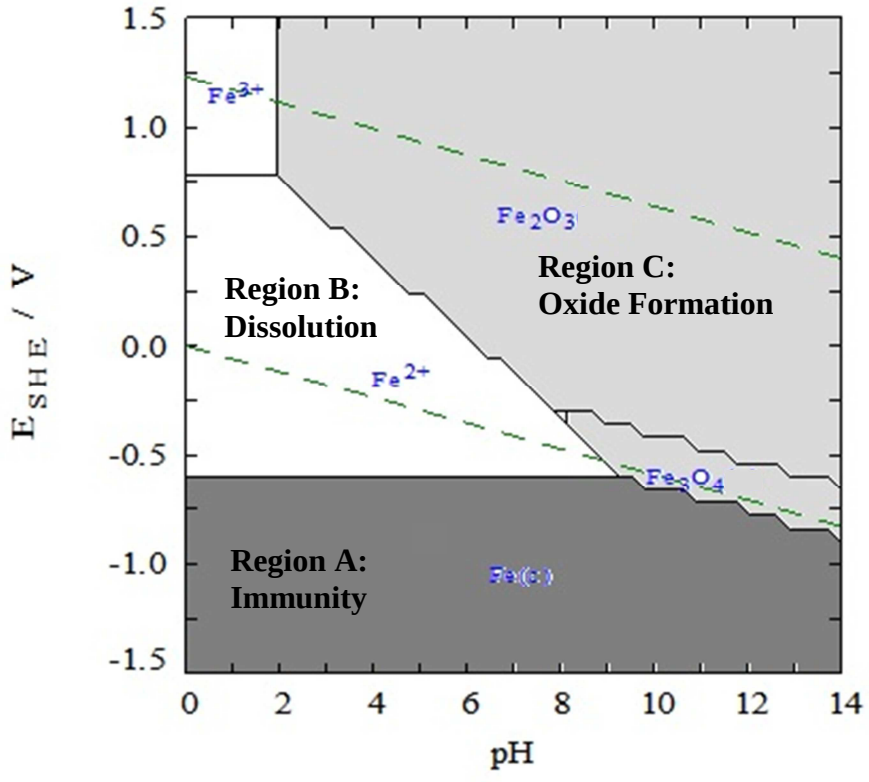

Figure 1.8: Pourbaix diagram for iron in water (dissolved iron concentration is 1.0×10^{-5} mol L^{-1} and the temperature is 25 °C). Only Fe, Fe_3O_4, Fe_2O_3 as solid products are considered. The diagram was realised with the MEDUSA software developed by Puigdomenech [19] at the KTH Royal Institute of Technology, Sweden and based on the SOLGASWATER algorithm [20].

The rate of the oxidation and reduction reactions increase as the potential is displaced from its equilibrium value [165]. A system is removed from equilibrium when the potential is displaced from the equilibrium potential by the application of an external voltage. This deviation in potential is defined as polarisation, η [160]:

$$\eta = \left| E - E_{eq} \right| \qquad \textbf{Eq. 1.24}$$

where, E_{eq} is the equilibrium potential. The magnitude of η depends mainly on the activation polarisation, concentration polarisation and resistance polarisation [134, 166]. When the rate of the electrochemical process is controlled by the charge transfer across the metal solution interface, then the system is under activation control. For such systems the relationship between the current density, *j*, and the potential, *E*, is given by the Butler–Volmer equation (Eq. 1.25) [166]:

$$j = j_0 \left(\exp\left[\frac{\alpha n F (E - E_{eq})}{RT} \right] - \exp\left[\frac{-(1-\alpha) n F (E - E_{eq})}{RT} \right] \right) \qquad \textbf{Eq. 1.25}$$

Here, j is the current density in A cm^{-2}, j_0 is the exchange current density in A cm^{-2}, defined as the rate of oxidation or reduction of the electrode at equilibrium, α is the charge transfer coefficient, n is the number of electrons involved, F is the Faraday constant (96,485 C mol^{-1}), R is the gas constant (8.314 J mol^{-1} K^{-1}) and T is the temperature in K.

For a sufficiently large value of anodic polarization from the equilibrium potential ($\eta_a > 50$ mV), the first term on the right side of Eq. 1.25 dominates the second term. Therefore, at large overpotentials, the Butler–Volmer equation simplifies to:

$$j = j_0 \exp\left[\frac{\alpha n F \eta_{a,a}}{RT} \right] \qquad \textbf{Eq. 1.26}$$

and rearranging the Tafel equation is obtained (Eq. 1.27):

$$\eta_{a,a} = \beta_a \log\left(\frac{j}{j_0} \right) \qquad \textbf{Eq. 1.27}$$

Here, $\eta_{a,a}$ is the anodic activation overpotential and $\beta_a = (2.303RT)/(\alpha nF)$ is the Tafel slope for the anodic reaction. A similar equation can be written for the cathodic half reaction.

When the transport of ions or molecules to or away from the metal surface determines the rate of the electrochemical process, then the system is said to be under concentration polarisation or transport control, η_c. For example, when the cathodic process in a corroding system depends on the reduction of dissolved oxygen, the diffusion of oxygen to the metal surface will often limit the rate of corrosion. The concentration polarisation can be expressed as:

$$\eta_c = \frac{RT}{nF}\ln\left(1-\frac{j}{j_{lim}}\right) \qquad \textbf{Eq. 1.28}$$

where, j_{lim} is the limiting current density which depends on the diffusivity of the reacting species.

Resistance polarisation, η_{IR}, arises as a consequence of the ohmic resistance in the system. It is the sum of all resistance elements present in the system. High-resistivity solutions and insulating films deposited at either the cathode or anode restrict the contact between the metal and the solution and will promote a high polarisation resistance. Consequently, the total polarisation, η_{tot}, across an electrochemical cell is the sum of these individual polarisations elements:

$$\eta_{tot} = \eta_a + \eta_c + \eta_{IR} \qquad \textbf{Eq. 1.29}$$

1.4.1.2 Mixed potential theory

Information on the kinetics of a corrosion reaction is usually presented as an Evans or polarisation diagram where the relationship between the electrode potential and current density is given for the reactions [134]. These diagrams are based on the principles of mixed-potential theory that was first developed by Wagner and Traud in 1938 [167]. In this analysis, any electrochemical reaction can be algebraically divided into separate oxidation and reduction half reactions with no net accumulation of electrical charge. As

a consequence, the rate of the oxidation reaction will equal the rate of the reduction reaction. Figure 1.9 shows the two half-cell reactions which occur when pure zinc is placed in an acid solution. In the corrosion of zinc, the oxidation half reaction corresponds to the dissolution of zinc, while the reduction of H^+ to liberate gaseous hydrogen gives the reduction half reaction. The potential of these two half-cell reactions are plotted as a function of the logarithm of the current density. When the corrosion reactions are controlled by activation polarisation, linear plots are observed. The corrosion potential, E_{corr}, and the corrosion current density values, j_{corr}, correspond to the intersection of the anodic and cathodic linear plots, as shown on the diagram. The value of the current at this intersection gives the rate of corrosion, j_{corr}. It is clear from this diagram that the slopes of the linear plots and the values of the exchange current densities, j_0, for the cathodic and anodic half reactions have a significant effect on the rate of corrosion.

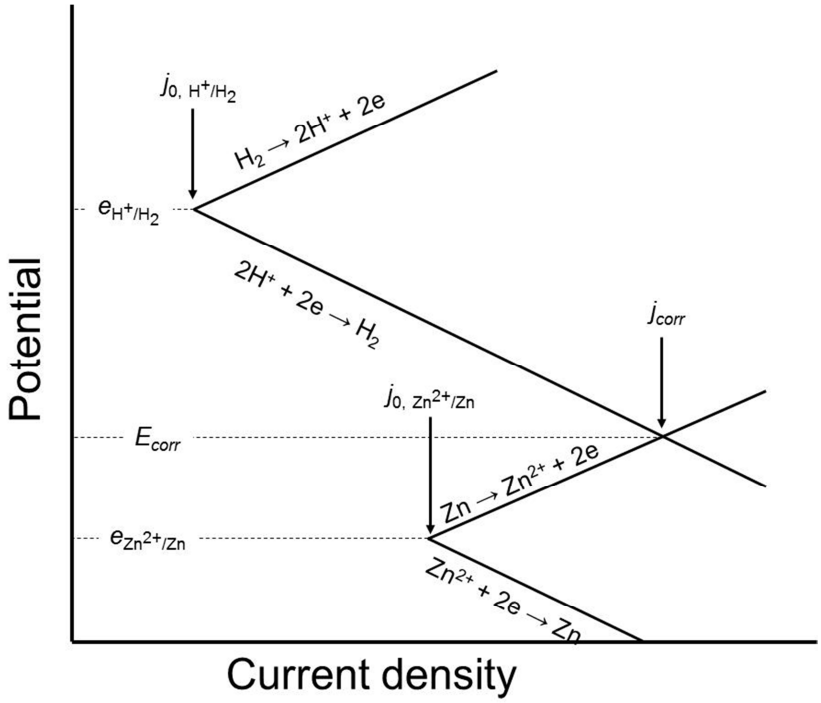

Figure 1.9: Evans diagram for zinc in HCl acid solution.

1.4.1.3 Types of corrosion

Metals and alloys are susceptible to different types of corrosion. The process may be quite complex, incorporating many factors, depending on the metal and the operating conditions. In this section, some forms of corrosion, with a specific focus on pitting corrosion, are introduced and discussed.

Uniform corrosion

Uniform corrosion, or general corrosion, proceeds evenly over the entire surface area, or a large fraction of the total area. General thinning takes place until failure. This is the most important and common form of corrosion in terms of amount of damage [134]. Measurements and predictions of uniform corrosion are relatively easy, making disastrous failures rare.

Galvanic corrosion

Galvanic corrosion takes place when two different or dissimilar metals are joined together in the presence of an electrolyte and a conductive path. Galvanic corrosion is easily identified by the presence of a build-up of corrosion at the joint between the dissimilar metals. When a galvanic couple forms, one of the metals in the couple, the less noble metal, acts as the anode and corrodes faster than it would by itself, while the other, the more noble metal, acts as the cathode and corrodes slower.

Intergranular corrosion

Intergranular corrosion is a form of localised attack which depends on the alloy composition. Indeed, it occurs along the grain boundaries, which are regions separating grains of different crystallographic orientation, or immediately adjacent to grain boundaries, while the bulk of the grains remain largely unaffected. This form of corrosion is usually associated with impurity segregation effects or specific phases precipitated on the grain boundaries.

Crevice corrosion

Crevice corrosion is a localised form of corrosion associated with a stagnant solution in small sheltered volumes. It occurs in localised areas such as crevices, joints, or bolted and threaded parts. Crevice corrosion is associated with variations in the concentration of salts, acids and moisture, which results in the development of an occluded corrosion

cell. The potential drop, the change in composition of the crevice electrolyte, caused by deoxygenation of the crevice, and a separation of electroactive areas drives the corrosion reaction. Small anodes are created within the crevice with the remainder of the body acting as a large cathode so corrosion in the crevice is highly accelerated.

Pitting corrosion

Pitting corrosion is a localised form of corrosion producing cavities or small pits in the material. Pitting corrosion may be difficult to detect. In addition, corrosion products often cover the pits. Pitting is initiated by localised chemical or mechanical damage to the protective oxide film. Factors that can cause breakdown of a passive film are acidity, low dissolved oxygen concentrations and the presence of halide anions, such as chlorides. Other favourable factors include the presence of inclusions. The processes involved in the formation of pits are complex and many still are not fully understood. However, three fundamental stages can be identified in the process, initiation, propagation and termination. The theories for passive film breakdown and pit initiation can be summarised and divided into three main mechanisms, adsorption, film breaking and film penetration [168]. These mechanisms are more relevant to pure metals, since pits are usually associated with inclusions or secondary-phase (intermetallic) particles in alloy systems.

The adsorption theory (Figure 1.10(a)) is based on the competitive adsorption of chloride ions and oxygen for sites on the metal surface. In this theory, the passive film is considered an adsorbed monolayer film of oxygen on the surface of the metal. Pits develop at sites where passivating oxygen is displaced by the presence of aggressive anions in order to overcome the repulsive forces between anions. The adsorbed halides induce pitting by weakening the bonding of the metal ions to the metal lattice or by thinning the passivating oxide film. According to Hoar and Jacobs [169] the adsorption of the aggressive anions leads to the formation of a surface complex, which separates from the surface and dissolves. As a consequence, the thinning of the oxide layer at a localised spot occurs and a high electrical field strength is produced, facilitating the migration of metal ions to the film/electrolyte interface. However, the breakdown can be inhibited or delayed when the adsorption of inhibiting ions, such as sulfate, takes place. On the other hand, Leckie and Uhlig [170] proposed a model where the passive film

consists of adsorbed oxygen rather than metal oxide. When O^{2-} is adsorbed, the metal passivates, while the adsorption of chlorides does not produce a passive surface. When anions other than chlorides are present, they also tend to adsorb on the passive metal/alloy surface displacing the chloride ions.

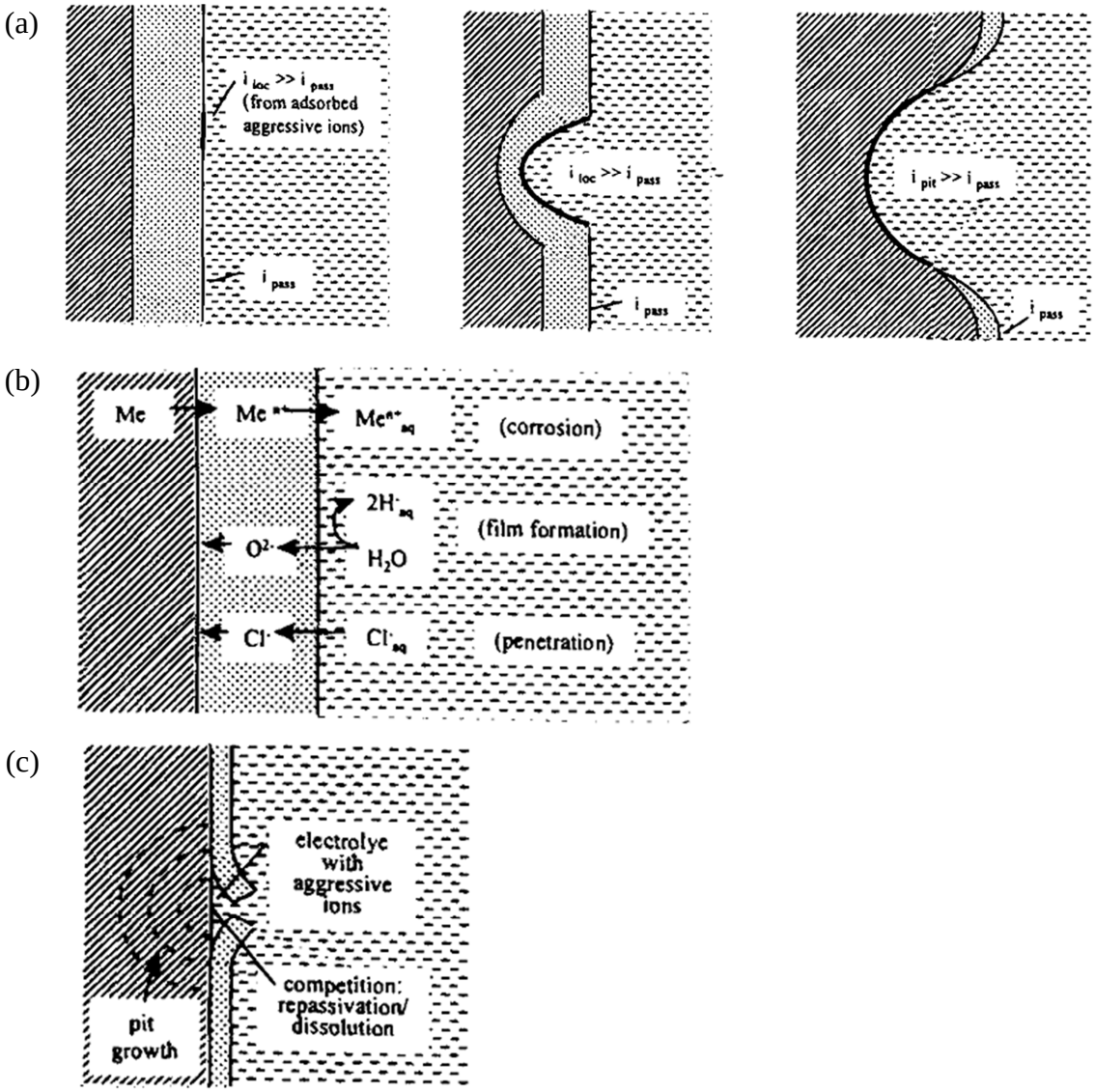

Figure 1.10: Schematic diagrams representing pit initiation by (a) adsorption and thinning, (b) penetration and (c) film breaking [168].

Metal Oxide passive layer Electrolyte

In the penetration mechanism (Figure 1.10(b)), the aggressive anions migrate and are incorporated throughout the film under the high electric field strength. The breakdown of passivity occurs when the anion reaches the metal/film interface [168, 171]. This migration requires an induction time, probably dependent on a critical concentration of

the anions in the inner oxide film [168, 172]. The anions can penetrate through the lattice via defects or through interactions with the oxide lattice. The presence of imperfections, such as grain boundaries, in the passive film can facilitate the entrance of aggressive anions into the film. The efficiency of the aggressive anions in the penetration of the film depends on their respective dimensions. The smaller anions, such as chlorides, penetrate more readily and therefore are considered more aggressive than bromide or iodide ions [73]. On the other hand, the incorporation of the aggressive anions at the outer surface of the oxide layer results in the formation of vacancies [172]. These vacancies diffuse to the metal/oxide surface where they are annihilated by the oxidative migration of cations from the metal. If the flux of these vacancies is larger than can be accommodated by oxidation, the vacancies will condense at the metal/oxide interface to form a void, which is believed to be the first step in the pitting process. The growth of these voids up to a critical size requires an incubation period. As a consequence, a semi-logarithmic dependence of the breakdown potential on chloride ion concentration is observed experimentally.

Pit initiation by film breakdown (Figure 1.10(c)) considers that the thin passive film is in a continuous state of breakdown and repair [168]. Mechanical stresses at the weak sites or flaws on the oxide film can lead to the local breakdown of the passive film [55]. However, in a non-aggressive environment the passive film can reform very rapidly, while the film reform will decrease rapidly in the presence of aggressive anions. As a result, the metal surface at these defective sites becomes activated. In this model, the role of chloride ions is restricted to prevent repassivation rather than promoting breakdown. It is worth noting that not all the breakdown events result in pitting corrosion. According to this model, breakdown will only lead to pitting corrosion where pit growth is possible. It is assumed that breakdown will always occur, but the passive film properties will influence the rate of its occurrence. Consequently, several researchers suggested a critical factor for pit stability mainly consisting of the product of pit depth and pit current density [173]. If this product exceeds a critical value, the pits are stable and do not passivate.

Subsequent to pit initiation, propagation occurs. The rate of pit growth depends on several factors, such as the composition of the metal, the electrolyte concentration around the pit and the mass-transport characteristics. Pit propagation occurs through the

establishment of local electrochemical cells, as shown in Figure 1.11. The anode is the area in which the metal dissolves, while the cathode forms the area in which the surface remains passive. The anodic metal dissolution reaction and the reduction reaction of dissolved oxygen are represented by Eq. 1.30 and Eq. 1.31:

Anodic $$M \rightarrow M^{n+} + ne^{-}$$ **Eq. 1.30**

Cathodic $$O_2 + H_2O + 4e^{-} \rightarrow 4OH^{-}$$ **Eq. 1.31**

Initially, the whole surface is in contact with the electrolyte containing dissolved oxygen, consequently oxygen reduction takes place across the surface. Due to the continuing metal dissolution, an excess of positive ions, M^{+}, is accumulated in the anodic area. In order to maintain charge neutrality, anions, such as chlorides, migrate from the electrolyte to the anodic area. The hydrolysis reaction of the cation, due to the metal dissolution, causes a decrease of the local pit pH:

$$M^{n+} + nH_2O \rightarrow M(OH)^{n+} + nH^{+}$$ **Eq. 1.32**

The acidity developed in the pit is not neutralised by the cathodic reaction because of the spatial separation of the anodic and cathodic reactions. The presence of H^{+} ions and chloride content prevents repassivation. As a result, pitting is considered to be autocatalytic in nature; once a pit starts to grow, the local conditions are altered such that further pit growth is promoted. The third stage of pitting is repassivation, which is usually associated with dilution of the local pit environment or a potential drop.

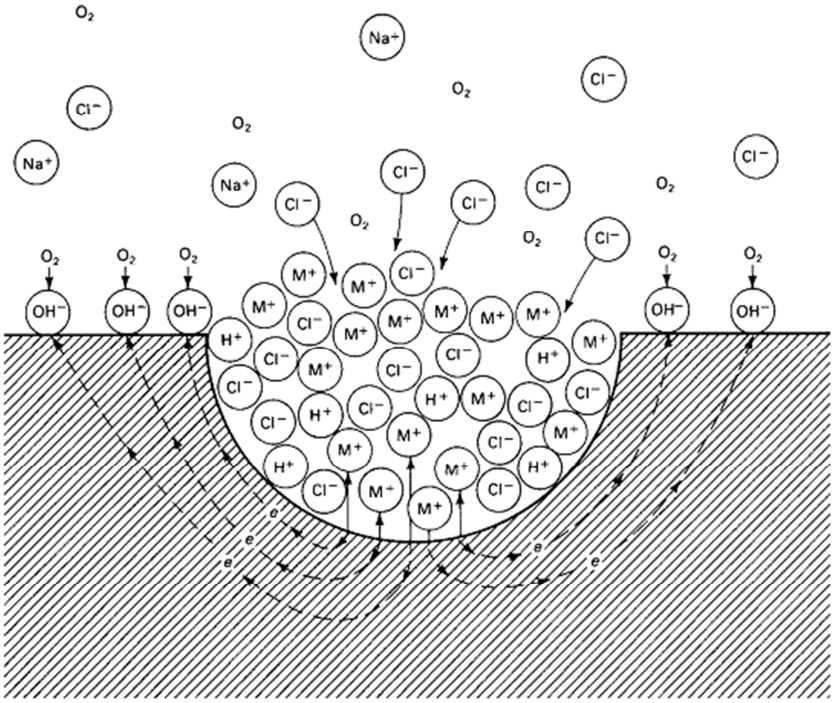

Figure 1.11: Schematic of an active corrosion pit on a metal in a chloride solution [174].

1.4.2 Corrosion properties of materials

In this section the electrochemistry of iron and aluminium and their alloys, which are used in the present thesis, is discussed. The analysis of the pure metals is performed using the Pourbaix diagrams, showing the stable domains of the metals as a function of pH and potential. In addition, a brief description of the classification of the iron and aluminium alloys and the effect of the alloying elements is given.

1.4.2.1 Iron

According to Evans [175], the corrosion of iron occurs when the metal surface is covered by an aqueous film in air. In such conditions, two reactions occur, the anodic dissolution or oxidation of iron and the reduction of dissolved oxygen. These reactions result in the dissolution of iron and the subsequent formation of iron hydroxides and oxides. In Figure 1.8 a simplified Pourbaix diagram for iron at 25 °C, giving the regions of stability of iron and its oxides in water is shown. Intermediate products such as $Fe(OH)_2$ are not shown as these oxidise further to Fe_3O_4 and Fe_2O_3. From the diagram it is seen that iron corrodes freely over a wide range of pH values and only a small region of passivity exists, where the surface is protected by a passive film. In this passive

region iron readily forms oxides, while under acidic conditions the dissolution of iron to Fe^{2+} and Fe^{3+} occurs. Indeed, the electrochemical behaviour of iron is very dependent on the solution pH. This pH effect was first reported by Kabanov *et al.* [176], who observed a significant increase in the dissolution of iron in alkaline environments. This was attributed to different dissolution mechanisms in acidic and alkaline media. However, Hurlen [177] suggested that the mechanism was the same but it involved a first-order catalytic interaction of the hydroxyl ions, according to the following:

$$2Fe + OH^- \leftrightarrows 2Fe^{2+} + OH^- + 4e^- \qquad \textbf{Eq. 1.33}$$

or

$$2Fe + OH^- \leftrightarrows Fe(OH)^+ + Fe^{2+} + 4e^- \qquad \textbf{Eq. 1.34}$$

In Figure 1.8 region C delineates the conditions where the passive layer is formed on the metal surface. For the chemical composition of this passive film, several models have been reported involving either single or double layers that contain different combinations and arrangements of the oxides, hydroxides, or oxyhydroxides, including Fe_3O_4 (magnetite), γ-Fe_2O_3 (maghemite), γ-FeOOH (lepicrocite), $Fe(OH)_2$ and a cation-deficient Fe_2O_3 ($Fe_{2-2x}G_xO_3$) [159, 178]. It appears that the passive film consists of a composite of iron oxides and hydroxides and is dependent on the potential applied in the growth of the film. The most common corrosion product formed on iron is due to the oxidation of the metal in the presence of air and water, forming an oxide layer, which is commonly known as rust. The process involves the oxidation of iron to give Fe^{2+} and subsequently the Fe^{3+} species. Then, these ions combine with oxygen to form ferric oxide, which is then hydrated according to the following equations:

$$2Fe + O_2 + 4H^+ \rightarrow 2Fe^{2+} + 2H_2O \qquad \textbf{Eq. 1.35}$$

$$2Fe + 1/2\,O_2 + (2+n)H_2O \rightarrow Fe_2O_3 \cdot nH_2O + H^+ \qquad \textbf{Eq. 1.36}$$

1.4.2.2 Stainless steel

Stainless steel is a general term used to indicate a large group of enhanced corrosion resistant alloy steels. These stainless steels are iron-based alloys containing at least 11 wt% chromium [179]. This amount of chromium gives the stainless steel the ability to

form a protective or passive film that resists corrosion. This film is self-forming and self-healing and is responsible for the resistance to corrosion of stainless steel. The corrosion resistance can be increased with increasing levels of chromium, nickel and molybdenum However, stainless steels cannot be considered to be 100% corrosion resistant. Indeed, the passive state can be broken down under certain conditions and then corrosion occurs locally.

According to Pardo *et al.* [180], the high corrosion resistance of stainless steels is primarily due to the oxide layer formed on its surface. Many studies have revealed that the passive film consists of a mixture of iron and chromium oxides with hydroxides and water-containing compounds in the outermost region of the film and chromium oxide at the metal–film interface [181-183]. Schweitzer [184] proposed that the passive film was duplex in nature, consisting of an inner barrier oxide film and an outer deposit of hydroxide or salt film. Indeed, a Cr-O-OH phase may be formed, which has better protective properties than the chromium oxide, Cr_2O_3 [181].

Stainless steels are divided into four main groups: austenitic, ferritic, martensitic and duplex. These groups are classified by their composition [179]. More specifically, a series identification (200, 300 and 400) was introduced by the American Institute of Steel and Iron, AISI, for a universal understanding of the components and the percentage of the components within stainless steel [181]. The austenitic steels, including the 200 and 300 series, are the most common stainless steels. This series contains a minimum of 18% chromium and low carbon contents. The austenitic stainless steels are known for high corrosion resistance and strength. The 300 series contains nickel as an austenite stabiliser, while the 200 series contains manganese and nitrogen stabilisers. The ferritic steels include the 400 series metals, with the chromium content ranging from 12% to 30% and low nickel contents, offering moderate corrosion resistance. The stability of the ferrite structure increases with an increase in the chromium content. The martensitic stainless steels contain the AISI 400 stainless steel, more specifically SS416 and SS420, commonly used for the manufacturing of cutlery and medical instruments [134]. The duplex family consists of an equal proportion of ferrite and austenite structures offering a high strength with approximately 23% chromium and 4% nickel. Duplex stainless steels display enhanced resistance to stress corrosion cracking and pitting corrosion in chloride solutions.

Although resistant to corrosion, stainless steels can suffer localised corrosion in the form of pitting and crevice corrosion when local breakdown of the protective passive film occurs [179]. The most significant environmental condition which influences the pitting corrosion behaviour of stainless steels is the chloride ion concentration. Once the breakdown of the passive film occurs, the corrosion of stainless steel is governed by the electrochemistry of iron, according to Figure 1.8. Indeed, it has been reported that the anodic polarisation of stainless steel leads to the selective dissolution of iron, leaving chromium enriched in the passive film [185, 186]. However, the composition of the passive films changes as the potential increases. This transformation involves the conversion of Cr(III) containing oxide species to a Cr(VI) containing soluble species, as shown in Figure 1.12. Depending on the pH of the solution, the conversion of Cr_2O_3 to CrO_4^{2-} is possible at potentials employed during the polarisation of the stainless steel.

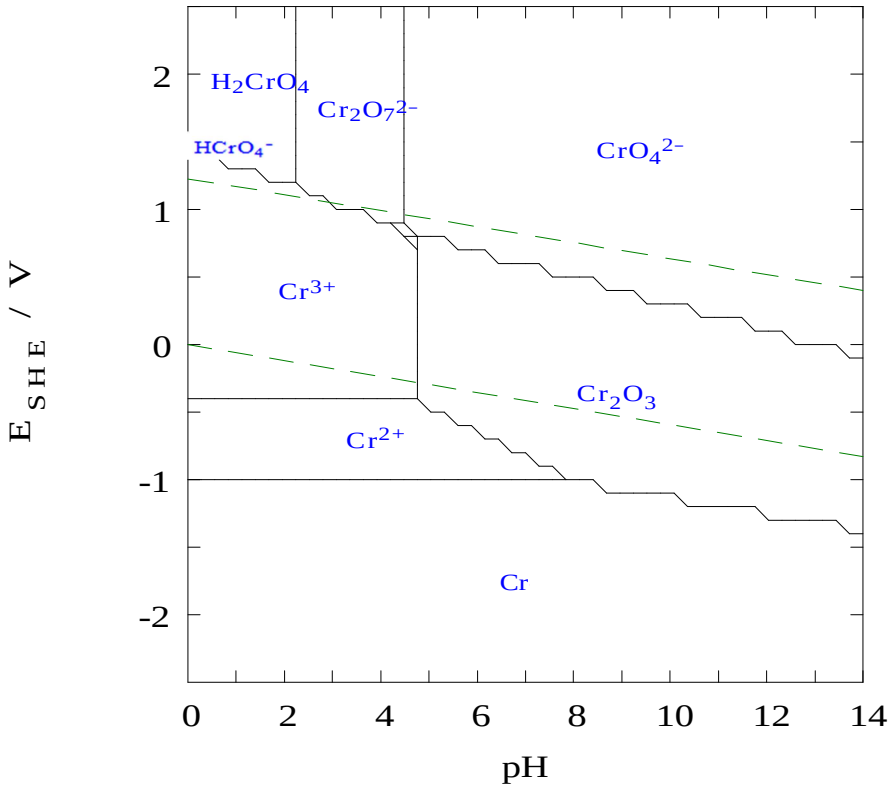

Figure 1.12: Simplified Pourbaix diagram for chromium in water (for a chromium concentration of 1.0×10^{-6} mol L^{-1} and a temperature of 25°C). The diagram was realised with the MEDUSA software developed by Puigdomenech [19] at the KTH Royal Institute of Technology, Sweden and based on the SOLGASWATER algorithm [20].

1.4.2.3 Aluminium

Freshly-formed aluminium easily reacts with air. Indeed, when it is exposed to the atmosphere, a layer of aluminium oxide is immediately formed on the surface. The thickness of the layer varies depending on the temperature and the presence of alloying elements. For example, oxide films formed at room temperature are 2 to 3 nm thick on pure aluminium [187]. At 425 °C the film thickness may reach 20 nm [187]. The natural oxide film corresponds to $A1_2O_3$, which is formed spontaneously according to Eq. 1.37. The Gibbs energy of this oxidation reaction is -1675 kJ mol^{-1} and this explains the very high affinity of aluminium towards oxygen.

$$2Al + 3/2\,O_2 \rightarrow Al_2O_3 \qquad \textbf{Eq. 1.37}$$

The Pourbaix diagram for the aluminium-water system at 25 °C is shown in Figure 1.13. In near neutral solution, between pH 4.0 and 8.6, the metal surface readily develops an insoluble oxide, which grows to sufficient thickness to limit the reactivity of the aluminium. Moreover, the diagram shows the amphoteric nature of the aluminium oxide. Indeed, under strongly acid or alkaline conditions, the protective layer is unstable and undergoes dissolution to form Al^{3+} or AlO_2^- species, respectively. Aluminium is susceptible to localised corrosion, especially pitting and crevice attack [188]. These forms of corrosion occur when species, such as chloride ions, compromise the integrity of the oxide film at local sites.

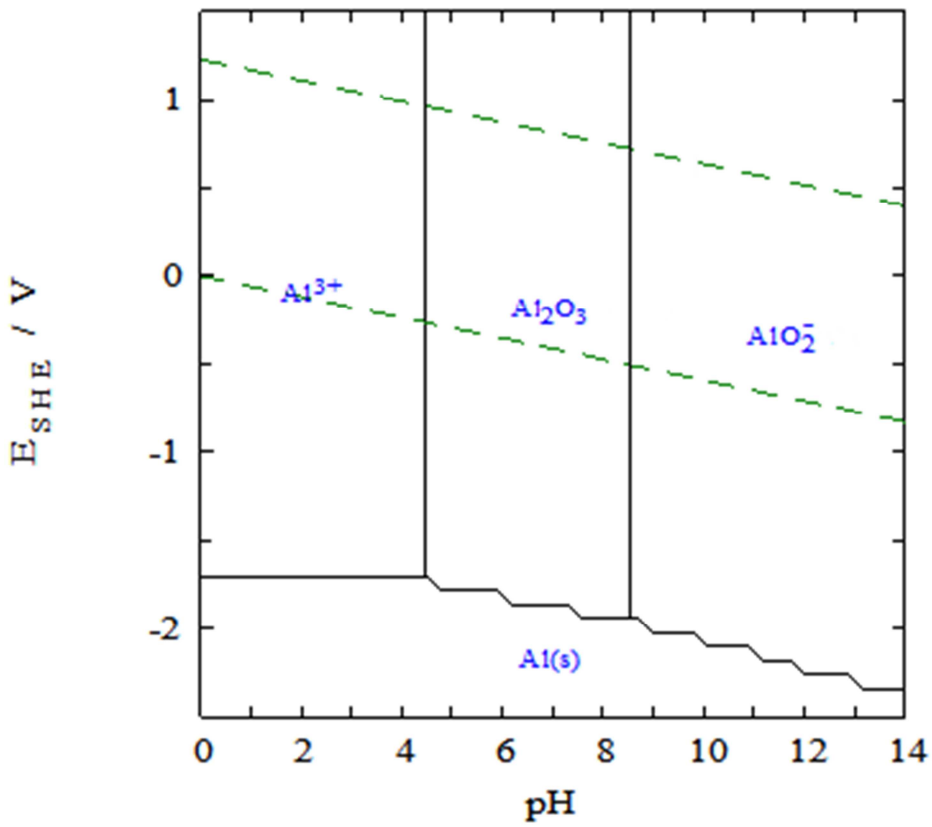

Figure 1.13: Simplified Pourbaix diagram for aluminium in water (for aluminium concentration of 1.0×10^{-5} mol L^{-1} and a temperature of 25°C). The diagram was realised with the MEDUSA software developed by Puigdomenech [19] at the KTH Royal Institute of Technology, Sweden and based on the SOLGASWATER algorithm [20].

1.4.2.4 Aluminium alloys

The properties of aluminium are altered by the addition of alloying elements [134]. The common alloying constituents are copper, magnesium, silicon, zinc, manganese and nickel. The cast alloys are cast directly into their desired forms, while the wrought alloys are cast in ingots or billets and are then worked mechanically into extrusions, forgings, sheets, foils, tubes and wires. The composition of the aluminium alloys is regulated by an internationally agreed classification system or nomenclature. According to the Aluminium Association, AA, system classification, which was adopted in the European Standard EN 573, each wrought alloy is assigned by a four digit number, with a further letter and number indicating the temper, or condition of the alloy, preceded by EN-AW (European Norm Wrought Product). For example, EN-AW 6082-T6 is a medium strength grade based on the aluminium-magnesium-silicon family, in the fully heat treated condition. Only the first digit has practical importance. It designates the

series to which the alloy belongs. Table 1.2 shows the series and corresponding alloying elements for the wrought aluminium alloys.

Table 1.2: Classification of aluminium wrought alloys.

Series	Alloy family
1xxx	None
2xxx	Copper
3xxx	Manganese
4xxx	Silicon
5xxx	Magnesium
6xxx	Magnesium and silicon
7xxx	Zinc (and copper)

As already mentioned, aluminium is highly corrosion resistant; however, it is soft and possesses a very low yield strength [187]. Consequently, it is often alloyed with various elements to improve its mechanical properties. The addition of these elements can also have an effect on the corrosion resistance. For example, the corrosion potential recorded on the addition of some major alloying elements to pure aluminium is shown in Figure 1.14. It can be seen that the addition of magnesium and zinc reduces the corrosion potential of aluminium, while additions of manganese, copper and silicon result in an increase in the corrosion potential. The alloying elements can also influence the corrosion properties. The equilibrium solubility of many metals in aluminium is very low and therefore the alloying additions as well as impurities often form intermetallic particles. These intermetallic particles may act as initiation sites for localised corrosion.

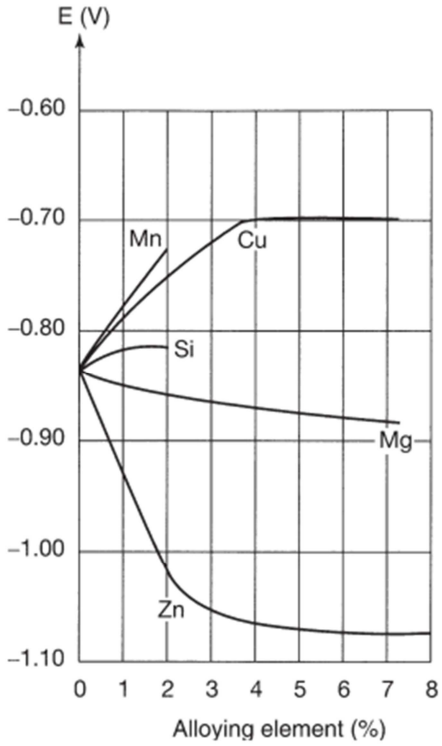

Figure 1.14: Influence of alloying elements on the dissolution potential of aluminium alloys [187].

1.5 Research presented in this thesis

The primary aim of this research is to investigate the feasibility of the electrocoagulation technique for the treatment of water using novel electrode materials, such as iron and aluminium alloys rather than the pure metals. Specifically, the objectives of the research are as follow: (i) to determine the removal efficiency of phosphates in terms of several parameters, such as the initial concentration of phosphates, current density, initial pH and the chloride concentration; (ii) to develop a kinetic and an adsorption model for the removal of phosphates; (iii) to relate the electrochemical and corrosion behaviour of some electrode materials in synthetic wastewaters containing several pollutants to their performance in terms of both removal and energy efficiencies.

In this chapter, an introduction to conventional wastewater treatments and the removal of the three pollutants subsequently used in the present study are given. This is followed by an overview of the basic principles of the electrocoagulation process that involve coagulation and flocculation. Finally, the electrochemistry of the electrode materials used in the present study is presented. The second chapter concerns the relevant

experimental techniques and apparatus employed, along with an overview of the theories and related equations and models used in this thesis.

The results and main findings are presented and discussed in Chapters 3-6. In Chapter 3, the efficiency of the electrocoagulation process for the removal of phosphate ions using an aluminium-magnesium alloy and a stainless steel is investigated. The efficiency is tested by varying parameters, such as the initial concentration of phosphates, current density, initial pH and sodium chloride concentration. The kinetics of the removal and the removal adsorption model are also presented. The electrocoagulation performance is then studied for the removal of phosphates from real wastewater samples.

In Chapter 4, results are presented on the electrochemical and corrosion behaviour of several electrode materials in synthetic wastewaters containing phosphates, an organic dye and zinc ions. The corrosion behaviour of pure aluminium and iron and some of their alloys has been extensively studied by several researchers [170, 173, 189-207]. However, few reports are available in the literature on the corrosion behaviour of these electrodes in solutions which contain a mixture of anions, as occurs in real wastewaters. In the present study, the effects of some common ions on the electrochemical behaviour of the electrode materials and on their corrosion morphology are discussed.

In Chapter 5, a study of the performance of the electrode materials is carried out. The test solutions are the synthetic wastewaters used in Chapter 4. The removal efficiencies of the three pollutants are compared and correlated to the electrochemical behaviour of the electrodes presented in Chapter 4. In addition, the energy consumption of the process is computed and shown for each electrode material. This study is the first attempt at relating the corrosion processes of the electrodes, in the presence of a mixture of ions, with the efficiency and energy performance for the simultaneous removal of various pollutants. Finally, conclusions are presented in Chapter 6.

1.6 References

[1] WHO/Unicef, *Global Water Supply and Sanitation Assessment 2000 Report*, World Health Organization and United Nations Children's Fund, 2000.
[2] Rajeshwar, K., Ibanez, J.G., Swain, G.M., *J. Appl. Electrochem.*, **24** (1994) 1077-1091.
[3] Holt, P.K., Barton, G.W., Mitchell, C.A., *Chemosphere*, **59** (2005) 355-367.
[4] Mollah, M.Y.A., Schennach, R., Parga, J.R., Cocke, D.L., *J. Hazard. Mater.*, **84** (2001) 29-41.
[5] Linares-Hernandez, I., Barrera-Diaz, C., Roa-Morales, G., Bilyeu, B., Urena-Nunez, F., *Chem. Eng. J.*, **148** (2009) 97-105.
[6] Crittenden, J.C., Trussel, R.R., Hand, D.W., Howe, K.J., Tchobanoglous, G., *MWH's Water Treatment: Principle and Design*, John Wiley, 2012.
[7] Cheremisinoff, N.P., *Handbook of Water and Wastewater Treatment Technologies*, Butterworth-Heinemann, 2002.
[8] Metcalf and Eddy, I., *Wastewater Engineering: Treatment and Reuse*, McGraw-Hill, 2003.
[9] Riffat, R., *Fundamentals of Wastewater Treatment and Engineering*, CRC Press, 2003.
[10] Chen, G.H., *Sep. Purif. Technol.*, **38** (2004) 11-41.
[11] Mollah, M.Y.A., Morkovsky, P., Gomes, J.A.G., Kesmez, M., Parga, J., Cocke, D.L., *J. Hazard. Mater.*, **114** (2004) 199-210.
[12] Gray, N.F., *Water Technology - An Introduction for Scientists and Engineers*, 2nd ed., Butterworth-Heinemann, 1999.
[13] Krishnan Rajeshwar, J.G.I., *Environmental Electrochemistry: Fundamentals and Applications in Pollution Sensors and Abatement*, Academic Press, 1997.
[14] WEF, *Biological and chemical systems for nutrient removal*, Water Environment Federation, 1998.
[15] Gray, A.V., *J. Inst. Wat. Eng. Scient.*, **39** (1985) 137-154.
[16] Ayoub, G.M., Koopman, B., Pandya, N., *Water Environ. Res*, **73** (2001) 478-485.
[17] Stevenson, F.J., *Cycles of soil*, John Wiley, 1986.
[18] Jenkins, D., Ferguson, J.F., Menar, A.B., *Water Res.*, **5** (1971) 369-&.
[19] Puigdomenech, I., *Windows software for the graphical presentation of chemical speciation, March 26-30*, in: 219th ACS National Meeting, San Francisco, CA, 2000, Am. Chem. Soc.
[20] Eriksson, G., *Anal. Chim. Acta*, **112** (1979) 375-383.
[21] Morse, G.K., Brett, S.W., Guy, J.A., Lester, J.N., *Sci. Total Environ.*, **212** (1998) 69-81.
[22] Thistleton, J., Berry, T.A., Pearce, P., Parsons, S.A., *Process Saf. Environ. Protect.*, **80** (2002) 265-269.
[23] Maurer, M., Boller, M., *Water Sci. Technol.*, **39** (1999) 147-163.
[24] Diagger, G.T., Sigmund, T.W., *Design and operation of chemical phosphorus removal facilities.*, in: R. Sedlak (Ed.) Phosphorus and nitrogen removal from municipal wastewater – principles and practice, Lewis Publishers, 1991.
[25] Nesbitt, J.B., *J. Water Pollut. Control Fed.*, **41** (1969) 701-713.
[26] Brett, S., Guy, J., Morse, G.K., *Phosphorus Removal and Recovery Technologies*, Seper Publications, 1997.
[27] Zollinger, H., *Color Chemistry - Synthesis, Properties and Application of Organic Dyes and Pigments*, VHCA and Wiley-VCH, 1991.
[28] Tauro, S., Coutinho, E., *J. Mol. Struc.-Theochem.*, **532** (2000) 23-29.
[29] Carneiro, P.A., Pupo Nogueira, R.F., Zanoni, M.V.B., *Dyes Pigments*, **74** (2007) 127-132.
[30] Freeman, H.S., Esancy, J.F., Claxton, L.D., *Dyes Pigments*, **13** (1990) 55-70.
[31] Crini, G., *Bioresour. Technol.*, **97** (2006) 1061-1085.
[32] Chen, J.P., *Decontamination of Heavy Metals: Processes, Mechanisms, and Applications*, Taylor & Francis Group, 2012.
[33] Duffus, J.H., *Pure Appl. Chem.*, **74** (2002) 793-807.

[34] Fu, F., Wang, Q., *J. Environ. Manage.*, **92** (2011) 407-418.
[35] Gakwisiri, C., Raut, N., Al-Saadi, A., Al-Aisri, S., Al-Ajmi, A., in: World Congress on Engineering, London, U.K., 2012, July 4 - 6.
[36] Srivastava, N.K., Majumder, C.B., *J. Hazard. Mater.*, **151** (2008) 1-8.
[37] Strokach, P.P., *Electrochem. Ind. Process. Bio.*, **55** (1975).
[38] Matteson, M.J., Dobson, R.L., Glenn, R.W., Kukunoor, N.S., Waits, W.H., Clayfield, E.J., *Colloids Surf., A*, **104** (1995) 101-109.
[39] Vik, E.A., Carlson, D.A., Eikum, A.S., Gjessing, E.T., *Water Res.*, **18** (1984) 1355-1360.
[40] Kobya, M., Can, O.T., Bayramoglu, M., *J. Hazard. Mater.*, **100** (2003) 163-178.
[41] Amosov, V.V., Zil'brtman, A.G., Kucheryavykh, E.I., Sorkin, E.I., Tsarik, L.Y., Eppel, S.A., Timoshek, V.E., Titov, I.P., *Chem. Technol. Fuels Oils*, **12** (1976) 850-852.
[42] Kaliniichuk, E.M., Vasilenko, I.I., Schepanyuk, V.Y., Sukhoverkhova, N.A., Makarov, I.A., *Int. Chem. Eng.*, **16** (1976) 434-435.
[43] Bochkarev, G.R., Lebedev, V.F., Nogin, N.M., *Sov. Min. Sci.*, **13** (1977) 35-38.
[44] Osipenko, V.D., Pogorelyi, P.I., *Metallurgist*, **21** (1977) 44-45.
[45] Gavrilyuk, A.I., *Sov. J. Water Chem. Technol.*, **3** (1981) 195-199.
[46] Gavrya, N.A., Novosel'tseva, L.V., Shevchenko, L.Y., Yutina, A.S., Kompaniets, V.I., Shatokhina, E.A., *Sov. J. Water Chem. Technol.*, **3** (1981) 527-528.
[47] Kharlamova, T.A., Gorokhova, L.T., *Sov. J. Water Chem. Technol.*, **4** (1982) 157-158.
[48] Novikova, S.P., Shkorbatova, T.L., Sokol, E.Y., *Sov. J. Water Chem. Technol.*, **4** (1982) 353-357.
[49] Nikolaev, N.V., Kozlovskii, A.S., Utkin, I.I., *Sov. J. Water Chem. Technol.*, **4** (1982) 244-247.
[50] Avetisyan, D.P., Tarkhanyan, A.S., Safaryan, L.N., *Sov. J. Water Chem. Technol.*, **6** (1984) 345-346.
[51] Gnusin, N.P., Vitul'skaya, N.V., Zabolotskaya, L.I., Belobrov, I.A., *J. Appl. Chem. (USSR)*, **50** (1997) 1663.
[52] Gnusin, N.P., Zabolotskaya, L.I., Vitul'skaya, N.V., *Sov. J. Water Chem. Technol.*, **7** (1985) 32.
[53] Pogrebnaya, V.L., Klimenko, A.A., Bokovikova, E.P., Tsymbal, E.P., Pronina, N.P., *Chem. Petrol. Eng.*, **31** (1995) 280.
[54] Beck, E.C., Giannini, A.P., Ramirez, E.R., *Food Technol.*, **22** (1974) 18.
[55] Chen, G.H., Chen, X.M., Yue, P.L., *J. Environ. Eng.*, **126** (2000) 858-863.
[56] Biswas, N., Lazarescu, G., *Int. J. Environ. Stud.*, **38** (1991) 65.
[57] Lawrence, J., Knieper, L., *Ind. Wastewater*, **1-2** (2000) 20.
[58] Do, J.S., Chen, M.L., *J. Appl. Electrochem.*, **24** (1994) 785-790.
[59] Gurses, A., Yalcin, M., Dogar, C., *Waste Manage. (Oxford)*, **22** (2002) 491-499.
[60] Ibanez, J.G., Singh, M.M., Szafran, Z., *J. Chem. Educ.*, **75** (1998) 1040-1041.
[61] Vlyssides, A.G., Loizidou, M., Karlis, P.K., Zorpas, A.A., Papaioannou, D., *J. Hazard. Mater.*, **70** (1999) 41-52.
[62] Vlyssides, A.G., Papaioannou, D., Loizidoy, M., Karlis, P.K., Zorpas, A.A., *Waste Manage. (Oxford)*, **20** (2000) 569-574.
[63] Xiong, Y., Strunk, P.J., Xia, H.Y., Zhu, X.H., Karlsson, H.T., *Water Res.*, **35** (2001) 4226-4230.
[64] Mameri, N., Yeddou, A.R., Lounici, H., Belhocine, D., Grib, H., Bariou, B., *Water Res.*, **32** (1998) 1604-1612.
[65] Panizza, M., Bocca, C., Cerisola, G., *Water Res.*, **34** (2000) 2601-2605.
[66] Tsai, C.T., Lin, S.T., Shue, Y.C., Su, P.L., *Water Res.*, **31** (1997) 3073-3081.
[67] Abuzaid, N.S., Bukhari, A.A., Al-Hamouz, Z.M., *Adv. Environ. Res.*, **6** (2002) 325-333.
[68] Donnini, J.C., Kan, J., Hassan, T.A., Kar, K.L., *Can. J. Chem. Eng.*, **72** (1994) 667.
[69] Renk, R.R., *Energy Prog.*, **8** (1988) 205.

[70] Szynkarczuk, J., Kan, J., Hassan, T.A.T., Donini, J.C., *Clays Clay Miner.*, **42** (1994) 667-673.
[71] Belongia, B.M., Haworth, P.D., Baygents, J.C., Raghavan, S., *J. Electrochem. Soc.*, **146** (1999) 4124-4130.
[72] Pretorius, W.A., Johannes, W.G., Lempert, G.G., *Water SA*, **17** (1991) 133-138.
[73] Phutdhawong, W., Chowwanapoonpohn, S., Buddhasukh, D., *Anal. Sci.*, **16** (2000) 1083-1084.
[74] Balasubramanian, N., Madhavan, K., *Chem. Eng. Technol.*, **24** (2001) 519– 521.
[75] Chiang, L.C., Chang, J.E., Tseng, S.C., *Water Sci. Technol.*, **36** (1997) 123-130.
[76] Pouet, M.F., Grasmick, A., *Water Sci. Technol.*, **31** (1995) 275-283.
[77] Sharma, G., Choi, J., Shon, H.K., Phuntsho, S., *Desalin. Water Treat.*, **32** (2011) 381-388.
[78] Holt, P., Barton, G., Mitchell, C., *Electrocoagulation as a Wastewater Treatment*, in: The Third Annual Australian Environmental Engineering Research Event, Castlemaine, Victoria, 1999.
[79] Johnson, P.N., Amirtharajah, A., *J. Am. Water Works Ass.*, **75** (1983) 232-329.
[80] Moreno C, H.A., Cocke, D.L., Gomes, J.A.G., Morkovsky, P., Parga, J.R., Peterson, E., Garcia, C., *Ind. Eng. Chem. Res.*, **48** (2009) 2275-2282.
[81] Moreno-Casillas, H.A., Cocke, D.L., Gomes, J.A.G., Morkovsky, P., Parga, J.R., Peterson, E., *Sep. Purif. Technol.*, **56** (2007) 204-211.
[82] Bagotsky, V.S., *Fundamentals of Electrochemistry*, 2nd ed., John Wiley, 2006.
[83] Edeleanu, C., Evans, U.R., *Transactions of the Faraday Society*, **47** (1951) 1121-1135.
[84] Richards, J.A., Wood, G.C., *Corros. Sci.*, **10** (1970) 313-316.
[85] Drazic, D.M., Popic, J.P., *J. Appl. Electrochem.*, **29** (1999) 43-50.
[86] Knörnschild, G., Kaesche, H., *Formation, Properties and Significance for Advanced Luminescent Materials*, in: 192th Meeting of The Electrochem. Society, Montreal, May,1997.
[87] Pickering, H.W., Frankenthal, R.P., *J. Electrochem. Soc.*, **119** (1972) 1297-1303.
[88] Canizares, P., Jimenez, C., Martinez, F., Saez, C., Rodrigo, M.A., *Ind. Eng. Chem. Res.*, **46** (2007) 6189-6195.
[89] Barrera-Diaz, C., Bilyeu, B., Roa, G., Bernal-Martinez, L., *Sep. Purif. Rev.*, **40** (2011) 1-24.
[90] Pizzi, N.G., *Water Treatment*, American Water Works Association, 2010.
[91] Harif, T., Khai, M., Adin, A., *Water Res.*, **46** (2012) 3177-3188.
[92] Benefield, L.D., Judkins, J.F., Weand, B.L., *Process Chemistry for Water and Wastewater Treatment*, Prentice-Hall, Inc., 1982.
[93] Wiesner, M.R., Klute, R., *Properties and Measurements of Particulate Contaminants in Water* in: J.B. McEwen (Ed.) Treatment Process Selection for Particle Removal, American Water Works Association, 1998.
[94] Eilbeck, W.J., Mattock, G., *Chemical processes in Waste Water Treatment*, Ellis Horwood, Ltd, 1987.
[95] Israelachvili, J.N., *Intermolecular and Surface Forces*, Acadamic Press, 2011.
[96] Bockris, J., Devanathan, M., Muller, K., *Proc. R. Soc. London A*, **274** (1963) 55-79.
[97] Tripathy, T., De, B.R., *J. Phys. Sci.*, **10** (2006) 93-127.
[98] Letterman, R.D., Amirtharajah, A., O'Melia, C.R., *Coagulation and Flocculation*, in: R.D. Letterman, A.W.W. Association (Eds.) Water Quality and Treatment, A Handbook of community water supplies, McGraw-Hill, 1999.
[99] Bratby, J., *Coagulation and Flocculation in Water and Wastewater Treatment*, IWA Publishing, 2006.
[100] Thomas, D.N., Judd, S.J., Fawcett, N., *Water Res.*, **33** (1999) 1579-1592.
[101] Holt, P.K., Barton, G.W., Wark, M., Mitchell, C.A., *Colloids Surf., A*, **211** (2002) 233-248.
[102] Duan, J.M., Gregory, J., *Adv. Colloid Interface Sci.*, **100** (2003) 475-502.
[103] Baes, C.F., Mesmer, R.E., *The hydrolysis of cations*, Wiley, 1976.

[104] Wesolowski, D.J., Palmer, D.A., *Geochim. Cosmochim. Acta*, **58** (1994) 2947-2969.
[105] Flynn, C.M., *Chem. Rev.*, **84** (1984) 31-41.
[106] Weber, W.J., *Physicochemical Processes for Water Quality Control*, John Wiley, 1972.
[107] Ben Sasson, M., Calmano, W., Adin, A., *J. Hazard. Mater.*, **171** (2009) 704-709.
[108] Bagga, A., Chellam, S., Clifford, D.A., *J. Membr. Sci.*, **309** (2008) 82-93.
[109] Katal, R., Pahlavanzadeh, H., *Desalination*, **265** (2011) 199-205.
[110] Gomes, J.A.G., Daida, P., Kesmez, M., Weir, M., Moreno, H., Parga, J.R., Irwin, G., McWhinney, H., Grady, T., Peterson, E., Cocke, D.L., *J. Hazard. Mater.*, **139** (2007) 220-231.
[111] Akbal, F., Camci, S., *Desalination*, **269** (2011) 214-222.
[112] Chou, W.-L., Wang, C.-T., Huang, K.-Y., *J. Hazard. Mater.*, **167** (2009) 467-474.
[113] Vasudevan, S., Lakshmi, J., Jayaraj, J., Sozhan, G., *J. Hazard. Mater.*, **164** (2009) 1480-1486.
[114] Vasudevan, S., Jayaraj, J., Lakshmi, J., Sozhan, G., *Korean J. Chem. Eng.*, **26** (2009) 1058-1064.
[115] Vasudevan, S., Lakshmi, J., Sozhan, G., *Clean-Soil Air Water*, **38** (2010) 506-515.
[116] Vasudevan, S., Lakshmi, J., Sozhan, G., *Desalination*, **275** (2011) 260-268.
[117] Vasudevan, S., Lakshmi, J., *Environ. Eng. Sci.*, **29** (2012) 563-572.
[118] Khemis, M., Tanguy, G., Leclerc, J.P., Valentin, G., Lapicque, F., *Process Saf. Environ. Protect.*, **83** (2005) 50-57.
[119] Arslan-Alaton, I., Kabdasli, I., Vardar, B., Tuenay, O., *J. Hazard. Mater.*, **164** (2009) 1586-1594.
[120] Kabdasli, I., Vardar, B., Arslan-Alaton, I., Tuenay, O., *Chem. Eng. J.*, **148** (2009) 89-96.
[121] SenthilKumar, P., Umaiyambika, N., Gayathri, R., *Environ. Eng. Manage. J.*, **9** (2010) 1031-1037.
[122] Bukhari, A.A., *Bioresour. Technol.*, **99** (2008) 914-921.
[123] Kabdasli, I., Keles, A., Oelmez-Hanci, T., Tuenay, O., Arslan-Alaton, I., *J. Hazard. Mater.*, **171** (2009) 932-940.
[124] Abuzaid, N.S., Al-Hamouz, Z., Bukhari, A.A., Essa, M.H., *Water Air Soil Pollut.*, **109** (1999) 429-442.
[125] Murthy, Z.V.P., Parmar, S., *Desalination*, **282** (2011) 63-67.
[126] Kabdasli, I., Arslan, T., Oelmez-Hanci, T., Arslan-Alaton, I., Tuenay, O., *J. Hazard. Mater.*, **165** (2009) 838-845.
[127] Golder, A.K., Samanta, A.N., Ray, S., *J. Hazard. Mater.*, **141** (2007) 653-661.
[128] Ghosh, D., Medhi, C.R., Purkait, M.K., *Chemosphere*, **73** (2008) 1393-1400.
[129] Wang, C.-T., Chou, W.-L., Kuo, Y.-M., *J. Hazard. Mater.*, **164** (2009) 81-86.
[130] Asselin, M., Drogui, P., Benmoussa, H., Blais, J.-F., *Chemosphere*, **72** (2008) 1727-1733.
[131] Bayramoglu, M., Eyvaz, M., Kobya, M., *Chem. Eng. J.*, **128** (2007) 155-161.
[132] Can, O.T., Kobya, M., Demirbas, E., Bayramoglu, M., *Chemosphere*, **62** (2006) 181-187.
[133] Mouedhen, G., Feki, M., Wery, M.D.P., Ayedi, H.F., *J. Hazard. Mater.*, **150** (2008) 124-135.
[134] Uhlig, H.H., Revie, R.W., *Uhlig's Corrosion Handbook*, 2nd ed., John Wiley & Sons, 2000.
[135] Trompette, J.L., Vergnes, H., *J. Hazard. Mater.*, **163** (2009) 1282-1288.
[136] Comninellis, C., Chen, G.E., *Electrochemistry for the Environment*, Springer, 2010.
[137] Hu, C.Y., Lo, S.L., Kuan, W.H., *Water Res.*, **37** (2003) 4513-4523.
[138] Chen, X.M., Chen, G.H., Yue, P.L., *Sep. Purif. Technol.*, **19** (2000) 65-76.
[139] Adhoum, N., Monser, L., Bellakhal, N., Belgaied, J.E., *J. Hazard. Mater.*, **112** (2004) 207-213.
[140] Shafaei, A., Pajootan, E., Nikazar, M., Arami, M., *Desalination*, **279** (2011) 121-126.
[141] Balasubramanian, N., Kojima, T., Basha, C.A., Srinivasakannan, C., *J. Hazard. Mater.*, **167** (2009) 966-969.

[142] Escobar, C., Soto-Salazar, C., Toral, M.I., *J. Environ. Manage.*, **81** (2006) 384-391.
[143] Al Aji, B., Yavuz, Y., Koparal, A.S., *Sep. Purif. Technol.*, **86** (2012) 248-254.
[144] Golder, A.K., Samanta, A.N., Ray, S., *Sep. Purif. Technol.*, **53** (2007) 33-41.
[145] Zongo, I., Leclerc, J.-P., Maiga, H.A., Wethe, J., Lapicque, F., *Sep. Purif. Technol.*, **66** (2009) 159-166.
[146] Emamjomeh, M.M., Sivakumar, M., *J. Environ. Manage.*, **90** (2009) 1663-1679.
[147] Martinez-Huitle, C.A., Brillas, E., *Appl. Catal., B*, **87** (2009) 105-145.
[148] Can, O.T., Bayramoglu, M., Kobya, M., *Ind. Eng. Chem. Res.*, **42** (2003) 3391-3396.
[149] Daneshvar, N., Oladegaragoze, A., Djafarzadeh, N., *J. Hazard. Mater.*, **129** (2006) 116-122.
[150] Ogutveren, U.B., Koparal, S., *J. Environ. Sci. Health., Part A*, **32** (1997) 2507-2520.
[151] Kumar, P.R., Chaudhari, S., Khilar, K.C., Mahajan, S.P., *Chemosphere*, **55** (2004) 1245-1252.
[152] Merzouk, B., Gourich, B., Sekki, A., Madani, K., Chibane, M., *J. Hazard. Mater.*, **164** (2009) 215-222.
[153] Heidmann, I., Calmano, W., *J. Hazard. Mater.*, **152** (2008) 934-941.
[154] Koparal, A.S., Ogutveren, U.B., *J. Hazard. Mater.*, **89** (2002) 83-94.
[155] Lacasa, E., Canizares, P., Saez, C., Fernandez, F.J., Rodrigo, M.A., *Chem. Eng. J.*, **171** (2011) 1012-1017.
[156] Irdemez, S., Demircioglu, N., Yildiz, Y.S., *J. Hazard. Mater.*, **137** (2006) 1231-1235.
[157] Irdemez, S., Demircioglu, N., Yildiz, Y.S., Bingul, Z., *Sep. Purif. Technol.*, **52** (2006) 218-223.
[158] Irdemez, S., Yildiz, Y.S., Tosunoglu, V., *Sep. Purif. Technol.*, **52** (2006) 394-401.
[159] Kruger, J., *Passivity*, in: ASM Handbook Volume 13A: Corrosion: Fundamentals, Testing, and Protection, ASM International, 2003.
[160] Fontana, M.G., *Corrosion Engineering*, McGraw-Hill, 1987.
[161] Sato, N., Okamoto, G., *Comprehensive Treatise of Electrochemistry,*, Plenum Press, 1981.
[162] Buchanan, E.E., Stansbury, R., *Fundamentals of Electrochemical Corrosion*, ASM International, 2000.
[163] Scully, J.C., *The Fundamentals of Corrosion*, Pergamon Press, 1975.
[164] Pourbaix, M., *J. Electrochem. Soc.*, **123** (1976) C25-C36.
[165] Roberge, P.R., *Corrosion Engineering, Principles and Practice*, McGraw-Hill, 2008.
[166] Bard, A.J., Faulkner, L.R., *Electrochemical Methods: Fundamentals and Applications*, Wiley, 2001.
[167] Wagner, C., Traud, W., *Z. Elektrochem. Ang. Physik. Chemie*, **44** (1938) 391.
[168] Frankel, G.S., *J. Electrochem. Soc.*, **145** (1998) 2186-2198.
[169] Hoar, T.P., Jacob, W.R., *Nature*, **216** (1967) 1299-1301.
[170] Leckie, H.P., Uhlig, H.H., *J. Electrochem. Soc.*, **113** (1966) 1262-1267.
[171] Heine, M.A., Pryor, M.J., *J. Electrochem. Soc.*, **114** (1967) 1001-&.
[172] Lin, L.F., Chao, C.Y., Macdonald, D.D., *J. Electrochem. Soc.*, **128** (1981) 1194-1198.
[173] Galvele, J.R., *J. Electrochem. Soc.*, **123** (1976) 464-474.
[174] Frankel, G.S., *Pitting Corrosion*, in: ASM Handbook Volume 13A: Corrosion: Fundamentals, Testing, and Protection, ASM International, 2003.
[175] Evans, U.R., *Nature*, **206** (1965) 980-982.
[176] Kabanov, B., Burstein, R., Frumkin, A., *Discuss. Farady Soc.*, **1** (1947) 259-269.
[177] Hurlen, T., *Electrochim. Acta*, **8** (1963) 609-619.
[178] Cornell, R.M., Schwertmann, U., *The Iron Oxides: Structure, Properties, Reactions, Occurrences and Uses*, John Wiley, 2006.
[179] Sedriks, A.J., *Corrosion of Stainless Steel*, John Wiley and Sons, New York, USA, 1979.

[180] Pardo, A., Merino, M.C., Coy, A.E., Viejo, F., Arrabal, R., Matykina, E., *Corros. Sci.*, **50** (2008) 780-794.
[181] Olsson, C.O.A., Landolt, D., *Electrochim. Acta*, **48** (2003) 1093-1104.
[182] Haupt, S., Strehblow, H.H., *Corros. Sci.*, **37** (1995) 43-54.
[183] Abreu, C.M., Cristobal, M.J., Losada, R., Novoa, X.R., Pena, G., Perez, M.C., *Electrochim. Acta*, **49** (2004) 3049-3056.
[184] Schweitzer, P.A., *Fundamentals of metallic corrosion: Atmospheric and media corrosion of metals*, in: Corrosion Engineering Handbook, CRC Press, 2006.
[185] Heine, B., Kirchheim, R., *Corros. Sci.*, **31** (1990) 533-538.
[186] Heusler, K.E., *Corros. Sci.*, **31** (1990) 597-606.
[187] Vargel, C., *Corrosion of Aluminium*, Elsevier, 2001.
[188] Snodgrass, J., *Corrosion Resistance of Aluminum Alloys*, in: ASM Handbook, Vol. 13A,Corrosion:Fundamentals, Testing, and Protection, ASM International, 2003.
[189] Alvarez, M.G., Galvele, J.R., *Corros. Sci.*, **24** (1984) 27-48.
[190] Bird, H.E.H., Pearson, B.R., Brook, P.A., *Corros. Sci.*, **28** (1988) 81-86.
[191] Galvele, J.R., in: R.P. Frankenthal, J. Kruger (Eds.) Passivity of Metals, The Electrochemical Society, Princeton, NJ, 1978, pp. 285-327.
[192] Horvath, J., Uhlig, H.H., *J. Electrochem. Soc.*, **115** (1968) 791-795.
[193] Lakatos-Varsányi, M., Falkenberg, F., Olefjord, I., *Electrochim. Acta*, **43** (1998) 187-197.
[194] Laycock, N.J., Newman, R.C., *Corros. Sci.*, **39** (1997) 1771-1790.
[195] Laycock, N.J., Newman, R.C., *Corros. Sci.*, **40** (1998) 887-902.
[196] MacDougall, B., Bardwell, J.A., *J. Electrochem. Soc.*, **135** (1988) 2437-2441.
[197] Nobe, K., Tobias, R.F., *Corrosion*, **20** (1964) 263.
[198] Szklarska-Smialowska, Z., Staehle, R.W., *J. Electrochem. Soc.*, **121** (1974) 1393-1401.
[199] Bohni, H., Uhlig, H.H., *J. Electrochem. Soc.*, **116** (1969) 906-910.
[200] Breslin, C.B., Friery, L.P., Carroll, W.M., *Corros. Sci.*, **36** (1994) 85-97.
[201] Brillas, E., Cabot, P.L., Centellas, F., Garrido, J.A., Perez, E., Rodriguez, R.M., *Electrochim. Acta*, **43** (1998) 799-812.
[202] Lee, W.J., Pyun, S.I., *Electrochim. Acta*, **45** (2000) 1901-1910.
[203] Munoz, A.G., Saidman, S.B., Bessone, J.B., *Corros. Sci.*, **44** (2002) 2171-2182.
[204] Pyun, S.I., Moon, S.M., *J. Solid State Electrochem.*, **3** (1999) 331-336.
[205] Pyun, S.I., Moon, S.M., Ahn, S.H., Kim, S.S., *Corros. Sci.*, **41** (1999) 653-667.
[206] Pyun, S.I., Na, K.H., Lee, W.J., Park, J.J., *Corrosion*, **56** (2000) 1015-1021.
[207] Shalaby, L.A., El Sobki, K.M., Abdul Azim, A.A., *Corros. Sci.*, **16** (1976) 637-643.

2 Experimental

2.1 Introduction

The present research is concerned with the corrosion behaviour and electrocoagulation performance of iron and aluminium and their alloys. The corrosion behaviour of these metals was investigated using potentiodynamic and cyclic potentiodynamic polarisation tests and open-circuit potential measurements. The morphology of the surfaces affected by localised corrosion was monitored using light microscopy. The efficiency of the electrocoagulation process was determined by measuring the removal of the pollutants using either UV-Visible or atomic absorption spectroscopy. In particular, the removal of phosphates by stainless steel and aluminium alloys was studied in detail. In addition, the kinetics of the removal was modelled using simple models and the adsorption process was fitted to standard isotherm equations. Furthermore, the speciation of the iron electrodissolution from the steel alloy was studied using rotating disk voltammetry, RDV. A screening chemometric study was carried out on the electrocoagulation process with the steel electrodes to determine the most relevant factors affecting the process efficiency.

In this chapter, the materials, methods and models used throughout the present work are described in detail. A brief description of the theoretical background of the experimental techniques is also presented.

2.2 Chemicals and electrode materials

2.2.1 Chemicals and test electrolytes

The chemicals used in the present work were potassium dihydrogen phosphate (ACS reagent, ≥ 99.0%), ammonium molybdate tetrahydrate (ACS reagent, ≥ 99.0%), ammonium metavanadate (99%), sodium chloride (AR grade, ≥ 99%), Orange II sodium salt (dye content, > 85%), calcium chloride dehydrate (ACS reagent, ≥ 99%), magnesium sulfate heptahydrate (ACS reagent, ≥ 98%), nitric acid (ACS reagent, 70%), sulfuric acid (reagent grade, 95-98%), sodium hydroxide (reagent grade, ≥ 98%), sodium sulfate (ACS reagent, ≥ 99.0%), zinc sulfate heptahydrate (99.999%), potassium chloride (super purum, 99.999+ %), ethanol (ACS reagent, ≥ 99.5%), ammonium iron(II) sulfate hexahydrate (ACS reagent, 99%) and iron(III) chloride hexahydrate (ACS reagent, 97%). All chemicals were supplied by Sigma-Aldrich® and used as received. All the electrolyte solutions were prepared using distilled water, except for the RDV experiments, which were carried out in Milli-Q purified water (14 MΩ, pH = 5.0).

The composition of the electrolyte solutions used in the corrosion tests is shown in Table 2.1. The ion concentrations were determined according to the OECD synthetic sewage [1].

Table 2.1: Composition of the electrolyte solutions used in corrosion (Chapter 4) and electrocoagulation tests (Chapter 5).

	KH_2PO_4 / M	NaCl / M	$CaCl_2.2H_2O$ / M	$MgSO_4.7H_2O$ / M	Na_2SO_4 / M	Orange II / M	$ZnSO_4.7H_2O$ / M
	-	1.7×10^{-2}	-	-	-	-	-
	-	1.7×10^{-1}	-	-	-	-	-
	-	1.7×10^{-2}	-	-	8.1×10^{-4}	-	-
	1.6×10^{-2}	-	-	-	-	-	-
sww 1	1.6×10^{-2}	1.2×10^{-2}	2.7×10^{-3}	8.1×10^{-4}	-	1.4×10^{-4}	1.5×10^{-3}
sww 2	1.6×10^{-2}	1.7×10^{-1}	2.7×10^{-3}	8.1×10^{-4}	-	1.4×10^{-4}	1.5×10^{-3}
	6.5×10^{-3}	-	-	-	-	-	-
	6.5×10^{-3}	5.0×10^{-4}	-	-	-	-	-

The electrolyte solutions employed for electrocoagulation tests are divided into three main categories. In Chapter 3, the electrolytes used were phosphate-containing solutions in sodium chloride prepared in distilled water and, where necessary, the pH was adjusted using HCl or NaOH to give the required value. In addition, two real samples from treatment facilities were employed. The conductivity levels of these samples are displayed in Table 2.2. In Chapter 5, the electrocoagulation tests were performed on two electrolyte solutions, sww 1 and sww 2, and the composition of these solutions is shown in Table 2.1.

Table 2.2: Conductivity levels for the real samples used for the electrocoagulation tests in Chapter 3.

Sample no.	**κ / mS cm^{-1}**
1	0.32
2	1.00

2.2.2 Electrode materials and sample preparation

The chemical composition and the exposed surface area of the various metals and alloys employed in the present study are shown in Table 2.3. All the electrode materials were supplied by Goodfellow© in rod, wire or sheet forms, which were then cut to provide the exposed surface area displayed in Table 2.3. The rotating disk electrode was platinum and this was purchased from Princeton Applied Research (Ametek).

Table 2.3: Chemical composition and surface area of electrodes.

Electrode	**Composition / wt. %**	**Geometric surface area / cm^2**	
		corrosion tests	**electrocoagulation tests**
Al	99.999	0.031	-
Al-2Mg (EN AW-5251)	Mg 1.7-2.4, Fe 0.5, Mn 0.5-0.1, Si 0.4, balance Al	0.50	40.8 – 38.7
Al-3Zn-0.02In	Zn 3, In 0.02, Fe 0.12, Si 0.08, Cu 0.006, balance Al	0.38	38.7
Pure Fe	99.99	0.071	38.7
AISI 310	Cr 24-26, Ni 19-22, Mn 2, Si 1.5, C 0.25, balance Fe	0.58	38.7
AISI 420	Cr 13-14, Mn 1, Si 1, C 0.3, balance Fe	0.63	36.9 – 38.7
		corrosion tests	**RDV**
Pt	100	> 1	0.1257

The samples used as working electrodes in the corrosion tests were set in a Teflon® holder with epoxy resin. An electrical contact was made attaching a copper wire to the sample with highly conductive silver-loaded resin. The quality of the electrical contact was checked with a multimeter to ensure that the resistance between the surface of the electrode and the connection was lower than 1.0 Ω. Prior to each experiment the exposed electrode surface was abraded on a Buehler® Metaserve grinder polisher with water lubricated Buehler® SiC grinding papers to a 2500 grit finish. The electrodes were then polished to a mirror finish with successively finer grades of Buehler® MetaDi monocrystalline diamond suspensions ranging from 30 to 1 μm on Buehler® polishing microcloths. Finally, they were rinsed with distilled water and ethanol, sonicated in a Branson 1510 ultrasonic bath and dried in a stream of air.

The samples used in the electrocoagulation tests were cut to form plates and the electrical connections were made using crocodile clips. The exposed area of each sample was defined by a mask of beeswax. Prior to each experiment they were abraded with water lubricated Buehler® silicon carbide paper (Grit P 320). They were then washed with distilled water and dried in a stream of air. If the electrodes were covered by a layer of oxides, they were dipped in HCl solution (5% v/v) for 10 min and rinsed thoroughly with water, before abrasion with SiC paper.

A platinum wire, with a high surface area, was used as the counter electrode in corrosion tests and in the RDV experiments. It was periodically abraded with Buehler® silicon carbide paper (Grit P 2500) and sonicated in distilled water to maintain a clean surface. The reference electrode was a saturated calomel electrode, SCE (0.242 V vs. NHE). The potential of the SCE reference electrode was regularly checked against a virgin SCE. Moreover, the aqueous KCl solution in the reference electrode was replaced periodically with a saturated solution of super purum KCl.

2.3 Experimental techniques

The experimental procedures and the equations employed in the present work are described in this section, along with a brief explanation of the parameters involved in the experiments. Additional information and representative calibration curves are given where necessary.

2.3.1 Electrochemical experiments

All the electrochemical experiments were carried out with a Solartron SI 1285A potentiostat, which was controlled by a computer unit. The software package used was CorrWare® for Windows version 3.2c by Scribner Associates, Inc. For the RDV experiments, the Pt electrode, described in Section 2.2.2, was rotated using a Princeton Applied Research Model 636 Ring-Disk Electrode System apparatus.

A basic diagram of a potentiostat controlling a three-electrode cell is presented inFigure 2.1. In this figure, the working, WE, reference, RE, and counter, CE electrodes are identified and connected to the potentiostat, which, in turn, is interfaced to a function generator. The potentiostat controls either the potential difference, V_{WE}, between the WE and the RE (potentiostatic mode) or the current flow, I_{RE}, between the WE and the CE (galvanostatic mode). The potential of the WE, V_{WE}, is varied by controlling the potential difference between WE and RE, V_{WR} ($V_{WR} = V_{WE} - V_{RE}$), since V_{RE} is constant. The current flow in the cell is $I_{CE} = I_{RE} + I_{WE}$. However, I_{RE} is taken as zero since the RE is connected to a high input impedance element. Consequently, the current flow in the cell is between WE and CE, $I_{WE} = I_{CE}$.

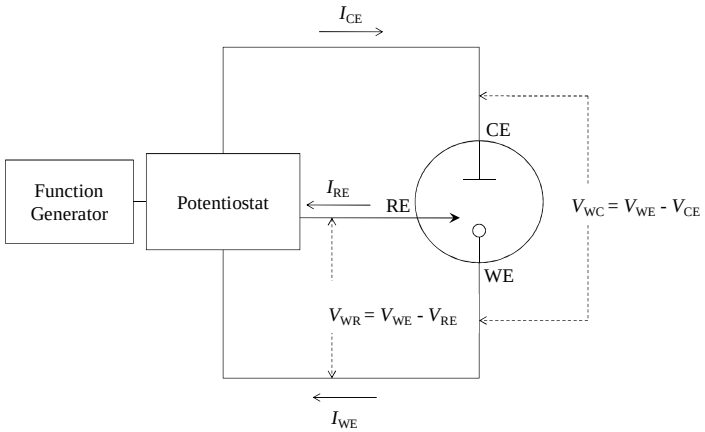

Figure 2.1: Basic diagram of a potentiostat (WE = working electrode, RE = reference electrode, CE = counter electrode).

2.3.1.1 The electrochemical cell for corrosion and RDV experiments

A typical three-electrode cell employed in the corrosion and RDV measurements is shown in Figure 2.2. This set-up consists of a working electrode, WE, a reference electrode, RE, and a counter electrode, CE. The electrode materials and their preparation are discussed in Section 2.2.2. The electrochemical cell was a glass cylinder of 10 mL in volume capped with a Teflon® lid holding the electrodes. A 100 mL glass cell was used for the RDE experiments. The three electrodes were immersed in the electrolyte solution and connected to the potentiostat. All the experiments were performed at room temperature. In some experiments, a micropipette was used to add known aliquots of chemicals to the electrolyte solution.

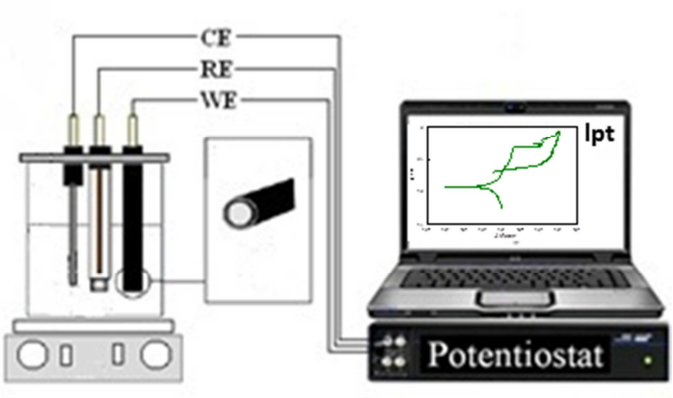

Figure 2.2: A schematic representation of the electrochemical cell used for corrosion and RDV experiments (WE = working electrode, RE = reference electrode, CE = counter electrode, lpt = laptop).

2.3.1.2 The electrochemical cell for electrocoagulation experiments

The electrocoagulation experiments were carried out using a standard three-electrode cell, presented in Figure 2.2 and a two-electrode set-up, which is shown in Figure 2.3, with an anode as the working electrode, WE, and a cathode as the counter electrode, CE. This two-electrode configuration is usually employed when precise control of the interfacial potential across the WE is not critical and the behaviour of the whole cell is under investigation. For example, in the present study it was used to estimate the energy consumption of the process, since its calculation required the cell voltage. The electrode materials and their preparation are presented in Section 2.2.2. In both electrochemical set-ups, a glass cell with a volume of 400 mL was equipped with a magnetic stirrer to

ensure good mixing during each experiment. The distance between the anode and the cathode was maintained at 1 cm for all the experiments.

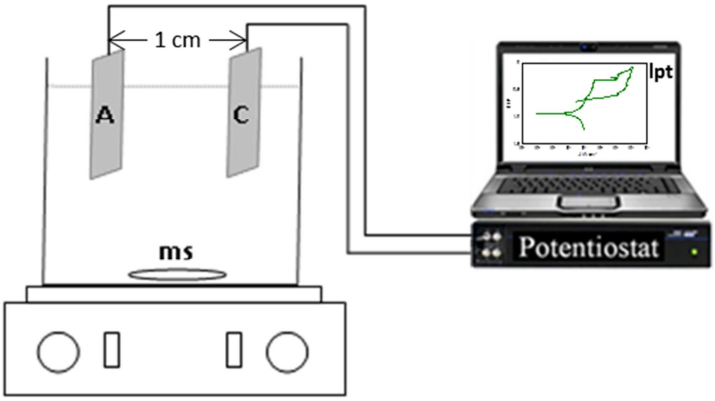

Figure 2.3: A schematic representation of the electrochemical cell used for electrocoagulation experiments (A = anode, C = cathode, ms = magnetic stirrer, lpt = laptop).

2.3.1.3 Corrosion techniques

Corrosion measurements are designed to predict the behaviour of a material before it is used in an environment. They can be broadly classified as destructive or non-destructive techniques [2]. A measurement is said to be destructive if it alters the corrosion process during the measuring process (e.g., potentiodynamic polarisation tests) or if the material is physically removed from the environment (e.g., weight loss measurements). Non-destructive techniques, which include open-circuit potential, linear polarisation resistance, electrochemical impedance spectroscopy and electrochemical noise, could be used to make repeated measurements at different time intervals. In the present study, two techniques were used for corrosion tests; open-circuit potential, OCP, measurements and potentiodynamic and cyclic potentiodynamic polarisation tests.

Open-circuit potential measurements

The open-circuit potential, OCP, or rest potential, is the potential exhibited by an electrode when no net current flows through the external circuit of the electrochemical cell. It is a relatively simple technique where the voltage between the WE and the RE is monitored as function of time [3]. By measuring the OCP it is possible, for example, to determine whether the corrosion is in the active or the passive state, gain information on the stability of the sample surface and obtain data for corrosion monitoring. The number

of data points collected determines the resolution and in these experiments data points were collected per second.

Potentiodynamic polarisation

The potentiodynamic polarisation technique for corrosion studies was introduced in the 1960s and became popular especially during the 1970s as a simple technique for routine use [2, 4]. It is useful for the prediction of the corrosion property of passivating metals or alloys prone to localised corrosion. This technique is based on the fact that when the potential of a freely corroding metal surface is changed by connecting it with an external power source, the metal will be polarised. ASTM [5] defines the term polarisation as "the change for the open-circuit potential as a result of the passage of current". The most common approach in polarisation methods involves changing the potential of the WE and monitoring the current which is produced. The potential is scanned at a fixed rate between two set values and the current is measured at periodic intervals [6]. In potentiodynamic polarisation tests, the measurement starts far away from the corrosion potential (> 100 mV) and gives a curve of the type shown in Figure 2.4. Potentiodynamic polarisation over a wide range of potentials, such as seen in Figure 2.4, provides important information about the system, for example the determination of the electrode behaviour over that range of potential. An active, passive and transpassive region can be identified and critical potentials, such as the corrosion potential, E_{corr}, breakdown potential, E_{br}, passivation potential, E_{pass}, or the slope of the polarisation curve at the corrosion potential, E_{corr}, can be estimated. However, according to Silverman [2, 4], the polarisation scan should not be used to estimate general or uniform corrosion rates. Making such an estimate from the potentiodynamic polarisation scan requires the assumption that the corrosion mechanism does not change over the wide potential range used for the scan. Other methods, such as electrochemical impedance spectroscopy or polarisation resistance, can be used for this purpose.

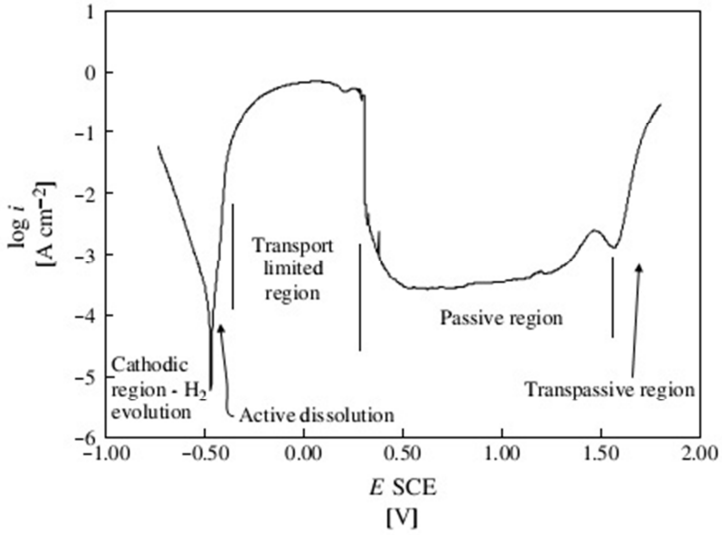

Figure 2.4: Representative potentiodynamic polarisation curve [6].

In the present study, potentiodynamic polarisation tests were performed on several electrode materials, listed in Section 2.2.2, and are shown in Chapter 4. The scans were started at a potential about 300 mV below the OCP and progressed in the anodic direction until visible breakdown of the electrode occurred, or a current density of 1 mA cm^{-2} was reached. Further details on the potentials and scan rates employed are given in the relevant sections of Chapter 4.

Under steady state conditions, electrochemical reactions under kinetic control obey the Tafel equations, Eq. 2.1 and Eq. 2.2, for large overpotentials.

anodic reaction $$\eta = \mathrm{a} + \beta_{\mathrm{a}} \log(j)$$ **Eq. 2.1**

cathodic reaction $$\eta = \mathrm{a}' + \beta_{\mathrm{c}} \log(j)$$ **Eq. 2.2**

Here, a and a' are the anodic and the cathodic constants, $a = (-2.303RT/\alpha nF)\log(j_0)$ and $a' = (2.303RT/(1-\alpha)nF)\log(j_0)$, respectively, and β_a and β_c are the anodic and the cathodic Tafel slopes, respectively (Section 1.4.1.1). Accordingly, a plot of the logarithm of the current, log(*j*), as a function of the overvoltage gives the Tafel plot. Many corrosion systems are kinetically controlled and consequently they follow Eq. 2.1 and Eq. 2.2. In a Tafel plot, a linear portion on both sides of the corrosion potential, E_{corr}, is indicative of kinetic control. Classical Tafel analysis is performed by

extrapolating the linear portion of a log current versus potential plot back to their intersection, as shown in Figure 2.5, giving the estimation of parameters such as corrosion current density, j_{corr}, and Tafel slopes, β_a and β_c.

In the present study, the Tafel analysis was performed using the CorrView2™ Version 3.0 analysis package under the following assumptions: (i) the Tafel region (linear portion of the semilogarithmic plot) extends for at least one order of magnitude of current [7]; (ii) the rate of polarization in the potentiodynamic scans is between 0.1 and 1 mV s^{-1} in order to determine steady state behaviour [7]. However, the first condition was not achievable in all the potentiodynamic scans due to interference from concentration polarization or other processes, such as surface roughening or film formation, which may alter the electrode surface [7]. The Appendix at the end of this thesis summarises the parameters evaluated using the Tafel analysis, such as the corrosion current density, j_{corr}, in A cm^{-1} and the anodic and the cathodic tafel slopes, β_a and β_c, respectively, in mV $decade^{-1}$.

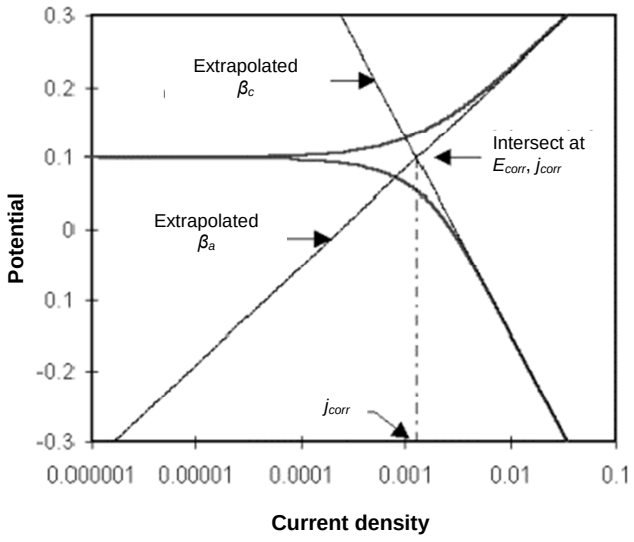

Figure 2.5: Classical Tafel analysis.

Cyclic potentiodynamic polarisation

In cyclic potentiodynamic polarisation measurements the voltage is first increased in the anodic direction (forward scan), then it is reversed at some chosen current or potential and then scanned in the cathodic direction (backward or reverse scan). The scan is

terminated usually at the corrosion potential, E_{corr}. The cyclic potentiodynamic polarisation provides information on the propensity for localised corrosion. In particular, the occurrence of a hysteresis loop between the forward and the reverse portions of the scan is considered a measure of the susceptibility of the sample to suffer localised corrosion [4]. However, hysteresis in cyclic potentiodynamic polarisation curves is not always associated with pitting or crevice corrosion and, consequently, it is necessary to examine the electrode surface following testing to establish the nature of the attack [8].

In Chapter 4, the cyclic potentiodynamic polarisation tests are presented for several electrode materials. The electrodes were polarised from a potential about 300 mV lower than the corrosion potential, E_{corr}, and the scan was reversed at 1 mA cm^{-2}, unless otherwise stated. Then the potential was cycled in the reverse direction until the corrosion potential, E_{corr}, was reached. Further details on the potentials and scan rates employed are given in the relevant sections of Chapter 4.

2.3.1.4 Electrocoagulation techniques

Electrocoagulation consists in either applying a constant current (galvanostatic mode) or a constant potential (potentiostatic mode) to the electrochemical cell described in Figure 2.2 and Figure 2.3. As a consequence, dissolution of the anode or WE occurs with simultaneous formation of hydroxyl ions, while hydrogen gas is usually produced at the cathode as a result of water reduction.

In the present study, the electrocoagulation tests were carried out under the galvanostatic mode in order to have consistent and reproducible anodic dissolution rates. The test electrolytes, listed in Table 2.1 and Table 2.2, were placed in the electrochemical cell, the solution pH was adjusted using either NaOH or NaCl when necessary and a constant stirring rate was employed throughout each experiment. All the electrocoagulation experiments were performed at room temperature, except for the adsorption isotherm studies. A constant current density was then applied using the potentiostat. Accordingly, the potential varied slightly depending on the resistance of the system. Samples were periodically taken from the reactor and allowed to settle for 15 min. Then the supernatant was filtered with Whatman™ filter paper (Grade 1, pore

size 11 μm) and analysed for the required quantitative determinations. The efficiency of removal, η, was computed according to Eq. 2.3, where C_0 is the initial concentration of the species and C_t is the concentration of the species at time t.

$$\eta(\%) = \frac{C_0 - C_t}{C_0} \times 100 \qquad \textbf{Eq. 2.3}$$

Different operating settings were used for the electrocoagulation experiments, consequently further details, such as the current density, solution pH or the surface area to the solution volume ratio, SA/V, in cm^{-1}, are given in the relevant chapters.

The adsorption isotherm studies were carried out with 74.0 mg L^{-1} of Al^{3+} or 361.3 mg L^{-1} of Fe^{2+} and phosphate solutions having concentrations ranging from 2.0 to 150.0 mg L^{-1} PO_4-P with a pH of 5.0 and the temperature of the electrochemical cell was controlled and maintained at 25 ± 1 ºC. The mass of the adsorbent (Al^{3+} or Fe^{2+}) used was calculated according to Faraday's laws of electrolysis and taking into account the composition of the electrode material used, as discussed in the relevant sections of Chapter 3.

2.3.1.5 Rotating disk voltammetry, RDV

Rotating disk voltammetry, RDV, is an electrochemical technique where the potential of the working electrode is swept between two chosen potential limits and the change in current is monitored. Unlike other electrochemical techniques, the working electrode, rotating disk electrode, RDE, is rotated at a controlled angular speed, ω (rad s^{-1}). The rotation motion determines a well-defined flow pattern of solution towards the surface of the RDE, as is shown in Figure 2.6. The electrode acts as a pump, pulling the solution upwards and perpendicular to the electrode surface [9]. However, the perpendicular flux of solution falls to zero at the electrode surface. Consequently, the layer of solution adjacent to the electrode surface manages to cling to the electrode and appears to be motionless from the perspective of the RDE. In this layer, where the solution is stagnant, the transport of the species is only by diffusion. The thickness of the layer, δ, in cm, is governed by the rate of the rotation and is inversely proportional to $\omega^{1/2}$, according to Eq. 2.4 [10].

$$\delta = 1.61 \frac{D^{1/3} \nu^{1/6}}{\omega^{1/2}} \qquad \textbf{Eq. 2.4}$$

Here, D is the diffusion coefficient, in $cm^2\ s^{-1}$, of the electroactive species, ν is the kinematic viscosity, in $cm^2\ s^{-1}$, of the solvent and ω is the angular velocity in rad s^{-1}.

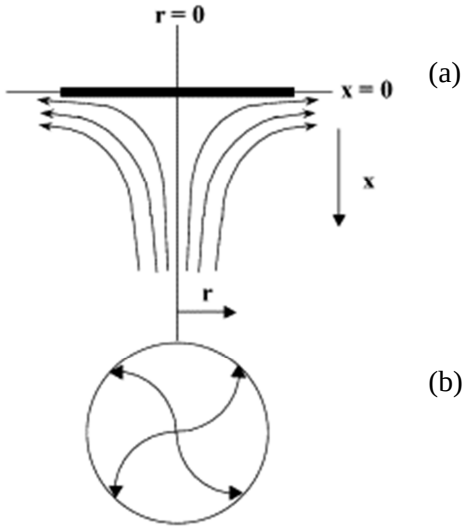

Figure 2.6: Schematic showing the flow patterns to the rotating disk electrode, RDE [10]. (a) The solution flow perpendicular to the electrode. (b) The electrode surface viewed from below.

A classical RDV experiment consists of a linear sweep voltammogram performed at a given scan rate, 1 to 50 mV s^{-1}, while the current is recorded as a function of the applied potential. The resulting voltammogram exhibits a typical sigmoidal wave, as is shown in Figure 2.7. At potentials where the rate of the electron transfer is high, a plateau is observed because the current is limited by the rate of mass transport. The limiting current, I_L, is given by the Levich equation, shown in Eq. 2.5

$$I_L = 0.62 nFAD^{2/3} \omega^{1/2} \nu^{-1/6} C^{\infty} \qquad \textbf{Eq. 2.5}$$

In this equation, n is the number of electrons transferred, F is the Faraday's constant (96,485.34 C mol^{-1}) and C^{∞} is the bulk concentration of the species in mol cm^{-3}. It is apparent from this equation that the limiting current, I_L, is linearly dependent on the square root of the rotational speed, $\omega^{1/2}$. Indeed, this is a useful test to determine if the current is mass-transport controlled [9].

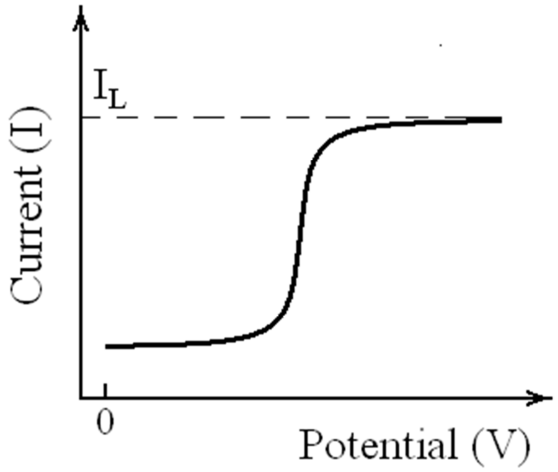

Figure 2.7: Typical diffusion controlled voltammetric response under mass-transfer-limiting condition.

In the present work, the RDV was used for the simultaneous detection of ferrous and ferric species, which were electrogenerated during electrocoagulation with a stainless steel electrode. RDV was first used to obtain the calibration curves for Fe(II) and Fe(III) in order to test the feasibility of the method. Then, the method was applied to the solutions after the electrocoagulation process. At the end of the electrocoagulation tests, 1.0 M H_2SO_4 was added to the solutions in order to have complete dissolution of the iron flocs formed during the process. After 24 h, samples of 25 mL were taken from each solution and used in RDV measurements using a potential range of -0.2 to 1.2 V vs. SCE, a scan rate of 10 mV s^{-1} and a rotation speed of the electrode of 3000 rpm. Due to the complexity of the sample matrix, a standard addition method was used [11]. In the standard addition method, small known concentrations of the analyte to be determined were added to aliquots of the unknown samples [12]. In these experiments, serial increments of the standard, V_s, were added to a constant volume, V_x, of the solution. With this method, additions of both Fe(II) and Fe(III) were made to the same samples keeping the IR drop and the ionic strength of the solution relatively constant. The linear response, Y, which was obtained for each solution is expressed by Eq. 2.6:

$$\underbrace{(V_x + NV_s)I_L}_{Y} = \underbrace{kV_xC_x}_{b} + \underbrace{kV_sC_s}_{m}\underbrace{N}_{x} \qquad \textbf{Eq. 2.6}$$

In this equation, V_x (25 mL) and V_s (0.25 mL) are the volumes of the unknown and the standard, respectively, C_x and C_s (0.5 M) are the concentrations of the unknown and the standard, respectively, N is the multiple units of addition (0, 1, 2, etc.) and I_L is the

limiting current from the RDV measurements. By plotting Y, the entire left hand side of Eq. 2.6, versus N a straight line results with an intercept, b, and a slope, m:

$$b = kV_x C_x \qquad m = kV_s C_s \qquad \textbf{Eq. 2.7}$$

Then, the unknown concentration, C_x, can be obtained from m and b:

$$C_x = \frac{bV_s C_s}{mV_x} \qquad \textbf{Eq. 2.8}$$

Figure 2.8 shows typical calibration curves for the Fe(II) and Fe(III) and a representative standard addition plot obtained for the determination of Fe(II).

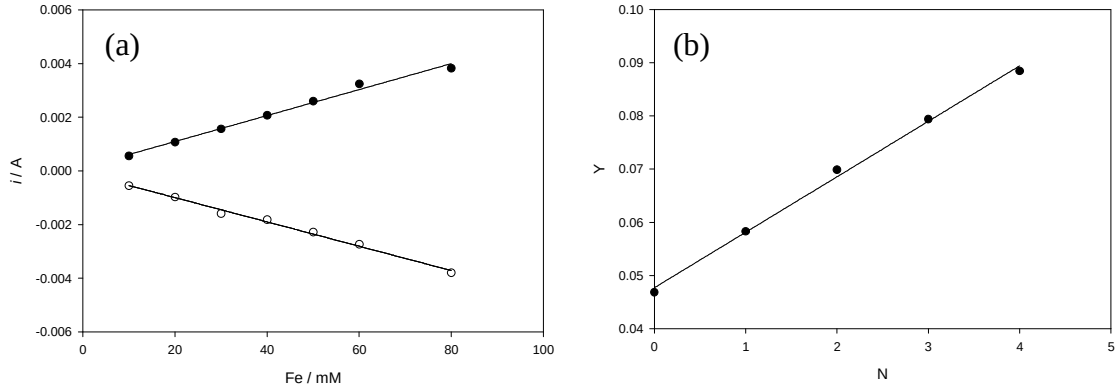

Figure 2.8: (a) Calibration curves for ● Fe(II) (R^2 = 0.990) and ○ Fe(III) (R^2 = 0.994) and (b) representative standard addition plot for ● Fe(II) (R^2 = 0.997).

2.3.2 Microscopy

The standard optical microscope, which is still the most widely used type of microscope, consists essentially of a combination of two lenses, an objective and an eyepiece. The product of these magnifications produces the magnification of the final image. The eyepiece can be replaced by a camera and the final image can be analysed on a computer unit. The main disadvantage of the optical microscope is the resolution limit, which restricts the minimum size of detail that can be seen at about 0.2 μm [13]. This limit cannot be overcome, since it is imposed by the wavelength of visible light, which is of the same order. The optical microscope is very widely used in

metallography, since it enables examination of materials and provides a magnified image of the micro- and macrostructures. Indeed, optical microscopy is used to characterise structures by revealing grain boundaries, phase boundaries, inclusion distribution and evidence of surface deformation [14].

In the present work, optical microscopy was used to examine the electrode surface after the corrosion tests were performed and to establish the nature of the localised corrosion. This technique was also used to ensure an adequate grinding and polishing of the samples prior to each experiment. The samples were washed thoroughly with distilled water, dried with a stream of air and observed carefully using an Olympus® BX51M at different magnifications in a dark-field mode. The micrographs were taken with a computer interfaced to a CCD camera (Leica DFC 2280 digital camera) and Olympus® DP version 3.2 software.

2.3.3 Spectroscopy

2.3.3.1 UV-Visible

UV-Visible (UV-Vis) spectroscopy consists in the measurement of the attenuation of a light beam after it passes through a sample. The intensity of the light absorbed is related to the concentration of the absorbing species, according to the Beer-Lambert law [15], Eq. 2.9:

$$A = \varepsilon_{\lambda} \mathrm{b} C \qquad \textbf{Eq. 2.9}$$

In this equation, A is the absorbance, ε_{λ} is the molar absorbtivity at a specific wavelength, λ, b is the path length and C is the concentration of the absorbing species.

In the present work, UV-Vis spectroscopy was used to determine the concentration of phosphate and Orange II, an organic dye, at the end of the electrocoagulation process in order to compute the efficiency of removal, as shown in Eq. 2.3. A Unicam Thermo Spectronic® UV 540 double-beam spectrometer was used. It comprises tungsten and deuterium lamps, a holographic grating monochromator and a photomultiplier tube detector. In all cases, a quartz cuvette with a path length of 1 cm was used. These data

were recorded using Vision 32 PC software and analysis was done using SigmaPlot™ Version 12.2.0.45 by Systat Software, Inc.

Colorimetric tests

The phosphate concentration was measured according to the vanadomolybdophosphoric acid colorimetric method [16]. This method consists of the reaction between phosphates and ammonium molybdate in acidic conditions to form a heteropoly acid, molybdophosphoric acid. When vanadium is added to the solution, vanadomolybdophosphoric acid, which has a yellow colour, is formed. To avoid interferences with ferric iron, the absorbance was measured at 470 nm. The calibration curve, obtained with phosphate concentrations ranging from 0.5 to 15.0 mg L^{-1}, is shown in Figure 2.9. It was used to calculate the concentration of phosphates in solution. The concentration of phosphates was expressed in units of mg L^{-1} PO_4-P, indicating the concentration of phosphorus in the form of phosphates. The limit of detection, DL, of the technique, defined as in Eq. 2.10, was estimated using the regression line of the calibration curve, according to Miller and Miller [17]. The value of the intercept of the calibration curve was used as an estimate of the blank signal, y_B, while the random error in the y-direction was used in place of the standard deviation of the blank, s_B [18].

$$DL = y_B + 3s_B \qquad \textbf{Eq. 2.10}$$

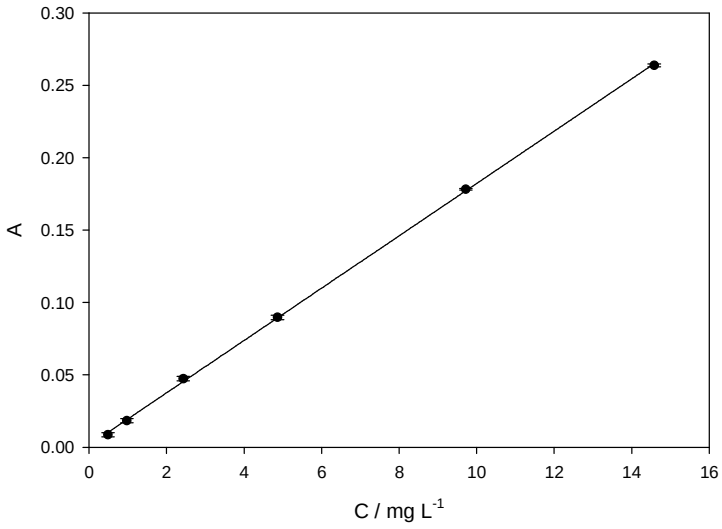

Figure 2.9: Calibration curve for PO_4-P determination (λ = 470 nm). The limit of detection, LD, was estimated as 0.25 mg L^{-1}. (R^2 = 0.999).

The structure of Orange II azo dye and its UV-Vis spectrum at a pH of approximately 10.0 are shown in Figure 2.10 (a) and (b), respectively. The chemical structure shows that this azo dye exhibits tautomerism between the azo and hydrazone forms by a proton exchange effect. In aqueous medium, the hydrazone form is the predominant species [19]. The azo dye colour is the result of the conjugation between the azo bond and the aromatic rings present in the dye molecule [20]. The UV-Vis spectrum has an absorption band at 485 nm and a shoulder at 405 nm in the visible region due to the chromophore-containing azo linkage and two bands at 310 and 230 nm in the UV region due to the aromatic rings. The 485 and 405 nm bands are attributed to the π-π^* transition of the hydrazine form and to the n-π^* transition of N=N azo group, respectively [19]. The other two peaks located in the UV region are assigned to the π-π^* transitions of the aromatic naphthalene and benzene rings [19].

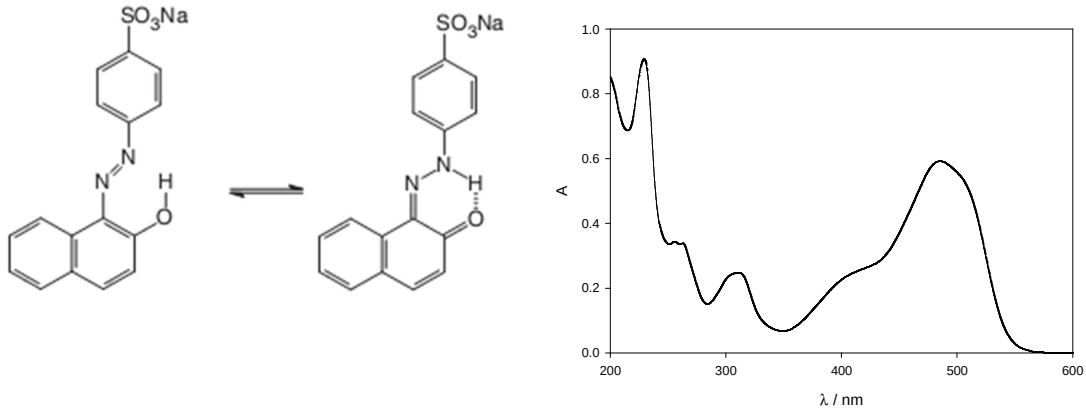

(a) (b)

Figure 2.10: Orange II dye (a) azo-hydrazone tautomerism and (b) representative UV-Vis spectrum.

In this work, the concentration of Orange II in solution was measured using the hydrazone band intensity at 485 nm. The calibration curve, obtained with concentrations ranging from 0.5 to 10.0 mg L^{-1} of Orange II, is shown in Figure 2.11. The limit of detection of the technique was estimated according to Eq. 2.10.

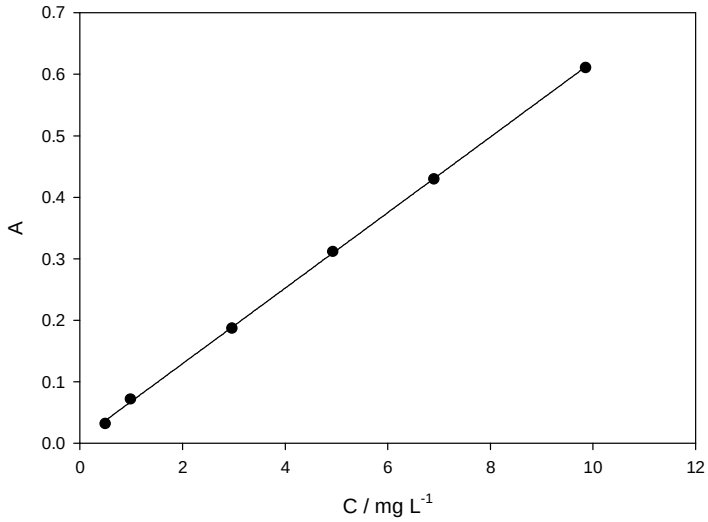

Figure 2.11: Calibration curve for Orange II dye determination (λ = 485 nm). The limit of detection, LD, was estimated as 0.18 mg L^{-1}. (R^2 = 0.999).

The concentrations of phosphates presented in Chapter 5 were measured in samples which also contained the Orange II dye. The spectra of these two species have some regions where both species absorb. In order to avoid any interference in the reading of the absorbance, the spectrophotometric determination of phosphates and Orange II was carried out by solving the simultaneous linear equations given in Eq. 2.11. In this equation, A_{470} and A_{485} are the absorbance values from the spectrum of the mixture at 470 and 485 nm, ε^{P}_{470} and ε^{P}_{485} are the molar absorbtivities of phosphates at 470 and 485 nm computed from the spectrum of pure phosphates. Likewise, ε^{O}_{470} and ε^{O}_{470} are the molar absorbtivities of Orange II dye at 470 and 485 nm, computed from the spectrum of the Orange II dye only, and C_P and C_O are the concentrations of phosphates and Orange II dye, respectively. This method is usually used in the analysis of a mixture of components. Provided that the spectra of the pure components are available, this method allows the determination of the concentrations of the individual components by analysing the spectrum of the mixture [21]. For the spectrophotometric determination of the two components in a binary system, such as the one in the present work, absorbance measurements at two different wavelengths are necessary. The resulting calculation to solve the set of equations is simple and yields a determinant ratio which can be evaluated readily by using Cramer's rule [22].

$$A_{470} = \varepsilon_{470}^{P} C_P + \varepsilon_{470}^{O} C_O$$

$$A_{485} = \varepsilon_{485}^{P} C_P + \varepsilon_{485}^{O} C_O \qquad \textbf{Eq. 2.11}$$

2.3.3.2 Atomic absorption spectroscopy

Atomic absorption, AA, spectroscopy relies on the fact that metal ions adsorb a specific wavelength within the light spectrum. Applying the Beer-Lambert law, the concentration of the metal is determined from the amount of absorption [23].

In the present work, AA spectroscopy was used to measure the concentration of Zn^{2+} ions in solution. A Perkin Elmer Analyst 200 atomic absorption spectrometer, with a premix burner, hollow-cathode lamp, air-acetylene flame atomiser, echelle grating monochromator and solid state detector, was employed. The wavelength was set at 213.9 nm. The standard solutions, used to obtain the calibration curve shown in Figure 2.12, were prepared by dissolving metallic zinc in HNO_3. The limit of detection of the technique was estimated according to Eq. 2.10.

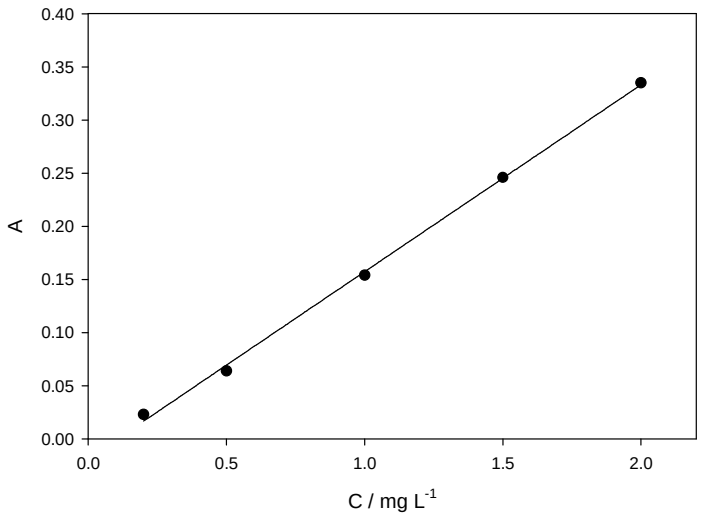

Figure 2.12: Calibration curve for Zn determination. The limit of detection, LD, was estimated as 0.09 mg L^{-1}. (R^2 = 0.998).

2.3.4 Kinetic analysis of phosphate removal by electrocoagulation

Chemical kinetics deals with the rate at which chemical reactions take place. The study of chemical kinetics is based on the law of mass action, published by Guldberg and Waage during 1864-1867 [24]. One of the key terms in reaction kinetics is the rate of reaction, *r*, defined as the number of molecules of a chemical species being converted or produced per unit volume with respect to time. Considering A reacting with B to produce C: aA + bB → cC, the rate of reaction is given by Eq. 2.12, where r_A, r_B and r_C are the rates of reaction with respect to species A, B and C, respectively, *a*, *b* and *c* are the stoichiometric coefficients for A, B and C, respectively, N_A, N_B and N_C represent the number of moles of A, B and C, respectively, and *V* is the volume containing the species.

$$r = r_A = r_B = r_C$$

$$r_A = -\frac{1}{a \cdot V}\frac{dN_A}{dt} \qquad r_B = -\frac{1}{b \cdot V}\frac{dN_B}{dt} \qquad r_C = \frac{1}{c \cdot V}\frac{dN_C}{dt} \qquad \textbf{Eq. 2.12}$$

From experimental observations and based on the above mentioned law of mass action and the collision theory, it was found that the rate of reaction can be expressed as the rate law [25]:

$$r = k[A]^x[B]^y \qquad \textbf{Eq. 2.13}$$

Here *k* is a proportionality factor called the rate coefficient or rate constant, which is dependent on the temperature through the Arrhenius equation and *x* and *y* are the partial orders with respect to A and B, respectively. The overall order of the reaction is equal to the sum of the partial orders.

In the present study, the kinetics of phosphate removal by electrocoagulation using steel and aluminium alloys is presented in Chapter 3. For this purpose, first- and second-order kinetic reactions were used in order to fit the experimental data. After integration of the rate laws, the first-order kinetics was expressed as a logarithmic relationship [15].

$$\ln\frac{[A]}{[A_0]} = -kt \qquad \textbf{Eq. 2.14}$$

The second-order kinetics was given by a linear equation between the reciprocal of the concentration and the time [15]:

$$\frac{1}{[A]} - \frac{1}{[A_0]} = kt \qquad \textbf{Eq. 2.15}$$

The experimental data were analysed and fitted to these proposed equations using SigmaPlot™ Version 12.2.0.45 by Systat Software, Inc. The linear regression analysis was based on the method of least squares with the Levenberg–Marquardt algorithm.

2.3.5 Fitting of phosphate removal by electrocoagulation to adsorption isotherms

The phenomenon of adsorption on a solid is related to the unsaturated and unbalanced forces that are present on solid surfaces. When a solid surface is brought into contact with a liquid or gas, the solid surface tends to balance these forces by attracting and retaining on its surface the molecules, atoms, or ions, of the liquid or gas. As a consequence, a greater concentration of the gas or liquid occurs in the vicinity of the solid than in the bulk. In this study, only the liquid-solid interface is relevant and is discussed.

The adsorption falls into two broad categories; physisorption and chemisorption [15]. Physisorption is a non-specific loose binding of the adsorbate to the surface due to weak interactions, such as van der Waals forces. On the other hand, chemisorption involves a more specific binding, such as the exchange or sharing of electrons between the adsorbate molecules and the solid surface, resulting in a chemical reaction. As a consequence, only monolayer adsorption is possible.

The adsorption isotherm indicates how the adsorption molecules distribute between the liquid phase and the solid phase, once the adsorption process reaches the equilibrium state. The adsorption process can be modelled using different approaches and the most used models are Langmuir's isotherm, Freundlich's isotherm and Temkin's isotherm. In

1932 Irving Langmuir was awarded the Nobel Prize for his studies concerning surface chemistry [26]. Langmuir's isotherm, describing the adsorption of adsorbate (A) onto the surface of the adsorbant (S), is based on three important assumptions: the surface of the solid has a specific number of sites, with the same energy, where the solute molecules can be adsorbed, the adsorption involves the attachment of only one layer of molecules to the surface, i.e., monolayer adsorption, and there are no interactions among the adsorbates [15]. The monolayer adsorption and the corresponding equilibrium constant, K_{ads}, can be represented as follows:

$$A + S \leftrightarrows AS \qquad K_{ads} = \frac{[AS]}{[A][S]} \qquad \textbf{Eq. 2.16}$$

Introducing the fraction of the adsorption sites to which a solute molecule has attached, θ, the final form of the Langmuir isotherm is obtained in Eq. 2.17.

$$\theta = \frac{K_{ads}[A]}{1 + K_{ads}[A]} \qquad \textbf{Eq. 2.17}$$

However, in liquid-solid adsorption, it is common to express θ as the ratio of the amount of adsorbate molecules per mass of adsorbant, q_e in mg g^{-1}, to the maximum adsorption capacity, q_m in mg g^{-1}, to give Eq. 2.18. The Langmuir isotherm is limited to a monolayer. It applies well to chemical adsorption and physical adsorption when saturation is approached.

$$q_e = \frac{q_m K_{ads}[A]}{1 + K_{ads}[A]} \qquad \textbf{Eq. 2.18}$$

In 1906, Herbert F. Freundlich presented the earliest known adsorption isotherm equation [27]. This empirical model is applied to adsorption on heterogeneous surfaces and multilayer processes. The model was derived by assuming an exponential decay of the adsorption site energy distribution and it is expressed by the following equation:

$$q_e = K_F [A]^{1/n} \qquad \textbf{Eq. 2.19}$$

where K_F, in mg g^{-1} L, and n (dimensionless) represent the Freundlich's temperature-dependent constants.

The Temkin adsorption isotherm removes the restriction in the Langmuir model that the heat of adsorption is independent of surface coverage θ. Indeed, it allows for a linear decrease in the heat of adsorption with coverage [28]. The Temkin's isotherm is expressed by Eq. 2.20:

$$q_e = \frac{RT}{b_T} \ln(K_T[A]) \qquad \textbf{Eq. 2.20}$$

where b_T is the Temkin constant related to heat of sorption in J mol^{-1}, K_T is the Temkin isotherm constant in L g^{-1}, R is the gas constant (8.314 J mol^{-1} K^{-1}), and T is the absolute temperature in K.

In the present study, the Langmuir, Freundlich and Temkin equations were used to model the electrocoagulation removal of phosphates by steel and aluminium alloys. These data were analysed using SigmaPlot™ Version 12.2.0.45 by Systat Software, Inc. A nonlinear regression method based on the Levenberg-Marquardt algorithm was used to fit the experimental data with these equations and the goodness of fit was obtained using the adjusted R^2 values.

2.3.6 Calculation of energy consumption during electrocoagulation

For water treatment it is essential to estimate the electrical energy consumption, EEC, in order to determine if the process is a financially viable method. In the present study, the energy consumption to carry out the electrocoagulation process was calculated as the electrical power in Wh, using the values of the potential of the cell, E_{cell}, and of the applied current, I, according to Eq. 2.21. The E_{cell} was obtained from the electrocoagulation tests performed using the electrochemical set-up illustrated in Figure 2.3. However, it remained almost constant during the tests and, consequently, its average value, $\overline{E}_{cell}$, was used. Since the electrocoagulation tests were performed under galvanostatic mode, the current, I, remained constant throughout the duration of the test.

$$\mathrm{EEC}\left(\mathrm{Wh}\right) = I\int_{0}^{t} E_{cell}\,\mathrm{d}t \times t = I\overline{E}_{cell}t \qquad \textbf{Eq. 2.21}$$

2.3.7 Statistical methods for chemometric study on phosphate removal

Statistical techniques are useful tools in process optimisation. One of the simplest approaches is the OFAT method (one factor at a time). A single factor is varied during the experiment and measurements are taken at each of the factor levels. Next, another factor is varied and measurements are taken. Generally, the goal is to maximise the response and, accordingly, a maximum is identified from the first set of experiments. Then, the second factor is varied in an attempt to obtain an increase in the response, which corresponds to the maximum for the selected response. However, the calculated optimum conditions may be far from the true values as the factors influencing the response are not independent. In chemometrics, this is called 'interaction'. The major limitation of this approach is that it does not allow the identification of important interactions among the experimental variables. The Design of Experimental (DoE) methods is a radical departure from the OFAT approach. The main objective of DoE is to develop methods which simultaneously account for, or model, the effect of a set of variables affecting the process under investigation. In particular, the use of the DoE method is an efficient procedure for planning experiments so that the data obtained can be analysed to yield valid and objective conclusions [29].

Chemometrics can be seen as a concept, or a tool box, containing tools that can be used to effectively plan and evaluate experiments within almost any area of research. For example, both computational and wet experiments usually generate a lot of information but this information is encoded in the experimental data. Information in the data that is relevant is often hidden with non-relevant information. For example, in the case of spectroscopic data, this may be due to fluctuations in the measuring equipment (noise). The DoE approach offers a statistical method when planning the experiments to maximise the amount of relevant information in the data gathered. In addition, DoE is a useful tool to extract maximum information with minimum experimentation and to draw meaningful conclusions from the data using statistical techniques. A DoE approach usually aims at one of the following:

• determining which variables are most influential on the response;
• determining the variable settings by which the process is optimised.

The optimisation may take several forms, such as maximising the yield of a reaction or minimising the variability of a process.

In the DoE approach, the mathematical models, the design matrices and the screening models are all important aspects of the analysis. Usually experimental data are described by mathematical relationships between the factors or variables, such as temperature, and a response, such as synthetic yield, reaction time or percentage impurity. Since the outcome of an experiment is dependent on the experimental conditions [30], the result can be described as a function based on the experimental variables:

$$y = f(x) \qquad \textbf{Eq. 2.22}$$

The function in Eq. 2.22 is approximated by a polynomial function and represents a good description of the relationship between the experimental variables and the responses. Considering two variables, x_1 and x_2, the simplest empirical model is a polynomial one, which contains only linear terms and describes the linear relationship between the experimental variables and the responses. In a linear model, the two variables x_1 and x_2 are expressed as:

$$y = b_0 + b_1x_1 + b_2x_2 \qquad \textbf{Eq. 2.23}$$

The next level of polynomial models contains additional terms that describe the interaction between different experimental variables. Thus, a second-order interaction model contains the following terms:

$$y = b_0 + b_1x_1 + b_2x_2 + b_{12}x_1x_2 \qquad \textbf{Eq. 2.24}$$

The two models shown in Eq. 2.23 and Eq. 2.24 are mainly used to investigate the experimental system, i.e., with screening studies or robustness tests. To be able to

determine an optimum response, quadratic terms are introduced into the model. By introducing these terms in the model, it is possible to determine nonlinear relationships between the experimental variables and responses. The following polynomial function describes a quadratic model with two variables:

$$y = b_0 + b_1 x_1 + b_2 x_2 + b_{11} x^2_{1+} b_{22} x^2_2 + b_{12} x_1 x_2 \qquad \textbf{Eq. 2.25}$$

The polynomial functions described in these equations, Eq. 2.23 to Eq. 2.25, contain a number of unknown parameters (b_0, b_1, b_2, etc.) that are to be determined. The use of a DoE allows the determination of these parameters by means of an appropriate experimental design. The design that is chosen depends on the proposed mathematical model, the shape of the domain and the objectives of the study (screening, factor influence, optimisation, etc.). For example, factorial or Plackett-Burman designs are used for screening, while central composite designs, CCDs, are employed in optimisation processes. In the present work, only factorial designs are presented and discussed.

For different mathematical models, different types of experimental design are needed and each experimental design gives a different series of experiments to be performed. In order to determine the parameters of the model, it is convenient to work using matrices and a +/- code. The list of experiments to be performed is usually displayed in a matrix called a design matrix, D. In the design matrix the rows refer to the experiments and the columns refer to factors. On the other hand, the results or responses of each experiment form a vector, called *y*. In addition, to determine the coefficient b_0 of the model another vector, called b, is introduced. Consequently, the relationship between the response, the coefficients and the experimental conditions can be expressed in a matrix form by Eq. 2.26:

$$y = D \,.b \qquad \textbf{Eq. 2.26}$$

This relationship is illustrated in Figure 2.13 for an example of the influence of temperature and the reaction time on the yield of a chemical reaction. Using multiple linear regression techniques and knowing D and *y*, it is surprisingly easy to calculate the

coefficients of the mathematical model, representing the studied system. Once the parameters of the model are known, it is possible to use the model to gain the following information [31]:

- Ascertain the significance of the coefficients and, consequently, the relevant factors affecting the process or system. This type of information is usually used in screening experiments.
- Determine the coefficients to construct a model of the response, thus establishing the optimum conditions for obtaining the best response.
- Produce a quantitative model in order to predict the response in the whole experimental domain.

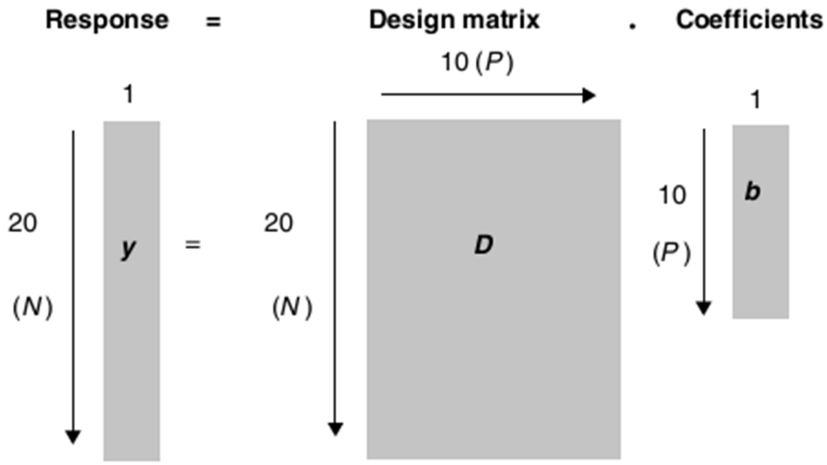

Figure 2.13: Relationship between response, design matrix and coefficients [31].

When an experiment is very large with multiple factors, it is often appropriate for a screening experiment to be conducted [32]. Screening experiments allow an identification of the factors that are of most importance. The factors that represent the greatest amount of information about the response variable can then be further analysed. Two-level screening designs, such as fractional factorial and Plackett–Burman designs, are usually applied for this purpose [33]. In factorial designs, all possible combinations of the two levels of the factors are tested. For example, a 2^n factorial design is comprised of all possible 2^n combinations of the n factors, where each factor has only two levels or settings. Consequently, it consists of 2^n runs. A factorial design provides information on all possible factorial effects, where a factorial effect is either the main

information or an interaction between two or more factors. Eq. 2.27 presents a 2^2 design, i.e., a two-level factorial design testing two factors. The two design factors are denoted by A and B and the two levels are represented by a +/- coding. Using this notation, the $2^2 = 4$ runs can be listed as the rows of the design matrix.

$$\begin{matrix} A & B \\ \begin{pmatrix} - & - \\ + & - \\ - & + \\ + & + \end{pmatrix} \end{matrix} \qquad \textbf{Eq. 2.27}$$

The main drawback of full factorial designs is the large number of experiments to be performed. Indeed, as n, the number of factors increases, it is clearly apparent that the required number of experiments may become prohibitive. However, higher order interactions are usually negligible, such as three-factor interactions and higher [34]. Consequently, information about all the remaining main effects and interactions can be obtained by running only a subset or fraction of the 2^n factorial design [32]. In general, a 2^{n-k} design is defined as a fractional design with n factors, each at two levels, and consists of 2^{n-k} treatment combinations or runs. As it is evident, a 2^{n-k} design is a 2^{-k}-th fraction that is 1/2, 1/4, 1/8 etc., of the 2^n full factorial design. The drawback with fractional factorials is that effects cannot be measured without the distortion risk from aliased effects. Indeed, as the number of experiments is reduced, the amount of information is correspondingly reduced. This implies that factors and interactions can be confounded with each other. However, not all interactions are significant and the purpose of a preliminary experiment is simply to sort out which factors should be studied in detail later.

In general, the following steps are used to construct the experimental design and interpret the results.

1. The first step is to choose a high and low level for each factor. The value of each factor is usually coded as – (low) and + (high), as already mentioned.
2. Then, the experiments are performed and the response is observed.
3. The next step is to analyse the data by setting up a design matrix based on the mathematical model, which has already been chosen.

4. Using statistical techniques, the coefficients of the model are calculated and interpreted.

In Chapter 5, a screening study on the electrocoagulation removal of phosphates by steel electrodes is presented. This study was performed using a fractional factorial design in order to determine the most influential factors affecting the electrocoagulation process. The DoE and the corresponding statistical tests were carried out using Design-Expert® Version 8.0.7.1 by Stat-Ease, Inc. The details of the chosen experimental design are given in Chapter 5, Section 5.4. In this section, the design matrix used to carry out the experiments and the statistical testing routines, which were then used to analyse the data, are presented and discussed.

A 2^{5-1} fractional factorial design with two replicates and blocking was used. The factors studied were, current density (A), electrocoagulation time or EC time (B), surface area of the electrode to the volume of the solution ratio or SA/V (C), flocculation time or floc time (D) and settlement time or settl time (E). The five factors and the design matrix of the experiments are given in Table 2.4.

Table 2.4: Design matrix for the 2^{5-1} fractional factorial design. Each experiment was duplicated for a total of 32 experiments.

Experimental run	Current density, A / mA cm^{-2}	EC time, B / min	SA/V, C / m^{-1}	Floc time, D / min	Settl time, E / min
1	2	5	9.1	2	10
2	5.5	5	9.1	2	10
3	2	60	9.1	2	10
4	5.5	60	9.1	2	10
5	2	5	12.6	2	10
6	5.5	5	12.6	2	10
7	2	60	12.6	2	10
8	5.5	60	12.6	2	10
9	2	5	9.1	30	60
10	5.5	5	9.1	30	60
11	2	60	9.1	30	60
12	5.5	60	9.1	30	60
13	2	5	12.6	30	60
14	5.5	5	12.6	30	60
15	2	60	12.6	30	60
16	5.5	60	12.6	30	60

The use of a fractional design involves the occurrence of confounding, which indicates that the values of a main effect (e.g., A, B, C, etc.) come from both the main effect itself and also contamination or bias from higher order interactions (e.g., AB, AC, ABC, etc.) [29]. In DoE when the estimate of an effect also includes the influence of one or more effects, usually higher order interactions, the effects are said to be aliased. In the 2^{5-1} fractional factorial design used for the present work, the main effects were aliased or confounded with 3-factor interactions. However, some of the 2-factor interactions were aliased with other 2-factor interactions. Table 2.5 shows the effects which were aliased. The use of blocking also entails confounding the effects, since the blocks were considered as an additional factor that was added to the design. Four blocks were used in this study, each one corresponding to a day in which the experiments were performed. The effects of the blocks were aliased with 3-factor effects as is possible to see from Table 2.5. Higher order interactions, such as 3-factor, are usually negligible and were not considered in this analysis.

Table 2.5: Confounding for the main effects, interactions and blocks in the 2^{5-1} fractional factorial design.

Estimated Terms	Aliased Terms
Main effects	
[A]	A + BCE
[B]	B + ACE
[C]	C + ABE
[D]	D
[E]	E + ABC
Interactions	
[AB]	AB + CE
[AC]	AC + BE
[AD]	[AD]
[AE]	AE + BC
[BD]	BD
[CD]	CD
[DE]	DE
Blocks	
[Block 1]	Bock 1 – ABD + CDE
[Block 2]	Bock 2 + ABD + CDE
[Block 3]	Bock 3 – ABD - CDE
[Block 4]	Bock 4 + ABD + CDE

The general approach to the statistical analysis of a factorial design was proposed by Montgomery [32] and is summarised in Table 2.6. It consists of four steps.

Table 2.6: Analysis procedure for a factorial design [32].

1	Estimate factor effects
2	Form initial model
3	Perform statistical testing
4	Analyse residuals

The first step consists of estimating the factor effects and examining their signs and magnitudes. In the present study, normal probability plots were used to assess the importance of the factor effects. The principle of normal probability plots is that if a series of numbers is randomly selected, they will form a normal distribution in the absence of systematic effects [31]. Consequently, According to Daniel [35], in DoE the effects that are negligible are normally distributed, with mean zero and variance σ^2 and fall along a straight line on the plot, while important effects have nonzero means and do not lie along the straight line. By selecting only the significant effects involving important factors and interactions, the initial model can be formulated (Step 2).

The formulated model is then tested using statistical techniques in the third step. F-test and *p*-value were used in the present work. F-test can be used to test the utility of a model in predicting the experimental data and with this purpose it was used in Chapter 5. In this case the null hypothesis, H_0, was that all the parameters of the model were zero, while the alternative hypothesis, H_1, was that at least one parameter was nonzero. To test H_0 versus H_1, the F-test was used, Eq. 2.28. In this equation, SS are the sum of squares, dof the degrees of freedom and MS the mean square.

$$F_0 = \frac{SS_{model} / dof}{SS_{error} / dof} = \frac{MS_{model}}{MS_{error}} \qquad \textbf{Eq. 2.28}$$

The F statistics can be seen as the ratio of the explained variability (the model) and the unexplained variability (the error), each divided by the corresponding degrees of freedom. Once a significance level, α, of the test has been specified, F_0 is compared to the critical value at the given significance level, F_α. If $F_0 \geq F_\alpha$, H_0 can be rejected in

favour of H_1. Setting a specific α-value or level of significance is often inadequate because it gives no idea about whether the computed value of the test statistic was just barely in the rejection region or far into this region [32]. Therefore, the *p*-value approach has been adopted. The *p*-value provides information about the weight of evidence against H_0 and can be defined as the smallest level of significance that would lead to rejection of the null hypothesis.

The last step, Step 4, consists in checking for model adequacy and assumptions. The analysis of variance, carried out in Step 3, is an exact test of the hypothesis of no difference. If the assumptions are valid, the errors are normally and independently distributed with mean zero and constant σ^2 [32]. Consequently, violations of the basic assumptions are investigated by examining residual graphs. The residuals from a fitted model are the differences between the observed responses and the corresponding predictions of the response computed using the regression function. If the model fit to the data is correct, the residuals appear to behave randomly. As a consequence, in a normal probability plot, the effects would lie on a straight line. A plot of the residuals versus the predicted values would be structureless [32], with no obvious pattern, since the residuals should not be related to any other variable including the predicted response.

2.4 References

[1] OECD, Test No. 303: Simulation Test - Aerobic Sewage Treatment - A: Activated Sludge Units; B: Biofilms, in: OECD Guidelines for the Testing of Chemicals, Adopted 22 January 2011.
[2] Uhlig, H.H., Revie, R.W., *Uhlig's Corrosion Handbook*, 2nd ed., John Wiley & Sons, Inc., New York, 2000.
[3] Ahmad, Z., *Principles of Corrosion Engineering and Corrosion Control*, Butterworth-Heinemann, Oxford, 2006.
[4] Silverman, D.C., *Tutorial on Cyclic Potentiodynamic Polarization Technique*, in: Corrosion 98, March 22 - 27, San Diego CA, 1998, NACE International.
[5] ASTM, in: Standard Terminology Relating to Corrosion and Corrosion Testing, G 15, 2008.
[6] Frankel, G.S., Rohwerder, M., *Electrochemical Techniques for Corrosion*, in: A.J. Bard, M. Stratmann, G.S. Frankel (Eds.) Corrosion and Oxide Films, Wiley, 2007.
[7] Bard, A.J., Stratmann, M., *Corrosion and Oxide Films, Encyclopedia of Electrochemistry, Volume 4*, John Wiley, 2003.
[8] Beavers, J.A., Durr, C.L., Thompson, N.G., *Unique Interpretation of Potentiodynamic Polarization Technique*, in: Corrosion 98, March 22 - 27, San Diego CA, 1998, NACE International.

[9] Pletcher, D., Greef, R., Peat, R., Peter, L.M., Robinson, J., *Instrumental Methods in Electrochemistry*, Horwood Publising, 2002.
[10] Bard, A.J., Faulkner, L.R., *Electrochemical Methods: Fundamentals and Applications*, Wiley, 2000.
[11] Bader, M., *J. Chem. Educ.*, **57** (1980) 703-706.
[12] Reichenbacher, M., Einax, J.W., *Challenges in Analytical Quality Assurance*, Springer, 2011.
[13] Mertz, J., *Introduction to Optical Microscopy*, Roberts and Company Publisher, 2009.
[14] Louthan, M.R., *Optical Metallography*, in: R.E. Whan (Ed.) ASM Handbook, Volume 10: Material Characterizations, ASM International, 1986.
[15] Atkins, P., Paula, J.D., *Physical Chemistry*, 9th ed., Oxford University Press, 2010.
[16] APHA-AWWA-WPCF, *Standard Methods for the examination of Water and Wastewater*, 18th ed., New York, 1992.
[17] Miller, J.N., Miller, J.C., *Statistics and Chemometrics for Analytical Chemistry*, 5th ed., Pearson Prentice Hall, Harlow, 2005.
[18] Hubaux, A., Vos, G., *Anal. Chem.*, **42** (1970) 849-855.
[19] Gonzales, G., Touraud, E., Spinelli, S., Thomas, O., *Organic Constituents*, in: O. Thomas, C. Burgess (Eds.) UV-Visible Spectrophotometry of Water and Wastewater, Elsevier, 2007.
[20] Mollah, M.Y.A., Gomes, J.A.G., Das, K.K., Cocke, D.L., *J. Hazard. Mater.*, **174** (2010) 851-858.
[21] de Levie, R., *Advanced Excel for Scientific Data Analysis*, Oxford University Press, 2008.
[22] de Levie, R., *J. Chem. Sci.*, **121** (2009) 617-627.
[23] Harris, D.C., *Quantitative Chemical Analysis*, W. H. Freeman, 2006.
[24] Marin, G.B., Yablonsky, G.S., *Kinetics of Chemical Reactions*, Wiley, 2011.
[25] Castellan, G.W., *Physical Chemistry*, Addison-Wesley Publishing Company, 1983.
[26] Langmuir, I., *J. Am. Chem. Soc.*, **40** (1918) 1361-1403.
[27] Freundlich, H., *J. Phys. Chem.*, **57A** (1906) 385-470.
[28] Temkin, M., Pyzhev, V., *Acta Physiochim. USSR*, **12** (1940) 217-222.
[29] NIST/SEMATECH, e-Handbook of Statistical Methods, http://www.itl.nist.gov/div898/handbook, 10/10/2012.
[30] Lundstedt, T., Seifert, E., Abramo, L., Thelin, B., Nystrom, A., Pettersen, J., Bergman, R., *Chemom. Intell. Lab. Syst.*, **42** (1998) 3-40.
[31] Brereton, R.G., *Chemometrics: Data Analysis for the Laboratory and Chemical Plant*, Wiley, 2003.
[32] Montgomery, D.C., *Design and Analysis of Experiments*, 7th ed., John Wiley & Sons, Inc., 2009.
[33] Box, G.E.P., Hunter, J.S., Hunter, W.G., *Statistics for experimenters: design, discovery, and innovation*, 2nd ed., Wiley, 2005.
[34] Myers, R.H., Montgomery, D.C., *Response surface methodology: process and product optimization using designed experiment*, 2nd ed., Wiley, 2002.
[35] Daniel, C., *Technometrics*, **1** (1959) 311-342.

3 Performance of Al-2Mg and AISI 420 Electrodes for the Removal of Phosphates by Electrocoagulation

3.1 Introduction

The electrode materials employed in electrocoagulation are usually aluminium and iron [1]. They are used for several applications, such as for treating wastewater containing heavy metals [2-4], foodstuff [5, 6], oil wastes [7, 8], textile dyes [9-14], fluoride [15], polymeric waste [16], organic matter from landfill leachate [17], suspended particles [18-21], chemical and mechanical polishing wastes [22], aqueous suspensions of ultrafine particles [23], nutrients [24], phenolic waste [25], arsenic [26] and refractory organic pollutants including lignin and EDTA [27]. This list is not exhaustive. Several authors have also attempted to use aluminium or iron electrodes for drinking water treatment [1, 28, 29].

Phosphorus occurs in natural water and wastewater mainly as inorganic phosphates, such as orthophosphates and polyphosphates [30]. The presence of excess phosphorus in the effluent discharged to natural water bodies has long been known to be the cause of algal bloom and eutrophication. Because of these problems, phosphate removal using chemical precipitation and coagulation has been carried out for a number of years [31, 32]. Recently, other physicochemical processes have been used to remove phosphates from wastewater as alternatives to the traditional methods. These techniques include adsorption, ion-exchange, electrodialysis, hybrid systems containing fly-ash adsorption and membrane filtration and electrocoagulation [33].

A number of studies have been reported on electrocoagulation and the removal of phosphates using pure iron or aluminium anodes [33-37]. However, alloys may have beneficial effects in terms of removal efficiency and energy consumption. Indeed, a few studies have been reported on the electrocoagulation process using aluminium and iron alloys [38]. In particular, the removal of phosphates using an aluminium-zinc alloy was investigated by Vasudevan *et al.* [39].

Although the removal of phosphates has been extensively investigated, the exact mechanism of its removal is not yet completely understood [32]. It may involve the precipitation and coagulation processes and is possibly influenced by the characteristics of the wastewater, such as the pH. In wastewater treatment, precipitation and coagulation are two distinct processes, although coagulation also involves precipitation [40]. Coagulation is based on the destabilisation-adsorption mechanism of stable particles in water, whereas precipitation involves the formation of insoluble compounds. The removal of phosphate can neither be explained in terms of the equilibrium model of a single chemical compound, such as $AlPO_4$, nor as a co-precipitation of $AlPO_4$ and $Al(OH)_3$ [32]. The degree of phosphate removal depends on the degree of hydrolysis of the coagulant and its concentration, the presence and the concentration of other ions and the pH. According to the model suggested by Hsu [41], phosphate removal is the result of the competitive action of phosphates, hydroxyls and other ions which react with aluminium and iron ions.

The coagulation process represents the preliminary stage for the removal of particles from solutions, which is commonly a two-phase process. In this preliminary phase, coagulants are added to the solution for the purpose of destabilising the pollutants either by charge-neutralisation or enmeshments in precipitates or, in the case of phosphate removal, formation of insoluble salts. However, as outlined previously, it is not always possible to identify a prevailing mechanism since it depends on different parameters that may change throughout the process, such as the initial coagulant concentration, pH, temperature, ionic strength and the presence of other species in solution. Flocculation is the second stage where the aggregation of destabilised particles and precipitation into larger particles, known as flocculant particles or flocs, take place. Coagulation typically occurs in less than 10 s [42] upon the addition of coagulants under rapid mixing

conditions and afterwards the aggregation of the destabilised particles takes place for several minutes under slow stirring. In chemical coagulation these two steps can be physically separated or differentiated on the basis of the time required for each of the processes. However, in electrocoagulation, the coagulation and flocculation phases occur simultaneously.

The two terms coagulation and flocculation are often used loosely to describe the overall process of aggregation. However, floc formation and growth can only take place if certain conditions are satisfied [43]. Firstly, there must be a supply of material, for example by direct nucleation on the particle surface, adsorption of material held in suspension or from inter-particle aggregation. Secondly, the solution must be destabilised to allow aggregation to proceed. The degree of destabilisation and transport factors determine the rate of floc formation. The conditions necessary for the formation of flocs can be satisfied regardless of the presence of pollutants in solution. Indeed, the supply of material might be the result of the introduction of aluminium or iron salts to the solution and the destabilisation of these particles might derive from processes of charge-neutralisation or precipitation to give the formation and growth of flocs. It is clear that the process of coagulation-flocculation is neither specific nor selective towards certain species of pollutants. The removal of pollutants or particles from solution is rather the result of competition between the hydrolysis of aluminium or iron ions and the adsorption, precipitation or formation of complexes of ions and particles, which are present in solution.

In this chapter results are presented and discussed on the removal efficiency of phosphates using aluminium-magnesium (Al-2Mg) and stainless steel (AISI 420) electrodes. The efficiency was investigated in terms of several parameters, such as the initial concentration of phosphates, current density, initial and final pH and the chloride concentration. The determination of a kinetic model for the removal is also attempted. To date no reports have been published on the removal of phosphates using Al-2Mg alloys or stainless steel anodes.

3.2 Al-2Mg electrode

In chemical coagulation, aluminium salts, such as $Al_2(SO_4)_3 \cdot nH_2O$, are frequently used to remove phosphates. When alum or other aluminium salts are added to water, they dissociate to give trivalent, Al^{3+}, ions, which hydrate to form the hexaaquoaluminium ion, $Al(H_2O)_6^{3+}$. The aquoaluminium ion undergoes a series of rapid hydrolysis reactions to form soluble monomeric and polymeric species as well as solid $Al(OH)_3$ [44], as shown in Figure 3.1.

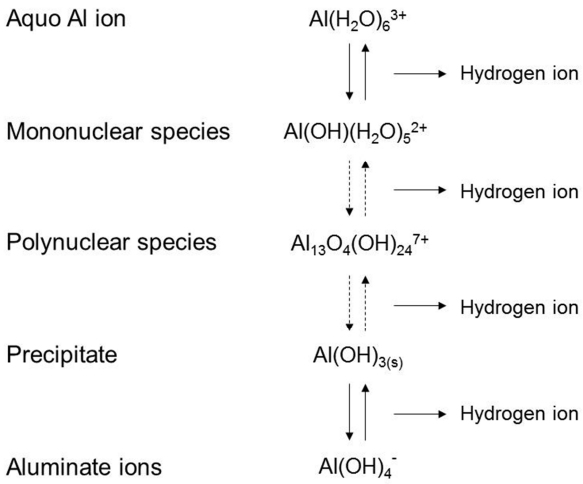

Figure 3.1: Aluminium hydrolysis products. The dashed lines denote an unknown sequence of reactions [22].

Aluminium and iron salts have been used extensively for the removal of phosphates, however the present understanding that the use of these salts leads to the direct formation of insoluble products, such as $AlPO_4$, is now considered to be too simple to explain the phosphate removal [40]. According to Aguilar *et al.* [45], the mechanism of the interaction between alum and phosphates may be due to one or any of the following processes:

- Direct adsorption of phosphate ions on the hydrolysis products shown in Figure 3.1, formed by the addition of alum to wastewater;
- Incorporation of the soluble phosphates to colloids in suspension;
- Formation of insoluble salts with aluminium, $Al^{3+} + H_nPO_4^{n-3} \leftrightarrow AlPO_4 + nH^+$.

However, the aluminium-orthophosphate system is complex, as discussed by Stumm and Morgan [46]. Recht and Ghassemi [47] have suggested that the removal of phosphates depends on the hydrolysis products of aluminium in addition to the Al^{3+} ion.

A significant contribution to the understanding of the removal of phosphates using coagulation was given by Hsu [41, 48]. He suggested that the Al-OH-Al and the Al-PO_4-Al linkages tend to integrate. Thus, the precipitation is governed by the integrated particles giving the formation of aluminium-hydroxy-phosphate complexes, $Al(OH)_{3-x}(PO_4)_x$, rather than the individual $AlPO_4$ and $Al(OH)_3$ species. These complexes either adsorb onto positively charged aluminium hydrolysis species or act as further centres of precipitation or nucleation points for aluminium hydrolysis products [40].

Although chemical and electrochemical coagulation are substantially different in terms of the dosing method of the coagulants, the mechanisms of coagulation-flocculation and the series of reactions and processes which occur in solution are similar [49]. However, the evolution of the chemical environment may differ in the two systems [50]. Considering the mechanisms reported previously for the removal of phosphates using chemical coagulation, Figure 3.2 attempts to summarise and draw a simplified scheme of the reactions which may occur during the electrocoagulation removal of phosphates. The first step involves the generation of the Al^{3+}, followed by the hydrolysis reactions, then particle destabilisation and finally the formation of large flocs, step IV. [51]

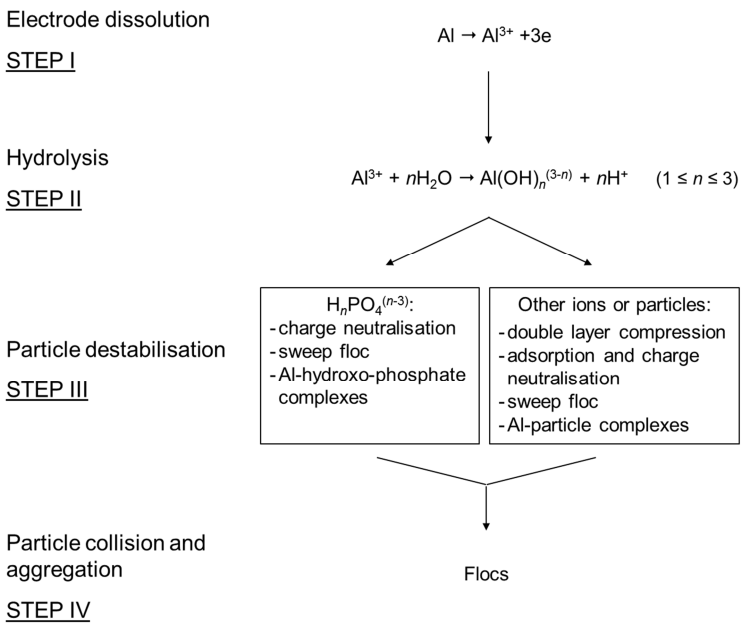

Figure 3.2: Simplified model for the removal of phosphates in electrocoagulation using aluminium electrodes.

In this section an aluminium alloy containing 2% magnesium (EN-AW 5251), Al-2Mg, was used as the anode material to remove phosphates. Several operational parameters, such as the initial concentration of phosphates, current density, initial and final pH and NaCl concentration, were investigated. Full experimental details are given in Section 2.3.1.4.

3.2.1 The effect of the initial concentration of PO_4-P

3.2.1.1 The efficiency of removal

In order to study the effect of the initial concentration of phosphates on the removal efficiency of solutions treated with the Al-2Mg electrode, electrocoagulation experiments were carried out by varying the initial concentration of phosphate, P_o. Figure 3.3 shows the normalised concentration of phosphate, P_t/P_o, plotted as a function of the electrocoagulation period in solutions containing 20.0, 60.0 and 150.0 mg L^{-1} of PO_4-P. The initial pH was fixed at 5.0, the NaCl concentration was maintained at 4.2×10^{-3} M, the current density was 11.0 mA cm^{-2} and the ratio of the surface area of the anode to the volume of solution, SA/V, was 11.7 m^{-1}. The corresponding data are shown in Table 3.1. It is clear from the data presented in Figure 3.3 and displayed in Figure 3.1, that, although after 60 min the concentration of phosphates was considerably reduced to very low levels for all three initial concentrations, the experiments performed at lower initial concentrations show higher removal efficiency. Indeed, as the initial concentration increased from 20.0 to 60.0 mg L^{-1}, the removal efficiency, after 20 min, decreased from 95% to 82%. These results are consistent with the findings of İrdemez *et al.* [34] and Bektaş *et al.* [36]. Both authors studied the removal of phosphates by electrocoagulation using pure aluminium electrodes and investigated the removal efficiency with several initial concentrations of phosphates, ranging from 10 to 200 mg L^{-1}. They found a decrease in the removal efficiency on increasing the initial concentration of phosphates. İrdemez *et al.* [34] reported a removal efficiency of 100% for 25, 50 and 100 mg L^{-1} phosphates and 88% for 150 mg L^{-1} phosphates at an initial pH of 3.0, a current density of 1.0 mA cm^{-2} and a SA/V ratio of 88.2 m^{-1}. Bektaş *et al.* [36] used an initial pH of 6.2 and a current density of 10.0 mA cm^{-2} and reported the complete removal of phosphate for initial phosphate concentrations of 25 and 50 mg L^{-1} and an efficiency of 90% for an initial concentration of 200 mg L^{-1} of PO_4-P. The

decrease in removal efficiency with increasing initial concentrations has been widely reported in electrocoagulation for several pollutants [34, 52-60] and it is generally ascribed to the amount of coagulant generated in solution relative to the concentration of the pollutant.

In a study on chemical coagulation, Stumm and O'Melia [61] observed that the dosage of coagulant necessary to bring about destabilisation of a solution depended upon the amount of particles. Thus, they concluded that the optimum coagulant dose was clearly proportional to the concentration of pollutants or colloids present in solution [42, 62]. O'Melia [63] described the residual turbidity observed in jar test experiments as a function of coagulant dosage by means of four curves, each one representing a different concentration of colloidal material. In each curve the author identified an area corresponding to low dosage where the coagulant added was insufficient to induce destabilisation of the particles present in solution. On increasing the coagulant dosage, destabilisation and aggregation were achieved [63]. Although this mechanism was suggested for chemical coagulation and for the removal of turbidity, it is reasonable to assume that it is generally valid for the removal of pollutants by electrogenerated coagulants. In electrocoagulation the coagulant dosage is clearly related to the electrolysis time through Faraday's laws of electrolysis. Consequently, the data displayed in Figure 3.3 may be seen as the residual concentration of phosphates as a function of the coagulant dosage. As the applied current was constant in each experiment, the coagulant dose also remained constant in the three sets of experiments shown in Figure 3.3. It is clearly evident from this figure that low initial concentrations of phosphates are removed faster and require less coagulant. In contrast, longer times are needed to treat the solution containing 150.0 mg L^{-1} of phosphates. At this higher initial concentration of phosphates, the amount of coagulant produced is not sufficient to destabilise the phosphate ions present in solution. These results are in good agreement with the work reported by O'Melia [63] for the removal of turbidity in chemical coagulation.

Interestingly, the amount of phosphates removed from the three initial concentrations shown in Figure 3.3 is not the same at each time interval. After 10 min of the electrocoagulation period, 16, 35 and 64 mg L^{-1} of PO_4-P are removed from initial

concentrations of phosphates of 20.0, 60.0 and 150.0 mg L^{-1}, respectively, as can be seen from the data presented in Table 3.1. It is clear that a greater amount of phosphates is removed from the solution when a high initial concentration is used, although the concentration of coagulants delivered to the solution is the same for all three experiments.

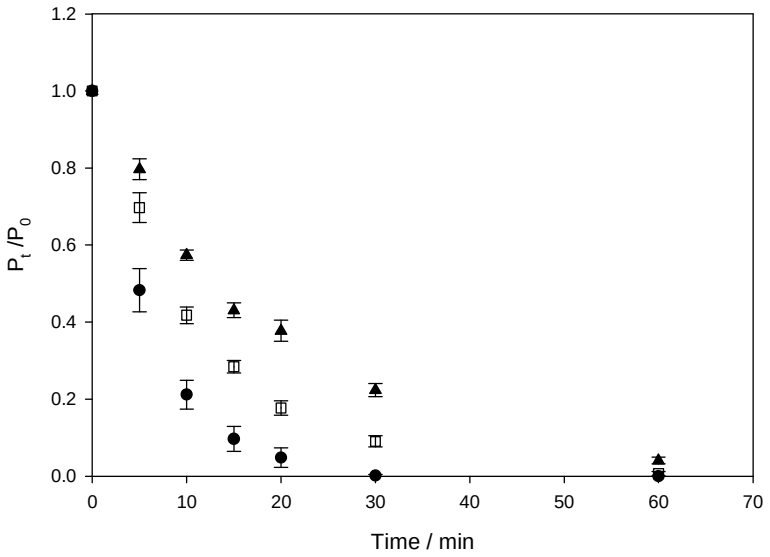

Figure 3.3: Normalised variation of the concentration, P_t/P_o, of phosphates plotted as a function of the electrocoagulation time in solutions containing initial concentrations, P_o, of ● 20.0 mg L^{-1}, □ 60.0 mg L^{-1} and ▲ 150.0 mg L^{-1} PO_4-P. (Anode/cathode = Al-2Mg/AISI 310, [NaCl] = 4.2×10^{-3} M, pH = 5.0, j = 11.0 mA cm^{-2}, SA/V = 11.7 m^{-1}).

Table 3.1: Residual concentration of phosphates, P_t, and removal efficiency, η, for different initial concentrations of PO_4-P. Each experiment was performed in triplicate (n = 3).

Time	$\mathbf{P_t}$	$\boldsymbol{\eta}$	$\mathbf{P_t}$	$\boldsymbol{\eta}$	$\mathbf{P_t}$	$\boldsymbol{\eta}$
/ min	**/ mg L^{-1}**	**/ %**	**/ mg L^{-1}**	**/ %**	**/ mg L^{-1}**	**/ %**
0	20.0	0	60.0	0	150.0	0
5	10.0 ± 1	52 ± 6	42 ± 2	30 ± 4	120 ± 4	20 ± 3
10	4.2 ± 0.8	79 ± 4	25 ± 1	58 ± 2	86 ± 2	43 ± 1
15	1.9 ± 0.7	90 ± 3	17 ± 1	72 ± 2	65 ± 3	57 ± 2
20	1.0 ± 0.5	95 ± 3	11 ± 1	82 ± 2	57 ± 4	62 ± 3
30	BDL*	99.8 ± 0.3	5.4 ± 0.9	91 ± 1	34 ± 3	78 ± 2
60	BDL*	100 ± 0	0.4 ± 0.3	99.3 ± 0.5	6 ± 1	95.9 ± 0.8

*BDL = Below Detection Limit (Section 2.3.3).

3.2.1.2 The rate constant for the removal of phosphates

As discussed previously in Section 3.1, the removal of pollutants upon addition of aluminium or iron ions is the result of a two-phase process, which involves coagulation and flocculation. Since in electrocoagulation these two phases occur simultaneously, it is clear that a series of complex reactions and processes is involved. While the coagulation phase depends primarily on the speciation of the coagulant, which, in turn, is governed by the solution pH and coagulant dosage [42], it has been reported that the flocculation phase is a function of the degree of destabilisation attained in the coagulation phase and the collision rate between the particles [43, 64]. Taking into account the complexity of these reactions, in the present study the removal of phosphates using the Al-2Mg electrode can be described by Eq. 3.1.

$$\frac{\mathrm{d}[\mathrm{P}]}{\mathrm{d}t} = -k[\mathrm{P}]^{x}\left[\mathrm{Al(OH)}_{n}^{(3-n)}\right]^{y} \qquad \textbf{Eq. 3.1}$$

Here, P is the concentration of phosphates, $Al(OH)_n^{(3-n)}$ is the concentration of the hydrolysis products of Al^{3+} ions, k is the rate constant and x and y are the partial orders of the reaction. As discussed in Section 3.2, it is believed that the removal of phosphates is attained by a combination of processes involving the $Al(OH)_n^{(3-n)}$ and aluminium hydroxide species (Step III in Figure 3.2). The final removal of phosphates is attained by particle collision and aggregation, as shown in Step IV in Figure 3.2. The chemistry of aluminium is quite complex and polynuclear species can form, although these products can often be ignored, especially in dilute and fresh solutions [65]. It is then clear that determining the rate constant, k, and the reaction orders, x and y, is extremely complicated, as the speciation of the hydrolysis products is governed by the pH and the coagulant dose. In electrocoagulation the coagulant is dosed in a continuous manner and the pH changes throughout the process. These conditions produce a dynamic system.

In an attempt to develop a kinetic model for the temporal variations of residual phosphates, it was assumed that the production and consumption rates of the hydrolysis products were equal. In this way the concentration of the $Al(OH)_n^{(3-n)}$ species can be considered constant (Step II in Figure 3.2) and Eq. 3.1 can be simplified to give Eq. 3.2.

$$\frac{\mathrm{d}[\mathrm{P}]}{\mathrm{d}t} = -k_{obs}[\mathrm{P}]^{x} \qquad \textbf{Eq. 3.2}$$

In this analysis, k_{obs} represents the observed rate constant. In this approximation the rate constant reflects the contribution of several reactions, involving both the coagulation and the flocculation phases (Figure 3.2). A similar approach was used to study the kinetics of electrochemical oxidation, ozonation and UV irradiation [66-70], where the elimination of pollutants in water was accomplished by the mediation of compounds generated in solution, such as 'active chlorine', ozone, hydrogen peroxide and other strong oxidising agents.

Several authors have reported that in electrocoagulation the removal of a wide variety of pollutants is described by pseudo first-order or pseudo second-order kinetics [15, 71-79]. Consequently, the data presented in Figure 3.3 were fitted to pseudo first (x = 1) and pseudo second-order (x = 2) models and the R^2 values were used to attest the goodness of the fit. These data are summarised in Table 3.2 and plotted in Figure 3.4(a) and (b). They clearly show that the removal of phosphates using the Al-2Mg electrode is better described by a pseudo first-order reaction. The R^2 values show excellent linearity. The pseudo first-order relationship is expressed in Eq. 3.3.

$$\ln\frac{P_t}{P_0} = -k_{obs}t \qquad \textbf{Eq. 3.3}$$

Here, P_0 is the initial phosphate concentration in mg L^{-1}, P_t is the phosphate concentration at time t in mg L^{-1}, k_{obs} is the rate constant in min^{-1} and t is the time in min. Typical plots where the logarithm of (P_t/P_0) is shown as a function of time are presented in Figure 3.4(a) and the values of k_{obs}, obtained as the slope of the linear regression analysis, are presented in Table 3.2. It is clearly evident that the rate constant, k_{obs}, decreases with increasing initial concentration of phosphates. In particular, the k_{obs} values vary from 0.1531 min^{-1} for 20.0 mg L^{-1} to 0.0525 min^{-1} for 150.0 mg L^{-1} of PO_4-P.

The dependence of k_{obs} on the initial concentration of phosphates suggests that the rate-determining step involves the phosphate ions. El-Ashtoukhy and Amin [78] reported a similar dependence of the rate constant for the removal of acid green dye 50 from wastewater using anodic oxidation as well as electrocoagulation. They suggested that the decrease of the pseudo first-order rate constant with increasing initial concentrations of the dye was due to an association of the dye molecules in the solution at high concentrations. However, dimerisation does not occur for phosphate ions.

Table 3.2: Rate constant, k_{obs}, and R^2 values for pseudo first-order and second-order kinetics.

Initial concentration, P_0 / mg L^{-1}	**Pseudo first-order kinetics** $\ln\frac{P_t}{P_0} = -k_{obs}t$		**Pseudo second-order kinetics** $\frac{1}{P_t} = k_{obs}t + \frac{1}{P_0}$	
	k_{obs} / min^{-1}	**R^2**	**k_{obs} / min^{-1}**	**R^2**
20.0	0.1531	0.999	0.0477	0.870
60.0	0.0832	0.999	0.0410	0.810
150.0	0.0525	0.997	0.0026	0.864

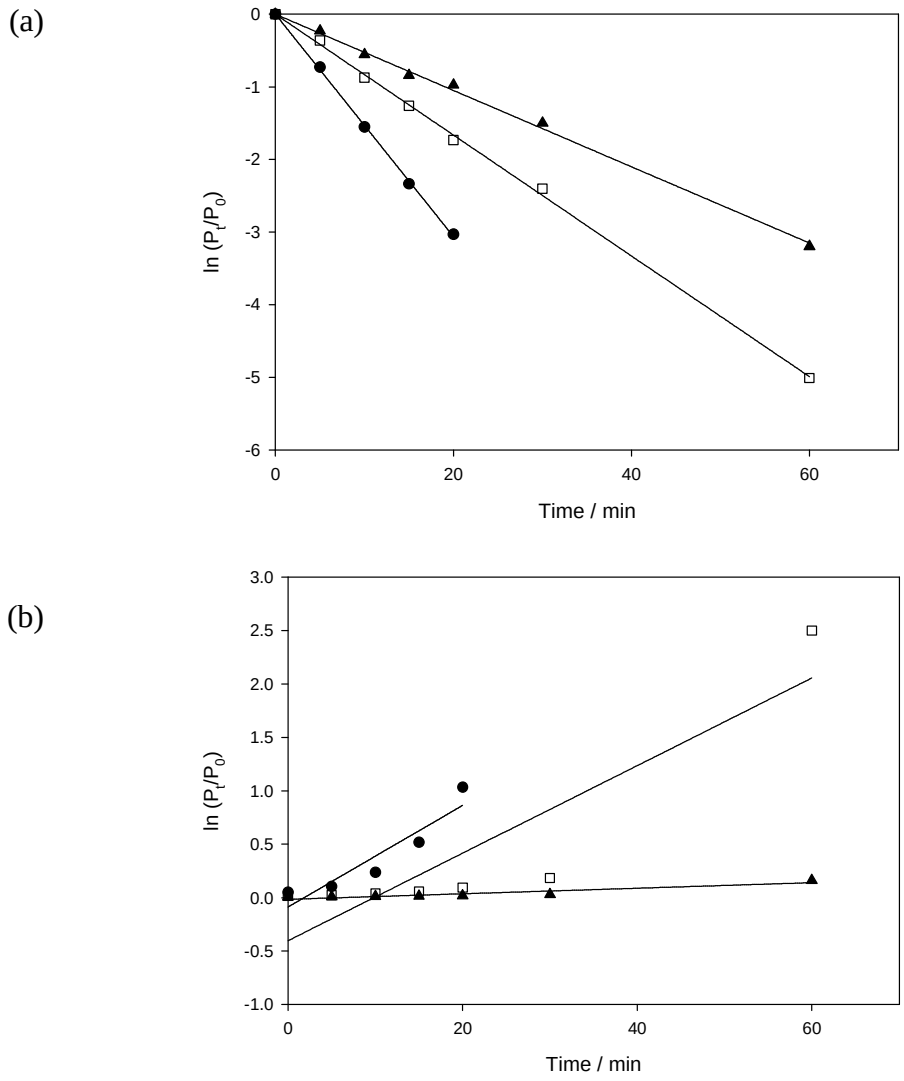

Figure 3.4: (a) Pseudo first-order and (b) pseudo second-order kinetics of phosphate removal at different initial concentrations of phosphates, P_0: ● 20.0 mg L^{-1}, □ 60.0 mg L^{-1} and ▲ 150.0 mg L^{-1} PO_4-P. (Anode/cathode = Al-2Mg/AISI 310, [NaCl] = 4.2×10^{-3} M, pH = 5.0, j = 11.0 mA cm^{-2}, SA/V = 11.7 m^{-1}).

It has been reported that the formation of hydroxycomplex species (Step II in Figure 3.2) shown in Figure 3.1 occurs rather rapidly, within microseconds for monomeric species and within 1 second if polymeric species are involved [80-83]. For example, according to Baes and Mesmer [81], half of the Al^{3+} ions hydrolyse to $Al(OH)^{2+}$ within 1×10^{-5} s at a pH of 4.0. Hanh and Stumm [83], in studying the coagulation of silica dispersions with Al^{3+}, compared the rate of destabilisation in the coagulation phase, i.e., the rate of aluminum hydroxycomplexes adsorption on the particle surface and the rate of particle collision in the flocculation stage. They concluded that the latter was the rate-determining step, which can be identified as Step IV in Figure 3.2. Also, the formation of aluminium hydroxide for entrapment of colloidal particles (sweep coagulation) is completed within 1 to 7 s [84]. Therefore, the flocculation phase is the rate-determining step and, in particular, the collision frequency and collision efficiency are the parameters which affect the overall coagulation-flocculation rate [83]. According to Smoluchowski [85, 86], the frequency f_{ij} of binary collisions between particles of type *i* and *j* is given by Eq. 3.4.

$$f_{ij} = E_{ij} k_{ij} C_i C_j \qquad \textbf{Eq. 3.4}$$

Here, E_{ij} is the efficiency factor for collisions between *i*- and *j*-type particles, k_{ij} is a collision frequency factor that depends on the specific mechanism responsible for the collision, C_i and C_j are the respective concentrations of the two types of particles. In the present work, C_i and C_j correspond to phosphate ions and aluminium hydroxycomplex species. According to Eq. 3.4, provided that the collision mechanism does not change upon the progression of the electrocoagulation process, the rate of particle collision is a function of the particle concentrations. However, increasing the concentration of phosphates does not result in an increase of the overall removal rate (as shown in Figure 3.4(a) and Table 3.2), which is determined by the collision frequency. The collision frequency in Eq. 3.4 also comprises the efficiency factor, E_{ij}, which is introduced because not every collision will result in an successful attachment [87]. Whether or not the particles remain attached after a collision depends on the net interparticle forces [88], that is the magnitude of the repulsive force between the particles. In other words, a successful particle aggregation depends on the destabilisation degree attained in the coagulation phase [42, 50]; if particles have been destabilised completely, then E_{ij} is

equal to 1 [42, 88] and each collision will lead to adhesion. In coagulation, and consequently in electrocoagulation, the degree of destabilisation is strictly dependent on the ratio of coagulant dosage to the concentration of pollutants [89], the so called 'stoichiometry of coagulation'.

Provided that the concentration of Al^{3+} ions dissolved from the electrode is constant and the hydrolysis of Al^{3+} (Step II in Figure 3.2) is rapid, then in solutions containing high initial concentrations of phosphates, the number of destabilised particles is small. In this case, the ratio of coagulant, aluminium hydroxycomplex species, to phosphate ions is low. As a consequence, the number of successful collisions between a coagulant particle and a destabilised particle is also low [50], since the efficiency factor E_{ij} in Eq. 3.4 is lower than 1. Therefore, the observed rate constant, k_{obs}, for the removal of phosphates will decrease as the concentration of phosphates is increased, as reported in Table 3.2.

3.2.2 The effect of the current density

In electrocoagulation, the current density is an important parameter for controlling the reaction rate. It is well known that the current density determines the amount of Al^{3+} ions released from the anode and, consequently, the coagulant dosage. At the same time, the rate and size of the H_2 bubbles produced at the cathode also depend on the applied current density [90]. When large current densities are used, the potential might assume high values resulting in a significant decrease in current efficiency and an increase of the energy consumption of the system [1].

To investigate the effect of the current density on the efficiency of phosphate removal, electrocoagulation experiments were carried out using various current densities. Figure 3.5 shows the residual concentration of phosphates, P_t, as a function of the electrocoagulation time for current densities of 5.3 and 11.0 mA cm^{-2}. It can be seen from the figure that, at the end of the process, the phosphates were removed almost completely for both values of current density, however the removal rate was rapid with the high current density. Indeed, as the current density increases from 5.3 to 11.0 mA cm^{-2}, the removal efficiency, after 30 min, increases from 77% to 91%.

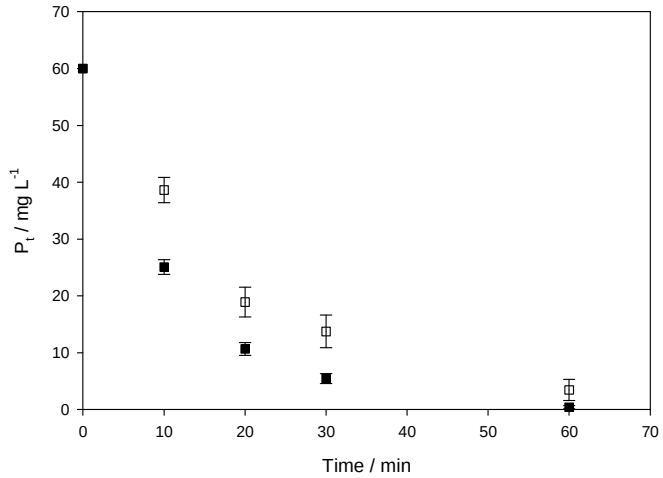

Time / min	P_t / mg L^{-1}	
	5.3 mA cm^{-2}	**11.0 mA cm^{-2}**
0	60.0	60.0
10	39 ± 2	25 ± 1
20	19 ± 3	11 ± 1
30	13.7 ± 2.9	5.4 ± 0.9
60	3.4 ± 1.9	0.4 ± 0.3

Figure 3.5: Variation of the concentration of phosphates, P_t, plotted as a function of the electrocoagulation time in solutions containing initial concentration, P_0, of 60.0 mg L^{-1} PO_4-P at different current densities: □ 5.3 mA cm^{-2} and ■ 11.0 mA cm^{-2}. Each experiment was performed in triplicate (n = 3). (Anode/cathode = Al-2Mg/AISI 310, [NaCl] = 4.2×10^{-3} M, pH = 5.0, SA/V = 11.7 m^{-1}).

The influence of the current density was studied by comparing the rate constants for the removal of phosphate at 5.3 and 11.0 mA cm^{-2}. In Figure 3.6 typical plots are shown of the logarithm of the concentration ratio, P_t/P_0, plotted as a function of the electrocoagulation time for initial concentrations of phosphates of 20.0, 60.0 and 150.0 mg L^{-1} at a current density of 5.3 mA cm^{-2} and an initial pH of 5.0. The experimental data were fitted by linear regression analysis and the resulting values of the observed pseudo first-order rate constants and R^2 are provided in Figure 3.6. The high values of R^2 indicate excellent agreement with pseudo first-order kinetics. The same model was valid with a current density of 11.0 mA cm^{-2} as shown in Section 3.2.1, Figure 3.4. As it can be seen from the table shown in Figure 3.6, the observed rate constant, k_{obs}, was 0.0877 min^{-1} for an initial phosphate concentration of 20.0 mg L^{-1}, while it was reduced to 0.0274 min^{-1} when the initial phosphate concentration is 150.0 mg L^{-1}.

From Figure 3.6 it is clear that k_{obs} decreased with increasing initial concentrations of phosphates. This result is in good agreement with the analysis provided in Section 3.2.1.2. Furthermore, by comparing the values of the k_{obs} obtained at 11.0 and 5.3 mA cm^{-2} in Figure 3.4(a) and Figure 3.6, respectively, it is evident that low current densities reduced the rate of phosphate removal. Indeed, for an initial concentration of phosphates of 60.0 mg L^{-1}, the k_{obs} ranges from 0.0832 to 0.0487 min^{-1} for current

densities of 11.0 and 5.3 mA cm^{-2}, respectively. These results are in good agreement with the data reported by Mameri *et al.* [15] on the defluoridation of Sahara waters by electrocoagulation. It was shown that the removal of fluoride depends on the current density and the temperature of the solution, with more efficient removal at a higher current density. As shown in Section 3.2.1, a smaller degree of destabilisation of phosphate ions is obtained in solutions containing a lower ratio of the coagulant to phosphate concentrations. According to Faraday's law, the concentration of Al^{3+} ions dissolved from the anode and delivered to the solution is proportional to the applied current. Accordingly, the amount of coagulant delivered is reduced at the lower current density. A smaller amount of coagulant in solution leads to a lower degree of destabilisation of phosphate, consequently, the collision efficiency seen in Eq. 3.4 diminishes and in turn the k_{obs} decreases. In addition, the chemical composition of solutions treated with different current densities is substantially different. For example, Lacasa *et al.* [33] demonstrated that lower current densities result in lower final pH values. In Section 3.2.3 it will be shown that the initial pH has an influence on the removal efficiency and it also determines the final pH of the solution.

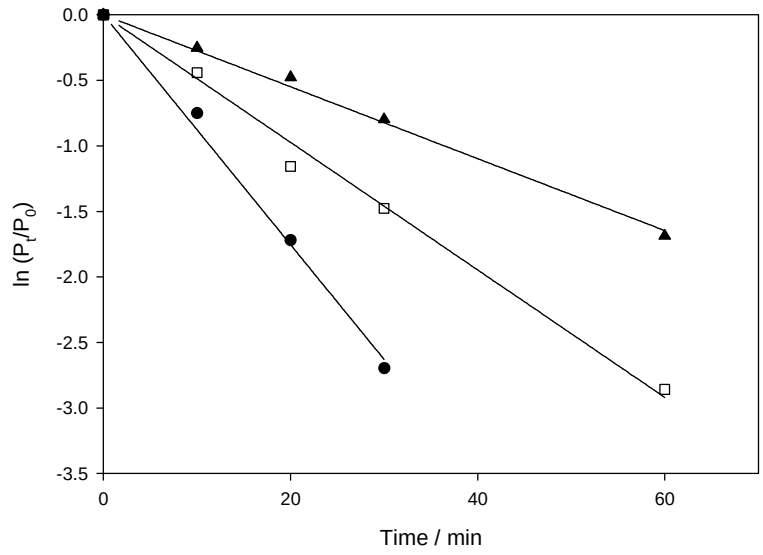

P_0 / mg L^{-1}	k_{obs} / min^{-1}	R^2
20.0	0.0877	0.995
60.0	0.0487	0.992
150.0	0.0274	0.995

Figure 3.6: Kinetics of phosphate removal at different initial concentrations of phosphates, P_0: ● 20.0 mg L^{-1}, □ 60.0 mg L^{-1} and ▲ 150.0 mg L^{-1} PO_4-P. (Anode/cathode = Al-2Mg/AISI 310, [NaCl] = 4.2 ×10^{-3} M, pH = 5.0, j = 5.3 mA cm^{-2}, SA/V = 11.7 m^{-1}).

3.2.3 The effect of pH

The initial pH is an important parameter affecting the performance of electrochemical processes [1, 91, 92], since it affects the degree of hydrolysis of Al^{3+} ions. In electrocoagulation, the solution pH increases during the process as the result of hydrogen evolution at the cathode. Consequently, the final pH of the solution and, more importantly, the range of pH values that the solution exhibits throughout the electrocoagulation process play an important role in electrocoagulation.

3.2.3.1 The effect of initial pH

To investigate the effect of the pH on the electrocoagulation of phosphates using the Al-2Mg electrode, the initial pH of a solution containing 85.0 mg L^{-1} of PO_4-P was adjusted in the range of 3.2 to 7.5 and the removal of phosphates was monitored with time. The concentrations of phosphates remaining in solution as a function of the electrocoagulation period at pH values of 3.2, 5.3, 6.7 and 7.5 are displayed in Figure 3.7. As evident from this figure, the effect of the initial pH is highly significant. The maximum removal of phosphates at the end of the electrocoagulation experiments is achieved at pH 3.2 with a residual phosphate concentration of 1.1 mg L^{-1} after a 30 min period. On increasing the initial pH, a gradual decrease of the amount of phosphates removed from the solution is observed. Indeed, with an initial pH of 7.5 the final concentration of phosphates is 26.2 mg L^{-1}.

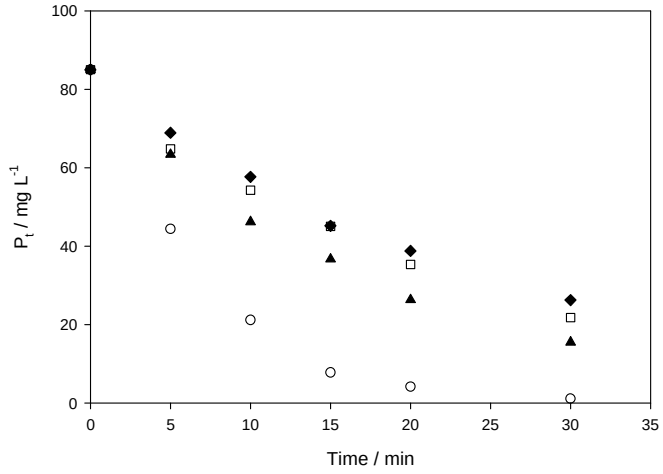

Time / min	P_t / mg L^{-1}			
	pH 3.2	**pH 5.3**	**pH 6.7**	**pH 7.5**
0	85.0	85.0	85.0	85.0
5	44.4	63.4	64.8	68.9
10	21.2	46.2	54.3	57.7
15	7.8	36.7	45.1	45.2
20	4.2	26.3	35.3	38.8
30	1.1	15.5	21.8	26.2

Figure 3.7: Variation of the residual phosphate concentration, P_t, plotted as a function of the electrocoagulation time in solutions containing 85.0 mg L^{-1} of PO_4-P at initial pH values of ○ 3.2, ▲ 5.3, □ 6.7 and ◆ 7.5. (Anode/cathode = Al-2Mg/AISI 310, [PO_4-P] = 85.0 mg L^{-1}, [NaCl] = 4.2 × 10^{-3} M, j = 11.0 mA cm^{-2}, SA/V = 11.7 m^{-1}).

The rate constants, k_{obs}, introduced in Section 3.2.1.2 were calculated for each initial pH used in the experiments shown in Figure 3.7 and these are summarised in Table 3.3. Again, high values of R^2 were obtained, indicating that the kinetics of phosphate removal follows the pseudo first-order model. The k_{obs} values depend on the initial pH values, varying from 0.1470 min^{-1} at pH 3.2 to 0.0396 min^{-1} at pH 7.5.

Table 3.3: Pseudo first-order constant, k_{obs}, and R^2 values for the removal of phosphates at different initial pH values.

Initial pH	k_{obs} / min^{-1}	R^2
3.2	0.1470	0.995
5.3	0.0574	0.999
6.7	0.0447	0.996
7.5	0.0396	0.998

Although it has been reported that the highest removal occurs near a pH of 7.0 with aluminium [1], it is well known that the performance also depends on the nature of pollutants present in the solution. In the literature there is no general agreement on the optimal initial pH required to remove phosphates. According to Bektaş *et al.* [36] the optimal initial pH for phosphate removal using pure aluminium is 5.0 to 6.0. A similar

finding was reported by Vasudevan *et al.* [39] in their study on the removal of phosphates using an aluminium-zinc electrode. In contrast, İrdemez and co-workers [34, 35] demonstrated that the highest efficiency removal of phosphates was achieved at an initial pH of 3.0, using aluminium and iron electrodes. This finding is in good agreement with the results obtained in the present study with the Al-2Mg electrode and shown in Figure 3.7 and suggests that a similar mechanism is involved with pure aluminium and the Al-2Mg electrode.

3.2.3.2 The effect of final pH

Figure 3.8 depicts the final pH of the solution after an electrocoagulation period of 30 min as a function of the initial pH. The removal efficiency of phosphates is also shown. It is clear that the final pH depends on the initial pH of the solution. When the initial pH is acidic, the final pH value shows a marked increase, from 3.2 to 7.1. On the other hand, solutions with initial pH values close to neutrality exhibit a more moderate rise, for example, from initial pH values of 6.7 and 7.5 to final values of 9.9 and 10.6, respectively. This is in good agreement with previous studies [92-94], which describe a levelling for the evolution of the pH in highly acidic or highly alkaline solutions. Regarding the pH variation observed during electrocoagulation, some authors [29, 94, 95] have attributed these pH changes to the hydrogen evolution reaction at the cathode. However, according to Chen *et al.* [93] the pH change may be due to other reasons. For example, the pH increase may occur because of the release of CO_2, which is over saturated in acidic solutions and enhanced by H_2 bubble evolution. The same authors also indicated that some anions, such as Cl^- and SO_4^{2-}, may exchange partly with OH^- in $Al(OH)_3$ to free OH^-, giving an increase of the solution pH.

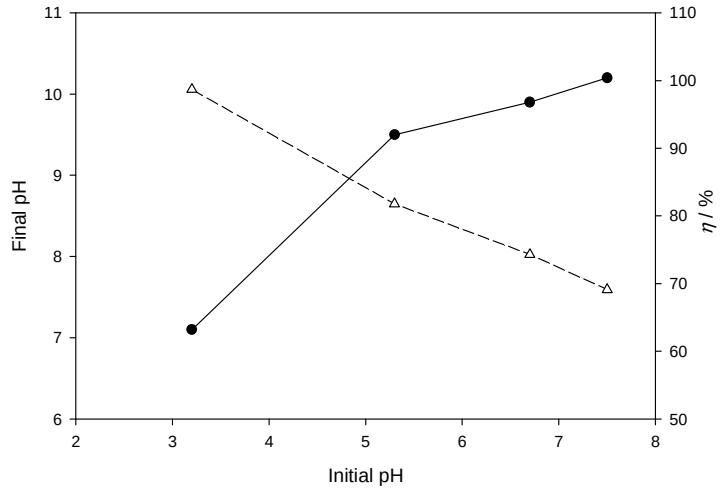

Initial pH	Final pH	η / %
3.2	7.1	98.7
5.3	9.5	81.8
6.7	9.9	74.3
7.5	10.6	69.1

Figure 3.8: Evolution of ● final pH and △ removal efficiency, η, plotted as a function of the initial pH. (Anode/cathode = Al-2Mg/AISI 310, [PO_4-P] = 85.0 mg L^{-1}, [NaCl] = 4.2 × 10^{-3} M, j = 11.0 mA cm^{-2}, SA/V = 11.7 m^{-1}).

The effect of the initial pH on the removal efficiency of phosphate can be explained in terms of the aluminium speciation. Cañizares and Rodrigo have published several works [96-101] on the electrocoagulation process using aluminium electrodes and on the speciation of aluminium. They characterised the hydrolysed aluminium species, generated during electrodissolution of the electrode (Figure 3.1), using a time-resolved spectrophotometric technique. This method involves the reaction between aluminium and ferron (8-hydroxy-7-iodo-5-quinolinesulfonic acid) to form a complex Al(ferron)$_3$ and allows the discrimination of monomeric, polymeric and precipitate species, since each of these species has a different time of reaction. Monomeric aluminium species react with ferron almost instantaneously (0 to 1 min), the fraction of aluminium reacting slower (1 to 20 min) is thought to include polynuclear aluminium species, whereas the fraction of aluminium that does not react with ferron is assumed to represent colloidal or solid-phase aluminium [102-105].

Cañizares *et al.* [97] claimed that the speciation of aluminium in aqueous solutions is dependent on the total concentration of aluminium and pH. They showed that at acidic pH, monomeric hydroxyaluminium cations are the primary species. Increasing the pH leads to a decline of the monomeric species with a gradual rise of aluminium hydroxide precipitates, which represent the main aluminium species at pH values close to neutrality. At alkaline pH, the precipitate dissolves to form monomeric anionic

hydroxyaluminium species in solution. In the light of these findings and taking into account that, as shown in Figure 3.8, the pH value increases with time in the range of pH investigated, it seems plausible that the removal of phosphates is accomplished through several mechanisms/reactions depending on the instantaneous pH of the solution.

The data shown in Figure 3.7 and supported by the study reported by İrdemez [34, 35] indicate that the highest removal of phosphates is achieved at an initial pH of 3.2. As evident from Figure 3.8, this corresponds to a final pH of 7.1. According to the findings of Cañizares *et al.* [97], at pH 3.2 the predominant coagulant species is represented by monomeric cations. At this pH the phosphate ions, which are negatively charged, are mainly removed by charge neutralisation by the hydroxyaluminium cations. As the solution pH increases with time, from 3.2 to 7.0, the primary removal mechanism changes to involve the hydroxide and the hydroxy-phosphate precipitates in a process of adsorption-precipitation and/or of sweep coagulation. It is important to note that in the same pH range (5.5 to 6.5) $AlPO_4$ has its minimum solubility.

When the initial pH is higher at 5.3, 6.7 or 7.5 a smaller pH change is observed during the electrocoagulation experiment and the final solution is alkaline. As suggested by Cañizares *et al.* [97], at a pH of 5.0 or higher the removal is attained prevalently as adsorption-precipitation and/or sweep coagulation. Furthermore, at pH values above 8.0, the predominant species is the anionic monomeric hydroxyaluminium, which is soluble and negatively charged [106]. Consequently, both species, the aluminate and phosphate ions, have negative charge, repelling each other and therefore cannot interact, decreasing the efficiency of the removal process [44]. Clearly, the initial pH affects the final pH value and the pH evolution throughout the electrocoagulation experiment determines the removal mechanism and the removal efficiency.

As outlined previously, some authors [36, 39] reported that the maximum removal efficiency of phosphates is achieved at initial pH values in the range of 5.0 to 7.0. Their findings are not consistent with the results shown in the present work and by İrdemez *et al.* [34, 35], where the optimum initial pH was found at a pH of 3.0. However, on examining the final pH of the solutions, it is evident that the authors who observed the

highest removal efficiencies at initial pH values in the range of 5.0 to 7.0 recorded final pH values of 6.5 to 6.7 [36] and 7.3 [39]. A comparable value of the final pH was observed in the present work, 7.1, for an initial pH of 3.2, which corresponds to the highest removal efficiency, as shown in Figure 3.8. This finding emphasises the role of the final pH and the pH evolution in the electrocoagulation removal of phosphates.

3.2.4 The effect of chloride concentration

The effect of chloride concentration on electrocoagulation has been investigated in a number of studies [1, 60, 71, 92, 97, 107]. The addition of NaCl leads to an increase of the conductivity of the solution. Consequently, working in a galvanostatic mode, the consumed electrical energy will decrease since the necessary voltage for attaining a certain current density diminishes. Conversely, in a potentiostatic mode, an increase of the conductivity leads to an increase of the current density and, in turn, higher amounts of Al^{3+} ions are dissolved. Furthermore, it is well known that chloride ions can destroy the passive film formed on the surface of aluminium [108]. Indeed, some authors have recommended that the solution contains 20% of Cl^- ions to ensure a normal operation of the electrocoagulation process [1]. However, the addition of NaCl to wastewaters with a low conductivity will affect the operating cost of the process, due to the increasing cost of chemicals.

Kabdaşlı *et al*. [71] claimed that increasing NaCl concentrations might suppress the efficiency of the process. The author did not provide any further explanation but, since the chloride anions were connected to a lower efficiency, then it appears that the counter ions influence the aluminium speciation and, in turn, the removal efficiency. Counter ions have an active role in the stepwise hydrolysis process shown in Figure 3.1, since they can compete with hydroxy ligands in the hydration shell of the aluminium complexes [109]. It has been reported that the tendency of an anion to alter the coagulation behaviour of hydrolysing metals is related to its electronegativity and its tendency to react with the metal ion or positively charged sites on the metal hydroxide precipitate [62, 110]. Chloride ions have a weak coordination capacity with metal ions [62], consequently the presence of chloride does not strongly affect the speciation of the aluminium hydrolysis products. X-ray and neutron diffraction studies carried out on

aluminium trichloride hexahydrate ($AlCl_3 \cdot 6H_2O$) demonstrated that the crystal structure contains six tightly bound aqua ligands in the primary coordination sphere and three chloro ligands in the secondary sphere. This indicates that the chloro ligands are less tightly bound compared to the aqua ligands [111]. Moreover, according to the hard and soft acid-base, HSAB, theory, introduced by Pearson [112], Al^{3+} ions have a greater tendency to bind the hard base H_2O rather than forming halo complexes. Stumm and Morgan [113] have shown that for ions like Al^{3+}, also called A-type metal cations, chloro complexes are weak and occur mostly in acidic solutions, where unfavourable competition of OH^- occurs. However, if the $[Cl^-]/[OH^-]$ ratio is sufficiently high, hydroxyl ions are displaced from the coordination sphere of the metal ion complexes by chloride ions [62] and consequently the removal efficiency might be suppressed.

In order to determine the effect of NaCl concentration on the removal of phosphates using the Al-2Mg electrode, electrocoagulation experiments were carried out by varying the concentration of NaCl. Figure 3.9 shows the residual concentration of phosphates after 30 min in solutions containing 4.2, 7.0, 10.0, 25.0 and 44.0×10^{-3} M NaCl. The initial concentration of phosphates was 85.0 mg L^{-1} and the initial pH was 5.0. A 10-fold increase in the NaCl concentration, from 4.2 to 44.0×10^{-3} M, results in a slight increase of the removal efficiency from 85.2% to 88.8%. This moderate increase of the removal efficiency recorded with increasing NaCl concentrations may be due to a higher degree of destabilisation attained in solution. Duan and Gregory [65] outlined that the solution destabilisation can also be brought about by an increase in the ionic strength, since it produces a compression of the electrical double layer of the particles. Consequently, the presence of NaCl in solution promotes the coagulation of phosphates. On the other hand, as already outlined, an excess concentration of Cl^- ions tends to displace the hydroxyl ions from the coordination sphere of Al^{3+} ions [62].

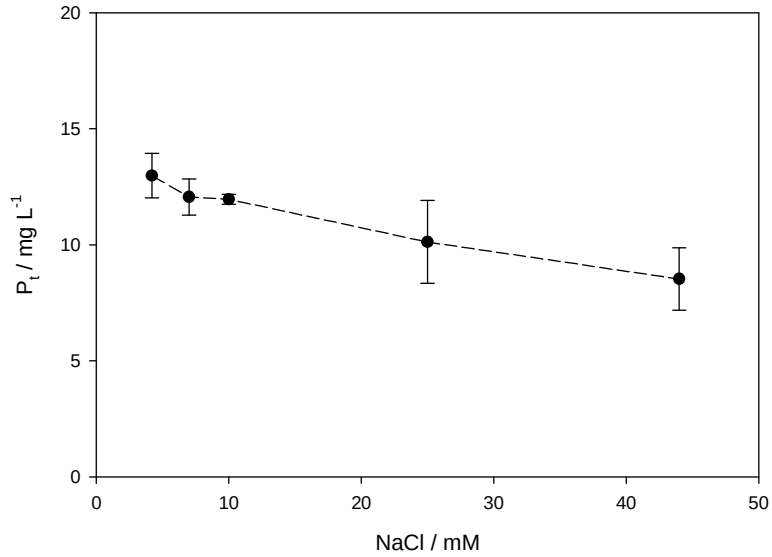

NaCl / mM	P_t / mg L^{-1}
4.2	13 ± 1
7.0	12.1 ± 0.8
10.0	12.0 ± 0.2
25.0	10 ± 2
44.0	9 ± 1

Figure 3.9: Residual phosphate concentration, $P_{t,}$ as a function of NaCl concentration. The concentrations of NaCl used were: 4.2, 7.0, 10.0, 25.0 and 44.0 × 10^{-3} M. Each experiment was performed in duplicate (n = 2). (Anode/cathode = Al-2Mg/AISI 310, [PO_4-P] = 85.0 mg L^{-1}, pH = 5.0, j = 11.0 mA cm^{-2}, t = 30 min, SA/V = 11.7 m^{-1}).

The NaCl concentration has a marked, important effect on the energy consumption of the system. Indeed, the increase of the solution conductivity due to the presence of NaCl has a direct effect on the potential between the electrodes. As shown in Figure 3.10, the potential of the anode decreases as the concentration of NaCl increases and, consequently, the conductivity of the solution increases. In solutions containing 4.2 × 10^{-3} M NaCl the average potential, $\overline{E}$, is 2.2 V vs. SCE. Towards the end of the electrocoagulation experiment, the potential exhibited a gradual increase and reached values close to 3.0 V vs. SCE. At these potentials, concurrent reactions not resulting in the dissolution of Al^{3+} ions may occur at the anode, such as the oxidation of water (1.23 V vs. SHE) or the formation of chlorine-oxygen compounds, as reported by several authors [60, 90, 98, 114]. Although these parasitic reactions may help flotation or pollutant oxidation, they give rise to a lower current efficiency of the process. Consequently, the amount of the generated Al^{3+} ions is lower and, in turn, a small amount of phosphate is removed, as was observed in Figure 3.9 for the solution containing 4.2 × 10^{-3} M NaCl. In solutions containing 7.0 and 10.0 × 10^{-3} M NaCl, the lower potentials of the anode, as shown in Figure 3.10, prevents these concurrent reactions.

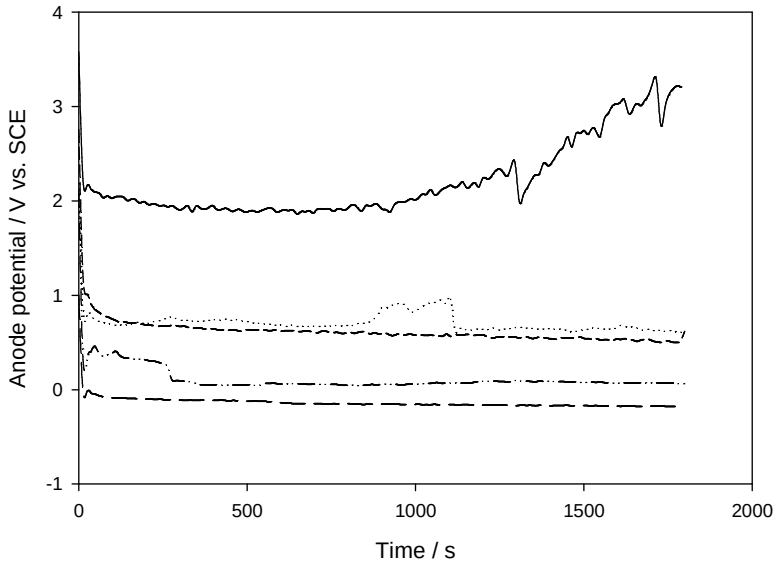

NaCl / mM	$\overline{E}$ / V vs. SCE
4.2	2.22
7.0	0.71
10.0	0.62
25.0	0.11
44.0	-0.14

Figure 3.10: Variation of the anode potential as a function of the electrolysis time in solutions containing −−− 4.2, · · · 7.0, − − − 10.0, − ·· − 25.0 and −− −− −− 44.0 × 10^{-3} M NaCl. (Anode/cathode = Al-2Mg/AISI 310, [PO_4-P] = 85.0 mg L^{-1}, pH = 5.0, j = 11.0 mA cm^{-2}, t = 30 min, SA/V = 11.7 m^{-1}).

3.2.5 Adsorption isotherms

In Section 3.2.1.2 it was shown that the electrocoagulation removal of phosphates follows pseudo first-order kinetics and the rate-determining step would appear to be associated with the flocculation stage, represented by Step IV in Figure 3.2, rather than the coagulation phase that involves the destabilisation of the solution, Step III in Figure 3.2. Then, in Section 3.2.3 it was reported that the destabilisation of phosphate ions is highly dependent on the solution pH, which determines the primary mechanism involved in the removal of the phosphates. Step III in Figure 3.2 lists the possible mechanisms. However, the solution pH changes throughout the electrocoagulation process, consequently the removal of phosphates cannot be adequately described on the basis of a single steady-state mechanism.

As indicated by Step III in Figure 3.2, one of the mechanisms responsible for the removal of phosphates involves either the adsorption of the Al-hydroxy-phosphate complexes on positively charged aluminium hydrolysis products, or the adsorption of phosphate ions on the aluminium hydrolysis products, mainly the amorphous $Al(OH)_3$ [40]. The phenomenon of adsorption was first observed in 1773 by C. W. Scheele for

gases and subsequently in 1930 for solutions by Lowitz [115] and has become a widely used operation for purification of water and wastewater [116]. It involves the accumulation of substances at a surface and can occur at an interface between any two phases, such as liquid-liquid, gas-liquid, gas-solid or liquid-solid interfaces. With the intention of determining whether adsorption was the primary mechanism for the electrocoagulation removal of phosphates at pH values close to neutrality, adsorption isotherm studies were carried out on phosphate-containing solutions at an initial pH of 5.0 and analysed using three important two-parameter adsorption models, the Langmuir, Freundlich and Temkin models [117-119].

A number of studies have been reported in the literature on the adsorption isotherm models in order to describe the phosphate removal using several adsorbents [44, 120-122]. These studies were performed by varying the initial phosphate concentration in jar test experiments using a constant amount of adsorbent and measuring the amount of phosphates adsorbed at equilibrium. In the electrocoagulation process performed at constant current density, the adsorbent or coagulant is dosed to the solution in a continuous manner, generating an extremely dynamic system, thus the equilibrium is attained progressively upon increasing the adsorbent concentration. Consequently, it is not possible to carry out batch experiments to determine the equilibration time, as it is usually done in adsorption isotherm studies. However, it is reasonable to assume that in electrocoagulation, the process of adsorption is relatively rapid and does not represent the rate-determining step, which instead corresponds to the flocculation phase (Step IV in Figure 3.2), as reported in Section 3.2.1.2. This implies that at the end of the electrocoagulation process the equilibrium for the adsorbed phosphates has been achieved and, consequently, the concentration of phosphates at equilibrium, P_e, is equal to the final concentration of phosphates in solution, P_t. To support this assumption, the residual concentration of phosphate in solution was measured as a function of time immediately after stopping the coagulant dosing. It was observed that equilibrium was achieved in the first 2 min as there was no further change in the residual concentration of phosphates after that interval of time. In the present work the concentration of phosphates at equilibrium was measured after 15 min to ensure that the adsorption process achieved the state of equilibrium. The test solutions contained initial concentrations of phosphates ranging from 2.0 to 150.0 mg L^{-1} and 4.2×10^{-3} M NaCl at

pH 5.0. The experimental procedure and fitting models are provided in more detail in Sections 2.3.1.4 and 2.3.5.

Once equilibrium was reached, the adsorption capacity was obtained using a mass equilibrium equation which is expressed by Eq. 3.5.

$$q_e = \frac{(P_0 - P_e)V}{M} \qquad \textbf{Eq. 3.5}$$

Here, q_e is the amount of PO_4-P adsorbed at equilibrium per unit mass of adsorbent in mg g^{-1}, P_0 and P_e are the initial and the equilibrium concentrations of PO_4-P, respectively, in mg L^{-1}, *V* is the volume of the solution in L and M is the amount of adsorbent in g. The adsorption isotherm was constructed expressing the amount of PO_4-P adsorbed per unit weight of adsorbent, q_e, as a function of P_e, the concentration of PO_4-P remaining in solution. The composition of the electrogenerated adsorbent involved in the removal of phosphates is not known, since it may comprise $Al(OH)_3$ as well as other hydrolysis products of aluminium. Consequently, the amount of adsorbent generated, M, was considered as the amount of Al^{3+} ions generated by electrodissolution of the Al-2Mg electrode, m_{Al}, and was calculated using Faraday's law. According to Faraday's law, the amount of substance deposited or dissolved, *m*, by the same quantity of charge is proportional to the chemical equivalent weight (EW) of the material, Eq. 3.6.

$$m = \frac{It(EW)}{F} = \frac{ItW}{nF} \qquad \textbf{Eq. 3.6}$$

Here, *m* is the mass in g, *I* is the current in A, *t* is the time in s, *EW* is the gram equivalent weight of the material (or *W*/*n* where *W* is the gram atomic weight and *n* is the valency of dissolution) and *F* is Faraday's constant (96,485 C mol^{-1}). The evaluation of *m* is very simple for pure metals. However, it becomes difficult when the electrode is made up of an alloy. In the present work an aluminium-magnesium alloy was used. Since the experiments were carried out in galvanostatic mode, the potential varies and therefore it can be assumed that the anode oxidation does not occur selectively towards any of the components of the alloy [123]. In this case, the alloy composition needs to be taken into account and this was achieved using Eq. 3.7 [123, 124]:

$$m = m_{Al} + m_{Mg} = \frac{It}{F}\left(\frac{W_{Al}}{n_{Al}} f_{Al} + \frac{W_{Mg}}{n_{Mg}} f_{Mg}\right) \quad \textbf{Eq. 3.7}$$

In this analysis, W is the atomic weight, f is the mass fraction and n is the valence of the elements present in the alloy. It is common to include in the calculation only elements of the alloy above 1% by mass [123].

The literature on the electrocoagulation removal of pollutants using aluminium electrodes presents several works [39, 107, 125-132] attempting to fit the experimental data with adsorption isotherm models. In the present study three models were used, the Langmuir equation, the Freundlich equation and the Temkin equation since they find common use for describing isotherms for water and wastewater treatment applications [133]. The Langmuir equation was derived in the 1900s to describe the adsorption of gas molecules on a planar surface [134]. Later this model was extended to liquid systems involving species in solution. The model suggests that adsorption occurs by monolayer adsorption without interaction between the adsorbed molecules. Eq. 3.8 describes the Langmuir model,

$$q_e = \frac{q_m K_L P_e}{1 + K_L P_e} \quad \textbf{Eq. 3.8}$$

where q_m is the maximum sorption capacity in mg g^{-1} and K_L is a constant related to the affinity of the binding sites in L mg^{-1}.

On the other hand, the Freundlich model proposes multilayer adsorption with a heterogeneous energetic distribution of active sites accompanied by interactions between adsorbed species [135]. The Freundlich model is expressed by Eq. 3.9,

$$q_e = K_F P_e^{1/n} \quad \textbf{Eq. 3.9}$$

where K_F (mg g^{-1} L) and n (dimensionless) represent the Freundlich's temperature-dependent constants, characteristic for the system. It has been suggested that these constants are associated with the adsorption capacity (K_F) and intensity (n) [136].

Values of n > 1 represent favourable adsorption conditions and the smaller the values of 1/n the stronger is the adsorption bond. The greater values of K_F correspond to a greater capacity of the adsorbent.

Temkin and Pyzhev considered the effects of some indirect adsorbate/adsorbate interaction on adsorption isotherms and suggested that because of these interactions the heat of adsorption of all the molecules in the layer would decrease linearly with coverage [137]. The Temkin isotherm has been generally applied in the following form (Eq. 3.10):

$$q_e = \frac{RT}{b_T} \ln(K_T P_e) \qquad \textbf{Eq. 3.10}$$

where b_T is the Temkin constant related to heat of sorption in J mol^{-1}, K_T is the Temkin isotherm constant in L g^{-1}, R is the gas constant (8.314 J mol^{-1} K^{-1}), and T is the absolute temperature in K.

Figure 3.11 shows the amount of PO_4-P adsorbed at equilibrium per unit mass of Al^{3+} ions, q_e, as a function of the final concentration of phosphates, P_e. The experiments were carried out by varying the initial concentration of phosphates from 2.0 to 150.0 mg L^{-1} in solutions containing 4.2×10^{-3} M NaCl at an initial pH of 5.0 and at a temperature of 25 ± 1 ºC. Each experiment was performed in triplicate. The experimental data were fitted by a nonlinear regression, since the transformation of the data into a linear form may distort the experimental error or alter the relationship between the variables [138]. The nonlinear regression plot for the Langmuir, the Freundlich and the Temkin models (Eq. 3.8, Eq. 3.9 and Eq. 3.10, respectively) are displayed in Figure 3.11. R^2 was not used to test the applicability of the two isotherm models, since it is traditionally defined for linear and not for curved relationship [139] and is long known within the mathematical literature that it is an inadequate measure for the goodness of fit in nonlinear models [140]. The goodness of fit of the two models was instead tested using the adjusted R^2 value, which accounts for the degrees of freedom. The adjusted R^2 values and the parameters of the Langmuir, Freundlich and Temkin isotherms are listed in Table 3.4. Clearly, the Freundlich model gives a better fit than the Langmuir and Temkin isotherm for the adsorption of phosphates using the Al-2Mg electrode. As

reported in Table 3.4, the value of K_F is 146 (mg g^{-1}) (L mg^{-1}) and the parameter n is higher than 1, indicating favourable adsorption. This result suggests that adsorption is indeed the primary mechanism for the removal of phosphates at the conditions used in this study.

Georgantas and Grigoropoulou [44] reported that the adsorption of orthophosphates and metaphosphates using alum or aluminium hydroxide is best described by the Freundlich isotherm. Nitrate, another negatively charged pollutant, has been shown to be removed in electrocoagulation according to the Freundlich model [128]. In studying the adsorption properties of sand for phosphorus, Del Bubba *et al.* [141] reported that the Langmuir model is useful to describe adsorption phenomena, whereas the Freundlich model fitted well the phosphate removal even if precipitation, other than adsorption, occurs. Consequently, it is not surprising that the electrocoagulation removal of phosphates also follows the same adsorption model. This may be because the Freundlich equation, although empirical, implies that the affinity for the adsorption sites decreases exponentially with increasing saturation [142]. This assumption seems more realistic than a constant binding energy inherent in the Langmuir equation. As already outlined, the electrocoagulation process is extremely complex and it is reasonable to suppose a heterogeneous surface of the adsorbent and a probable interaction among the adsorbate, the phosphate ions or other particles present in the solution.

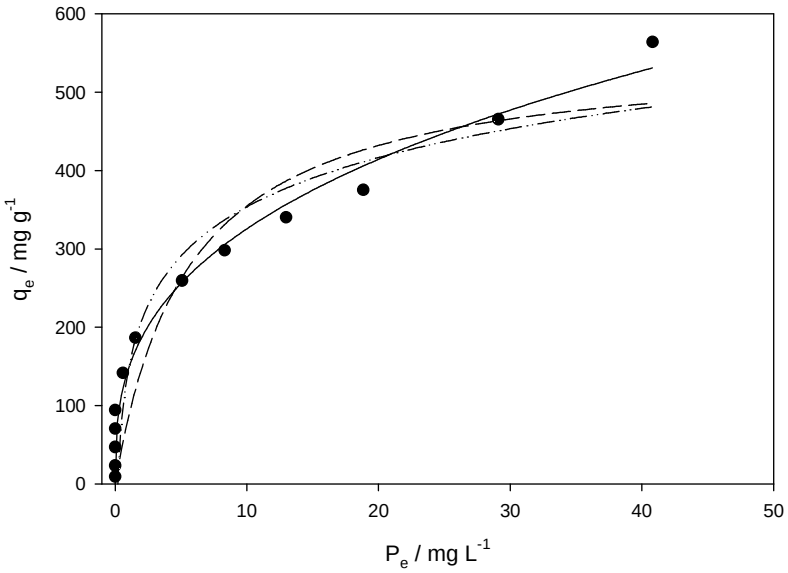

Figure 3.11: ● Experimental data, −−− Freundlich isotherm, − − − Langmuir isotherm and −·−·− Temkin isotherm fitting at 25 ± 1 ºC. (Anode/cathode = Al-2Mg/AISI 310, [PO_4-P] = 2.0 to 150.0 mg L^{-1}, [NaCl] = 4.2 × 10^{-3} M, pH = 5.0, j = 11.0 mA cm^{-2}, t = 30 min, SA/V = 11.7 m^{-1}).

Table 3.4: Langmuir, Freundlich and Temkin isotherm model constants and adjusted R^2 values.

Langmuir model		
K_L / L mg^{-1}	q_m / mg g^{-1}	Adjusted R^2
0.18 ± 0.08	552 ± 69	0.883
Freundlich model		
K_F / (mg g^{-1})(L mg^{-1})	n	Adjusted R^2
146 ± 22	2.9 ± 0.1	0.943
Temkin model		
K_T / L g^{-1}	B / J mol^{-1}	Adjusted R^2
5 ± 3	91 ± 14	0.911

3.2.6 The removal of phosphates from real samples

Given the positive results obtained for the removal of phosphates, the Al-2Mg electrode was used as an anode material to treat real samples obtained from two wastewater facilities. The samples were collected at the primary settlement areas and their conductivity levels are presented in Table 3.5. As shown in Table 3.5, the conductivity of the sample no. 1 was 0.32×10^{-3} S cm^{-1}, while for the sample no. 2 it was 1.00×10^{-3} S cm^{-1}.

Table 3.5: Conductivity levels for the real samples.

Sample no.	**κ / mS cm^{-1}**
1	0.32
2	1.00

The samples were used in electrocoagulation tests without any pre-treatment. Figure 3.12 shows the concentration of phosphates, P_t, plotted as a function of the electrocoagulation period for both samples. The current density was 4.2 mA cm^{-2} and the ratio of the surface area of the anode to the volume of solution, SA/V, was 13.0 m^{-1}. It is clear from Figure 3.12 that at the end of 15 min the phosphate ions are completely removed from both samples. The removal is relatively fast, indeed, after just 5 min, the concentration of phosphates is reduced by 73.3% and 91.3% for the sample no.1 and the sample no. 2, respectively.

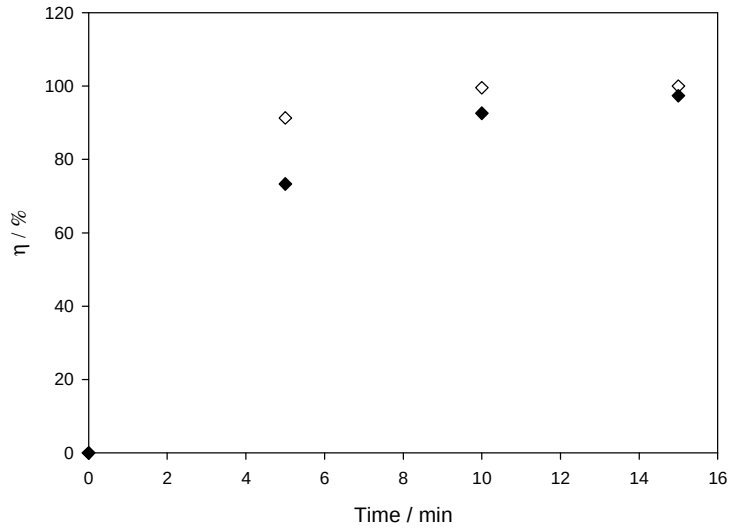

Time / min	**η / %**	
	sample no. 1	**sample no. 2**
0	0	0
5	73.3	91.3
10	92.6	BDL*
15	97.4	BDL*

*BDL = Below Detection Limit (Section 2.3.3).

Figure 3.12: Removal efficiency, η, plotted as a function of the electrocoagulation time in ◆ sample no. 1 and ◇ sample no. 2 (Table 3.5). (Anode/cathode = Al-2Mg/AISI 310, j = 4.2 mA cm^{-2}, SA/V = 13.0 m^{-1}).

Table 3.6 gives the observed rate constant, k_{obs}, for the data recorded with both samples shown in Figure 3.12. The high values of R^2 suggest that the removal of phosphates in real wastewater samples follows the pseudo first-order model, in good agreement with the data presented earlier. The values of k_{obs} were computed as 0.2440 and 0.5438 min^{-1} for the sample no. 1 and the sample no. 2, respectively.

Table 3.6: Pseudo first-order constant, k_{obs}, and R^2 values for the removal of phosphates from the real samples.

Sample no.	**k_{obs} / min^{-1}**	**R^2**
1	0.2444	0.997
2	0.5438	0.997

Although the removal of phosphates is rapid and complete for both samples, important differences were observed in terms of the anode potential. In Figure 3.13 the potentials recorded during the electrocoagulation experiments, shown in Figure 3.12, are presented as a function of the electrocoagulation period. An average value, $\overline{E}$, of about 1.31 V vs. SCE was recorded for the sample no. 1, while the average potential adopted in the sample no. 2 was considerably lower at 0.03 V vs. SCE. This difference is mainly due to the conductivity of the two samples. As reported in Table 3.5, the conductivity of the sample no. 2 is considerably higher. This is in good agreement with the results presented in Section 3.2.4 on the effect of the concentration of NaCl and, consequently, of the conductivity solution on the anode potential. It is clear that the treatment of a solution with conductivity levels similar to the sample no. 1 would have a strong impact on the energy consumption of the process.

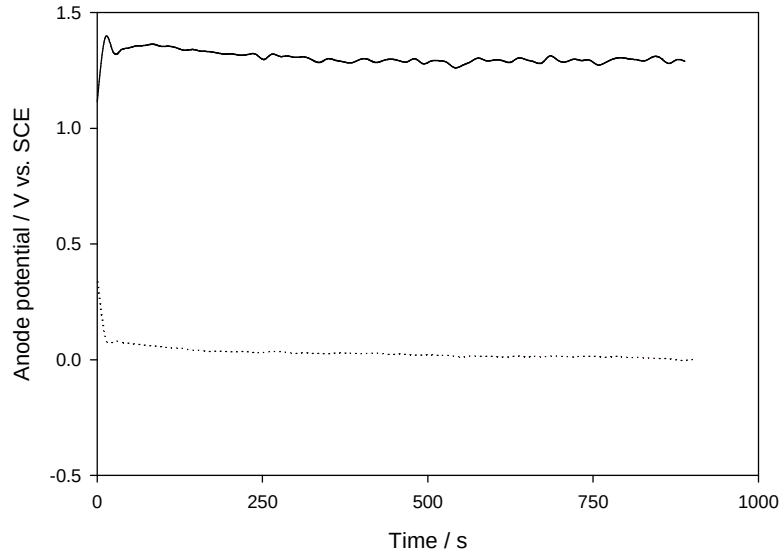

Sample no.	$\overline{E}$ / V vs. SCE
1	1.31
2	0.03

Figure 3.13: Variation of the anode potential as a function of the electrocoagulation period in −−− sample no. 1 and · · · sample no. 2 (Table 3.5). (Anode/cathode = Al-2Mg/AISI 310, j = 4.2 mA cm^{-2}, SA/V = 13.0 m^{-1}).

3.3 AISI 420 electrode

The chemical removal of phosphates is usually achieved by the addition of salts of di- and tri-valent metal ions. Iron(II), iron(III) and aluminium(III) are most frequently used in wastewater treatment because they form easily settleable flocs within short times [143]. When iron salts are added to the solution, the metal ions react with the water molecules to form hydrolysis products, as already outlined for aluminium ions in Section 3.2 [63, 144, 145]. As postulated by Brønsted more than 60 years ago, the hexaaquoiron(II) complex ion participates in a series of consecutive proton transfer reactions, which are illustrated in Figure 3.14.

The hydrolysis products listed in Figure 3.14 are all known and identified, however the intermediate steps are frequently complicated. Furthermore, the formation of polymeric species has also been reported especially in solutions of high metal concentrations, similarly to the case of Al^{3+} hydrolysis products [113].

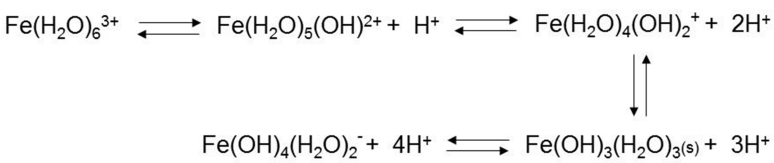

Figure 3.14: Monomeric iron (III) hydrolysis products [113].

It has been suggested that for iron(II) salts the removal of phosphates depends on its conversion to iron(III), since iron(III) complexes show better flocculation characteristics [143], whereas iron(II) appears as finely dispersed colloids that can be washed out to the effluent [146, 147]. The oxidation of Fe^{2+} ions to the Fe^{3+} form is dependent mainly on pH and oxygen concentration [148]. Indeed, Stumm and Lee [149] demonstrated that at pH values higher than 5.0 the oxidation rate is first order with respect to both the concentrations of Fe^{2+} and dissolved oxygen and second order in the solution pH ($[OH^-]$), as shown in Eq. 3.11:

$$-\frac{\mathrm{dFe(II)}}{\mathrm{d}t} = k[\mathrm{Fe(II)}][\mathrm{OH}^-]^2\, p_{O_2} \qquad \textbf{Eq. 3.11}$$

Here, k is the rate constant in $min^{-1}\ atm^{-1}\ L^2\ M^{-2}$, Fe(II) is the concentration of Fe^{2+} ions in M, OH^- is the concentration of hydroxyl ions in M and p_{O_2} is the partial pressure of oxygen in atm. Leprince *et al.* [145] pointed out that appreciable differences exist between the chemistry of iron and aluminium ions in solution. In particular, the hydrolysis of iron is more rapid and, consequently, more difficult to control [150]. Despite these differences, it has been suggested that a similar mechanism is involved in the removal of phosphates using both iron and aluminium salts [41, 48, 151]. As outlined in Section 3.1, the chemical reactions which take place between phosphates and, in this case, ferric ions in wastewater are very complex and result in the formation of Fe-hydroxo-phosphate complexes, $Fe(OH)_{3-x}(PO_4)_x$ [151]. According to SEM analysis and a mathematical chemical precipitation model developed by Fytianos *et al.* [152], the main precipitating species depends on the molar ratio of phosphates to the iron salts. In particular, at a molar ratio, Fe:P > 1:1, a solid phase of $Fe_{2.5}PO_4(OH)_{4.5}$ was identified. Similarly to the removal of phosphate by Al^{3+} salts presented in Section 3.2, the main mechanisms involved in the removal of phosphates in the presence of Fe^{3+} salts are [40]:

- Adsorption of phosphate ions on the Fe^{3+} hydrolysis products, mainly amorphous $Fe(OH)_3$;
- Adsorption of the Fe-hydroxo-phosphate complexes onto positively charged Fe^{3+} hydrolysis species;
- Incorporation of phosphate ions in the precipitation of Fe-hydroxo-complexes and Fe^{3+} hydrolysis products.

It can be reasonably assumed that in the electrocoagulation removal of phosphates a similar mechanism exists [49]. However, the process may be somewhat different since different conditions develop in the chemical and the electrochemical systems. Figure 3.15 shows a simplified model for the removal of phosphates when iron based electrodes are used. Unlike the scheme presented in Figure 3.2 for aluminium electrodes, a further step, Step II, is added. This step is connected with the oxidation of Fe^{2+} ions to Fe^{3+} due to the dissolved oxygen. As reported previously in Eq. 3.11, this reaction is strongly dependent on the solution pH. Several studies have indeed reported that iron dissolves from the anode as Fe^{2+} [147, 153, 154].

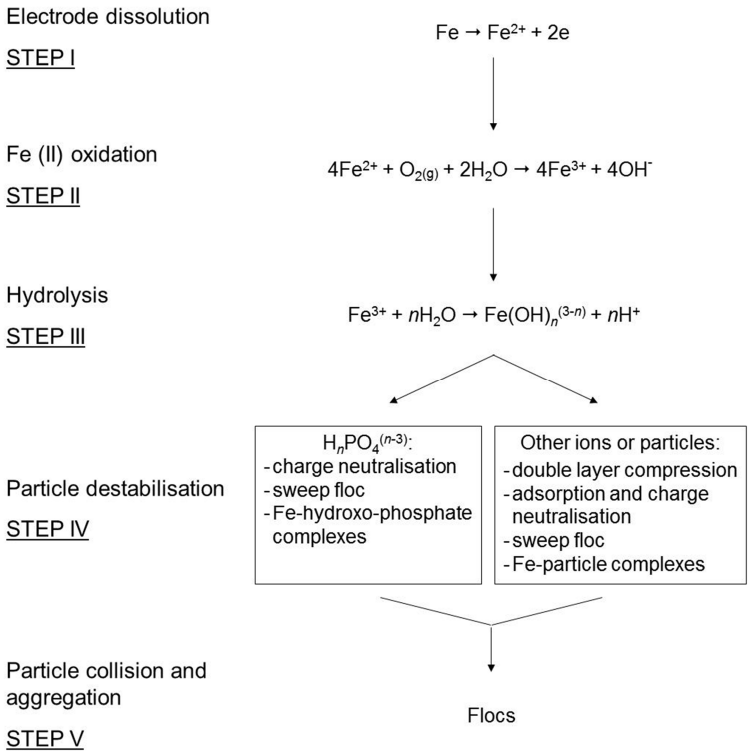

Figure 3.15: Simplified model for the removal of phosphates in electrocoagulation using stainless steel electrodes.

In this section the removal efficiency of phosphates using stainless steel AISI 420 (Fe86.7/Cr13.0/C0.3) as the anode material is presented. The removal performances were tested by varying the operational parameters, such as the initial concentration of phosphates, current density, initial pH and supporting electrolyte concentration. Furthermore, the speciation of iron dissolved from the anode was determined using, for the first time, an electrochemical method and the kinetics of phosphate removal was investigated.

3.3.1 Iron speciation in electrocoagulation

The electrochemical oxidation of iron based anodes, such as the stainless steel AISI 420 used in the present research, can result in the generation of ferrous (Fe^{2+}) or ferric (Fe^{3+}) ions, according to Eq. 3.12 and Eq. 3.13.

$$Fe_{(s)} \rightarrow Fe^{2+} + 2e^{-} \qquad E^0 = 0.44 \text{ V vs. SHE} \qquad \textbf{Eq. 3.12}$$

$$Fe_{(s)} \rightarrow Fe^{3+} + 3e^{-} \qquad E^0 = 0.037 \text{ V vs. SHE} \qquad \textbf{Eq. 3.13}$$

In the literature there is no general agreement on the species of iron that are produced at the anode in electrocoagulation applications. Some studies [155-157] report that Fe(II) is produced and then it hydrolyses to form insoluble hydroxide species, $Fe(OH)_2$. Other works [93, 147, 157, 158] claim that the dissolution of Fe(II) at the anode is followed by its oxidation to Fe(III) by dissolved oxygen. Conversely, Fe(III) has been reported as the iron species produced at the anode [26, 90, 159, 160]. In the electrocoagulation process it is crucial to clearly establish what iron species is dissolved. This information affects the number of electrons that are involved in the anode dissolution and, consequently, the total amount of coagulant generated and the consumption of the electrode. These parameters are important to determine the efficiency and the economic feasibility of the electrocoagulation process. Furthermore, as previously reported in Section 3.3, it has been suggested that Fe(III), rather than Fe(II), and its hydrolysis products are responsible for the removal of particles and pollutants from wastewater [143, 146, 147, 150].

Some attempts have been made to differentiate between Fe(II) and Fe(III). For example, Lakshmanan *et al.* [153] demonstrated that Fe^{2+} ions were produced at the anode. They compared the total iron measured by atomic absorption spectroscopy, AAS, to the theoretical total iron generated according to Faraday's law (Eq. 3.6) for ferrous (n = 2) and ferric (n = 3) iron. Their experimental data agreed with a two-electron transfer at all pH values investigated. A similar approach was used by Bagga *et al.* [147] to determine whether Fe(II) or Fe(III) was generated in the pre-treatment of surface water prior to microfiltration. However, this approach suffers from limitations, particularly as chemical dissolution of iron occurs [96, 154] or other reactions, such as oxygen evolution, take place at the anode [33, 154]. On the other hand, Sasson *et al.* [154] showed that Fe(II) was released from the iron anode at pH values between 5.0 and 9.0. In this study, 1,10-phenanthroline was used in order to complex the Fe^{2+} ions and prevent their oxidation. Subsequently, the concentration of Fe(II) was determined by UV-Vis spectroscopy. Although this approach is simple to operate, it may give inaccurate results since the addition of 1,10-phenanthroline only delays the oxidation of Fe(II) to Fe(III) [154]. As shown in Section 3.3, the oxidation reaction is extremely rapid especially at high pH values. Moreover, it has been reported that the determination of Fe(II) with 1,10-phenanthroline in the presence of Fe(III) gives rise to less reliable results owing to the redox processes induced by the chelating reagent on the Fe(II)-Fe(III) system [161, 162]. Indeed, the presence of 1,10-phenanthroline seems to promote the reduction of Fe(III) and the formation of the corresponding coloured iron(II) chelate compound, according to Eq. 3.14:

$$Fe^{3+} + 3(phen) + e^{-} \rightarrow [Fe(phen)_3]^{2+} \qquad \textbf{Eq. 3.14}$$

Furthermore, it has been reported that the presence of strong complexing agents, such as phosphates, might interfere with the spectrophotometric determination of iron with 1,10-phenanthroline [163, 164].

With the aim of determining whether the Fe(II) or Fe(III) ions were dissolved from the anode at the conditions used in the present study, an electrochemical technique was employed to simultaneously detect the concentration of ferrous and ferric species using a rotating disk electrode, RDE. This technique was proposed by Jin and Botte [165] and

has the advantage of being simple, rapid and does not require any pre-treatment procedures, expensive reagents or instruments. It is based on the reduction-oxidation reaction of Fe(III) and Fe(II):

$$Fe^{3+} + e^- \rightarrow Fe^{2+} \qquad E^0 = 0.77 \text{ V vs. SHE} \qquad \textbf{Eq. 3.15}$$

This generates a sigmoidal wave when rotating disk voltammetry, RDV, is used. The height of the sigmoidal wave which corresponds to the limiting current, I_L, is described by the Levich equation, Eq. 3.16.

$$I_L = 0.62nFAD^{2/3}\omega^{1/2}\nu^{-1/6}C^{\infty} \qquad \textbf{Eq. 3.16}$$

Here, n is the number of electrons transferred in the half reaction, F is Faraday's constant (96,485.34 C mol^{-1}), A is the surface area of the electrode (cm^2), D is the diffusion coefficient (cm^2 s^{-1}), ω is the angular velocity of the rotating electrode (rad s^{-1}), ν is the kinematic viscosity of the solution (cm^2 s^{-1}) and C^{∞} is the bulk concentration of the species (mol cm^{-3}). Under steady state conditions, the limiting currents, I_L, are measured and related to the concentrations of the cations present in solution. In particular, for the determination of the iron species, it has been found that the upper limiting current, I_{UL}, is related to the analytical signal of Fe(II) ions, while the lower limiting current, I_{LL}, is proportional to the analytical signal of Fe(III) ions.

Figure 3.16(a) shows representative voltammograms recorded in 1.0 M H_2SO_4 solutions containing 20.0×10^{-3} M Fe(II) or 80.0×10^{-3} M Fe(III), while in Figure 3.16 (b) the voltammogram recorded in a solution containing a mixture of 20.0×10^{-3} M Fe(II) and 80.0×10^{-3} M Fe(III) is compared with the data recorded in 20.0×10^{-3} M Fe(II) and in 80.0×10^{-3} M Fe(III). These data were recorded by scanning the potential from -0.2 to 1.2 V vs. SCE at 1000 rpm at a scan rate of 50 mV s^{-1}. The upper limiting current, I_{UL}, was monitored at 1.0 V vs. SCE and the lower limiting current, I_{LL}, was obtained at -0.1 V vs. SCE. Figure 3.16(c) and (d) provide the calibration curves for Fe(II) and Fe(III) generated from the single solutions of the ions and from the mixtures, respectively. The slopes of the curves were computed as 4.84×10^{-5} and 4.87×10^{-5} A mM^{-1} for Fe(II) in the single and in the mixture solutions, respectively, and -4.53×10^{-5}

and -4.39 × 10^{-5} A mM^{-1} for Fe(III) in the single and in the mixture solutions, respectively. It is apparent that the values of the slope computed in single solutions are consistent with those observed in the mixture. Consequently, it is clear from these data that the concentration of each of the iron species can be determined simultaneously.

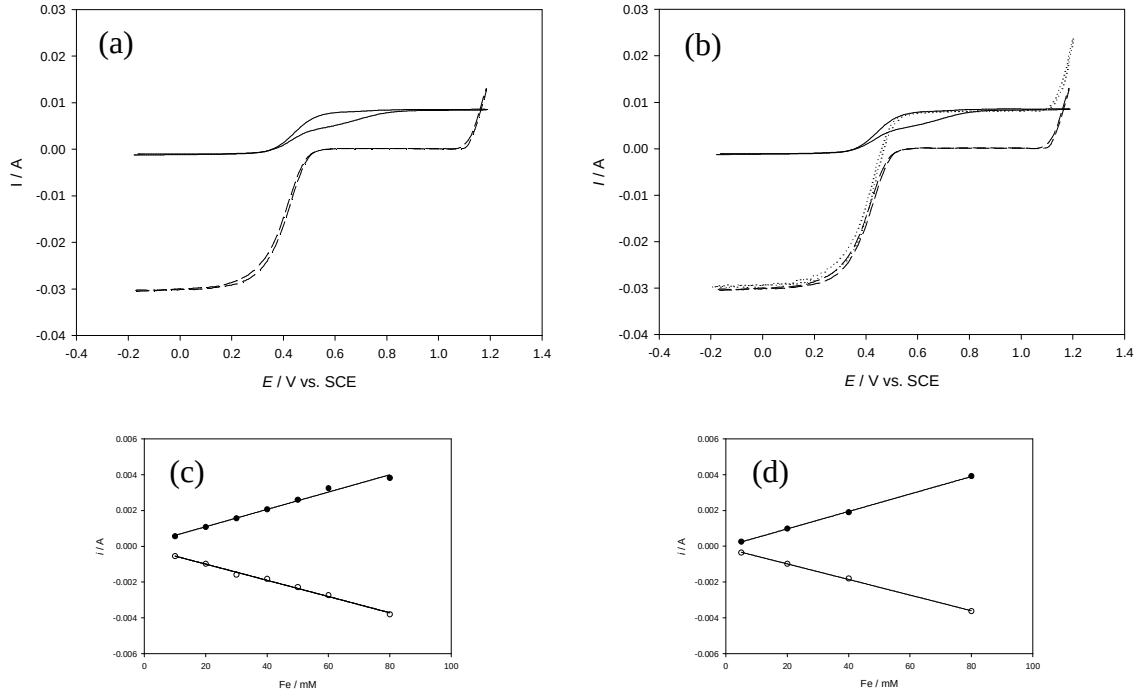

Figure 3.16: Voltammograms recorded in 1.0 M H_2SO_4 containing: (a) −−− 20.0 × 10^{-3} M Fe(II), − − − 80.0 × 10^{-3} M Fe(III) and (b) · · · a mixture of 20.0 × 10^{-3} M Fe(II) and 80.0 × 10^{-3} M Fe(III). The potential was scanned from -0.2 to 1.2 V vs. SCE at a scan rate of 50 mV s^{-1} and the rotation of the disk electrode was set at 1000 rpm. Calibration curves for ● Fe(II) and ○ Fe(III) plotted from (c) the single solutions of Fe(II) and Fe(III) and (d) the mixtures of Fe(II) and Fe(III).

The Levich equation presented in Eq. 3.16 is valid under steady-state and mass transfer limited conditions [166]. In the present study, a steady-state condition was achieved after the third cycle. Furthermore, linear plots were obtained when the limiting current, I_L, was plotted as a function of the square root of the rotation speed, $\omega^{½}$, indicating that the system was under mass transport control.

In Figure 3.17(a) typical voltammograms recorded in a 4.2 × 10^{-3} M NaCl solution collected at the end of an electrocoagulation test are shown. The voltammograms were recorded at a scan rate of 10 mV s^{-1} and at 500, 1000, 1500, 2000, 2500, 3000 and 4000 rpm. The upper and lower limiting currents, I_{UL} and I_{LL}, were plotted as a function of the

square root of the rotation speed, $\omega^{½}$, and these plots are shown in Figure 3.17(b) and (c). Linear plots, with correlation coefficients between 0.999 and 0.989, were obtained in both cases in good agreement with the Levich equation (Eq. 3.16).

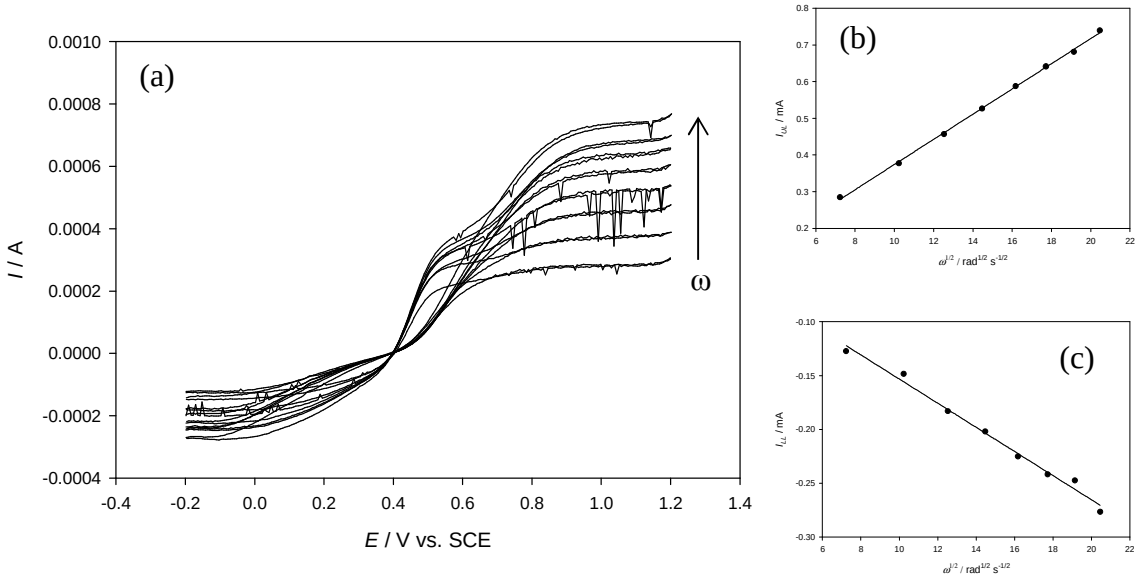

Figure 3.17: (a) Voltammograms recorded in a 4.2 × 10^{-3} M NaCl solution collected at the end of an electrocoagulation test at 500, 1000, 1500, 2000, 2500, 3000, 3500 and 4000 rpm. The potential was scanned from -0.2 to 1.2 V vs. SCE at a scan rate of 10 mV s^{-1}. Levich plots for (b) the upper and (c) lower limiting currents, I_{UL} and I_{LL}, read at 1.1 and -0.1 V vs. SCE, respectively, from the voltammograms.

To determine the oxidation state of the iron species generated at the AISI 420 anode during electrocoagulation, the total iron concentration, computed as the sum of the concentrations of Fe^{2+} and Fe^{3+} ions measured using this electrochemical technique, was compared with the theoretical iron concentration according to Faraday's law. Firstly, the concentration of Fe^{2+} and Fe^{3+} ions were measured by a standard addition method at the end of the electrocoagulation tests carried out in 4.2 × 10^{-3} M NaCl without phosphates for 45 min. The initial pH of the solutions was 5.0 and the current density was fixed at 11.0 mA cm^{-2}. Full experimental details are given in Section 2.3.1.5. Figure 3.18(a) shows the voltammograms of a representative solution and the relative stepwise standard addition of the aliquots. Typical standard addition plots for Fe(II) and Fe(III) are presented in Figure 3.18(b) and (c), indicating very good linearity.

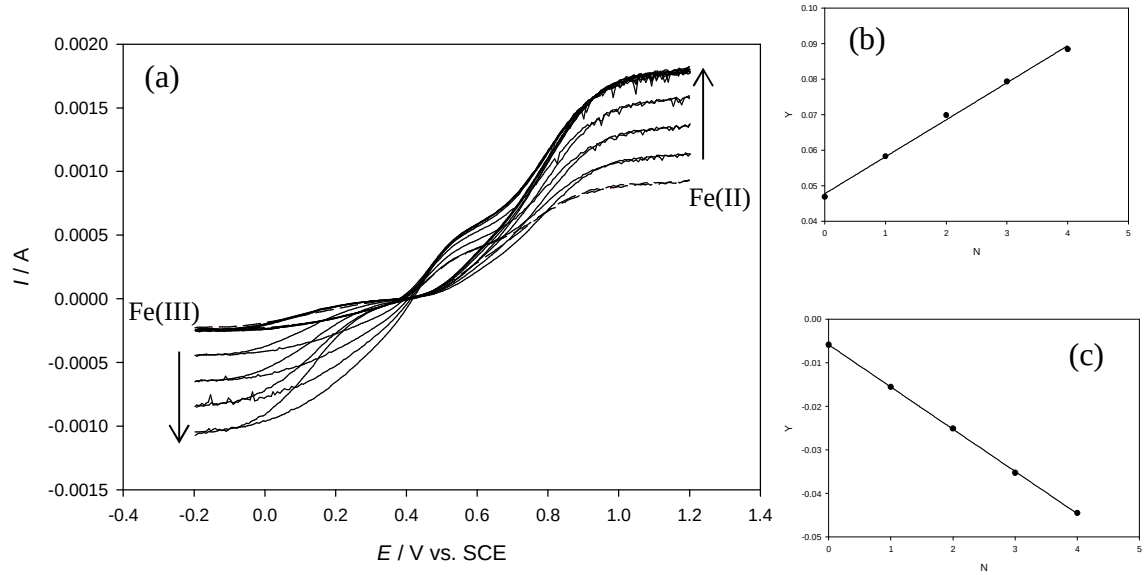

Figure 3.18: (a) Voltammograms of a solution recorded at the end of the electrocoagulation test in 4.2×10^{-3} M NaCl. The potential was scanned from -0.2 to 1.2 V vs. SCE at a scan rate of 10 mV s^{-1} and the rotation of the disk electrode was set at 3000 rpm. Standard addition plots for (b) Fe(II) and (c) Fe(III).
Fe(II): $y = 0.0477 + 0.0104\ x$, $R^2 = 0.997$.
Fe(III): $y = 0.00584 + 0.00970\ x$, $R^2 = 0.999$.

In Table 3.7 the concentrations of Fe(II) and Fe(III) obtained by this standard addition method are shown and compared to the theoretical total ion concentration. The theoretical iron concentrations were obtained using Faraday's law by considering a two- or three-electron transfer reaction. Taking into account the composition of the stainless steel AISI 420 electrode, the amount of iron is expressed by Eq. 3.17.

$$m_{Fe} = \left(\frac{It}{F}\right)\left(\frac{W_{Fe}}{n_{Fe}}\ f_{Fe}\right) \qquad \textbf{Eq. 3.17}$$

In this analysis, m_{Fe} is the mass of iron in g, I is the current in A, t is the time in seconds, F is Faraday's constant (96,485 C mol^{-1}), W_{Fe} is the atomic weight of iron in g mol^{-1}, n_{Fe} is the valence of iron ($n = 2$ or $n = 3$) and f_{Fe} is the mass fraction of iron in the alloy. By comparing the concentrations obtained using the experimental and theoretical analyses from Table 3.7, it is clear that better agreement is achieved using the Fe(II) species. This suggests that Fe(II) ions are generated at a pH of 5.0 and at a current density of 11.0 mA cm^{-2} on oxidation of the AISI 420 electrode.

Table 3.7: Concentrations of the experimental $Fe^{2+}$and Fe^{3+} ions, measured using the standard addition method, the experimental total Fe, computed as the sum of Fe(II) and Fe(III) and the theoretical total Fe, computed according to Faraday's law in Eq. 3.17. Each measurement was performed in triplicate (n = 3).

Experimental			**Theoretical (from Faraday's law)**	
Fe(II) / mM	**Fe(III) / mM**	**Fe_{TOT} / mM**	**Fe_{TOT} / mM**	
			n = 2 (Eq. 3.17)	*n* = 3 (Eq. 3.17)
11.8 ± 0.8	1.60 ± 0.03	13.4 ± 0.8	13.86	9.24

3.3.2 The effect of the initial concentration of PO_4-P

3.3.2.1 The efficiency of removal

The effect of the initial concentration of phosphate on the removal efficiency of solutions treated with the stainless steel AISI 420 electrode was evaluated by monitoring the residual concentration of PO_4-P as a function of time in solutions containing different initial concentrations. Figure 3.19 shows the normalised concentrations, P_t/P_o, obtained as a function of the electrocoagulation period for solutions containing 20.0, 60.0 and 150.0 mg L^{-1} of PO_4-P. The electrocoagulation tests were carried out for 60 min using 4.2×10^{-3} M NaCl as a supporting electrolyte, the initial pH of the solutions was 5.0 and the applied current density was 11.0 mA cm^{-2}. The results are further summarised in Table 3.8 where the residual concentration of phosphates and the removal efficiency are presented as a function of the initial phosphate concentrations. As evident from Figure 3.19 and Table 3.8, the removal efficiency of phosphates decreases on increasing the initial concentration. After 20 min the removal efficiency was calculated as 75%, 57% and 40.5% for initial concentrations of phosphates of 20.0, 60.0 and 150.0 mg L^{-1}, respectively.

These results are consistent with the studies reported in the literature. For example, İrdemez *et al.* [34] studied the effect of the initial concentration of phosphates on the removal efficiency from wastewater using iron plate electrodes. After 20 min the complete removal of phosphate was achieved with initial concentrations of 25 and 50 mg L^{-1} PO_4-P, while a removal efficiency of 95% and 75% was reached with 100 and 150 mg L^{-1} PO_4-P, respectively. Also, Behbahani *et al.* [167] observed a decrease in the removal efficiency on increasing the initial concentration of phosphates. For

example, after 20 min of electrocoagulation with iron electrodes at an initial pH of 7.0, 8.33 mA cm^{-2} and a SA/V ratio of 12 m^{-1}, a removal efficiency of 100% was observed for initial concentrations of 25 and 100 mg L^{-1} PO_4-P, while the efficiency was lowered to 63.3% for an initial concentration of 400 mg L^{-1} PO_4-P. A similar trend has been reported for the electrochemical removal of several pollutants [34, 52-60] and this was also observed in Section 3.2.1.1 for the removal efficiency of phosphates with the Al-2Mg electrode. There is a general consensus that this is the result of a low coagulant to pollutant ratio at high initial concentrations of pollutants, which is inadequate to bring about an overall destabilisation of the solution.

Although the efficiency of phosphate removal declines with increasing initial concentrations of phosphates, a greater amount of phosphate is removed at the higher concentration, as shown in Table 3.8. This was also observed with the Al-2Mg electrode in Section 3.2.1.1. A similar effect was reported by Zheng *et al.* [168] on studying the removal of phosphates from human urine with iron electrodes. The removal efficiency decreased with increasing urine dosage, however the amount of phosphates removed increased.

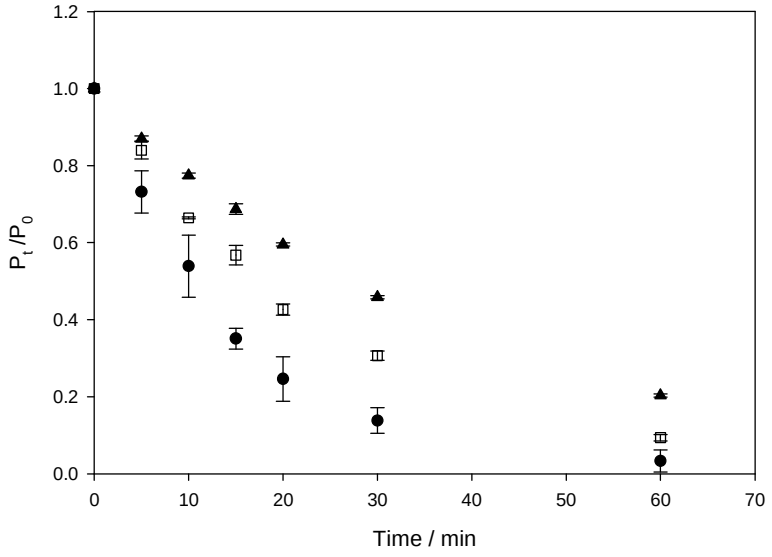

Figure 3.19: Plot of normalised variation of the concentration of phosphates, P_t/P_0, as a function of time in solutions containing initial concentrations, P_0, of ● 20.0 mg L^{-1}, □ 60.0 mg L^{-1} and ▲ 150.0 mg L^{-1} PO_4-P. (Anode/cathode = AISI 420/AISI 310, [NaCl] = 4.2×10^{-3} M, pH = 5.0, j = 11.0 mA cm^{-2}, SA/V = 10.5 m^{-1}).

Table 3.8: Residual concentration of phosphates, P_t, and removal efficiency, η, for different initial concentrations of PO_4-P. Each experiment was performed in triplicate (n = 3).

Time	$\mathbf{P_t}$	$\boldsymbol{\eta}$	$\mathbf{P_t}$	$\boldsymbol{\eta}$	$\mathbf{P_t}$	$\boldsymbol{\eta}$
/ min	**/ mg L^{-1}**	**/ %**	**/ mg L^{-1}**	**/ %**	**/ mg L^{-1}**	**/ %**
0	20.0	0	60.0	0	150.0	0
5	15 ± 1	27 ± 5	50 ± 1	16 ± 2	131 ± 1	13 ± 1
10	11 ± 2	46 ± 8	39.9 ± 0.2	33.5 ± 0.3	116 ± 1	23 ± 1
15	7.0 ± 0.5	65 ± 3	34 ± 2	43 ± 3	103 ± 2	31 ± 1
20	5 ± 1	75 ± 6	26 ± 1	57 ± 1	89 ± 1	40.5 ± 0.4
30	2.8 ± 0.7	86 ± 3	18.4 ± 0.7	69 ± 1	69 ± 0.7	54.2 ± 0.4
60	0.7 ± 0.6	97 ± 3	5.6 ± 0.5	90.6 ± 0.8	30 ± 0.7	79.7 ± 0.4

3.3.2.2 The rate constant for the removal of phosphates

In Section 3.2.1.2 it has been shown that, in a simplified model, the removal of phosphates using the Al-2Mg electrode comprises four steps (Figure 3.2) and the last step, Step IV, is the rate-determining step for the removal process. This step involves the phosphate ions. As shown in Section 3.2.1.2, the removal of phosphates is best described by a pseudo first-order reaction. However with the AISI 420 electrode, an additional step is needed to be considered. Indeed, as shown in Figure 3.15 by Step II and as has been reported in Section 3.3.1, the dissolution of iron from the anode generates the Fe^{2+} ions. This species is subsequently oxidised to Fe^{3+} which has been identified as the iron species responsible for the removal of particles or pollutants in solution [143, 147, 150, 169]. Considering this further step, the kinetics for the removal of phosphate using the AISI 420 electrode can be described by Eq. 3.18.

$$-\frac{\mathrm{d}[\mathrm{P}]}{\mathrm{d}t} = k[\mathrm{Fe(III)}][\mathrm{P}]^{x}\left[\mathrm{Fe(OH)}_{n}^{(3-n)}\right]^{y} \qquad \textbf{Eq. 3.18}$$

Here, P is the concentration of phosphate, Fe(III) is the concentration of Fe^{3+} ions resulting from the oxidation of Fe^{2+} ions, $Fe(OH)_n^{(3-n)}$ is the concentration of the hydrolysis products of Fe^{3+} ions, k is the rate constant and x and y are the partial orders of the reaction. As shown in Eq. 3.11, the rate of Fe^{2+} oxidation increases sharply with increasing pH. Morgan and Lahv [170] demonstrated that in oxygen saturated solutions and at a pH between 5.0 and 8.0, Fe^{2+} is readily oxidised to Fe^{3+}. Furthermore, Sasson *et al.* [154] and Lakshmanan *et al.* [153] observed complete oxidation of Fe(II) during

electrocoagulation operated at pH > 7.0. In the present research the experiments were carried out at an initial pH of 5.0 and, as will be shown in Section 3.3.4, the pH increases sharply as the electrocoagulation reactions proceed. As in the case of the Al-2Mg electrode in Section 3.2.1.2, it can be assumed that the production and the consumption rates of the hydrolysis products of iron are equal. Consequently, the concentrations of Fe^{3+} and the hydrolysis products of iron, $Fe(OH)_n^{(3-n)}$, can be considered constant and Eq. 3.18 can be simplified as:

$$-\frac{d[P]}{dt} = k_{obs}[P]^x \qquad \textbf{Eq. 3.19}$$

Here, k_{obs} is the observed rate constant and x can be measured experimentally. In this approximation the rate constant reflects the contribution of several reactions, involving both the coagulation and the flocculation phases (Figure 3.15).

To determine the order of the coefficient x in Eq. 3.19, the data shown in Figure 3.19 were fitted to pseudo first (x = 1) and pseudo second (x = 2) order models and the R^2 value was used to attest the goodness of the fit. Similarly to the Al-2Mg electrode, a better fit was obtained for the pseudo first-order kinetics, as shown in Table 3.9. To fit the experimental data to Eq. 3.19, the logarithm of (P_t/P_0) was plotted as a function of time and these plots are shown in Figure 3.20. The values of the observed rate constant, k_{obs}, obtained as the slope of the linear regression analysis, are presented in Table 3.9. As already observed in Section 3.2.1.2 for the Al-2Mg electrode, the values of the observed rate constant, k_{obs}, for the removal of phosphates decrease with increasing initial concentrations. For example, k_{obs} varies from 0.0600 min^{-1} for 20.0 mg L^{-1} of PO_4-P to 0.0263 min^{-1} for 150.0 mg L^{-1} of PO_4-P. These values are clearly lower than those found for the Al-2Mg electrode in Table 3.2.

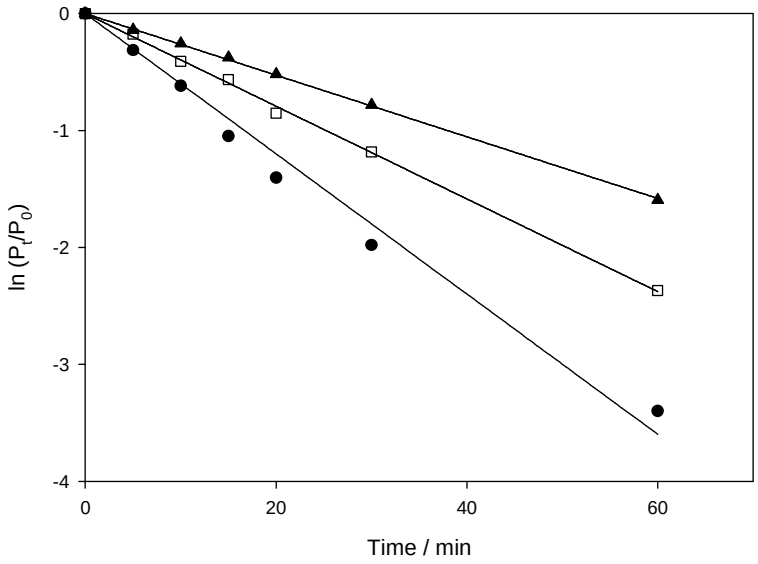

Figure 3.20: Plot of kinetics of phosphate removal at different initial concentrations of phosphates, P_0: ● 20.0 mg L^{-1}, □ 60.0 mg L^{-1} and ▲ 150.0 mg L^{-1} PO_4-P. (Anode/cathode = AISI 420/AISI 310, [NaCl] = 4.2×10^{-3} M, pH = 5.0, j = 11.0 mA cm^{-2}, SA/V = 10.5 m^{-1}).

Table 3.9: Rate constant, k_{obs}, and R^2 values for pseudo first- and second-order kinetics.

Initial concentration, P_0 / mg L^{-1}	**Pseudo first-order kinetics** $\ln \frac{P_t}{P_0} = -k_{obs}t$		**Pseudo second-order kinetics** $\frac{1}{P_t} = k_{obs}t + \frac{1}{P_0}$	
	k_{obs} / min^{-1}	**R^2**	**k_{obs} / min^{-1}**	**R^2**
20.0	0.0600	0.983	0.0244	0.905
60.0	0.0396	0.999	0.0027	0.918
150.0	0.0263	0.999	0.0004	0.949

3.3.3 The effect of the current density

The effect of the applied current density was studied using a current density of 2.6 and 11 mA cm^{-2} for the electrocoagulation of solutions containing 60.0 mg L^{-1} of phosphates. The initial pH of the solutions was 5.0 and the electrolysis time was 30 min. Figure 3.21 shows the concentration of phosphates, P_t, plotted as a function of the electrolysis time at current densities of 2.6 and 11.0 mA cm^{-2} in solutions containing 60.0 mg L^{-1} of phosphates. As the current density increases from 2.6 to 11.0 mA cm^{-2}, the removal efficiency, after 30 min, increases significantly from 46% to 69%. This

result is clearly related to the low amount of iron dissolved from the anode at the lower current density.

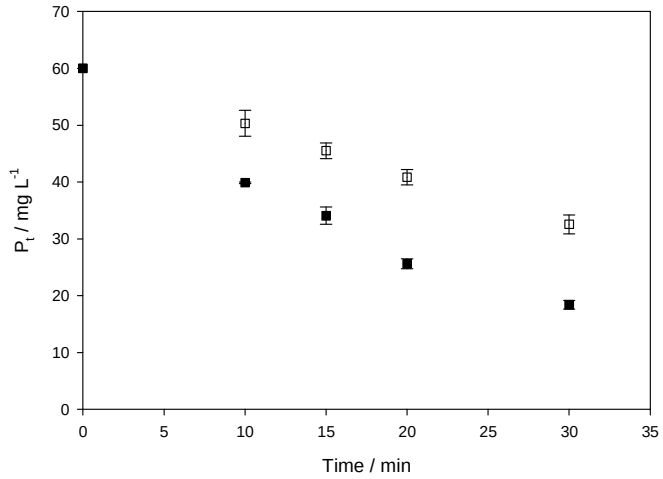

Time / min	P_t / mg L^{-1}	
	2.6 mA cm^{-2}	**11.0 mA cm^{-2}**
0	60.0	60.0
10	50 ± 2	39.9 ± 0.2
15	46 ± 1	34 ± 2
20	41 ± 1	26 ± 1
30	32.6 ± 1.7	18.4 ± 0.7

Figure 3.21: Graph illustrating the variation of the concentration of phosphates, P_t, as a function of the electrocoagulation time in solutions containing initial concentration, P_0, of 60.0 mg L^{-1} PO_4-P at different current densities: □ 2.6 mA cm^{-2} and ■ 11.0 mA cm^{-2}. Each experiment was performed in triplicate (n = 3). (Anode/cathode = AISI 420/AISI 310, [NaCl] = 4.2×10^{-3} M, pH = 5.0, SA/V = 10.5 m^{-1}).

The effect of the applied current density was also investigated by comparing the rate constant, k_{obs}, for the electrocoagulation of solutions containing 20.0, 60.0 and 150.0 mg L^{-1} of phosphate using a current density of 2.6 mA cm^{-2}. The initial pH of the solutions was 5.0 and the electrolysis time was 30 min. The plots obtained by plotting the logarithm of (P_t/P_0) as a function of time for the three phosphate-containing solutions are shown in Figure 3.22. A linear regression analysis was used to fit the experimental data and to provide the values of the observed rate constants, k_{obs}. As can be seen from Figure 3.22, high values of R^2 were obtained for the three different initial concentrations of phosphates, indicating that the data fit well the proposed pseudo first-order model kinetics. In Section 3.3.2.2 it has been shown that the same kinetics model was valid for the Al-Mg alloys using a current density of 11.0 mA cm^{-2}.

It is evident from Figure 3.22 that the values of k_{obs} decrease with increasing initial concentrations of phosphate. The computed k_{obs} is 0.0257 min^{-1} for initial phosphate concentration of 20.0 mg L^{-1} while it is reduced to 0.0122 min^{-1} when the initial concentration is 150.0 mg L^{-1}. The same trend was observed in Section 3.3.2.2 for an

applied current density of 11.0 mA cm^{-2}. These results can be explained by the low coagulant to phosphate ratio when higher concentrations of phosphate are used.

Similarly to the Al-2Mg electrode in Section 3.2.2, by comparing the values of the k_{obs} obtained at 11.0 and 2.6 mA cm^{-2} in Figure 3.20 and Figure 3.22, it is evident that low current densities reduce the rate of phosphate removal. Accordingly, k_{obs} decreases from 0.0369 min^{-1} to 0.0196 min^{-1} for current densities of 11.0 and 2.6 mA cm^{-2}, respectively.

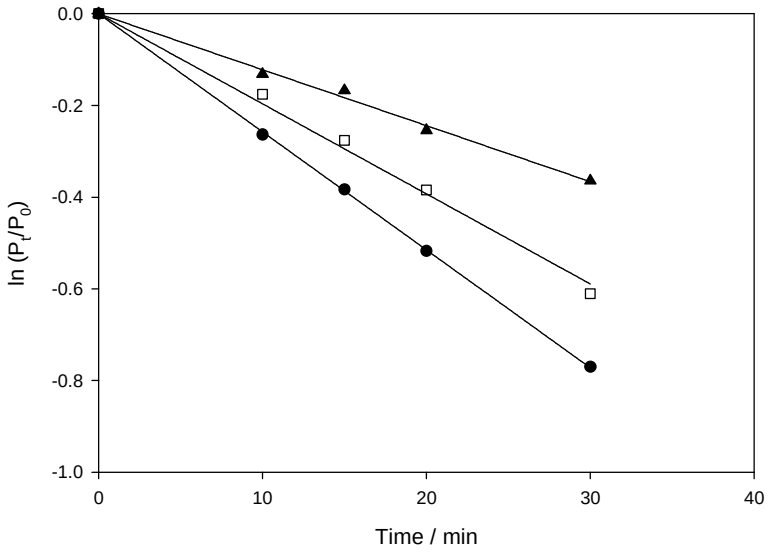

P_0 / mg L^{-1}	k_{obs} / min^{-1}	R^2
20.0	0.0257	0.999
60.0	0.0196	0.994
150.0	0.0122	0.994

Figure 3.22: Plot showing kinetics of phosphate removal at different initial concentration of phosphates, P_0: ● 20.0 mg L^{-1}, □ 60.0 mg L^{-1} and ▲ 150.0 mg L^{-1} PO_4-P. (Anode/cathode = AISI 420/AISI 310, [NaCl] = 4.2×10^{-3} M, pH = 5.0, j = 2.6 mA cm^{-2}, SA/V = 10.5 m^{-1}).

3.3.4 The effect of pH

The electrochemically produced iron ions from the AISI 420 electrode are involved in hydrolysis reactions and these reactions will depend on the pH of the solution, thus affecting the electrocoagulation performance. As for the Al-2Mg electrode, the initial pH, the final pH and the changes in the pH during the electrocoagulation process are important.

3.3.4.1 The effect of initial pH

The influence of the initial pH on the removal of phosphate using the AISI 420 electrode was studied by varying the initial pH in solutions containing 85.0 mg L^{-1} of PO_4-P. The pH was adjusted to 3.0, 7.2 and 9.7. The current density was 11.0 mA cm^{-2} and the electrocoagulation time was 30 min. The concentrations of phosphates at the different initial pH values are shown as a function of the electrocoagulation time in Figure 3.23. It is clear from this figure that the removal of phosphates is highly dependent on the initial pH of the solution. At the lowest initial pH, pH of 3.0, the highest removal efficiency of 97.1% was obtained. However, the removal efficiency decreases on increasing the initial pH. Indeed, the removal efficiency was reduced to 67.8% and 56.7% for initial pH values of 7.2 and 9.7, respectively. These results are consistent with the literature on the removal of phosphates using iron electrodes. İrdemez *et al.* [171] reported removal efficiencies of 86% for an initial pH of 3.0, 71% for an initial pH of 6.0 and a lower efficiency of 64% at an initial pH of 9.0 on using iron electrodes. These results were obtained using an initial concentration of phosphates of 100 mg L^{-1}, a current density of 1 mA cm^{-2} and a surface area to volume ratio, SA/V, of 88.2 m^{-1}. Similarly, Behbahani *et al.* [167] found removal efficiencies of 85%, 69% and 58% for initial pH values of 3.0, 7.0 and 10.0, respectively, at the end of 40 min with an initial phosphate concentration of 400 mg L^{-1} and at 2.5 mA cm^{-2} using iron electrodes.

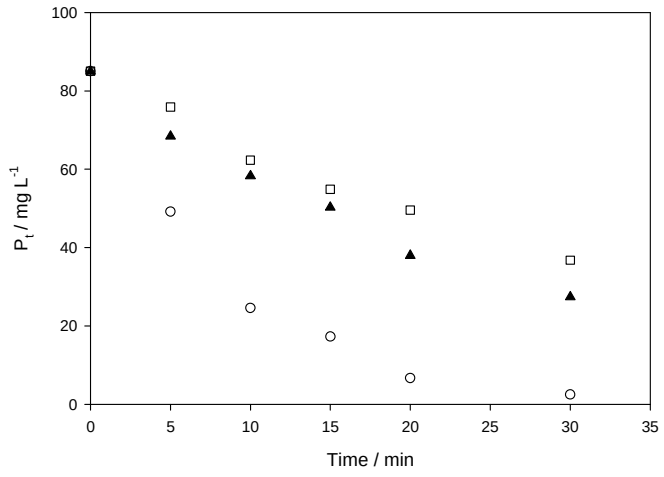

Time / min	P_t / mg L^{-1}		
	pH 3.0	pH 7.2	pH 9.7
0	85.0	85.0	85.0
5	49.2	68.4	75.9
10	24.6	58.3	62.3
15	17.3	50.3	54.9
20	6.7	38.0	49.6
30	2.5	27.4	36.8

Figure 3.23: Variation of the residual phosphate concentration, P_t, plotted as a function of the electrocoagulation time in solutions containing 85.0 mg L^{-1} of PO_4-P at initial pH values of ○ 3.0, ▲ 7.2 and □ 9.7. (Anode/cathode = AISI 420/AISI 310, [PO_4-P] = 85.0 mg L^{-1}, [NaCl] = 4.2×10^{-4} M, j = 11.0 mA cm^{-2}, SA/V = 10.5 m^{-1}).

In Table 3.10 the rate constants, k_{obs}, calculated for each initial pH value used in the data presented in Figure 3.23, are shown. The corresponding R^2 values for the linear regression analysis carried out on the experimental data are provided. It is clear from the R^2 values that the removal of phosphates follows the pseudo first-order model for all the initial pH values investigated. As clearly evident from this table, the k_{obs} values decrease with increasing initial pH values. The k_{obs} is high for an initial pH of 3.0, at 0.1186 min^{-1}, while for initial pH values of 7.2 and 9.7 the k_{obs} values are much lower at 0.0381 min^{-1} and 0.0280 min^{-1}, respectively.

Table 3.10: Pseudo first-order constant, k_{obs}, and R^2 values for the removal of phosphate at different initial pH values.

Initial pH	**k_{obs} / min^{-1}**	**R^2**
3.0	0.1186	0.992
7.2	0.0381	0.994
9.7	0.0280	0.995

3.3.4.2 The effect of final pH

As already shown in Section 3.2.3.2, the solution pH changes abruptly during the electrocoagulation process using the Al-2Mg electrode. Similarly, in the electrocoagulation removal of phosphate with AISI 420 electrode, the pH increases with the electrolysis time. This is shown in Figure 3.24, where the final pH and the removal efficiency of phosphates are presented as a function of the initial pH after an electrocoagulation period of 30 min. The initial concentration of phosphates was 85.0 mg L^{-1} and the current density was 11.0 mA cm^{-2}. Clearly, the initial pH strongly affects the value of the final pH. Indeed, an initial acidic pH leads to a neutral value of the final pH, varying from 3.0 to 7.2. The final pH values recorded for a neutral, pH value of 7.2 and an alkaline solution, pH value of 9.7, are similar reaching pH values of 10.9 and 11.3, respectively. Similar final pH values were found in Section 3.2.3.2 for the Al-2Mg electrode at a current density of 11.0 mA cm^{-2}. This result is in good agreement with the findings of Lacasa *et al.* [33], who reported that, regardless of the type of electrode employed, the final pH is related to the current density used during the electrocoagulation process. They found that higher current densities resulted in higher

final pH values. The final pH values observed in the present work are also in good agreement with the data reported by İrdemez *et al.* [171] and Behbahani *et al.* [167].

It is evident from Figure 3.24 that the removal efficiency decreases with increasing the final pH values. The highest removal efficiency was observed with an initial pH of 3.0, which results in a final pH of 7.4. According to Jiménez *et al.* [172], who characterised the hydrolysed iron species by the ferron method, at this neutral pH the main hydrolysis products are iron hydroxide precipitates and the charge of the flocs is positive. They explained this result in terms of adsorption of soluble monomeric species, generated at acidic pH values, on the metal hydroxide precipitate formed. On the other hand, Lacasa *et al.* [33] measured negative values of the zeta-potential when phosphates were present in solution. After an initial decrease, then the zeta-potential increased up to a value close to zero in the case of electrocoagulation with iron electrodes. The negatively charged particles might be related in this case to the adsorption of phosphate ions on the surface of the precipitates, leading to a gradual neutralisation of the zeta-potential. As in the case of the Al-2Mg electrodes presented in Section 3.2.3.2, at an initial pH of 3.0 the removal is attained through different mechanisms as the pH varies during the electrocoagulation process. This may include charge neutralisation at acidic pH values by means of monomeric hydrolysis species and adsorption on hydroxide precipitates, as the pH increases, as shown in Figure 3.15.

Jiménez *et al.* [172] reported that the main hydrolysis species in alkaline solutions are iron hydroxide precipitates and that charged flocs are only observed at pH values below 9.0. This finding was explained by the absence of soluble species in the solution that can be adsorbed on the precipitate. However, when phosphate ions are present in solution, as in the present research, it would be expected that these adsorb onto the formed flocs facilitating their subsequent removal. As shown in Figure 3.24, at neutral or alkaline initial pH values the removal efficiencies are low and correspond to final pH values close to 11.0. Also, Behbahani *et al.* [167] found lower removal efficiencies associated with high final pH values. A plausible explanation is provided by the presence of a large quantity of hydroxyl ions, which compete with the phosphate ions for adsorption on the iron precipitates. An extensive study on the variation of pH in electrocoagulation using iron electrodes has been carried out by Moreno-Casillas *et al.*

[173], where it was concluded that the formation of the final electrocoagulation products involves green rust, which consists of alternating positively charged Fe(II)-Fe(III) hydroxide layers and hydrated anion layers [117]. However, this does not form if pH conditions in the bulk solution are too acidic or alkaline [173].

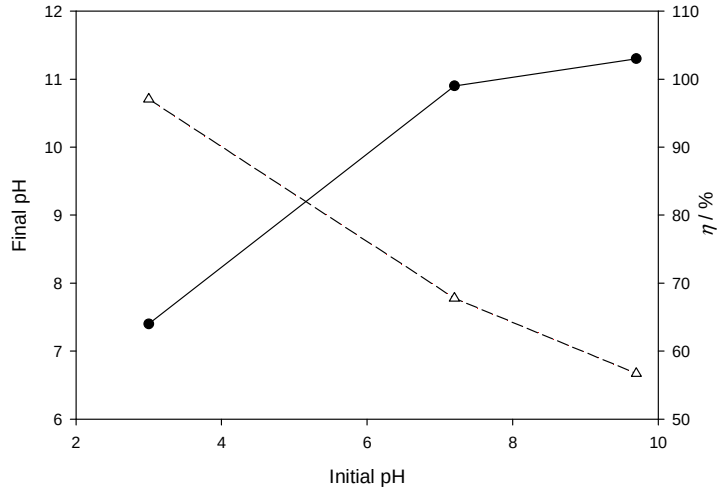

Initial pH	Final pH	η / %
3.0	7.4	97.1
7.2	10.9	67.8
9.7	11.3	56.7

Figure 3.24: Evolution of ● final pH and △ removal efficiency, η, plotted as a function of the initial pH. (Anode/cathode = AISI 420/AISI 310, [PO_4-P] = 85.0 mg L^{-1}, [NaCl] = 4.2 × 10^{-3} M, j = 11.0 mA cm^{-2}, SA/V = 10.5 m^{-1}).

3.3.5 The effect of chloride concentration

In electrocoagulation, the conductivity of the solution is a significant parameter. As already outlined in Section 3.2.4 for the Al-2Mg electrode, it affects the current density, the anode potential, the current efficiency and the usage of the electrical energy. To overcome these problems, small amounts of a supporting electrolyte, usually sodium chloride, are added to the solutions, resulting in an increase of the solution conductivity and a reduction of the energy consumption. Furthermore, aggressive anions, such as chlorides, are responsible for the breakdown of the protective chromium oxide layer present on the surface of stainless steels [174]. Consequently, when stainless steel is used as the anode material, the presence of chloride ions may reduce the voltage required to overcome the electrode passivation. On the other hand, it is well known that chlorides give rise to pitting attack at the passivated surface of stainless steels. As a result, a high concentration of chloride ions may lead to an uneven consumption of the electrode due to pitting corrosion.

As discussed previously in Section 3.2.4, high concentrations of the supporting electrolyte may adversely affect the removal efficiency in the electrocoagulation process. Indeed, the presence of counter ions can promote competition with the hydroxy ligands in the hydrolysis process of iron, shown in Figure 3.14. However, it has been reported that chloride ions, used in the present study as the supporting electrolyte, have a weak coordination capacity with metal ions [62]. Moreover, according to the hard and soft acid-base, HSAB, concept introduced by Pearson [112], Fe^{3+} ions have a greater tendency to bind the hard base H_2O rather than forming halo complexes.

In this study, sodium chloride, NaCl, was used as the supporting electrolyte for the electrocoagulation removal of phosphate using the AISI 420 electrode. The effect of chloride ions on the removal efficiency of phosphates was investigated in solutions containing different concentrations of chloride. Figure 3.25 shows the residual concentration of phosphates, P_t, after 60 min in solutions containing 2.8, 4.2, 10.0, 25.0 and 44.0×10^{-3} M NaCl. The initial concentration of phosphate was 85.0 mg L^{-1} and the initial pH was maintained at 5.0. When the concentration of NaCl increases from 2.8×10^{-3} to 4.2×10^{-3} M, the removal efficiency improves slightly from 75% to 85%. However, no significant improvement was observed when the concentration of NaCl was above 4.2×10^{-3} M. Indeed, as the NaCl concentration varies from 4.2×10^{-3} to 44.0×10^{-3} M, the residual concentration of phosphates, after 60 min, ranges from 11 to 9.1 mg L^{-1}, giving very little difference in the extent of phosphate removal. These findings are in good agreement with several reports on the electrocoagulation of phosphates with iron electrodes [175-177], where an increase in the removal efficiency is observed, however this effect is lost on further increasing the concentration of the supporting electrolyte.

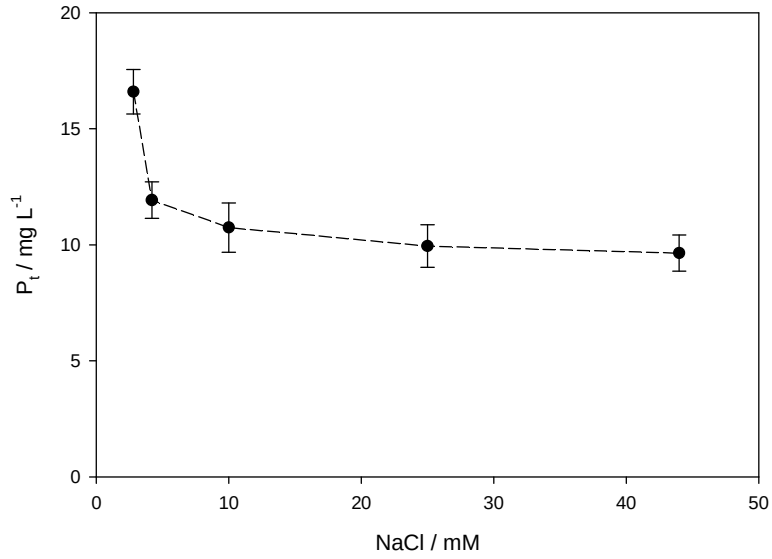

NaCl / mM	P_t / mg L^{-1}
2.8	20 ± 2
4.2	12.5 ± 0.6
10.0	11 ± 1
25.0	10.0 ± 0.9
44.0	9.1 ± 0.8

Figure 3.25: Residual phosphate concentration, P_t, as a function of NaCl concentration. The concentrations of NaCl used were: 4.2, 7.0, 10.0, 25.0 and 44.0 × 10^{-3} M. Each experiment was performed in duplicate (n = 2). (Anode/cathode = AISI 420/AISI 310, [PO_4-P] = 80.0 mg L^{-1}, pH = 5.0, j = 11.0 mA cm^{-2}, t = 60 min, SA/V = 10.5 m^{-1}).

The variation of the anode potential as a function of the electrocoagulation time is reported in Figure 3.26 for 80.0 mg L^{-1} phosphate solutions containing 2.8, 4.2, 10.0, 25.0 and 44.0 × 10^{-3} M NaCl. As can be seen from this figure the average anode potential, $\overline{E}$, increases as the concentration of NaCl decreases. Similar results were reported by İrdemez *et al.* [34] in solutions of low conductivity using iron plates electrodes. By comparing the average values of the anode potential of the AISI 420 electrode with those of the Al-2Mg electrode at different NaCl concentrations, shown in Figure 3.26 and Figure 3.9, respectively, it is evident that the Al-2Mg electrode exhibits lower potentials. This result is in agreement with the findings of Izquierdo *et al.* [178], who reported that the cell potential required with the iron electrodes to allow the same current density was significantly higher than with aluminium plates. It is clear that in the solution containing 2.8 × 10^{-3} M NaCl the average anode potential, $\overline{E}$, is 3.2 V vs. SCE, Figure 3.26. However, values up to 4.7 V vs. SCE were observed in the first few minutes of the electrocoagulation experiment. As discussed previously in Section 3.2.4, concurrent reactions may also occur at the anode, competing with the dissolution of iron, at these high potentials. Consequently, the coagulant dosage and, in turn, the removal efficiency would be lower. This may explain the lower removal efficiency of phosphates observed in the 2.8 × 10^{-3} M NaCl solution, shown in Figure 3.25.

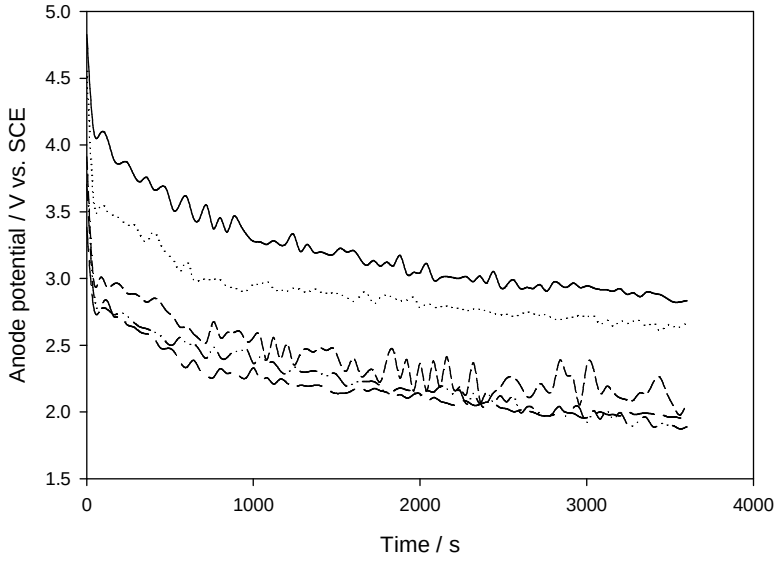

NaCl / mM	$\overline{E}$ / V vs. SCE
2.8	3.21
4.2	2.90
10.0	2.41
25.0	2.24
44.0	2.19

Figure 3.26: Variation of the anode potential as a function of the electrolysis time in solutions containing −−− 2.8, · · · 4.2, − − − 10.0, − ·· − 25.0 and −− −− −− 44.0 × 10^{-3} M NaCl. (Anode/cathode = AISI 420/AISI 310, [PO_4-P] = 80.0 mg L^{-1}, pH 5.0, j = 11.0 mA cm^{-2}, t = 60 min, SA/V = 10.5 m^{-1}).

3.3.6 Adsorption isotherms

In the simplified model drawn in Figure 3.15 to describe the process of phosphate removal using the AISI 420 electrode, the mechanism involves either the adsorption of phosphate ions on the Fe^{3+} hydrolysis products or the adsorption of the Fe-hydroxo-phosphate complexes onto positively charged Fe^{3+} hydrolysis species (Step IV in Figure 3.15). In order to determine whether adsorption was the primary mechanism for the removal of phosphate-containing solutions at an initial pH of 5.0, adsorption isotherm studies were performed and the resulting data were compared to the Langmuir, Freundlich and Temkin models, introduced in Section 3.2.5.

In Figure 3.27 the amount of P-PO_4 adsorbed at equilibrium per unit mass of Fe^{2+} ions, q_e, as a function of the final concentration of phosphates, P_e is shown. The q_e values were calculated according to Eq. 3.5, where in this case M represents the amount of Fe^{2+} ions generated by electrodissolution of the stainless steel AISI 420 electrode and was calculated using Faraday's law, taking into account the composition of the material, given in Section 2.2.2. The test solutions contained initial concentrations of phosphates ranging from 2.0 to 150.0 mg L^{-1} and 4.2 × 10^{-3} M NaCl at pH 5.0. The solutions were

stirred throughout the experiment and the temperature was kept constant at 25 ± 1 ºC. The final concentration of phosphates, P_e, was measured after 15 min from the end of the electrocoagulation test in order to ensure that the adsorption equilibrium had been achieved. The details of the experiments are given in Sections 2.3.1.4 and 2.3.5. The experimental data were fitted by nonlinear regression analysis, according to the Langmui, Freundlich and Temkin models (Eq. 3.8, Eq. 3.9 and Eq. 3.10, respectively), and are shown in Figure 3.27. As evident from Table 3.11, a higher value of the adjusted R^2 was obtained for the Freundlich adsorption model. The high value of the adjusted R^2 indicates that adsorption is the primary mechanism for the removal of phosphates using the AISI 420 electrode at the conditions used in the present study. The values of K_F and n were computed as 17 (mg g^{-1}) (L mg^{-1}) and 2.2, respectively. Also the adsorption of phosphates using the Al-2Mg electrode was better described by the Freundlich equation, as reported in Section 3.2.5. However, on comparing the values of the parameters K_F and n presented in Table 3.4 and Table 3.10 for the Al-2Mg electrode and the AISI 420 electrode, respectively, it is evident that the aluminium system has a greater affinity for the adsorption of phosphate ions. Indeed, the Freundlich constants K_F and n are 146 (mg g^{-1}) (L mg^{-1}) and 3.1 for the Al-2Mg system, while for the AISI 420 system they are considerably lower.

Different adsorbents that have been used for removing phosphates include iron based materials, such as iron-rich and iron oxide [179-185]. However, there are no studies carried out on the adsorption of phosphates using iron based electrodes. Lacasa *et al*. [128] reported that nitrate ions, negatively charged pollutants similar to phosphate ions, are removed according to the Freundlich model using iron electrodes. This is in good agreement with the results presented in this section.

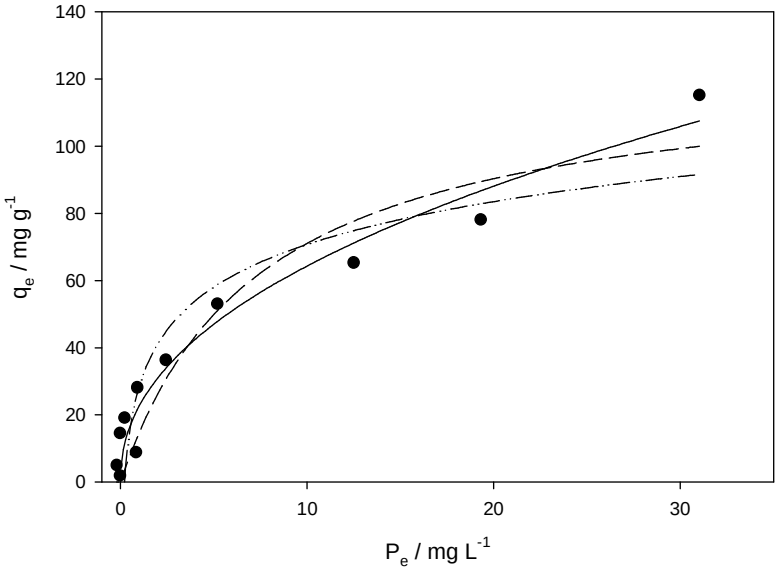

Figure 3.27: ● Experimental data, −−− Freundlich isotherm, − − − Langmuir isotherm and −·−·− Temkin isotherm fitting at 25 ± 1 ºC. (Anode/cathode = AISI 420/AISI 310, [PO_4-P] = 2.0 to 150.0 mg L^{-1}, [NaCl] = 4.2 × 10^{-3} M, pH = 5.0, j = 11.0 mA cm^{-2}, t = 60 min, SA/V = 10.5 m^{-1}).

Table 3.11: Langmuir, Freundlich and Temkin isotherm model constants and adjusted R^2 values.

Langmuir model		
K_L / L mg^{-1}	q_m / mg g^{-1}	Adjusted R^2
0.13 ± 0.06	124 ± 21	0.883
Freundlich model		
K_F / (mg g^{-1})(L mg^{-1})	n	Adjusted R^2
23 ± 3	2.2 ± 0.1	0.949
Temkin model		
K_T / L g^{-1}	B / J mol^{-1}	Adjusted R^2
5 ± 2	18 ± 3	0.858

3.3.7 The removal of phosphates from real samples

The two real samples, treated with the Al-2Mg electrode in Section 3.2.6, were used to investigate the feasibility of the AISI 420 electrode to remove phosphates from real wastewater samples. The conductivity levels of the samples are given in Table 3.5.

The current density was 4.1 mA cm^{-2} and the ratio of the surface area of the anode to the volume of solution, SA/V, was 13.4 m^{-1}. The removal efficiencies of phosphates for the two samples as a function of the electrocoagulation time are given in Figure 3.28. The removal of phosphates in the sample no. 1 was somewhat slow and after 15 min only 12% of the initial content of phosphates was removed from the sample. On the other hand, complete removal was achieved for the sample no. 2.

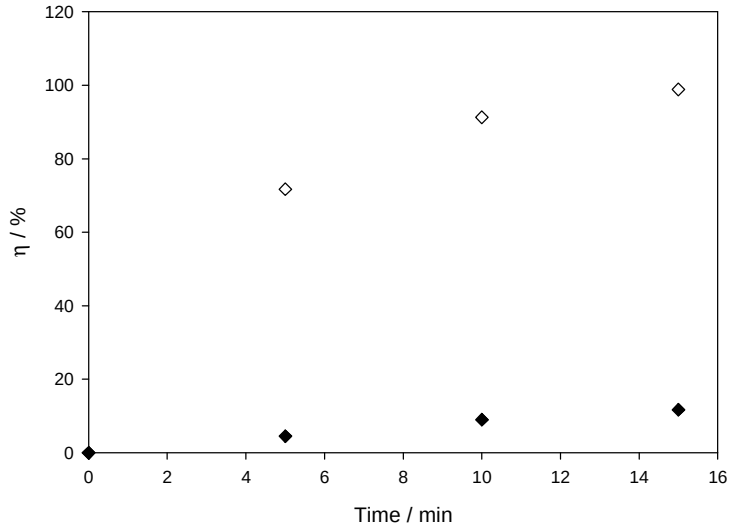

Time / min	**η / %**	
	sample no. 1	**sample no. 2**
0	0	0
5	4.5	71.7
10	9.0	91.3
15	11.7	BDL*

*BDL = Below Detection Limit (Section 2.3.3).

Figure 3.28: Removal efficiency, η, plotted as a function of the electrocoagulation time in ◆ sample no. 1 and ◇ sample no. 2 (Table 3.5). (Anode/cathode = AISI 420/AISI 310, j = 4.1 mA cm^{-2}, SA/V = 13.4 m^{-1}).

The values of the observed rate constant, k_{obs}, are presented in Table 3.12 and the corresponding R^2 values are also included. It is clear from the high R^2 values that the removal of phosphates from the real wastewater samples followed pseudo first-order kinetics. The k_{obs} value is remarkably low for the sample no. 1, at 0.0084 min^{-1}, while for the sample no. 2 a much higher value of 0.2949 min^{-1} is obtained. By comparing this value with the k_{obs} value of 0.5438 min^{-1}, obtained from the electrocoagulation removal of phosphates using the Al-2Mg electrode and shown in Table 3.6, it is clear that phosphate ions are removed faster and more efficiently when the Al-2Mg electrodes are used. Nevertheless, at the end of a 15 min period, the concentration of phosphates is lower than the threshold limit for discharge in receiving water bodies in both cases.

Table 3.12: Pseudo first-order constant, k_{obs} and R^2 values for the removal of phosphate from the real samples.

Sample no.	k_{obs} **/ min^{-1}**	R^2
1	0.0084	0.991
2	0.2949	0.981

The variation of the anode potential during the electrocoagulation removal of phosphates from the real samples is shown in Figure 3.29. These data were recorded under the same conditions as that described in Figure 3.28. Clearly, the potential for the sample no. 1 is relatively high, with an average value, $\overline{E}$, of 3.29 V vs. SCE, however it is not unexpected since the sample has a low conductivity, Table 3.5. As already discussed in Section 3.3.5, high values of the anode potential imply not just high energy consumption for the process, they also mean that side reactions can take place at the anode, reducing the current efficiency. The low removal obtained for the sample no. 1, as evident from Figure 3.28, might indeed be explained in terms of low coagulant dosage due to the occurrence of these side reactions at the anode not resulting in the dissolution of Fe^{2+} ions. On the other hand, the average potential value, $\overline{E}$, for the sample no. 2 is 1.57 V vs. SCE. However, at the beginning of the experiment, the potential increases sharply up to values close to 2.0 V vs. SCE and then gradually declines. As listed in Table 3.6 and Table 3.12, the values of k_{obs} for the sample no. 2 were computed as 0.5438 and 0.2949 min^{-1} using the Al-2Mg and the AISI 420 electrode, respectively. Although the removal of phosphates was complete using both electrodes, it is clear that the performance of the Al-2Mg electrode is better. Again, the small value of k_{obs}, obtained using the AISI 420 electrode, is consistent with the parasitic reactions, occurring at the anode surface especially during the first few minutes of the experiments, which lower the amount of iron ions generated from the anode.

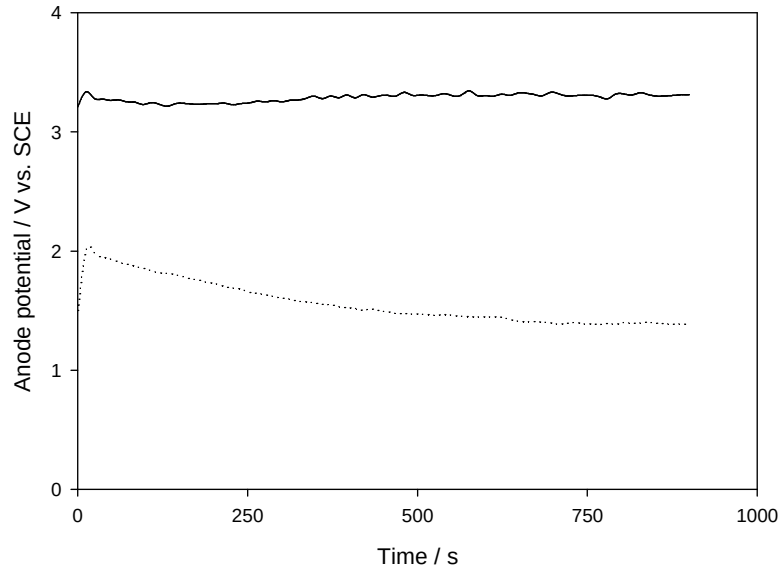

Sample no.	$\overline{E}$ / V vs. SCE
1	3.29
2	1.57

Figure 3.29: Variation of the anode potential as a function of the electrocoagulation period in −−− sample no. 1 and · · · sample no. 2 (Table 3.5). (Anode/cathode = AISI 420/AISI 310, j = 4.1 mA cm^{-2}, SA/V = 13.4 m^{-1}).

3.4 Summary

The present chapter is focused on the electrocoagulation removal of phosphates with two anode materials, Al-2Mg and stainless steel AISI 420 alloys. Both alloys are capable in removing phosphates under different operating conditions, although the Al-2Mg electrode is more effective.

The removal of phosphates from solution follows the pseudo first-order kinetics for the two anode materials. In both cases, the observed rate constant, k_{obs}, has been found dependent on the concentration of PO_4-P (Sections 3.2.1 and 3.3.2). Indeed, it decreased with increasing initial concentrations of phosphates. This dependence has been ascribed to the degree of destabilisation attained in solution due to the ratio of coagulant dosage to phosphate concentration. A small degree of destabilisation, which occurs in solutions with high initial concentrations of phosphates, reflects on less efficient collisions and aggregations of the destabilised particles (Figure 3.2) that, according to the literature, is the rate-determining step of the process.

As expected, for both alloys the observed rate constant, k_{obs}, is dependent on the current density of the process (Sections 3.2.2 and 3.3.3).

The removal efficiency of phosphates is significantly affected by the initial pH of the solution for both alloys (Sections 3.2.3.1 and 3.3.4.1). It has been observed that it decreases with increasing initial pH values. However, the final pH and the pH evolution also play a major role in the removal process (Sections 3.2.3.2 and 3.3.4.2). The highest removal efficiency was observed at acidic initial pH and at final pH values around 7.0 in both Al and Fe systems.

The concentration of chloride ions and the solution conductivity have a marginal effect on the removal efficiency using Al-2Mg as the anode material (Section 3.2.4). On the other hand, the performances of AISI 420 grade are strongly reduced in low conductive solutions (Section 3.3.5).

Both Al-2Mg and AISI 420 alloys remove phosphates according to the Freundlich adsorption isotherm model in the range of concentrations studied (Sections 3.2.5 and 3.3.6). This finding is consistent with removal mechanisms involving other processes other than just adsorption, as shown in the literature.

By means of rotating disk voltammetry, RDV, it has been shown that Fe(II) ions are generated at a pH of 5.0 and at a current density of 11.0 mA cm^{-2} on oxidation of the AISI 420 electrode.

The phosphate content has been removed efficiently from two real samples using the Al-2Mg alloy (Section 3.2.6), while it has been observed that the AISI 420 electrode is not effective in removing phosphates from the real sample with low conductivity (Section 3.3.7). This has been rationalised as the effect of the passive nature of this material. The combination of small chloride concentration and low conductivity results in the occurrence of concurrent reactions at the anode because of high potential values exhibiting by the anode during the electrocoagulation process. These reactions do not result in the dissolution of Fe^{2+} ions.

Although both alloys have shown to be effective in the removal of phosphates, some limitations have arisen from treating real samples with specific physico-chemical characteristics. In particular, the different performance observed for Al-2Mg and AISI

420 electrodes to treat the real samples are related to the different electrochemical behaviour and corrosion properties that these two alloys exhibit in a given medium. The electrochemical behaviour will, indeed, be the subject of Chapter 4. Several anode materials will be investigated in terms of their electrochemistry in two specific test solutions.

3.5 References

[1] Chen, G.H., *Sep. Purif. Technol.*, **38** (2004) 11-41.
[2] Gnusin, N.P., Vitul'skaya, N.V., Zabolotskaya, L.I., Belobrov, I.A., *J. Appl. Chem. (USSR)*, **50** (1997) 1663-1741.
[3] Pogrebnaya, V.L., Klimenko, A.A., Bokovikova, E.P., Tsymbal, E.P., Pronina, N.P., *Chem. Petrol. Eng.*, **31** (1995) 280-281.
[4] Gnusin, N.P., Zabolotskaya, L.I., Vitul'skaya, N.V., *Sov. J. Water Chem. Technol.*, **7** (1985) 32-35.
[5] Chen, G.H., Chen, X.M., Yue, P.L., *J. Environ. Eng.*, **126** (2000) 858-863.
[6] Beck, E.C., Giannini, A.P., Ramirez, E.R., *Food Technol.*, **22** (1974) 18.
[7] Lawrence, J., Knieper, L., *Ind. Wastewater*, **1-2** (2000) 20-25.
[8] Biswas, N., Lazarescu, G., *Int. J. Environ. Stud.*, **38** (1991) 65.
[9] Vlyssides, A.G., Papaioannou, D., Loizidoy, M., Karlis, P.K., Zorpas, A.A., *Waste Manage. (Oxford)*, **20** (2000) 569-574.
[10] Do, J.S., Chen, M.L., *J. Appl. Electrochem.*, **24** (1994) 785-790.
[11] Ibanez, J.G., Singh, M.M., Szafran, Z., *J. Chem. Educ.*, **75** (1998) 1040-1041.
[12] Vlyssides, A.G., Loizidou, M., Karlis, P.K., Zorpas, A.A., Papaioannou, D., *J. Hazard. Mater.*, **70** (1999) 41-52.
[13] Gurses, A., Yalcin, M., Dogar, C., *Waste Manage. (Oxford)*, **22** (2002) 491-499.
[14] Xiong, Y., Strunk, P.J., Xia, H.Y., Zhu, X.H., Karlsson, H.T., *Water Res.*, **35** (2001) 4226-4230.
[15] Mameri, N., Yeddou, A.R., Lounici, H., Belhocine, D., Grib, H., Bariou, B., *Water Res.*, **32** (1998) 1604-1612.
[16] Panizza, M., Bocca, C., Cerisola, G., *Water Res.*, **34** (2000) 2601-2605.
[17] Tsai, C.T., Lin, S.T., Shue, Y.C., Su, P.L., *Water Res.*, **31** (1997) 3073-3081.
[18] Donnini, J.C., Kan, J., Hassan, T.A., Kar, K.L., *Can. J. Chem. Eng.*, **72** (1994) 667.
[19] Abuzaid, N.S., Bukhari, A.A., Al-Hamouz, Z.M., *Adv. Environ. Res.*, **6** (2002) 325-333.
[20] Renk, R.R., *Energy Prog.*, **8** (1988) 205.
[21] Szynkarczuk, J., Kan, J., Hassan, T.A.T., Donini, J.C., *Clays Clay Miner.*, **42** (1994) 667-673.
[22] Belongia, B.M., Haworth, P.D., Baygents, J.C., Raghavan, S., *J. Electrochem. Soc.*, **146** (1999) 4124-4130.
[23] Matteson, M.J., Dobson, R.L., Glenn, R.W., Kukunoor, N.S., Waits, W.H., Clayfield, E.J., *Colloids Surf., A*, **104** (1995) 101-109.
[24] Pretorius, W.A., Johannes, W.G., Lempert, G.G., *Water SA*, **17** (1991) 133-138.
[25] Phutdhawong, W., Chowwanapoonpohn, S., Buddhasukh, D., *Anal. Sci.*, **16** (2000) 1083-1084.
[26] Balasubramanian, N., Madhavan, K., *Chem. Eng. Technol.*, **24** (2001) 519– 521.
[27] Chiang, L.C., Chang, J.E., Tseng, S.C., *Water Sci. Technol.*, **36** (1997) 123-130.
[28] Pouet, M.F., Grasmick, A., *Water Sci. Technol.*, **31** (1995) 275-283.

[29] Vik, E.A., Carlson, D.A., Eikum, A.S., Gjessing, E.T., *Water Res.*, **18** (1984) 1355-1360.
[30] Valsami-Jones, E., *Phosphorus in Environmental Technologies: Principles and Applications*, IWA Publishing, 2004.
[31] Kirk, P.W.W., Perry, R., Hunter, M., Lester, J.N., Matthews, P.J., *Environ. Technol. Lett.*, **9** (1988) 171-180.
[32] Diamadopoulos, E., Benedek, A., *J. Water Pollut. Control Fed.*, **56** (1984) 1165-1172.
[33] Lacasa, E., Canizares, P., Saez, C., Fernandez, F.J., Rodrigo, M.A., *Chem. Eng. J.*, **172** (2011) 137-143.
[34] Irdemez, S., Demircioglu, N., Yildiz, Y.S., Bingul, Z., *Sep. Purif. Technol.*, **52** (2006) 218-223.
[35] Irdemez, S., Yildiz, Y.S., Tosunoglu, V., *Sep. Purif. Technol.*, **52** (2006) 394-401.
[36] Bektas, N., Akbulut, H., Inan, H., Dimoglo, A., *J. Hazard. Mater.*, **106** (2004) 101-105.
[37] Vasudevan, S., Sozhan, G., Ravichandran, S., Jayaraj, J., Lakshmi, J., Sheela, S.M., *Ind. Eng. Chem. Res.*, **47** (2008) 2018-2023.
[38] Emamjomeh, M.M., Sivakumar, M., *J. Environ. Manage.*, **90** (2009) 1663-1679.
[39] Vasudevan, S., Lakshmi, J., Jayaraj, J., Sozhan, G., *J. Hazard. Mater.*, **164** (2009) 1480-1486.
[40] Jiang, J.Q., Graham, N.J.D., *Water SA*, **24** (1998) 237-244.
[41] Hsu, P.H., *Water Res.*, **10** (1976) 903-907.
[42] Crittenden, J.C., Trussell, R.R., Hand, D.W., Howe, K.J., Tchobanoglous, G., *MWH's Water Treatment: Principles and Design*, John Wiley & Sons, 2012.
[43] Bache, D.H., Gregory, R., *Flocs in Water Treatment*, IWA Publishing, 2007.
[44] Georgantas, D.A., Grigoropoulou, H.P., *J. Colloid Interface Sci.*, **315** (2007) 70-79.
[45] Aguilar, M.I., Saez, J., Llorens, M., Soler, A., Ortuno, J.F., *Water Res.*, **36** (2002) 2910-2919.
[46] Stumm, W., Morgan, J.J., *J. Am. Water Works Assoc.*, **54** (1962) 971-994.
[47] Recht, H.L., Ghassemi, M., Kinetics and mechanism of precipitation and nature of the precipitate obtained in phosphate removal from wastewater using aluminium (III) and iron (III) salts, in: Report No. 17010 EKI, 1970.
[48] Hsu, P.H., *Water Res.*, **9** (1975) 1155-1161.
[49] Donini, J.C., Frenette, R.G., Kasperski, K.L., Kelebek, S., Electrocoagulation - Final Report, Division Report CRL 89-82(CF), CANMET, Energy, Mines and Resources Canada, in: September 1989.
[50] Harif, T., Khai, M., Adin, A., *Water Res.*, **46** (2012) 3177-3188.
[51] Bayar, S., Yildiz, Y.S., Yilmaz, A.E., Irdemez, S., *Desalination*, **280** (2011) 103-107.
[52] Koparal, A.S., Ogutveren, U.B., *J. Hazard. Mater.*, **89** (2002) 83-94.
[53] Akbal, F., Camci, S., *Environ. Prog. Sustain. Energy*, **31** (2012) 340-350.
[54] Murthy, Z.V.P., Parmar, S., *Desalination*, **282** (2011) 63-67.
[55] Secula, M.S., Cretescu, I., Petrescu, S., *Desalination*, **277** (2011) 227-235.
[56] Behbahani, M., Moghaddam, M.R.A., Arami, M., *Desalination*, **271** (2011) 209-218.
[57] Mollah, M.Y.A., Gomes, J.A.G., Das, K.K., Cocke, D.L., *J. Hazard. Mater.*, **174** (2010) 851-858.
[58] Abdelwahab, O., Amin, N.K., El-Ashtoukhy, E.S.Z., *J. Hazard. Mater.*, **163** (2009) 711-716.
[59] Kobya, M., Demirbas, E., Can, O.T., Bayramoglu, M., *J. Hazard. Mater.*, **132** (2006) 183-188.
[60] Daneshvar, N., Oladegaragoze, A., Djafarzadeh, N., *J. Hazard. Mater.*, **129** (2006) 116-122.
[61] Stumm, W., O'Melia, C.R., *J. Am. Water Works Assoc.*, **60** (1968) 514-525.
[62] Bratby, J., *Coagulation and Flocculation in Water and Wastewater Treatment*, IWA Publishing, 2006.

[63] O'Melia, C.R., *Coagulation and Flocculation*, in: W.J. Weber (Ed.) Physicochemical Process for Water Quality Control, Wiley-Interscience, 1972.
[64] Schick, M.J., Hubbard, A.T., *Coagulation and Flocculation*, Taylor & Francis, 2005.
[65] Duan, J.M., Gregory, J., *Adv. Colloid Interface Sci.*, **100** (2003) 475-502.
[66] Szpyrkowicz, L., Kaul, S.N., Neti, R.N., Satyanarayan, S., *Water Res.*, **39** (2005) 1601-1613.
[67] Szpyrkowicz, L., Juzzolino, C., Kaul, S.N., Daniele, S., De Faveri, M.D., *Ind. Eng. Chem. Res.*, **39** (2000) 3241-3248.
[68] Szpyrkowicz, L., Kaul, S.N., Neti, R.N., *J. Appl. Electrochem.*, **35** (2005) 381-390.
[69] Murphy, U.N., Rekha, H.B., Bhavya, J.G., *Int. J. Environ. Sci. Develop.*, **2** (2011) 484-487.
[70] Khan, H., Ahmad, N., Yasar, A., Shahid, R., *Pol. J. Environ. Stud.*, **19** (2010) 83-92.
[71] Kabdasli, I., Keles, A., Oelmez-Hanci, T., Tuenay, O., Arslan-Alaton, I., *J. Hazard. Mater.*, **171** (2009) 932-940.
[72] Abuzaid, N.S., Al-Hamouz, Z., Bukhari, A.A., Essa, M.H., *Water Air and Soil Poll.*, **109** (1999) 429-442.
[73] Linares-Hernandez, I., Barrera-Diaz, C., Roa-Morales, G., Bilyeu, B., Urena-Nunez, F., *Chem. Eng. J.*, **148** (2009) 97-105.
[74] Ugurlu, M., Gurses, A., Dogar, C., Yalcin, M., *J. Environ. Manage.*, **87** (2008) 420-428.
[75] Fouad, Y.O.A., Konsowa, A.H., Farag, H.A., Sedahmed, G.H., *Chem. Eng. J.*, **145** (2009) 436-440.
[76] Kabdasli, I., Arslan, T., Oelmez-Hanci, T., Arslan-Alaton, I., Tuenay, O., *J. Hazard. Mater.*, **165** (2009) 838-845.
[77] Chou, W.-L., Wang, C.-T., Huang, K.-Y., *Desalination*, **251** (2010) 12-19.
[78] El-Ashtoukhy, E.S.Z., Amin, N.K., *J. Hazard. Mater.*, **179** (2010) 113-119.
[79] Linares-Hernandez, I., Barrera-Diaz, C., Bilyeu, B., Juarez-GarciaRojas, P., Campos-Medina, E., *J. Hazard. Mater.*, **175** (2010) 688-694.
[80] Rubin, A.J., Kovac, T.W., *Effect of Aluminum III Hydrolysis on Alum Coagulation*, in: A.J. Rubin (Ed.) Chemistry of Water Supply, Treatment and Distribution, Ann Arbor Science, 1974.
[81] Baes, C.F., Mesmer, R.E., *The Hydrolysis of Cations*, Wiley-Interscience, 1976.
[82] Hudson, H.E., Wolfner, J.P., *J. Am. Water Works Assoc.*, **70** (1967) 613-620.
[83] Hahn, H.H., Stumm, W., *J. Colloid Interface Sci.*, **28** (1968) 134-&.
[84] Letterman Rd, Quon, J.E., Gemmell, R.S., *J. Am. Water Works Assoc.*, **65** (1973) 716-722.
[85] Smoluchowski, M., *Physik. Z.*, **17** (1916) 557-585.
[86] Smoluchowski, M., *Z. Physik. Chem.*, **92** (1917) 129-168.
[87] Hogg, R., *Flocculation and Dewatering of Fine-Particle Suspensions*, in: H. Stechemesser, B. Dobias (Eds.) Coagulation and Flocculation, Taylor & Francis, 2005.
[88] Kusters, K.A., Wijers, J.G., Thoenes, D., *Chem. Eng. Sci.*, **52** (1997) 107-121.
[89] Stumm, W., O'Melia, C.R., *J. AWWA*, **60** (1968) 514-539.
[90] Mollah, M.Y.A., Morkovsky, P., Gomes, J.A.G., Kesmez, M., Parga, J., Cocke, D.L., *J. Hazard. Mater.*, **114** (2004) 199-210.
[91] Canizares, P., Jimenez, C., Martinez, F., Rodrigo, M.A., Saez, C., *J. Hazard. Mater.*, **163** (2009) 158-164.
[92] Mouedhen, G., Feki, M., Wery, M.D.P., Ayedi, H.F., *J. Hazard. Mater.*, **150** (2008) 124-135.
[93] Chen, X.M., Chen, G.H., Yue, P.L., *Sep. Purif. Technol.*, **19** (2000) 65-76.
[94] Adhoum, N., Monser, L., Bellakhal, N., Belgaied, J.E., *J. Hazard. Mater.*, **112** (2004) 207-213.
[95] Kobya, M., Hiz, H., Senturk, E., Aydiner, C., Demirbas, E., *Desalination*, **190** (2006) 201-211.

[96] Canizares, P., Jimenez, C., Martinez, F., Saez, C., Rodrigo, M.A., *Ind. Eng. Chem. Res.*, **46** (2007) 6189-6195.
[97] Canizares, P., Martinez, F., Jimenez, C., Lobato, J., Rodrigo, M.A., *Ind. Eng. Chem. Res.*, **45** (2006) 8749-8756.
[98] Canizares, P., Martinez, F., Jimenez, C., Lobato, J., Rodrigo, M.A., *Environ. Sci. Technol.*, **40** (2006) 6418-6424.
[99] Canizares, P., Martinez, F., Jimenez, C., Lobato, J., Rodrigo, M.A., *Sep. Sci. Technol.*, **42** (2007) 2157-2175.
[100] Canizares, P., Martinez, F., Jimenez, C., Saez, C., Rodrigo, M.A., *J. Hazard. Mater.*, **151** (2008) 44-51.
[101] Canizares, P., Martinez, F., Lobato, J., Rodrigo, M.A., *J. Hazard. Mater.*, **145** (2007) 233-240.
[102] Zhou, W.Z., Gao, B.Y., Yue, Q.Y., Liu, L.L., Wang, Y., *Colloids Surf., A*, **278** (2006) 235-240.
[103] Jardine, P.M., Zelazny, L.W., *Soil Sci. Soc. Am. J.*, **51** (1987) 889-892.
[104] Parker, D.R., Zelazny, L.W., Kinraide, T.B., *Soil Sci. Soc. Am. J.*, **52** (1988) 67-75.
[105] Feng, C., Shi, B., Wang, D., Li, G., Tang, H., *Colloids Surf., A*, **287** (2006) 203-211.
[106] Letterman, R.D., Amirtharajah, A., O'Melia, C.R., *Coagulation and Flocculation*, in: R.D. Letterman (Ed.) Water Quality and Treatment - A Handbook of Community Water Supplies, McGraw-Hill, 1999.
[107] Sengil, I.A., Ozacar, M., *J. Hazard. Mater.*, **137** (2006) 1197-1205.
[108] Frankel, G.S., *J. Electrochem. Soc.*, **145** (1998) 2970-2970.
[109] F.G.R., G., *Inorganic polymeric chemistry*, Butterworths and Co., 1963.
[110] Liang, Z., Wang, Y., Zhou, Y., Liu, H., Wu, Z., *Sep. Purif. Technol.*, **68** (2009) 382-389.
[111] Buchanan, D.R., Harris, P.M., *Acta Crystallogr. Sect. B: Struct. Sci.*, **B 24** (1968) 954-&.
[112] Pearson, R.G., *J. Am. Chem. Soc.*, **85** (1963) 3533-&.
[113] Stumm, W., Morgan, J.J., *Aquatic Chemistry: Chemical Equilibria and Rates in Natural Waters* 3rd ed., John Wiley & Sons, 1996.
[114] Martinez-Huitle, C.A., Brillas, E., *Appl. Catal., B*, **87** (2009) 105-145.
[115] Kraemer, E.O., *Colloids*, in: H.S. Taylor (Ed.) A Treatise on Physical Chemistry, D. Van Nostrand Company, New York, 1930.
[116] Weber, W.J., *Adsorption*, in: W.J. Weber (Ed.) Physicochemical Process for Water Quality Control, Wiley-Interscience, 1972.
[117] Cornell, R.M., Schwertmann, U., *The Iron Oxides: Structure, Properties, Reactions, Occurrences and Uses*, Viley-VCH, 2003.
[118] Xue, G., Gao, M., Gu, Z., Luo, Z., Hu, Z., *Chem. Eng. J.*, **218** (2013) 223-231.
[119] Crini, G., Badot, P.-M., *Sorption processes and pollution: conventional and non-conventional sorbents for pollutant removal from wastemasters*, Presses Universitaires de Franche-Comté, 2010.
[120] Boisvert, J.P., To, T.C., Berrak, A., Jolicoeur, C., *Water Res.*, **31** (1997) 1939-1946.
[121] Xie, W.M., Wang, Q.H., Ma, H.Z., Ogawa, H.I., *Int. J. Environ. Pollut.*, **23** (2005) 486-491.
[122] Tanada, S., Kabayama, M., Kawasaki, N., Sakiyama, T., Nakamura, T., Araki, M., Tamura, T., *J. Colloid Interface Sci.*, **257** (2003) 135-140.
[123] ASTM, in: G 102 - 89: Standard Practice for Calculation of Corrosion Rates and Related Information from Electrochemical Measurements, 1999.
[124] Cuevas-Arteaga, C., Porcayo-Calderon, J., *Mater. Sci. Eng., A*, **435** (2006) 439-446.
[125] Vasudevan, S., Lakshmi, J., *Water Sci. Technol.*, **65** (2012) 353-360.
[126] Vasudevan, S., Kannan, B.S., Lakshmi, J., Mohanraj, S., Sozhan, G., *J. Chem. Technol. Biotechnol.*, **86** (2011) 428-436.
[127] Vasudevan, S., Lakshmi, J., Sozhan, G., *Clean-Soil Air Water*, **38** (2010) 506-515.

[128] Lacasa, E., Canizares, P., Saez, C., Fernandez, F.J., Rodrigo, M.A., *Chem. Eng. J.*, **171** (2011) 1012-1017.
[129] Wang, C.-T., Chou, W.-L., Huang, K.-Y., *Sep. Sci. Technol.*, **45** (2010) 212-220.
[130] Xu, Y., Jiang, J.-Q., Quill, K., Simon, J., Shettle, K., *Desalin. Water. Treat.*, **2** (2009) 131-138.
[131] Chou, W.-L., *J. Hazard. Mater.*, **177** (2010) 842-850.
[132] Kalyani, K.S.P., Balasubramanian, N., Srinivasakannan, C., *Chem. Eng. J.*, **151** (2009) 97-104.
[133] Weber, W.J., *Pure Appl. Chem.*, **37** (1974) 375-392.
[134] Langmuir, I., *J. Am. Chem. Soc.*, **40** (1918) 1361-1403.
[135] Freundlich, H., *J. Phys. Chem.*, **57A** (1906) 385-470.
[136] Mead, J., *Aust. J. Soil. Res.*, **19** (1981) 3-342.
[137] Temkin, M., Pyzhev, V., *Acta Physiochim. USSR*, **12** (1940) 217-222.
[138] Brown, A.M., *Comput. Meth. Prog. Bio.*, **65** (2001) 191-200.
[139] Motulsky, H.J., Ransnas, L.A., *FASEB J.*, **1** (1987) 365-374.
[140] Spiess, A.-N., Neumeyer, N., *BMC pharmacology*, **10** (2010) 6-6.
[141] Del Bubba, M., Arias, C.A., Brix, H., *Water Res.*, **37** (2003) 3390-3400.
[142] Kuo, S., McNeal, B.L., *Soil Sci. Soc. Am. J.*, **48** (1984) 1040-1044.
[143] Thistleton, J., Clark, T., Pearce, P., Parsons, S.A., *Process Saf. Environ. Prot.*, **79** (2001) 339-344.
[144] Johnson, P.N., Amirtharajah, A., *J. Am. Water Works Assoc.*, **75** (1983) 232-239.
[145] Leprince, A., Fiessinger, F., Bottero, J.Y., *J. Am. Water Works Assoc.*, **76** (1984) 93-97.
[146] Recht, H.L., Ghassemi, M., Phosphate precipitation with ferrous iron, 17010 EKI 09/71, in: Water Pollution Control Research Series, 1971.
[147] Bagga, A., Chellam, S., Clifford, D.A., *J. Membr. Sci.*, **309** (2008) 82-93.
[148] Yeoman, S., Stephenson, T., Lester, J.N., Perry, R., *Environ. Pollut.*, **49** (1988) 183-233.
[149] Stumm, W., Lee, G.F., *Ind. Eng. Chem.*, **53** (1961) 143-146.
[150] Thistleton, J., Berry, T.A., Pearce, P., Parsons, S.A., *Process Saf. Environ. Prot.*, **80** (2002) 265-269.
[151] Hsu, P.H., *Environmental Letters*, **5** (1973) 115-136.
[152] Fytianos, K., Voudrias, E., Raikos, N., *Environ. Pollut.*, **101** (1998) 123-130.
[153] Lakshmanan, D., Clifford, D.A., Samanta, G., *Environ. Sci. Technol.*, **43** (2009) 3853-3859.
[154] Sasson, M.B., Calmano, W., Adin, A., *J. Hazard. Mater.*, **171** (2009) 704-709.
[155] Parga, J.R., Cocke, D.L., Valverde, V., Gomes, J.A.G., Kesmez, M., Moreno, H., Weir, M., Mencer, D., *Chem. Eng. Technol.*, **28** (2005) 605-612.
[156] Osipenko, V.D., Pogorelyi, P.I., *Metallurgist*, **21** (1977) 628-630.
[157] Mollah, M.Y.A., Schennach, R., Parga, J.R., Cocke, D.L., *J. Hazard. Mater.*, **84** (2001) 29-41.
[158] Hansen, H.K., Nunez, P., Grandon, R., *Miner. Eng.*, **19** (2006) 521-524.
[159] Kobya, M., Senturk, E., Bayramoglu, M., *J. Hazard. Mater.*, **133** (2006) 172-176.
[160] Moreno-Casillas, H.A., Cocke, D.L., Gomes, J.A.G., Morkovsky, P., Parga, J.R., Peterson, E., *Sep. Purif. Technol.*, **56** (2007) 204-211.
[161] Fadrus, H., Maly, J., *Analyst*, **100** (1975) 549-554.
[162] Lee, T.S., Kolthoff, I.M., Leussing, D.L., *J. Am. Chem. Soc.*, **70** (1948) 2348-2352.
[163] Pehkonen, S., *Analyst*, **120** (1995) 2655-2663.
[164] APHA-AWWA-WPCF, *Standard Methods for the examination of Water and Wastewater*, 18th ed., New York, 1992.
[165] Jin, X., Botte, G.G., *J. Appl. Electrochem.*, **39** (2009) 1709-1717.
[166] Pletcher, D., *Instrumental Methods in Electrochemistry*, Woodhead Publishing Paperback, 2011.

[167] Behbahani, M., Moghaddam, A.M.R., Arami, M., *Int. J. Environ. Res.*, **5** (2011) 403-412.
[168] Zheng, X.-y., Kong, H.-N., Wu, D.-y., Wang, C., Li, Y., Ye, H.-r., *Water Sci. Technol.*, **60** (2009) 2929-2938.
[169] Gendel, Y., Lahav, O., *J. Hazard. Mater.*, **183** (2010) 596-601.
[170] Morgan, B., Lahav, O., *Chemosphere*, **68** (2007) 2080-2084.
[171] Irdemez, S., Demircioglu, N., Yildiz, Y.S., *J. Hazard. Mater.*, **137** (2006) 1231-1235.
[172] Jimenez, C., Saez, C., Martinez, F., Canizares, P., Rodrigo, M.A., *Sep. Purif. Technol.*, **98** (2012).
[173] Moreno-Casillas, H.A., Cocke, D.L., Gomes, J.A.G., Morkovsky, P., Parga, J.R., Peterson, E., Garcia, C., *Ind. Eng. Chem. Res.*, **48** (2009) 2275-2282.
[174] Uhlig, H.H., Revie, R.W., *Uhlig's Corrosion Handbook*, 2nd ed., John Wiley & Sons, New York, 2000.
[175] Mollah, M.Y.A., Pathak, S.R., Patil, P.K., Vayuvegula, M., Agrawal, T.S., Gomes, J.A.G., Kesmez, M., Cocke, D.L., *J. Hazard. Mater.*, **109** (2004) 165-171.
[176] Modirshahla, N., Behnajady, M.A., Kooshaiian, S., *Dyes Pigm.*, **74** (2007) 249-257.
[177] Chou, W.-L., Wang, C.-T., Huang, K.-Y., *J. Hazard. Mater.*, **167** (2009) 467-474.
[178] Jimenez Izquierdo, C., Canizares, P., Rodrigo, M.A., Leclerc, J.P., Valentin, G., Lapicque, F., *Desalination*, **255** (2010) 15-20.
[179] Persson, P., Nilsson, N., Sjoberg, S., *J. Colloid Interface Sci.*, **177** (1996) 263-275.
[180] Mayer, T.D., Jarrell, W.M., *Water Res.*, **34** (2000) 3949-3956.
[181] Kreller, D.I., Gibson, G., vanLoon, G.W., Horton, J.H., *J. Colloid Interface Sci.*, **254** (2002) 205-213.
[182] Tzou, Y.M., Wang, M.K., Loeppert, R.H., *Arch. Environ. Contam. Toxicol.*, **44** (2003) 445-453.
[183] Rentz, J.A., Turner, I.P., Ullman, J.L., *Water Res.*, **43** (2009) 2029-2035.
[184] Seida, Y., Nakano, Y., *Water Res.*, **36** (2002) 1306-1312.
[185] Heal, K.V., Dobbie, K.E., Bozika, E., McHaffie, H., Simpson, A.E., Smith, K.A., *Water Sci. Technol.*, **51** (2005) 275-282.

4 Electrochemical Behaviour of Various Electrode Materials in Synthetic Wastewater

4.1 Introduction

The main objective of the work presented in this chapter is to compare the electrochemical properties and behaviour of iron and aluminium based anodes and to assess the feasibility of using these anode materials in the electrocoagulation process. Since electrocoagulation involves the oxidation of the electrode and the subsequent generation of high concentrations of cations, the selection of the anode material is one of the most important steps in developing a successful electrocoagulation unit. The composition of the electrode material has a marked impact on the rate of dissolution and several authors have identified it as a key factor in electrocoagulation applications [1-5].

The most widely used electrode materials are iron and aluminium as described by Vik *et al.* [6] and Novikova *et al.* [7] because they are cheap, readily available, and have proven effective [1, 2, 8]. For example, Do and Chen [9], on comparing the efficiency of iron and aluminium electrodes in removing dyes, concluded that the optimum conditions varied with the choice of iron or aluminium. Later, Baklan and Kolesnikova [4] carried out a study to correlate the size of the flocculants produced with the removal efficiency of organic substances. They conducted a single experiment and concluded that iron electrodes were more efficient because of the size of the flocculant particles, which ranged from 10 to 30 μm for Fe^{3+} compared to the smaller range from 0.05 to 1 μm

for Al^{3+}. On the other hand, Hülser *et al.* [10] investigated the cathodic corrosion of aluminium during the electrodeposition of paint and found that electrocoagulation was strongly enhanced with aluminium in comparison to steel. This was attributed to a higher efficiency of *in situ* formed aluminium hydroxide complexes by hydrolysis of the aluminate ion in acting as nuclei for the electrocoagulation process.

The choice of the electrode material can also affect the consumption of electrical energy supplied to the system in order to induce oxidation of the electrodes. The metal cations, which are necessary in forming the coagulation and flocculation of the pollutants, are generated by applying a constant current or a constant potential. The power consumption of this process depends mainly on the electrochemical properties of the anode material and its resistance to dissolution or corrosion. Accordingly, passive systems are likely to give rise to higher energy consumption. In the light of these considerations, the addition of alloying elements to iron or aluminium is interesting, as these alloying components have a significant effect on the electrochemical behaviour of the metals [11]. The alloying elements can be used to enhance the rate of dissolution or to alter the nature of the dissolution sites, varying from more localised to general dissolution. Indeed, some iron- and aluminium-based alloys, other than pure iron and aluminium, have already been used in electrocoagulation experiments [12].

The electrochemical behaviour of the electrode material is also determined by the nature and the concentration of ions present in the test solution. Some ions are known to have an inhibiting effect on the corrosion reactions, whereas other ions serve as activators, enhancing the rate of dissolution. For example, the presence of chloride anions may give rise to localised corrosion, such as pitting or crevice corrosion. This, in turn, gives high rates of metal dissolution at localised sites, while the remaining surface corrodes at a much lower rate. In contrast, the presence of inhibitors in the solution to be treated gives rise to a decrease in the efficiency of the electrocoagulation due to the release of lower concentrations of metal cations from the electrode [13]. Inhibitors and activators occur together in wastewater treatment facilities and, although the role of the most common ions on the electrode behaviour is well known from the literature, the effect of co-existing ions has not been the subject of a systematic study.

Localised corrosion gives rise to high rates of dissolution at specific sites and the production of high concentrations of metal cations. It is no surprise that several authors have pointed out that localised corrosion is desirable in electrocoagulation as high concentrations of the metal cations are delivered [5, 14, 15]. However, localised corrosion may adversely affect the lifetime of the electrode giving irregular dissolution across the surface [16]. Furthermore, if active pits repassivate, it becomes increasingly more difficult to induce metal dissolution at these passive sites. In contrast, uniform dissolution gives a near uniform rate of dissolution across the electrode surface and this rate of dissolution can be controlled to deliver the required concentration of metal cations.

In this study several iron and aluminium based electrodes were used as anode materials in electrocoagulation tests. The chemical composition of the electrode materials used is given in Section 2.2.1. Pure iron and two stainless steel electrodes, AISI 310 (austenitic grade) and AISI 420 (martensitic grade), were used as the iron-based system. The two stainless steel grades were selected on the basis of their chromium content in order to study the effect of the chromium addition on the removal efficiency in electrocoagulation. AISI 310 has a high chromium content, namely 25%, while AISI 420 has a lower level of chromium, i.e., 13%. Although iron is widely used in electrocoagulation applications, Chen and co-workers [1, 5] and indeed several other authors [17-23] have reported some limitations in its use. In particular, at the end of the treatment the effluent water developed a yellowish colour, thus affecting the overall quality of the water and preventing its discharge to the receiving water bodies. The yellowish colour has been attributed to the presence of fine particles of rust, which form as a result of the oxidation of the ferrous species by dissolved oxygen in water [1], as shown in Section 1.4.2.1. These particles are easily formed when the iron electrodes are used in non-continuous operation [2]. Indeed, the iron electrode corrodes at the open-circuit potential. With the intention of avoiding this negative effect of the rust on the effluent colour, the stainless steels were selected as the presence of chromium facilitates the formation of a protective or passive film preventing, or minimising, the formation of rust [24].

The aluminium-based electrodes included pure aluminium, and two alloys, Al-2Mg and Al-3Zn-0.02In. Along with iron, aluminium has been extensively used in electrocoagulation [8]. However, the existence of a passive film on its surface is one of the main drawbacks of using pure aluminium in electrocoagulation, as the presence of the passive film leads to an increase in the applied potential required to induce dissolution [5, 6, 8, 25]. Furthermore, aluminium corrodes mainly in the form of pitting, which has been recently considered a detrimental form of corrosion in electrocoagulation from an operational perspective [16]. For the purpose of minimising both the effects of the passive film and pitting corrosion, aluminium-magnesium and aluminium-zinc-indium alloys were chosen. Although the addition of magnesium as an alloying element does not have any significant effect in avoiding the pitting corrosion of the electrode, it is known that the corrosion resistance of pure aluminium is affected by the degree of purity of the metal and by the type of alloying elements [26, 27], as also shown in Section 1.4.2.4. Therefore, it is expected that Al-Mg alloys, although still showing good corrosion resistance [24], are less protective leading to more favourable dissolution and generation of Al^{3+} ions in the solution at lower applied potentials. On the other hand, it is known that zinc and indium have the ability to activate aluminium and alter the nature of the dissolution reaction to give more uniform dissolution [28-30].

In this chapter results are presented and discussed on the corrosion behaviour of various electrode materials, which are subsequently used in Chapter 5 to remove pollutants using the electrocoagulation technique. Corrosion parameters, such as the corrosion potential, breakdown potential, and corrosion current, were determined by potentiodynamic polarisation tests, whereas the propensity of the various electrodes to suffer localised corrosion was predicted by cyclic potentiodynamic polarisation measurements and confirmed by light microscopy. As discussed in Section 1.4, the form of corrosion depends on the electrode material and the solution composition and these tests are useful in gaining information about the form and rate of the corrosion reaction [11, 31].

The influence of the solution composition, particularly with regard to the nature and the concentration of some anions commonly present in wastewaters, was studied. The corrosion performance of the electrode materials was investigated in the solutions listed

in Table 4.1. Two synthetic wastewaters, sww 1 and sww 2, which ion concentrations were given from the OECD synthetic sewage [32], were selected in order to study the effect of co-existing ions. They contained three model pollutants, namely phosphates, an azo dye called Orange II (1.4×10^{-4} M), and zinc ions (1.5×10^{-3} M). The composition of the two solutions differs in the chloride ion concentration, 0.017 M in sww 1 and 0.170 M in sww 2. In addition, in order to study the single effect of the anions present in the two synthetic wastewaters, Cl^-, SO_4^{2-}, and PO_4^{3-}, the polarisation tests were also carried out in solutions containing these anions at the same concentration as in sww 1 and sww 2. Slightly higher and lower concentrations were also employed, as highlighted in Table 4.1. For the sake of comparison, results are first presented for the potentiodynamic polarisation and the cyclic potentiodynamic polarisation tests carried out in the single component solutions. Then, results are presented for the mixed solutions, sww 1 and sww 2. By presenting the results in this order, it is possible to discern the effect of the individual anions on the overall electrochemical behaviour of the electrodes in the synthetic wastewater test solutions.

Table 4.1: Composition of the electrolyte solutions used in the potentiodynamic polarisation and cyclic potentiodynamic polarisation tests. The two synthetic wastewaters, sww 1 and sww 2, also contained an azo dye called Orange II (1.4×10^{-4} M) and zinc ions (1.5×10^{-3} M). The pH was maintained at 5.0.

Solution no.		KH_2PO_4 / M	NaCl / M	$CaCl_2.2H_2O$ / M	$MgSO_4.7H_2O$ / M	Na_2SO_4 / M	Tot Cl^- / M
1		-	1.7×10^{-2}	-	-	-	1.7×10^{-2}
2		-	1.7×10^{-1}	-	-	-	1.7×10^{-1}
3		-	1.7×10^{-2}	-	-	8.1×10^{-4}	1.7×10^{-2}
4		1.6×10^{-2}	-	-	-	-	-
5	**sww 1**	1.6×10^{-2}	1.2×10^{-2}	2.7×10^{-3}	8.1×10^{-4}	-	1.7×10^{-2}
6	**sww 2**	1.6×10^{-2}	1.7×10^{-1}	2.7×10^{-3}	8.1×10^{-4}	-	1.7×10^{-1}
7		6.5×10^{-3}	-	-	-	-	-
8		6.5×10^{-3}	5.0×10^{-4}	-	-	-	5.0×10^{-4}

4.2 Pure iron

The potentiodynamic polarisation tests were carried out by polarising pure iron (99.99%) electrodes with a geometric surface area of 0.071 cm^2 in the anodic direction, from -0.900 V vs. SCE up to the breakdown potential, E_{br}, at a rate of 1 mV s^{-1}, unless

otherwise stated. To generate the cyclic potentiodynamic polarisation curves the iron electrodes were cycled at a rate of 1 mV s^{-1} from -0.900 V vs. SCE, but the scan was reversed at 1 mA cm^{-2} or 5 mA cm^{-2}. Then the potential was cycled in the reverse direction until the corrosion potential, E_{corr}, was reached.

4.2.1 The effect of Cl^- ions

Potentiodynamic polarisation curves of pure iron recorded in 0.017 M and 0.170 M NaCl solutions are shown in Figure 4.1. It is evident from the figure that increasing the chloride concentration causes a substantial shift of the corrosion potential, E_{corr}, towards less noble values. The shift reflects a greater susceptibility of iron to corrosion because a higher concentration of chloride ions creates a more aggressive environment. For the 10-fold increase in NaCl concentration, the extent of the shift is about 100 mV, varying from -0.360 V vs. SCE in 0.017 M NaCl to -0.460 V vs. SCE in 0.170 M NaCl. A higher corrosion current, j_{corr}, is also recorded in the more concentrated NaCl solution. At potentials higher than E_{corr}, passivation of the iron electrode occurs and this is characterised by a nearly constant current with increasing applied potential. However, at higher applied potentials, there is a sharp and rapid increase in the current. This marks the onset and initiation of pitting corrosion. The breakdown potential, E_{br}, which represents the potential at which pitting is initiated, is computed as -0.090 V vs. SCE in 0.017 M NaCl and -0.290 V vs. SCE in 0.170 M NaCl. Thus, it is evident that increasing chloride concentration shifts the breakdown potential to more active values. In addition, the extent of the passive range, ΔE_{pass}, calculated as the difference between the breakdown potential, E_{br}, and the corrosion potential, E_{corr}, increases with the decreasing chloride concentrations. In 0.017 M NaCl, ΔE_{pass} is approximately 0.270 V, while it is reduced to 0.180 V in the more concentrated 0.170 M NaCl solution.

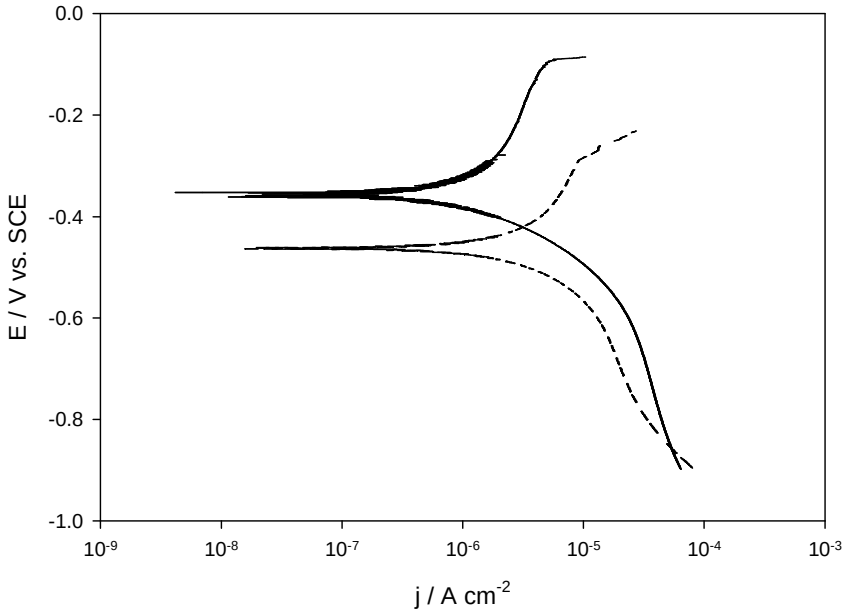

Figure 4.1: Potentiodynamic polarisation curves recorded at a scan rate of 1 mV s^{-1} for pure iron in ——— 0.017 M and – – – 0.170 M NaCl solutions at a pH of 5.0.

The effect of chloride ion concentration on the breakdown potential can also be shown by plotting the breakdown potential, E_{br}, as a function of the logarithm of the chloride concentration. In order to determine this relationship for the pure iron electrode, polarisation tests were carried out in 0.017, 0.100, 0.170, and 0.300 M NaCl solutions adjusted to a pH of 5.0, and the resulting plot is displayed in Figure 4.2. As evident from this figure, a linear relationship exists and, using linear regression analysis, the Eq. 4.1 is obtained.

$$E_{br} = -0.409 - 0.180[\mathrm{Cl}^-] \qquad \textbf{Eq. 4.1}$$

According to Eq. 4.1, as the chloride concentration decreases, the breakdown potential, E_{br}, is displaced to higher potentials. The value of the slope, which is represented by B, is somewhat higher than the values presented by Galvele and co-workers [33, 34]. In 1976 Galvele developed an extensive model on the mechanism of pitting corrosion [33] and he reported a logarithmic relationship between the breakdown potential, E_{br}, and the concentration of aggressive anions. Galvele accounted for this relationship, which is valid with several anions and other metals [35], by considering the effect of chloride concentration on the potential drop within the pit and this explanation was also used by

Laycock and Newman [36, 37] in their studies on stainless steel electrodes. According to Galvele, a value of 59 to 64 mV is obtained for pure iron in de-aerated NaCl solutions, at a pH of 10, if the migration of the chloride ions inside the pits is the only variable considered [33, 38]. However, several works reported different values of B for iron, most of them are listed in a review by Galvele [34], containing a comprehensive list of values for several electrode materials and environments. For pure iron in chloride solutions the B values range from 30 to 150 mV. The value shown in Eq. 4.1 is beyond that range, however it has to be considered that the value adopted by B can be affected by several variables, such as the pH of the solution, the presence of a buffer, the oxygen content, temperature, nature of the electrolyte, and roughness of the electrode surface [36]. The measurement technique and the can rate can also influence the magnitude of B. Indeed, several of the reported studies have been carried out using the potentiostatic technique rather than the potentiodynamic approach. The experimental value of B, shown in Eq. 4.1, can be used to compare the sensitivity of the various electrode materials to chloride concentration. Accordingly, this analysis was performed on the various electrodes and the B values were compared.

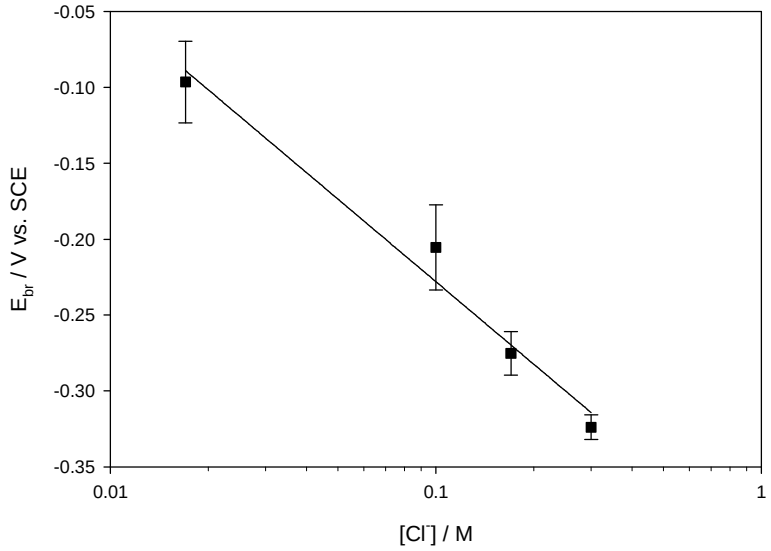

NaCl / M	E_{br} / V vs. SCE
0.017	-0.10 ± 0.03
0.100	-0.21 ± 0.01
0.170	-0.28 ± 0.03
0.300	-0.324 ± 0.008

Figure 4.2: Breakdown potential, E_{br}, of the pure iron plotted as a function of the logarithm of the chloride concentration. Each experiment was performed in triplicate (n = 3). The breakdown potential, E_{br}, was obtained from potentiodynamic polarisation tests at a scan rate of 1 mV s^{-1}. The experimental points were fitted by a linear regression analysis to E_{br} = A + B log [Cl^-], A = –0.409 ± 0.022 V, B = –0.180 ± 0.019 V, and R^2 = 0.976.

The susceptibility of the iron electrode to localised corrosion was investigated further using cyclic potentiodynamic polarisation tests. Representative data are shown in Figure 4.3(a) where the cyclic polarisation curves for pure iron in 0.017 M and 0.170 M NaCl are compared. The data recorded during the forward and reverse cycles are clearly different giving hysteresis. This phenomenon is usually associated with the onset of pitting attack and in some theories it is suggested that the larger the hysteresis, the more likely a localised corrosion site will propagate once initiated [24]. However, a post-scan microscopic examination of the sample is recommended in order to confirm the nature of the attack [39].

The surface of the electrode was examined using light microscopy after the cyclic polarisation tests were completed, and representative micrographs are shown in Figure 4.3(b) and (c). Pitting attack is clearly evident, with the size and distribution of the pits depending on the concentration of the chloride solution. From Figure 4.3(b) it is evident that in 0.017 M NaCl, the size of the pits ranges from 2 to 8 μm and these are evenly dispersed over the electrode surface. In contrast, the micrograph recorded in the presence of 0.170 M NaCl (Figure 4.3(c)) shows fewer pits, with the larger pits having a diameter from 20 to 25 μm and these are scattered among several smaller pits with a diameter of about 1 μm. These findings are consistent with the higher rates of dissolution in the 0.170 M NaCl solution. Once a pit is nucleated, the propagation step is more rapid at the higher chloride concentrations and this gives rise to larger pits. This attack continues at several isolated sites, while new sites are activated to give the smaller sized pits that are also observed on the surface. These sites are smaller as they are not nucleated at the breakdown potential, E_{br}, but sometime later during the forward or reverse cycle.

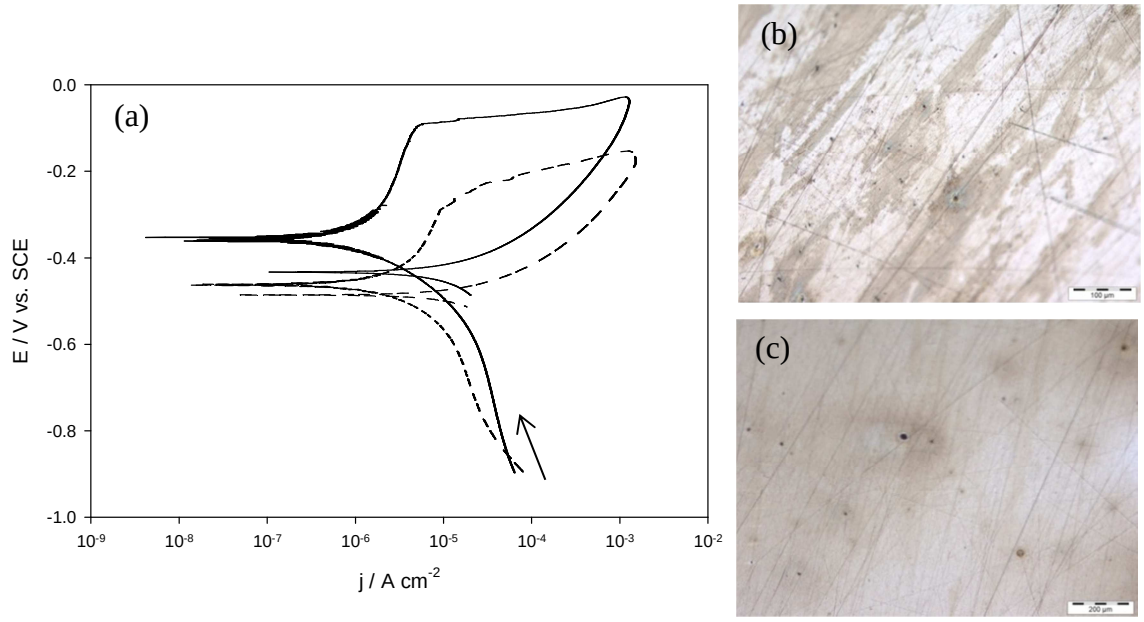

Figure 4.3: (a) Cyclic potentiodynamic polarisation curves recorded for the pure iron in —— 0.017 M and – – – 0.170 M NaCl solutions at a pH of 5.0 at a scan rate of 1 mV s^{-1}; micrographs of pure iron electrode at the end of the cyclic potentiodynamic polarisation scan in (b) 0.017 M NaCl, with the scale bar corresponding to 100 μm and (c) 0.170 M NaCl, with the scale bar corresponding to 200 μm.

4.2.2 The effect of SO_4^{2-} ions

Since the two synthetic wastewaters, sww 1 and sww 2, used as test solutions in the electrocoagulation experiments contain sulfate ions, potentiodynamic polarisation tests were carried out to investigate the effect of the presence of sulfate ions on the electrochemical behaviour of pure iron. However, the conductivity of the 8.1×10^{-4} M SO_4^{2-} solution was too low for the corrosion tests and 0.017 M NaCl was added to the Na_2SO_4 solution as shown in Table 4.1, while the pH was maintained at a value of 5.0. The resulting polarisation curve was compared to the data recorded in the absence of sulfate ions (Section 4.2.1) and these data are presented in Figure 4.4. As can be seen from the figure, the two curves are noticeably different. A clear passive region is evident in the 0.017 M NaCl solution, but with the addition of the sulfate ions there is a slight increase in the corrosion potential, E_{corr}, from -0.359 V vs. SCE in the absence of sulfate ions to -0.319 V vs. SCE in the presence of sulfate. There is a corresponding increase in the corrosion current from 9.29×10^{-7} A cm^{-2} to 1.90×10^{-6} A cm^{-2}, and the breakdown potential, E_{br} is lowered from -0.091 to -0.162 V vs. SCE. Moreover, the passive current density is higher and the passive region is less defined in the presence of the sulfate ions. However, the rapid increase in the current at -0.162 V vs. SCE is consistent with the onset of pitting attack.

The effect of sulfate ions on the breakdown and dissolution of iron has been described in several reports. For example, Vatankhah *et al.* [40] found that rotating iron disk electrodes exhibit uniform corrosion in 1.0 M solutions containing sulfate ions. Also, MacDougall and Bardwell [41] concluded that the passivation of iron is an efficient process in 0.15 M sulfate solutions at pH 3.0 or 8.4. However, when iron is polarised in a solution comprising chlorides and sulfates, localised dissolution and pitting attack is observed. Bird *et al*. [42] showed that the presence of sulfate ions reduces the pitting potential of iron as a result of competitive adsorption between the anions present in solution. Nobe and Tobias [43] reported similar findings for iron in 1.0 M Na_2SO_4 solutions with various amounts of chloride ions (from 0.00 to 0.05 M) at pH 3.0. Nobe and Tobias [43] observed an increase in the current density in the passive region with an increase in the concentration of chloride ions. However, the current density varied with the ratio of the sulfate to chloride concentration. The results presented in Figure 4.4 are consistent with these studies reported in sulfate solutions with added chlorides.

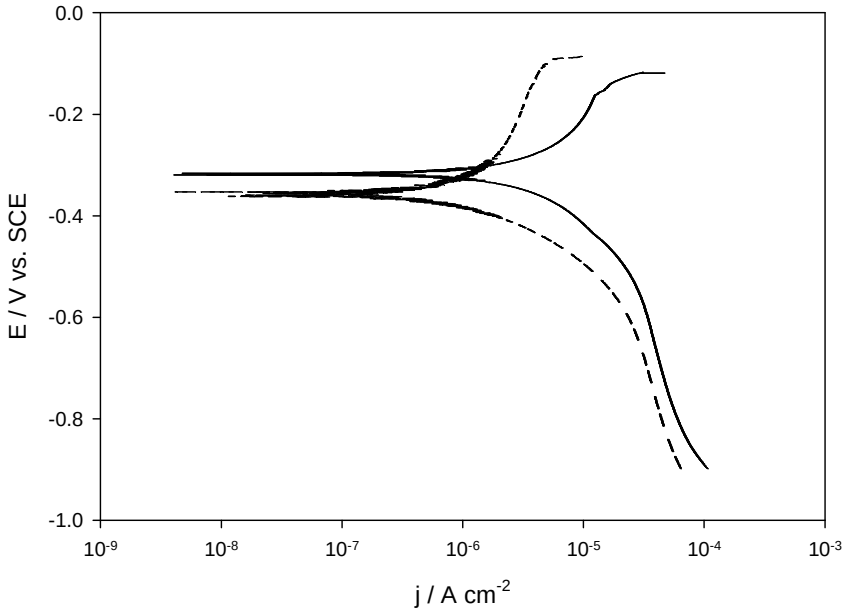

Figure 4.4: Potentiodynamic polarisation curves recorded for the pure iron in —— 0.017 M NaCl and 8.1×10^{-4} M Na_2SO_4 solution at a pH of 5.0 and – – – 0.017 M NaCl at a pH of 5.0, at a scan rate of 1 mV s^{-1}.

To confirm the onset of pitting corrosion of the pure iron electrode in the sulfate-containing solution, cyclic potentiodynamic polarisation tests were carried out in a

0.017 M NaCl and 8.1 × 10^{-4} M Na_2SO_4 solution (Table 4.1). The cyclic curve is displayed in Figure 4.5, and clearly shows hysteresis between the forward and reverse cycle, indicating pitting corrosion. Indeed, pits were found on examination of the electrode surface using light microscopy, as shown in Figure 4.5(b). This micrograph shows the presence of large pits with a diameter of about 2 μm, and several smaller pits distributed across the surface. These pits are smaller than the pits observed in the chloride solution in the absence of sulfate anions (Section 4.2.1, Figure 4.3). These results are consistent with the findings of Galvele [33], who observed inhibition of pitting corrosion in the presence of sulfate anions. As the pits start to grow, sulfate ions are accumulated inside the pits, since the anions with the higher charge are preferentially accumulated at the metal-solution interface. This build up in the concentration of the sulfate ions gives rise to repassivation of the pits. However, chloride ions eventually diffuse to the site, reducing the concentration of sulfates inside the pits. As a consequence, a continuous process of activation and deactivation of the pits is observed. It is clear from the micrograph and the polarisation tests that iron is susceptible to pitting attack in a solution containing 0.017 M NaCl and 8.1 × 10^{-4} M Na_2SO_4 at a pH of 5.0.

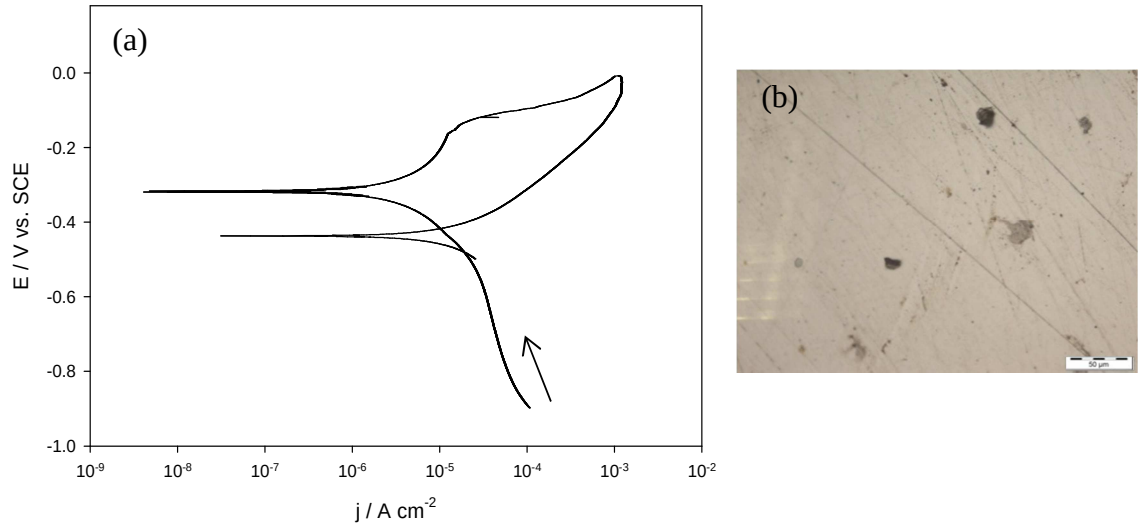

Figure 4.5: (a) Cyclic potentiodynamic polarisation curve for the pure iron recorded in —— 0.017 M NaCl and 8.1 × 10^{-4} M Na_2SO_4 solution at a pH of 5.0, at a rate of 1 mV s^{-1}; (b) micrograph, with the scale bar corresponding to 50 μm, of pure iron at the end of the cyclic potentiodynamic polarisation scan.

4.2.3 The effect of PO_4^{3-} ions

Phosphates are one of the most popular corrosion inhibitors employed in the corrosion protection of ferrous alloys [11, 44, 45]. In addition, phosphates were added to give the two synthetic wastewaters, sww 1 and sww 2, as detailed in Table 4.1. Therefore, corrosion studies were carried out in a phosphate-containing solution in order to investigate the effects of the phosphate ions on the iron electrode and then to allow a more direct comparison with the results obtained in the two synthetic wastewaters, sww 1 and sww 2. The polarisation plots were recorded in 0.016 M KH_2PO_4 (Table 4.1). A typical plot is presented in Figure 4.6 and it is clearly evident that the polarisation behaviour is very different to that observed in the chloride or sulfate solutions in Sections 4.2.1 and 4.2.2, respectively. The corrosion potential, E_{corr}, is -0.720 V vs. SCE, considerably lower than the value observed in the chloride or sulfate solutions, and the corrosion current, j_{corr}, is one order of magnitude higher, at 3.1×10^{-5} A cm^{-2}. These data clearly show that the corrosion rate is higher in the 0.016 M KH_2PO_4 solution. In addition, the anodic portion of the scan does not show any passive region. The current increases in a near linear manner from the corrosion potential, E_{corr}, to reach a value of about 1 mA cm^{-2} at -0.550 V vs. SCE. This indicates significant dissolution.

Phosphates are well known as film-forming corrosion inhibitors [44, 45] and phosphate-containing solutions have been proposed and used as environmentally acceptable alternatives to chromates in corrosion inhibition applications [46-48]. The corrosion protection is provided by the formation of precipitates on the surface of the metal, thereby forming a protective film [44, 45]. However, as shown by the work of Szklarska-Smialowska and Staehle [49], corrosion inhibition in phosphate-containing solutions is highly dependent on the solution pH. The authors conducted an ellipsometric study to elucidate the optical properties of the film growth on iron electrodes in 0.1 M sodium orthophosphate solutions at different pH values, from 4.5 to 12.3. The growth of the film was found regardless of the solution pH, but the type and nature of the film were considerably different. In particular, at pH 4.5 and 7.0 in the presence of $H_2PO_4^-$ ions in solution, a porous and non-protective film was formed, giving little or no corrosion protection. Similar results were reported by Pryor and Cohen [50]. The results obtained in Figure 4.6 are consistent with active dissolution of the pure iron electrode in the phosphate solution at a pH of 5.0 and are in good

agreement with these literature reports. Furthermore, this active dissolution at a pH of 5.0 is consistent with the optimum pH range, from a value of 5.0 to 7.0, reported by İrdemez *et al.* [51] in removing phosphates using electrocoagulation with iron electrodes.

Polarisation tests were also recorded with a lower concentration of phosphate anions, 6.5×10^{-3} M KH_2PO_4, however in this case chloride anions, 5.0×10^{-4} M NaCl, were added to the solution to increase the conductivity. Again, data similar to that presented in Figure 4.6 were obtained, indicating active dissolution of the iron electrode.

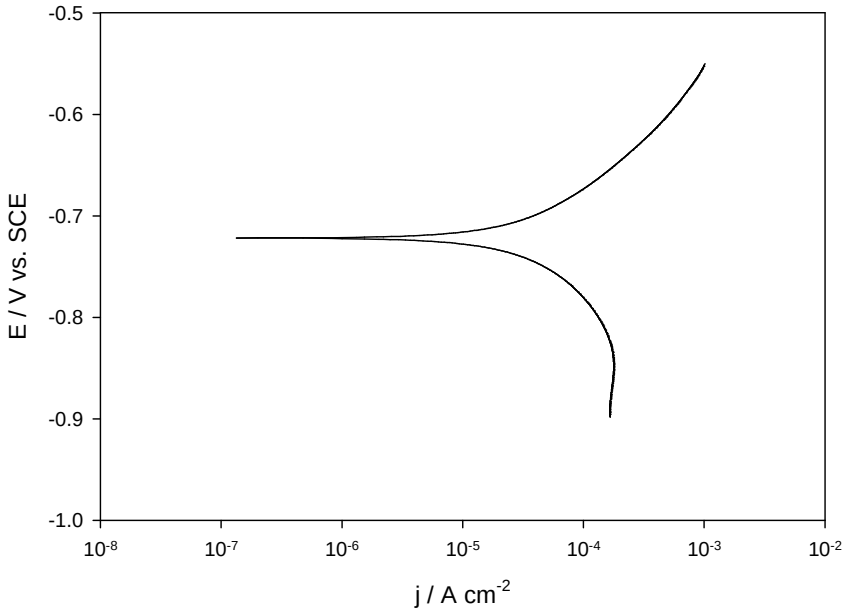

Figure 4.6: Potentiodynamic polarisation curve recorded at a scan rate of 10 mV s^{-1} for the pure iron electrode in —— 0.016 M KH_2PO_4 solution at a pH of 5.0.

In an attempt to obtain more information on the nature of the dissolution, cyclic potentiodynamic polarisation tests were recorded in 0.016 M KH_2PO_4 (Table 4.1). In Figure 4.7(a), a representative cyclic polarisation plot is presented and in this case there is little difference between the forward and reverse portions of the scan and there is no evidence of any significant hysteresis. This phenomenon has been explained by Silverman [52] in terms of relatively large amounts of charge and active or rapid corrosion that gives a sharp increase in current under slight polarisation. The small difference in current recorded at the same potential between the two portions of the scan

depends on the scan direction; in the reverse scan the current does not represent the steady state current at the applied potential because of the large charge that has passed in the forward scan. This finding is supported by the micrograph presented in Figure 4.7(b). This was recorded following the cyclic polarisation measurement. Several small active sites are present on the surface. However, it was also possible to identify some pits with a larger diameter of approximately 4 μm.

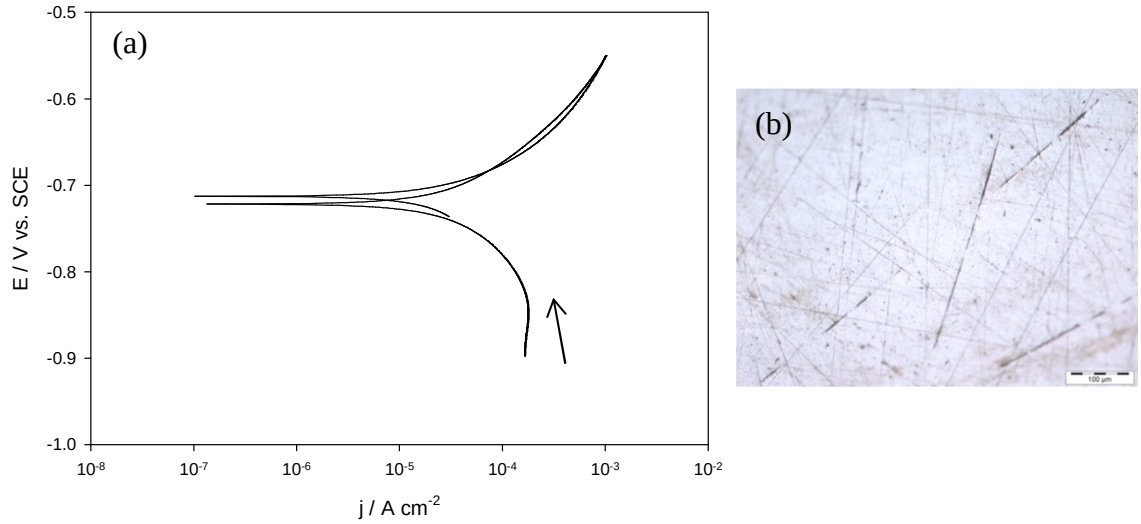

Figure 4.7: (a) Cyclic potentiodynamic polarisation curve recorded for the pure iron electrode at a scan rate of 1 mV s^{-1} in —— 0.016 M KH_2PO_4 solution, at a pH of 5.0; (b) micrograph of the pure iron electrode at the end of the cyclic potentiodynamic polarisation scan, scale bar corresponds to 100 μm.

These results are important in terms of electrocoagulation. It is clear that the iron electrode is not prone to significant passivation in the slightly acidic phosphate solution. Furthermore, the absence or the presence of chloride ions has little influence on the polarisation behaviour of the iron electrode. Accordingly, variations in the chloride concentration should not pose any significant issue in water treatment facilities since the electrochemical behaviour of iron remains almost constant.

4.2.4 The effect of co-existing anions in sww 1 and sww 2

The effect of the co-existing anions on the electrochemical properties of the pure iron was studied by polarising the electrode in sww 1 and sww 2 (Table 4.1). The potentiodynamic polarisation plots are shown in Figure 4.8 and, although the polarisation curves are similar, the corrosion potentials, E_{corr}, are slightly different at

approximately -0.710 V and -0.724 V vs. SCE in sww 1 and sww 2, respectively. This small difference is probably due to the 10-fold increase in the chloride concentration for the sww 2 solution (Table 4.1). However, the corrosion currents, j_{corr}, are nearly identical at 3.1×10^{-5} A cm^{-2} in sww 1 and 2.9×10^{-5} A cm^{-2} in sww 2. Interestingly, these values are significantly higher compared to the j_{corr} values obtained in the NaCl solutions (Section 4.2.1, Figure 4.1). Furthermore, the polarisation curves, shown in Figure 4.8, are very similar to that obtained in the KH_2PO_4 solution (Figure 4.6). Indeed both the corrosion potential, E_{corr}, and the corrosion current, j_{corr}, are similar and the shapes of the polarisation curves are nearly identical (Figure 4.6), indicating active dissolution of the electrode with little evidence of passivity. However, it has to be considered that in the two synthetic wastewaters the phosphates are present in relatively high concentrations with respect to the other electrolytes, thus potentially masking the effect of the other anions. However, a potentiodynamic polarisation scan (data not shown) performed in a solution with the same composition and concentration as in sww 1, but with 1.60×10^{-3} M KH_2PO_4, was similar. Although in this scan the corrosion potential, E_{corr}, was higher at -0.482 V vs. SCE and the corrosion current, j_{corr}, was considerably lower at 8.38×10^{-6} A cm^{-2}, there was no evidence of any passive region. It is clear from these results that the phosphate ions have a significant influence on the corrosion behaviour of pure iron in slightly acidic solutions, with a pH of 5.0.

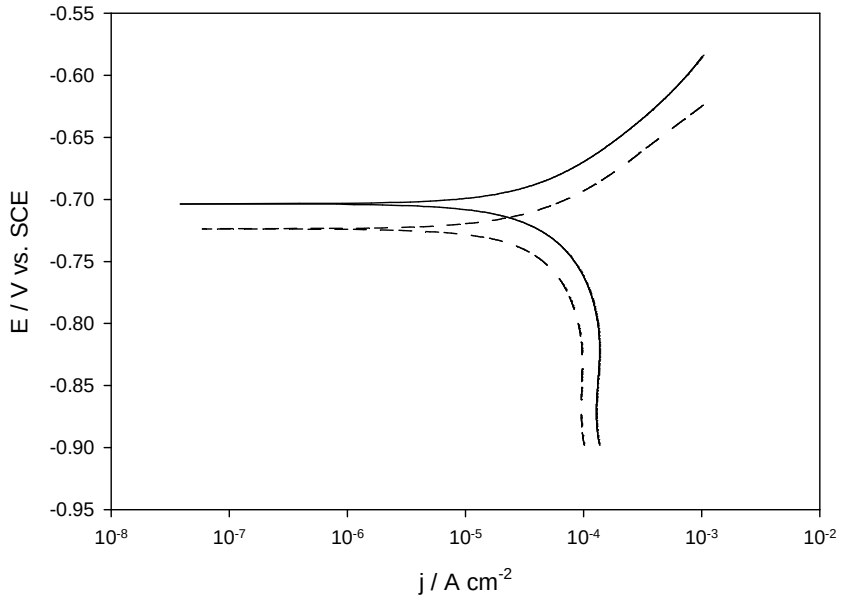

Figure 4.8: Potentiodynamic polarisation curves recorded at a scan rate of 1 mV s^{-1} for the pure iron electrode in —— sww 1 and – – – sww 2 solutions, at a pH of 5.0 (Table 4.1).

Again, cyclic potentiodynamic polarisation tests were carried out in sww 1 and sww 2 solutions and representative plots are presented in Figure 4.9(a). Clearly there is no significant hysteresis, with the forward and reverse cycles in relatively good agreement. These data are similar to that recorded in the phosphate solution (Section 4.2.3, Figure 4.7), highlighting the significant influence of the phosphate anions. Moreover, the 10-fold increase in the chloride concentration, sww 2, has little influence on the level of agreement between the forward and reverse cycles. There is no obvious hysteresis in either the sww 1 or sww 2 solutions. The surface of the electrodes was studied by post-scan examinations of the electrode surface by light microscopy. The micrographs of the iron electrode cycled in sww 2 are presented in Figure 4.9(b) and (c) and reveal that the electrode surface is covered by small dissolution sites, with no significant pits. A similar surface morphology was observed for the iron electrode after the cyclic scan in sww 1. These results indicate that pitting attack induced by the chloride ions, even at reasonably high concentrations, is mitigated or minimised in the presence of phosphate ions at a pH of 5.0. This can be explained by the lack of a passive region. Since in sww 1 and sww 2 the pure iron electrode shows no passive behaviour and more general-like dissolution or corrosion, it is a promising material in treating the two synthetic wastewaters using the electrocoagulation technique.

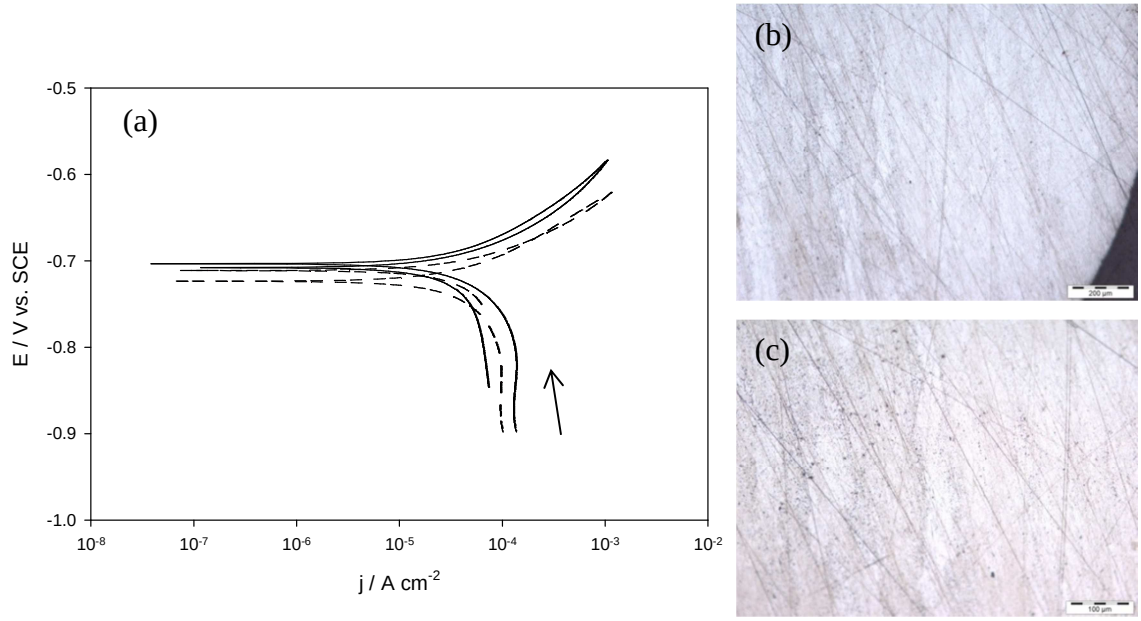

Figure 4.9: (a) Cyclic potentiodynamic polarisation curves for the pure iron electrode in —— sww 1 and – – – sww 2 solution, at a pH of 5.0 (Table 4.1) at a scan rate of 1 mV s^{-1}; micrographs of the pure iron electrode at the end of the cyclic potentiodynamic polarisation scan in sww 2 solutions (b) scale bar corresponding to 200 μm and (c) scale bar corresponding to 100 μm.

4.3 Stainless steel AISI 310

Similar experiments were carried out with the AISI 310 (Fe/Cr25/Ni20) stainless steel grade electrodes. The potentiodynamic polarisation tests were carried out by polarising the electrodes, with a geometric area of 0.58 cm^2, in the anodic direction, from an initial potential of -0.900 V vs. SCE up to a final potential of 1.100 V vs. SCE at a scan rate of 1 mV s^{-1}. In the cyclic potentiodynamic polarisation curves the scan was reversed when the current reached a value of 1 mA cm^{-2}. Again, the polarisation behaviour was studied in simple chloride, sulfate and phosphate solutions, and then studies in the synthetic wastewaters, sww 1 and sww 2, were performed. The pH of the solutions was maintained at 5.0.

4.3.1 The effect of Cl^- ions

AISI 310 belongs to the austenitic stainless steel family, containing chromium and nickel, as outlined in Section 1.4.2.2. In particular, the 310 grade is characterised by an excellent corrosion resistance because of a high chromium and nickel content (24-26% Cr, 19-22% Ni). The corrosion resistance of stainless steel is attributed to the formation of a thin, adherent and self-healing passive film consisting of mixed oxides of chromium and iron. The increasing chromium content in stainless steel enhances the stability of the passive film, while the presence of nickel delays the decrease in pH during pit growth by neutralising the solution in the pit [53]. Austenitic steels, however, are not immune to pitting corrosion, particularly in the presence of chloride ions [54]. The beneficial effects of chromium, nickel, and other alloying elements are determined by the pitting and crevice corrosion resistance index, known as the pitting resistance equivalent number, PREN [55]. The PREN is given by the relative contribution of the alloying elements, as shown in Eq. 4.2.

$$\mathrm{PREN} = [\mathrm{Cr}] + 3.3[\mathrm{Mo}] + 16[\mathrm{N}] + 1.65[\mathrm{W}] \qquad \textbf{Eq. 4.2}$$

In this equation, [Cr] indicates the % weight of Cr in the alloy, while [Mo], [Ni], and [W] give the contributions of the other alloying elements. In general, higher pitting and crevice corrosion resistance is achieved when the numerical value of PREN is high. The PREN value for AISI 310 has been computed as 25.0 [55].

The evidence of this high corrosion resistance is provided in Figure 4.10(a), which shows the potentiodynamic polarisation tests of the AISI 310 electrode in 0.017 M and 0.170 M NaCl (Table 4.1). There is no marked difference in the shape of the polarisation curves and the electrode exhibits a wide, extended passive range of approximately 500 mV in both solutions. The breakdown potentials, E_{br}, are 0.102 V vs. SCE and 0.054 V vs. SCE in 0.017 M and 0.170 M NaCl, respectively. Relatively low corrosion currents are measured, with j_{corr} values of 2.23×10^{-6} A cm^{-2} in 0.017 M and 2.03×10^{-6} A cm^{-2} in 0.170 M NaCl, showing that the chloride concentration has little influence. The extent of the passive region, ΔE_{pass}, does not increase with decreasing chloride concentrations, which is somewhat different to that observed with the iron electrode (Section 4.2.1).

The shift in the breakdown potential with increasing concentration of chloride is in good agreement with several reports on AISI 304, a stainless steel with 18% Cr and 8% Ni (Fe-Cr18-Ni8). For example, Leckie and Uhlig [56] carried out a study on the environmental factors affecting the breakdown potential of Fe-Cr18-Ni8. In a 0.1 M NaCl solution, the breakdown potential was observed at 0.116 V vs. SCE and lower breakdown potentials were recorded with increasing chloride concentrations. Several studies have also been carried out to investigate the effect of increasing the concentration of chromium in austenitic stainless steels. For example, Horvath and Uhlig [57] studied the effect of the concentration of the alloying elements of the Cr-Fe-Ni-Mo system in NaCl solutions. A significant increase in the breakdown potential, E_{br}, was observed for Cr concentrations between 25 and 40% in the Cr-Fe binary alloys in 0.1 M NaCl, indicating a greater resistance to pitting attack. Pitting attack was observed for the 48.8% Cr-Fe alloy, however pitting was not evident with the 57.8% Cr-Fe. With regard to the ternary systems, 15% Cr-Fe-Ni-Mo, an increase in the breakdown potential, E_{br}, was observed with an increase in the Ni concentration. The high breakdown potentials recorded for the AISI 310 stainless steel, which contains 25% Cr and 20% Ni, is consistent with these reports.

The AISI 310 electrode was polarised in a slightly acidic solution, with a pH of 5.0, and the concentration of the chloride anion was varied. The breakdown potential was measured as a function of the chloride concentration and a logarithmic relationship was

obtained with the breakdown potential, E_{br}, decreasing linearly with the logarithm of chloride concentration, as depicted in Figure 4.10(b). A similar linear dependence was found with the iron electrode polarised in NaCl solutions (Section 4.2.1) in agreement with the results reported by Galvele [34]. The linear relationship obtained for AISI 310, was found using linear regression analysis, and is shown in Eq. 4.3.

$$E_{br} = 0.018 - 0.046[\mathrm{Cl}^-] \qquad \textbf{Eq. 4.3}$$

The value of B was computed as 46 mV (Eq. 4.3). This is somewhat smaller than the value of approximately 88 mV reported for Fe-Cr18-Ni8 [56]. However, a smaller B value is expected for the AISI 310 because it is less susceptible to pitting corrosion. It is worth noting in Figure 4.10(a) that in 0.017 M NaCl a transition occurs at about -0.040 V vs. SCE, where the current increases to reach a maximum value before decaying again. This active-passive transition, which is also called the "anodic nose", has been reported for some austenitic stainless steel alloys in dilute acidic environments [52]. This behaviour has been explained in terms of a passivation process or a valency change. It is clear that this anodic nose is not present in the more concentrated 0.170 M NaCl solution.

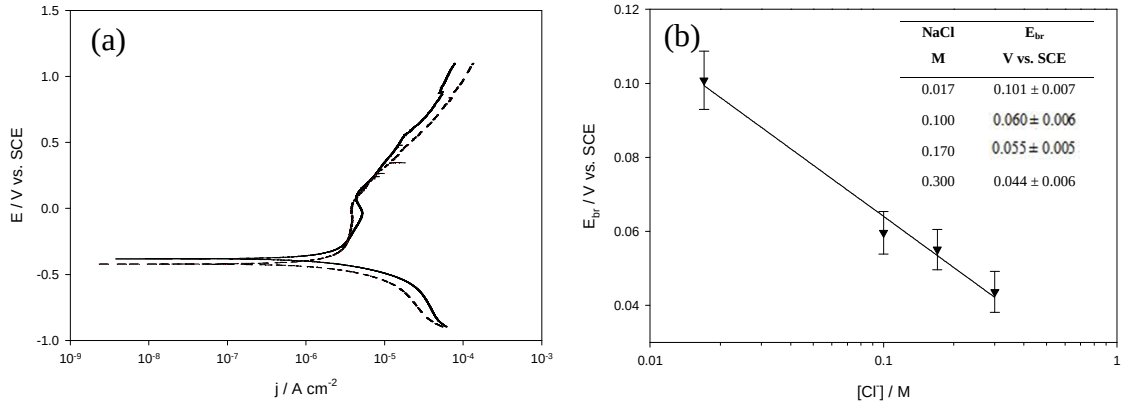

Figure 4.10: (a) Potentiodynamic polarisation curves for the AISI 310 electrode in —— 0.017 M and – – – 0.170 M NaCl solutions, at a pH of 5.0, recorded at a scan rate of 1 mV s^{-1}. (b) Breakdown potential, E_{br}, of AISI 310 as a function of the logarithm of the chloride concentration. The breakdown potential, E_{br}, was obtained from potentiodynamic polarisation tests. Each experiment was performed in triplicate (n = 3). The experimental points were fitted by a linear regression analysis to E_{br} = A + B log [Cl^-], A = 0.018 ± 0.004 V, B = –0.046 ± 0.004 V, R^2 = 0.986.

The cyclic potentiodynamic polarisation tests, recorded with the AISI electrode in 0.170 and 0.017 M NaCl at a pH of 5.0, are presented in Figure 4.11(a). In both cases, significant hysteresis is observed and this can be attributed to the growth of large pits as illustrated in the micrographs shown in Figure 4.11(b) and (c). Isolated pits with irregular shape and with a size of about 50 to 70 μm are evident on the electrode surface. This clearly shows that once the passive film is destroyed, the pits propagate at relatively high rates, but this is also connected to the potentials applied to the electrode, which extend to values in the vicinity of 1.40 V vs. SCE.

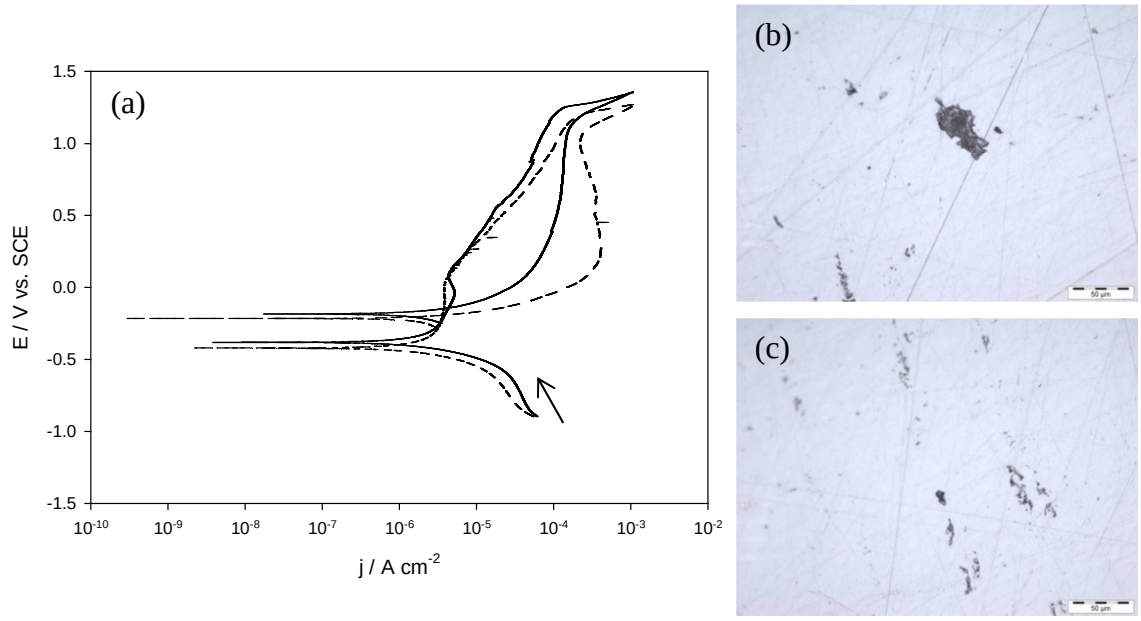

Figure 4.11: (a) Cyclic potentiodynamic polarisation curves for the AISI 310 electrode in —— 0.017 M and – – – 0.170 M NaCl solutions, at a pH of 5.0, recorded at a scan rate of 1 mV s^{-1}; (b) and (c) micrographs of the AISI 310 electrode at the end of the cyclic potentiodynamic polarisation scan in 0.170 M NaCl solution, with the scale bar corresponding to 50 μm.

4.3.2 The effect of SO_4^{2-} ions

The influence of sulfate anions on the polarisation behaviour of AISI 310 is shown in Figure 4.12, where the potentiodynamic polarisation curve recorded in 0.017 M NaCl solution is compared with the data obtained in 0.017 M NaCl with 8.1×10^{-4} M Na_2SO_4 (Table 4.1). Again, a clear passive region is evident in the sulfate-containing solution. Indeed, the passive current density is somewhat lower in the presence of the sulfate anions. The breakdown potential was computed as 0.131 V vs. SCE, which is slightly higher than the value observed in the NaCl solution (E_{br} = 0.102 V vs. SCE in 0.017 M NaCl).

It is well known that the breakdown potential in chloride-containing solutions depends on the concentration and nature of other anions in the solution [58]. In particular, Brauns and Schwenk [59] observed this behaviour for OH^- and SO_4^{2-} additions. Leckie and Uhlig [56] also found that the breakdown potential of Fe-Cr18-Ni8 stainless steel in 0.10 M NaCl increased with increasing Na_2SO_4 concentrations, and in 0.15 M Na_2SO_4 pitting did not occur. The data presented in Figure 4.12 are consistent with these findings and show that sulfate additions inhibit the pitting corrosion of AISI 310. According to Leckie and Uhlig [56, 58], the magnitude of the breakdown potential shift depends on the ratio of sulfate to chloride ions. On addition of 0.0125 M Na_2SO_4 to 0.100 M NaCl, they observed a 50 mV increase in the breakdown potential. A smaller increase of the breakdown potential, about 29 mV, is instead evident in Figure 4.12 for AISI 310, however, this can be explained in terms of the low SO_4^{2-}/Cl^- ratio. It is also evident from Figure 4.12 that although an anodic nose is observed at about 0.010 V vs. SCE, the current is lower and this feature is less pronounced in the presence of the sulfate anions. Moreover, when cyclic polarisation plots were recorded in the presence of sulfate, in 0.017 M NaCl and 8.1×10^{-4} M Na_2SO_4, although hysteresis was observed and pits were found on the surface, the pits were smaller in diameter (data not shown). Again, this highlights the role of sulfate anions as inhibitors in the pitting corrosion of AISI 310.

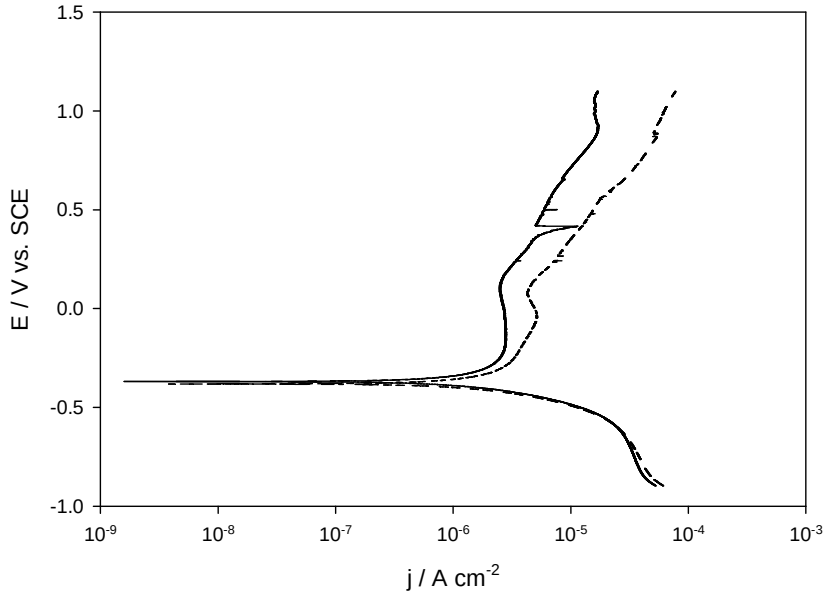

Figure 4.12: Potentiodynamic polarisation curves recorded for the AISI 310 at a scan rate of 1 mV s^{-1} in —— 0.017 M NaCl and 8.1×10^{-4} M Na_2SO_4, at a pH of 5.0 and – – – 0.017 M NaCl, at a pH of 5.0.

4.3.3 The effect of PO_4^{3-} ions

As mentioned in Section 4.2.3, phosphate ions are well known to have an inhibiting effect on the corrosion of ferrous alloys [11, 44, 45]. This property can adversely affect the energy demand in removing phosphates from water using the electrocoagulation technique. To investigate the extent of this effect, potentiodynamic polarisation tests were carried out on the AISI 310 electrode in 0.016 M KH_2PO_4 (Table 4.1) and a representative curve is shown in Figure 4.13(a). As illustrated in the figure, the electrode remains passive and low currents of the order of 1 μA cm^{-2} are evident from the corrosion potential, E_{corr}, to values in the vicinity of 1.00 V vs. SCE. Lakatos-Varsányi *et al.* [60] studied the influence of phosphate on the electrochemical behaviour of AISI 304 exposed to neutral chloride-containing solutions and found that phosphate ions enhance the repassivation properties of stainless steel. Indeed, this finding is consistent with the results obtained from the cyclic potentiodynamic polarisation curve, shown in Figure 4.13(b). In fact, the repassivation potential, which corresponds to the potential at which the forward and reverse scans cross each other, occurs at a very high potential of 1.10 V vs SCE. Below the repassivation potential a stable growing pit or crevice site will cease to grow.

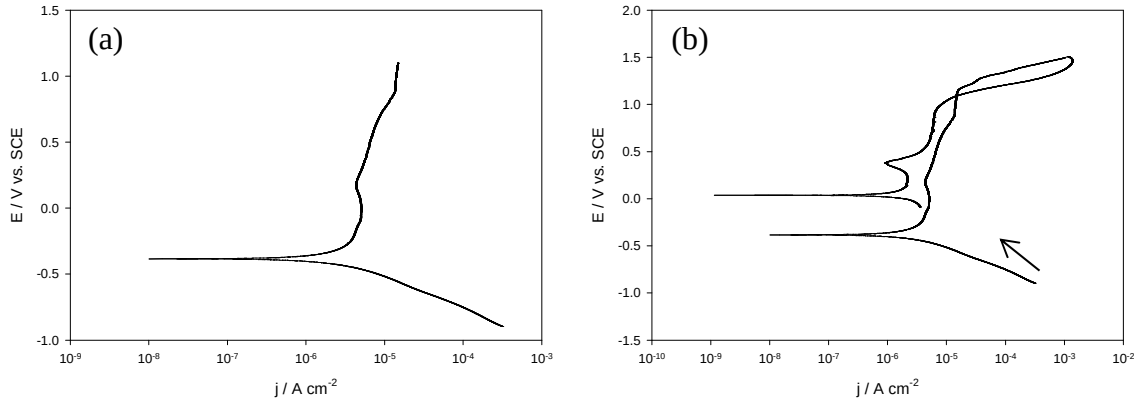

Figure 4.13: (a) Potentiodynamic polarisation curve and (b) cyclic potentiodynamic polarisation curve recorded for the AISI 310 electrode at a scan rate of 1 mV s^{-1} in —— 0.016 M KH_2PO_4 solution, at a pH of 5.0.

From the analysis of the polarisation and cyclic polarisation plots, it is evident that in phosphate containing solutions, phosphate ions passivate the AISI 310 electrode and, as reported by Lakatos-Varsányi *et al.* [60], improve the repassivation properties of the alloy.

4.3.4 The effect of co-existing anions in sww 1 and sww 2

The effect of the co-existing ions on the electrochemical behaviour of AISI 310 was studied by carrying out potentiodynamic polarisation tests in the multicomponent media of sww 1 and sww 2 (Table 4.1). Again, the pH was maintained at a value of 5.0. Representative polarisation plots are shown in Figure 4.14, and it is clear that the composition of the two solutions, which differ in the concentration of chloride anions, has a significant effect on the initiation, propagation and repassivation of pits. In sww 1 the anodic part of the curve exhibits an anodic nose at around -0.140 V vs. SCE, but then the current decays to reach values of approximately 2.0×10^{-6} A cm^{-2}, giving an extended passivation region. A small increase in the current is visible at about 0.600 V vs. SCE. The corrosion current was computed as 1.09×10^{-6} A cm^{-2} which is comparable to the values recorded in the sulfate-containing (2.62×10^{-6} A cm^{-2}, Section 4.3.2) and phosphate-containing solutions (2.28×10^{-6} A cm^{-2}, Section 4.3.3). However, the most significant variation between the data recorded in sww 1 and in 0.017 M NaCl is the extent of the passive region.

These results are consistent with competitive adsorption between the aggressive chloride anions and the sulfate and phosphate anions. As the chloride concentration, which is 0.017 M, is low compared to the relatively high levels of phosphates, adsorption of the chloride anions is inhibited. This is consistent with one of the most recognised theories on pitting corrosion of stainless steels [58], which was briefly presented in Section 1.4.1.3. According to the adsorption theory, pitting occurs as a result of a competitive adsorption of chloride anions at the passive film. The alloy has a greater affinity for oxygen, but as the potential is increased, the concentration of chloride at the electrode surface increases and eventually pitting is initiated. Other ions, such as sulfate or phosphate, compete with the chloride anions for the sites on the passive film, shifting the breakdown potential, E_{br}, to more positive values in order to reach a chloride concentration sufficient for a successful exchange with the adsorbed oxygen. However, there is a minimum anion concentration necessary to inhibit pitting in a chloride solution, and this depends on both the chloride concentration and the inhibitor anions ($\log [Cl^-] = k \times \log (\sum [\text{anions}]) + \text{constant}$). This relationship was derived assuming that the ions adsorb according to the Freundlich isotherm [61].

This theory also supports the dramatic change in the polarisation behaviour recorded when the electrode is polarised in sww 2, which contains a higher concentration of chloride ions, 0.170 M. As evident in Figure 4.14, a sharp increase of the current density takes place at around 0.150 V vs. SCE, which corresponds to the breakdown potential. This difference is evidently related to the ratio of inhibiting ions (sulfate and phosphate) to chloride anions.

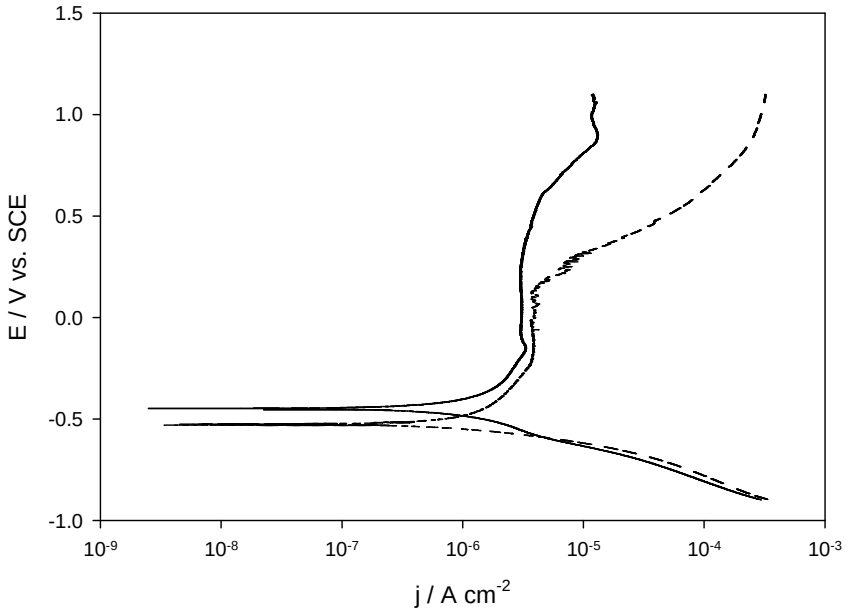

Figure 4.14: Potentiodynamic polarisation curves for the AISI 310 electrode in —— sww 1 and – – – sww 2 solutions, at a pH of 5.0, recorded at a scan rate of 1 mV s^{-1}.

The cyclic potentiodynamic polarisation tests were carried out on the AISI 310 electrode in sww 1 and sww 2 to establish the level of pitting attack compared to that observed in the simple chloride solutions. Representative plots are shown in Figure 4.15(a) and, although the data are very different, both curves exhibit significant hysteresis that is generally associated with the presence of pits on the electrode surface. There was no evidence of any pits on the AISI 310 electrode polarised in sww 1, however, pits were indeed found on examination of the surface of the electrode polarised in sww 2. The corresponding micrographs are presented in Figure 4.15(b) and (c). It is clear that these pits are very different to those observed in the simple chloride solutions, (Section 4.3.1, Figure 4.11). These pits have a round shape and are much closer together. However, the size of the pits is similar with an average diameter of about 50 μm. Furthermore, the pits are surrounded by rings of the corrosion products.

The use of AISI 310 to treat wastewaters poses a potential health risk. In fact, in all the potentiodynamic polarisation curves, Figure 4.10-Figure 4.15, at potentials between 0.800 and 0.900 V vs. SCE the current increases, then a partial repassivation of the electrode surface takes place, and eventually, above about 1.20 V vs. SCE, the current density rises sharply again. This behaviour may be connected with rapid pitting attack or the transformation of Cr(III) to Cr(VI). Indeed, the conversion to Cr(VI) is consistent with the potential-pH diagram for chromium shown in Section 1.4.2.2, Fig. 1.11, where the transformation occurs at around 1.00 V vs. SHE. This transformation leads to the formation of the most thermodynamically favoured species, $HCrO_4^-$, which is soluble, thus a less protective surface is formed. This seems to indicate that Cr(VI) is released during the electrolytic dissolution of the AISI 310 electrode at high potentials. This was further investigated and the results are presented in Section 5.2.2.

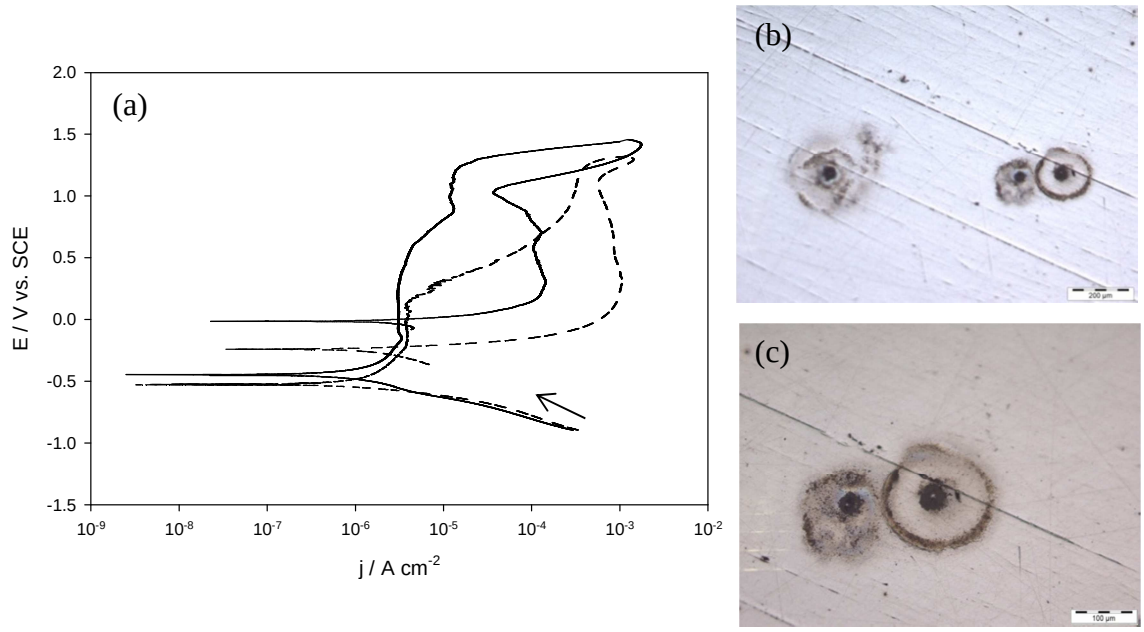

Figure 4.15: (a) Cyclic potentiodynamic polarisation curves for the AISI 310 electrode in —— sww 1 and – – – sww 2 solutions, at a pH of 5.0, at a scan rate of 1 mV s^{-1}; micrographs of the AISI 310 electrode at the end of the cyclic potentiodynamic polarisation scan in sww 2 solution at (b) scale bar corresponding to 200 μm and (c) scale bar corresponding to 100 μm.

It is evident that AISI 310 remains passive in both sww 1 and sww 2, but at some applied potential, which depends on the concentration of the chloride anions, breakdown of the passive film occurs. With a sufficient chloride concentration, the alloy suffers severe localised corrosion in the form of large pits. This behaviour can

negatively affect its use in electrocoagulation in terms of energy and electrode consumption and is discussed in Sections 5.2.2 and 5.2.3.

4.4 Stainless steel AISI 420

It is clear from Section 4.3 that the high chromium content of the AISI 310 stainless steel gives rise to passive conditions, which may adversely affect the energy consumption when used in electrocoagulation experiments. Moreover, the surface suffers from severe pitting attack, depending on the chloride concentration and the high applied potential. In view of these findings, a less corrosion resistant stainless steel, AISI 420, which is a martensitic stainless steel (Section 1.4.2.2), containing 13% chromium and 0.3% of carbon, was selected. The pitting resistance equivalent number, PREN [55], which was introduced in Section 4.3.1, is 13 for AISI 420. The martensitic stainless steels are generally used for their mechanical properties and the corrosion resistance is considerably lower in comparison with other stainless steels [11]. Consequently, there are fewer reports on the corrosion resistant properties of these alloys compared to other types of stainless steels.

The electrochemical behaviour of AISI 420 was studied using potentiodynamic polarisation tests, which were performed by polarising the AISI 420 electrode, with a geometric area of 0.63 cm^2, in the anodic direction, from -0.900 V vs. SCE up to the breakdown potential, E_{br}, or up to 1.00 V vs. SCE at a scan rate of 1 mV s^{-1}. Cyclic potentiodynamic polarisation tests were not carried out since from preliminary experiments it was evident that currents as low as 1.0×10^{-5} A cm^{-2} promoted the growth of deep and large pits. Although AISI 420 is more resistant than pure iron to corrosion, once corrosion or pitting is initiated, the damage caused by pitting is extensive and severe.

4.4.1 The effect of Cl^- ions

The potentiodynamic polarisation curves recorded for the AISI 420 electrode in 0.017 M and 0.170 M NaCl are displayed in Figure 4.16(a). In 0.017 M NaCl the electrode shows a typical active-passive transition before the breakdown potential, E_{br}, which occurs at about 0.010 V vs. SCE, is reached. The passive region, ΔE_{pass}, is

approximately 150 mV smaller than that observed for AISI 310 (0.333 V and 0.484 V for AISI 420 and AISI 310, respectively) and this confirms the lower corrosion resistance of this alloy due to its low chromium content. Indeed, it has been reported that the resistance of martensitic stainless steels in chloride solutions is only sufficient for short-term contact and they are not suitable for continuous immersion [11]. Type 410 stainless steel specimens (containing 11.5-13.5% Cr and 0.15% C) with a thickness of 6 mm, have been found completely perforated after 1 year of exposure to seawater in the Pacific Ocean [11]. On increasing the concentration of chloride, 0.170 M NaCl, there is considerable decrease in the breakdown potential from about 0.010 V vs. SCE in 0.017 M NaCl to -0.180 V vs. SCE in 0.170 M NaCl. There is a corresponding decrease in the passive region from 0.330 V to 0.16 V. As shown in Figure 4.16(a), the active-passive transition is not observed in 0.170 M NaCl. This is in good agreement with the results reported by de Cristofaro for a 13% Cr martensitic stainless steel in 0.7 M NaCl at pH 1.7 [62]. The concentration of chloride appears to have little effect on the corrosion potential, E_{corr}, which is approximately -0.340 V vs. SCE in both solutions, and the corrosion currents, j_{corr}, which were computed as 6.25×10^{-7} A cm^{-2} in 0.017 M NaCl and 6.63×10^{-7} A cm^{-2} in 0.170 M NaCl.

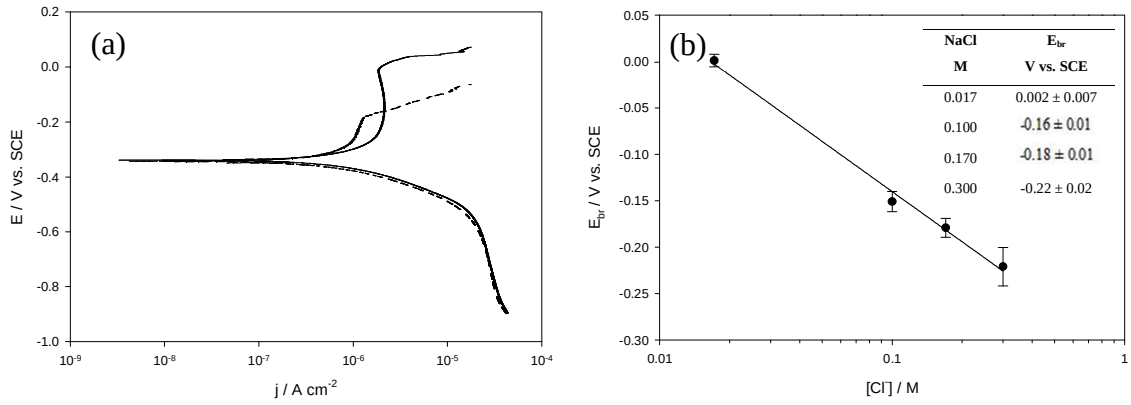

Figure 4.16: (a) Potentiodynamic polarisation curves for the AISI 420 electrode in —— 0.017 M and – – – 0.170 M NaCl solutions, at a pH of 5.0, recorded at a scan rate of 1 mV s^{-1}. (b) Breakdown potential, E_{br}, of AISI 310 as a function of the logarithm of the chloride concentration. The breakdown potential, E_{br}, was obtained from potentiodynamic polarisation tests recorded at 1 mV s^{-1}. Each experiment was performed in triplicate (n = 3). The experimental points were fitted by a linear regression analysis to E_{br} = A + B log [Cl$^-$], A = –0.319 ± 0.010 V, B = –0.179 ± 0.009 V, R^2 = 0.994.

The influence of the chloride concentration on the breakdown potential of AISI 420 is shown more clearly in Figure 4.16(b), where the breakdown potential is plotted as a function of the logarithm of the chloride concentration. By fitting the experimental points to a linear equation using linear regression analysis, the Eq. 4.4 was obtained.

$$E_{br} = -0.319 - 0.179[\mathrm{Cl}^-] \qquad \textbf{Eq. 4.4}$$

The value of the slope, which corresponds to B, is -0.179 V from Eq. 4.4, whereas for AISI 310 a slope of -0.046 V was found in Section 4.3.1, Eq. 4.3. Clearly, the susceptibility of AISI 420 to pitting corrosion by chloride ions is much higher than that found with AISI 310. However, the value of B is similar to that calculated for the iron electrode (Eq. 4.1) which was computed in Section 4.2.1. A clear comparison of the linear dependence of the breakdown potential, E_{br}, on the logarithm of chloride concentration is presented in Figure 4.17 for the three iron-containing electrodes. It is clear that the AISI 310 electrode is less sensitive to the concentration of chloride, as the slope of the linear plot, which is equivalent to B, is small, at -0.046 V. As the concentration of chloride ions may change from one electrocoagulation site to another or even at the same site over an extended time period, the ideal electrode should exhibit a low dependence on the chloride concentration. Although AISI 310 exhibits a relatively low dependence on the chloride concentration (Figure 4.17), this electrode is highly passive with high breakdown potentials and, as a consequence, high energy consumption is expected when AISI 310 is used in electrocoagulation applications. Lower breakdown potentials are found with AISI 420, however it shows a greater sensitivity to the presence of chloride in solution since the value of B is -0.179 V, as it is evident from Figure 4.17. A similar susceptibility to chloride ions is exhibited by the pure iron electrode, with a B value of -0.181 V. However, the pure iron electrode presents a positive characteristic, since it has low breakdown potentials, as shown from the data presented in Figure 4.17.

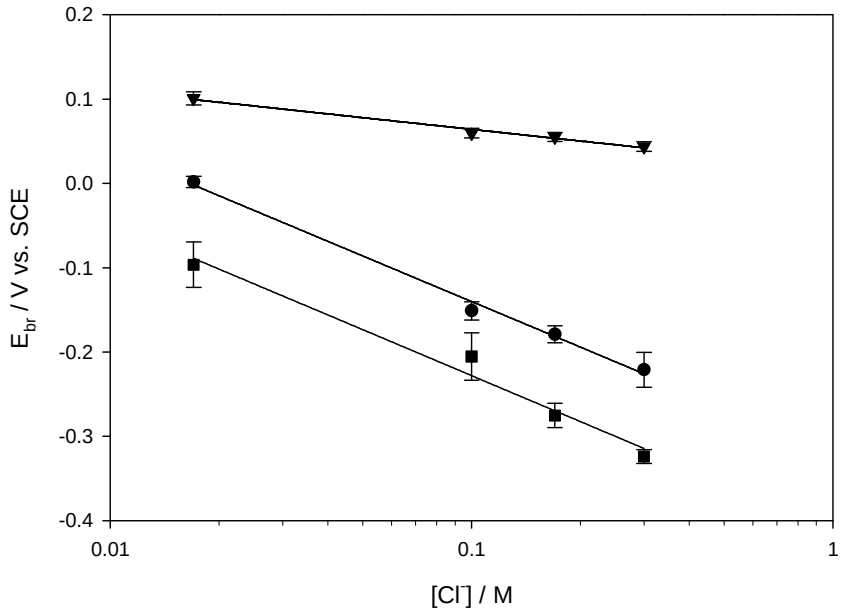

Figure 4.17: Breakdown potential, E_{br}, of ▼ AISI 310, ● AISI 420, and ■ iron electrodes as a function of the logarithm of the chloride concentration.

As detailed earlier, large and deep pits were observed on the surface of the AISI 420 electrode and, in an attempt to minimise the growth of these pits, the polarisation tests in 0.017 M and 0.170 M NaCl solutions were stopped at a current density of 1.8×10^{-5} A cm^{-2}. The surface morphology of the electrodes was then studied using light microscopy. Typical micrographs are shown in Figure 4.18(b)-(d). Even at this relatively low current density, large pits are evident. In 0.017 M NaCl solutions (Figure 4.18(a)) the pits grow as isolated active sites to reach a diameter of 60 to 70 μm. On the other hand, the density of the pits observed at the higher concentration, in 0.170 M NaCl, was much higher. The largest pits have a diameter of 120 to 130 μm (Figure 4.18(b)), however other smaller sized pits were evident on the electrode surface. The pits appear to adopt a reasonably circular geometry in both solutions, however the distance between the pits is considerably smaller at the higher chloride concentration, as evident in Figure 4.18(c).

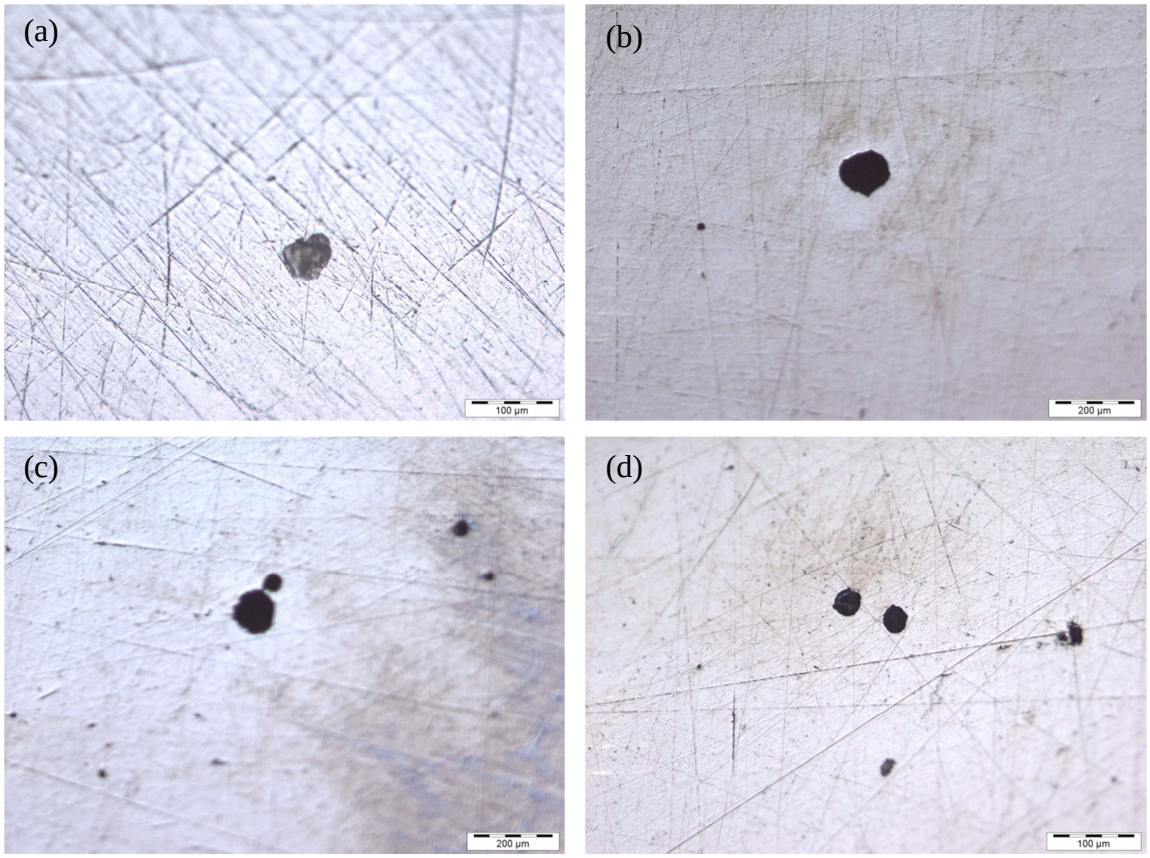

Figure 4.18: Micrographs for the AISI 420 electrode polarised in (a) 0.017 M NaCl at a pH of 5.0, scale bar corresponds to 100 µm and (b) and (c) 0.170 M NaCl solution at a pH of 5.0, scale bar corresponds to 200 µm (d) 0.170 M NaCl solution at a pH of 5.0, scale bar corresponds to 100 µm.

4.4.2 The effect of SO_4^{2-} ions

As detailed earlier for pure iron and AISI 310, the influence of sulfate anions on the polarisation behaviour of AISI 420 was studied by adding 8.1×10^{-4} M sulfate to 0.017 M NaCl and the pH of the solution was maintained at 5.0. Representative polarisation curves are shown in Figure 4.19(a). The potentiodynamic polarisation curve recorded for the AISI 420 electrode in 0.017 M NaCl and 8.1×10^{-4} M Na_2SO_4 is shown, while for comparison the polarisation curve recorded in 0.017 M NaCl is also presented. In the presence of sulfate ions, the corrosion potential, E_{corr}, is -0.277 V vs. SCE, about 60 mV more positive than that observed in 0.017 M NaCl. The anodic portion of the scan exhibits a passive region of about 300 mV, which extends up to the breakdown potential, E_{br}, at 0.170 V vs. SCE. There is a clear increase in the passive region on addition of the sulfate anions to the chloride-containing solution. Below the breakdown potential, some current oscillations are visible. These are usually the result of pits

nucleating and repassivating, and these nucleation and repassivation events continue until breakdown of the film and the growth of larger pits is achieved in the presence of the chloride ions at higher applied potentials [11]. It is clear that the addition of 8.1×10^{-4} M Na_2SO_4 to the chloride-containing solution shifts the breakdown potential by about 150 mV towards more noble values. As discussed by Leckie and Uhlig [56, 58] with Fe-Cr18-Ni8 stainless steel in 0.1 M NaCl, the magnitude of the shift depends on the ratio of sulfate to chloride ions. However, it is also evident from a comparison of the results presented in Section 4.3.2 with the results obtained with the AISI 310 electrode that the composition of the steel has an influence on the breakdown potential recorded in the presence of sulfates. A potential shift of 29 mV was evident with AISI 310 and this indicates that the Cr content has a role to play. Indeed, this is consistent with the enhanced resistance to pitting attack, which is observed on increasing the Cr content as an alloying element [57].

The micrographs recorded for the AISI 420 electrode polarised in 0.017 M NaCl and 8.1×10^{-4} M Na_2SO_4 are presented in Figure 4.19(b) and (c). Again, the electrodes were polarised to a maximum current density of 8.1×10^{-5} A cm^{-2} to minimise the formation of large and deep pits. The reasonably circular geometry of the pits present on the electrode surface is similar to that observed in the NaCl solutions (Section 4.4.1, Figure 4.18). However, in the presence of the sulfate anions the size of the pits is significantly smaller, with an average diameter of about 50 μm compared to the larger diameter of 60 to 70 μm found in the absence of the sulfate ions (Section 4.4.1). Similar results were found with the AISI 310 in the presence of sulfates (Section 4.3.2) and these results can be explained in terms of the inhibiting effects of the sulfate ions.

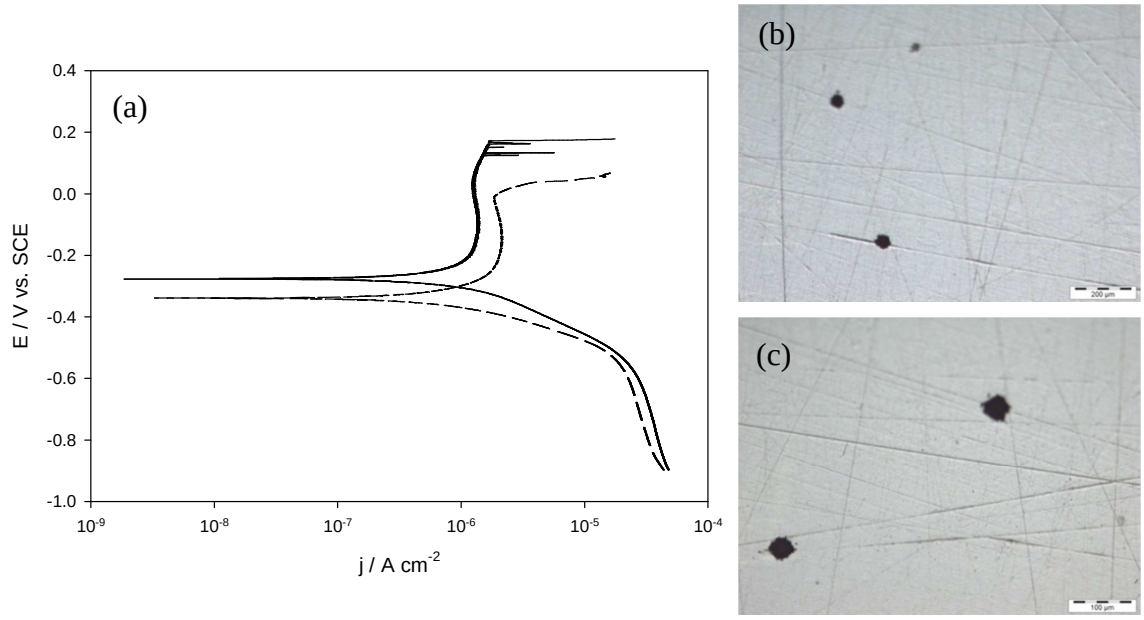

Figure 4.19: (a) Potentiodynamic polarisation curves for the AISI 420 electrode in —— 0.017 M NaCl and 8.1×10^{-4} M Na_2SO_4 at a pH of 4.8 and – – – 0.017 M NaCl at a pH of 5.0 recorded at a scan rate of 1 mV s^{-1}. (b) Micrographs of AISI 420 recorded at the end of the cyclic potentiodynamic polarisation scan in 0.017 M NaCl and 8.1×10^{-4} M Na_2SO_4 with the scale bar corresponding to 200 μm and (c) scale bar corresponding to 100 μm.

4.4.3 The effect of PO_4^{3-} ions

As discussed previously, phosphate ions act as corrosion inhibitors for ferrous alloys, thus AISI 420 may passivate in solutions containing phosphates. However, the passivation of the electrode may have negative consequences from the perspective of treating phosphate-containing solutions using electrocoagulation. In order to determine the extent of this passivation effect, polarisation plots were recorded in a slightly acidic, pH of 5.0, 0.016 M KH_2PO_4 solution. In Figure 4.20(a) the potentiodynamic polarisation plot, recorded for AISI 420 in the phosphate solution, is shown. The electrode exhibits an active-passive transition followed by a wide passive region which extends up to about 0.850 V vs. SCE. Then the potential enters the transpassive region, which corresponds to the end of the passive region and an increase in current density is observed. In the transpassive region, oxygen evolution and possibly increased corrosion is observed. For example, Uhlig [11] has attributed the loss of the protective nature of the passive film of stainless steel in the transpassive region to the oxidation of Cr(III), present in the protective layer, to the soluble species of Cr(IV). This explanation indicates that at high potentials the electrochemistry of chromium is predominant and it

dissolves in solution, similarly to that observed with AISI 310. The passivation effect by phosphate ions is supported by the micrographs of the electrode surface recorded at the end of the polarisation scan in 0.016 M KH_2PO_4 solution. A representative micrograph is shown in Figure 4.20(a). The electrode surface does not show any evidence of pits other than some imperfections already present on the electrode before the polarisation experiment.

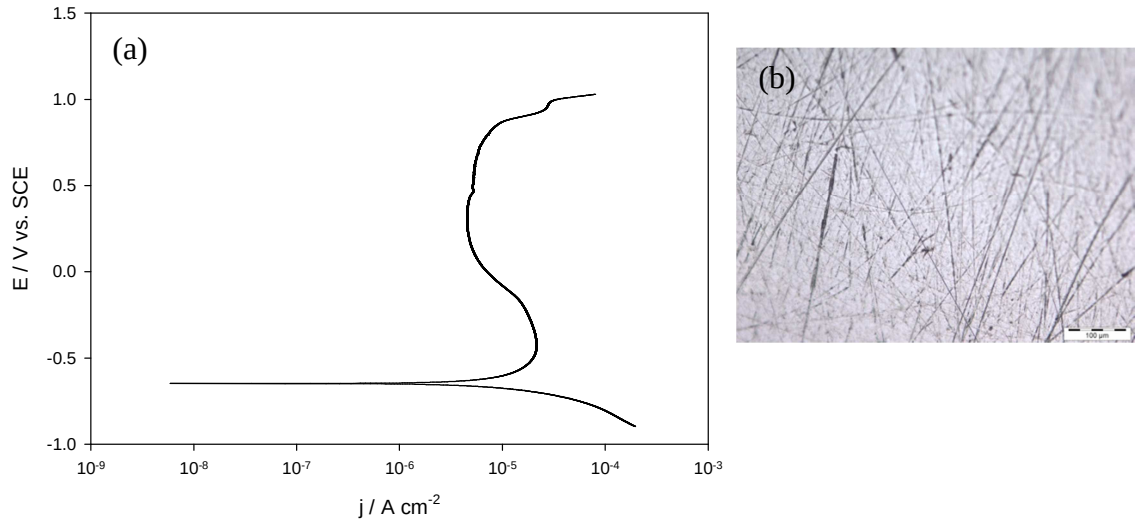

Figure 4.20: (a) Potentiodynamic polarisation curves for the AISI 420 electrode in —— 0.016 M KH_2PO_4 at a pH of 5.0, recorded at a scan rate of 1 mV s^{-1}. (b) Micrograph of AISI 420 at the end of the cyclic potentiodynamic polarisation scan, scale bar corresponds to 100 μm.

4.4.4 The effect of co-existing anions in sww 1 and sww 2

The electrochemical behaviour of AISI 420 in a multicomponent system was investigated by the potentiodynamic polarisation technique in the two formulated synthetic wastewaters, sww 1 and sww 2, and the resulting polarisation plots are shown in Figure 4.21(a). The corrosion potential, E_{corr}, is similar in both solutions, adopting a value of -0.650 V vs. SCE, whereas the corrosion current, j_{corr}, is higher in sww 2, reaching a value of 1.0×10^{-5} A cm^{-2}, compared to the somewhat lower value of 7.0×10^{-6} A cm^{-2} computed in sww 1. This is probably connected with the higher chloride anion concentration in sww 2. There is also a significant variation in the breakdown potentials. The breakdown potential, $E_{br,}$ in sww 1 occurs at about 0.112 V vs. SCE compared to the lower value of -0.088 V vs. SCE observed in sww 2. In

comparison with the 0.017 M and 0.0170 M NaCl solutions (Section 4.4.1), the breakdown potential is shifted to more positive values in the sww 1 and sww 2 solutions. The magnitude of the shift is about 100 mV in both cases. This suggests a competitive adsorption process between the anions present in the solution. A similar effect was observed with the AISI 310 (Section 4.3.4), where the presence of phosphate ions, which act as inhibitors and compete with chloride ions for adsorption on the passive film, gives rise to a shift of the breakdown potential to more noble values. The electrode surface was examined by light microscopy to reveal the presence of irregular-shaped pits, as can be seen in Figure 4.21(b) and (c). The pits grown in sww 1 solution have an average size of 30 to 50 μm (Figure 4.21(b)), whereas in sww 2, as the concentration of chloride is higher, the pits are wider with an average diameter of 50 to 80 μm (Figure 4.21(c)). Again, the pits developed in the two synthetic wastewaters are smaller in size compared to that observed in the corresponding NaCl solutions (Section 4.4.1, Figure 4.19) and this result supports the competitive action of the phosphate inhibiting ions.

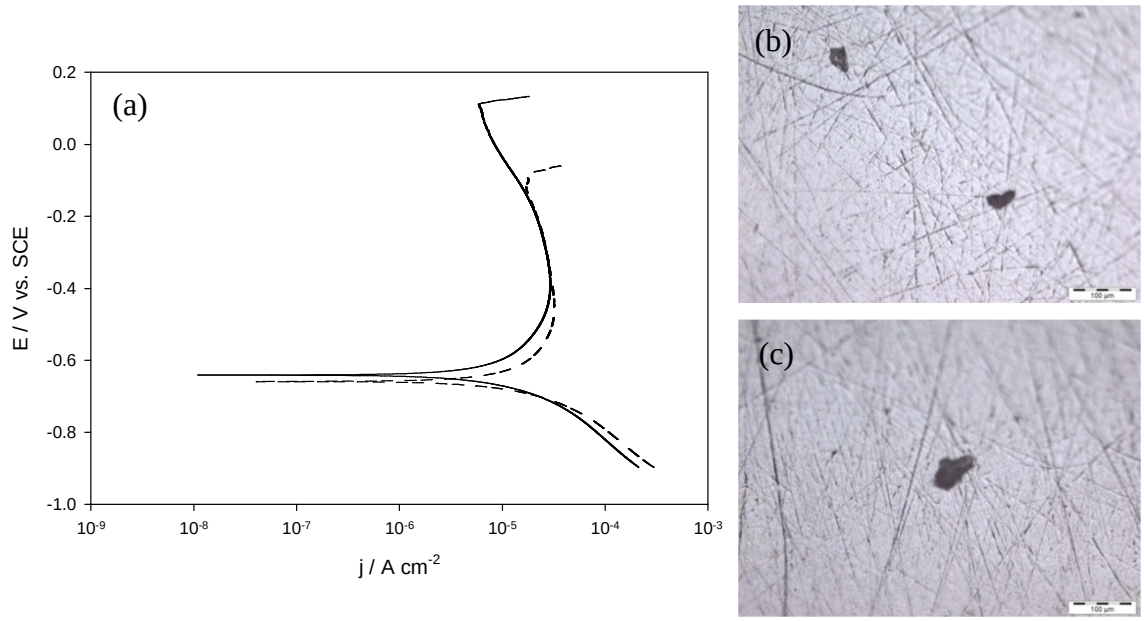

Figure 4.21: (a) Potentiodynamic polarisation curves for the AISI 420 electrode in ––– sww 1 and – – – sww 2 solutions, at a pH of 5.0, recorded at a scan rate of 1 mV s^{-1}. Micrographs of AISI 420 electrode at the end of the cyclic potentiodynamic polarisation scan in (b) sww 1, with scale bar at 100 μm and (c) sww 2, with scale bar at 100 μm.

4.5 Pure aluminium

As outlined in Section 1.4.2.3, aluminium is well known to be resistant against corrosion in aqueous media because of a uniform, natural oxide film, which is rapidly formed on the metal surface [26]. However, when aluminium is exposed to aggressive ions, such as chlorides, pitting attack occurs. The open-circuit potential measured on aluminium does not correspond to that of the metal, but represents a mixed potential between the oxide layer, which forms immediately (within 1 ms or even less), and the metal [26]. Consequently, in an aggressive environment the rest potential of aluminium is affected by the attack of the ions, causing fluctuations in the measured potential. For this reason, the potentiodynamic polarisation tests carried out on the as-received aluminium electrodes did not provide reproducible values of the corrosion potential, E_{corr}, although good reproducibility was obtained with the breakdown potential, E_{br}. In an attempt to increase the reproducibility of the corrosion potential, E_{corr}, several chemical and electrochemical pre-treatments of the electrode were considered. Good reproducibility was achieved using a slight modification of the method proposed by Van Gheem *et al.* [63]. After this pre-treatment the aluminium electrode was polarised in the anodic direction from -1.400 V vs. SCE, or some other initial potential below the corrosion potential, up to the breakdown potential, E_{br}, at a rate of 10.0, 1.0 or 0.5 mV s^{-1}. The exposed area of the working electrode was 0.031 cm^2.

4.5.1 The effect of Cl^- ions

In Figure 4.22(a) potentiodynamic polarisation curves are shown for pure aluminium recorded in a 0.100 M NaCl solution starting from an initial potential of -1.240 V vs. SCE. These data were obtained for the pure aluminium electrode without any chemical or electrochemical pre-treatment of the electrode surface. It is clearly evident from the presented figure that the corrosion potential, E_{corr}, varies considerably, ranging from -1.153 V to -0.828 V vs. SCE. On the other hand, the breakdown potential, E_{br}, is reproducible and occurs at about -0.730 V vs. SCE. The open-circuit potential was recorded in 0.100 M NaCl solution for 30 min immediately before the electrode was polarised and these data are shown in Figure 4.22(b). Potential fluctuations, exceeding 400 mV, are evident. These potential oscillations are related to pitting attack and indicate the occurrence of a process of activation and repassivation of the natural

passive layer [64]. Given that the breakdown potential, E_{br}, of pure aluminium in 0.100 M NaCl solution is -0.730 V vs. SCE, Figure 4.22(a), then the fluctuations of the open-circuit potential occur below the breakdown potential, E_{br}. This phenomenon is attributed to the occurrence of metastable pits on the electrode surface [64]. These metastable pits initiate and grow for a limited period before repassivation occurs and this accounts for the increase and rapid decrease in the open-circuit potential [65]. The reproducibility of the potentiodynamic polarisation curves is affected by this instability of the natural passive film due to the growth and the repassivation of the metastable pits.

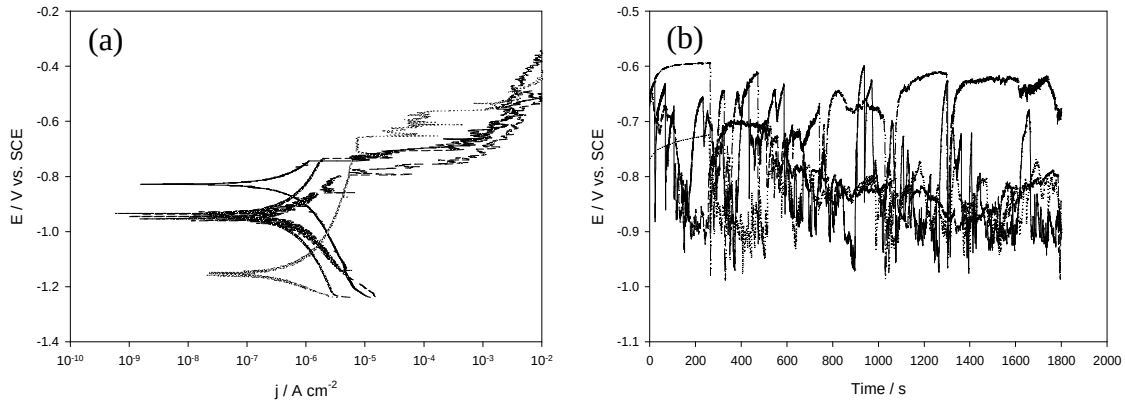

Figure 4.22: (a) Potentiodynamic polarisation curves recorded for the pure aluminium in 0.100 M NaCl at a pH of 5.0, at a scan rate of 0.5 mV s^{-1} and (b) the corresponding open-circuit potential plotted as a function of time without any pre-treatment of the electrode surface.

In order to promote a more stable passive film and, consequently, obtain reproducible experiments, several chemical and electrochemical pre-treatments were considered. Good reproducibility was achieved by modifying a method used by Van Gheem *et al.* [63] to obtain a reproducible surface composition. Before the polarisation tests, the specimen was immersed in 0.1 M NaOH solution at 70 °C for 60 s and subsequently in 1.0 M HNO_3 solution at 70 °C for 90 s. The data recorded following this pre-treatment are shown in Figure 4.23(a) and (b), where four potentiodynamic polarisation curves and the corresponding open-circuit potentials are shown. In the polarisation curves shown in Figure 4.23(a) the average corrosion potential of the four experiments is -1.344 ± 0.029 V vs. SCE and the average breakdown potential occurs at -0.803 ± 0.016 V vs. SCE. These results show an extremely high reproducibility in comparison with the data displayed in Figure 4.22. The average value of -0.800 V vs. SCE for the

breakdown potential is slightly lower than the values of -0.640 V vs. SCE reported by Böhni and Uhlig [66] for aluminium in 0.10 M NaCl. Also Broli and Holtan [67], McCaffrey [68], and Pyun and co-workers [69, 70] reported higher breakdown values. However, these studies used either a harsh surface pre-treatment or etching in alkaline solutions or a multi-step of immersion treatments. Using such conditions a relatively thicker surface oxide film may be developed and it might account for the higher breakdown potential recorded in these studies. Furthermore, the polarisation scans reported in Figure 4.23(a) were obtained in aerated NaCl solutions, whereas some of the cited studies are performed in deaerated solutions. It has been reported that in the absence of oxygen the breakdown potential of aluminium is shifted towards more positive values [27, 63]. For example, Pyun *et al.* [70] reported a breakdown potential of -0.720 V vs. SCE in aerated conditions, while Böhni and Uhlig [66] found that the pitting starts at -0.640 V vs. SCE in the absence of oxygen.

The open-circuit potential of the aluminium electrode after the chemical pre-treatment for the four experiments is presented in Figure 4.23(b). Although in the initial stage the open-circuit potential is significantly different for the four experiments, it shows a sharp increase followed by a gradual decline in all the experiments and then converges towards the same potential value of -1.30 V vs. SCE. Since this chemical pre-treatment of the electrode produced very reproducible results, it was then used to study the effect of the chloride concentration on the electrochemical behaviour of the pure aluminium electrode.

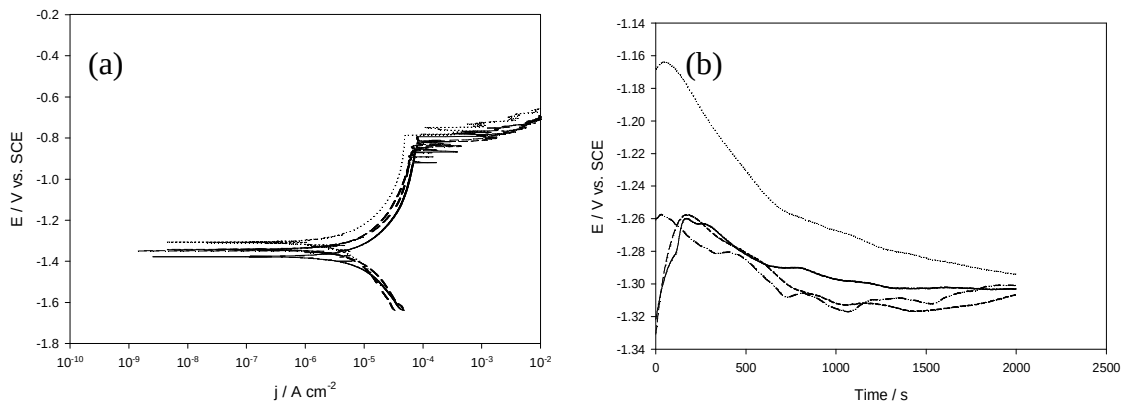

Figure 4.23: (a) Potentiodynamic polarisation curves recorded at a scan rate of 0.5 mV s^{-1} for the pure aluminium in 0.100 M NaCl at a pH of 5.0 and (b) the corresponding open-circuit potential plots for pure aluminium electrode in 0.100 M NaCl solution after immersing the electrode in 0.1 M NaOH solution for 60 s at 70 °C and then in 1.0 M HNO_3 solution for 90 s at 70 °C.

The influence of the chloride concentration is shown in Figure 4.24 where the potentiodynamic polarisation curves recorded in 0.005 M, 0.010 M, 0.100 M, 0.250 M and 0.500 M NaCl are shown. The corrosion potential, E_{corr}, decreased as the concentration of chloride ions was increased. There is also a significant variation in the breakdown potential, E_{br}, which ranges from -0.550 V vs. SCE in 0.005 M NaCl to 0.960 V vs. SCE in 0.500 M NaCl. Current fluctuations are also observed below the breakdown potential and these transients can be attributed to the occurrence of metastable pits on the electrode surface [65].

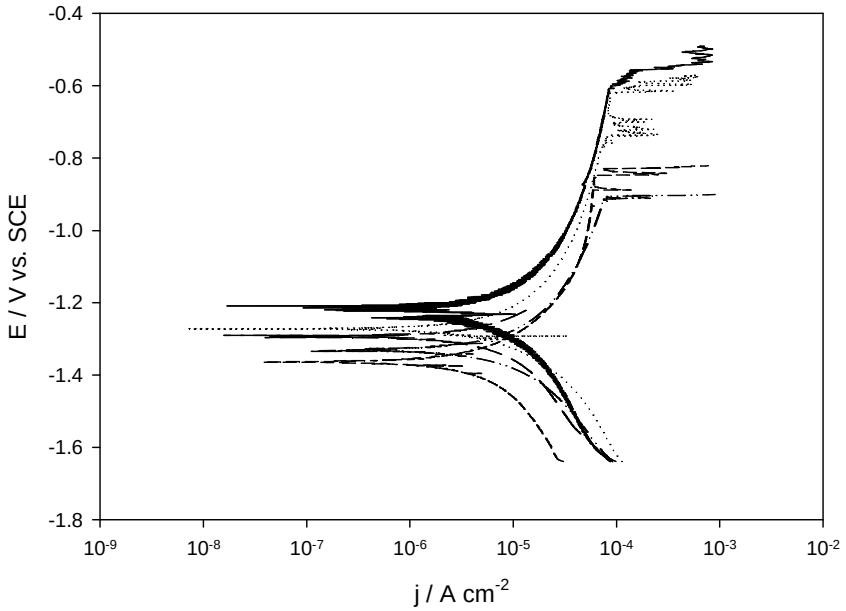

Figure 4.24: Potentiodynamic polarisation curves for the pure aluminium electrode in —— 0.005 M, · · · 0.010 M, – – – 0.100 M, – ·· – 0.250 M and —— —— 0.500 M NaCl solutions at a pH of 5.0, at a scan rate of 0.5 mV s^{-1}.

On plotting the breakdown potential, E_{br}, as a function of the logarithm of the concentration of chloride, a linear relationship was found [34] as displayed in Figure 4.25. The value of the slope, which is equivalent to B, obtained by fitting the experimental data using a linear regression analysis, is -0.204 V according to Eq. 4.5.

$$E_{br} = -1.026 - 0.204[\mathrm{Cl}^-] \qquad \textbf{Eq. 4.5}$$

This value is somewhat higher than the values obtained for pure iron, -0.181 V, and the two stainless steel grades implying a greater sensitivity of pure aluminium to variations

in the chloride concentration. In the review of the breakdown of passivity by Galvele [34], values of B are reported for pure aluminium and these range from -0.073 V to -0.139 V vs. SCE. However, as outlined previously, the pre-treatment of the electrode surface may have a significant impact on the thickness and protective properties of the passive film and this will influence the magnitude of B. The relatively mild pre-treatment, used in this study, was chosen in order to avoid any significant modifications of the passive film of aluminium. In the electrocoagulation tests the aluminium electrode was not subjected to any of these pre-treatments.

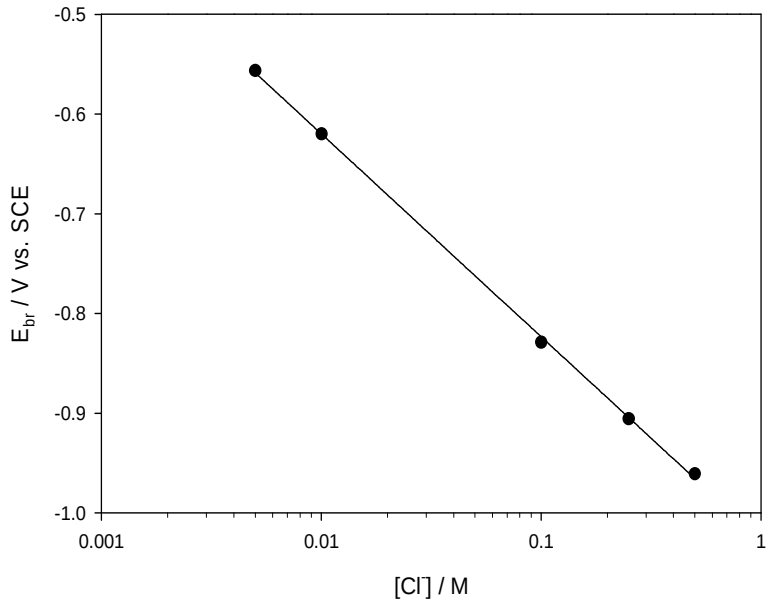

NaCl / M	E_{br} / V vs. SCE
0.005	-0.557
0.010	-0.620
0.100	-0.829
0.250	-0.906
0.500	-0.961

Figure 4.25: Breakdown potential, E_{br}, of the pure aluminium as a function of the logarithm of the chloride concentration. The breakdown potential, E_{br}, was obtained from potentiodynamic polarisation tests recorded at a rate of 0.5 mV s^{-1}. The experimental points were fitted by a linear regression analysis to E_{br} = A + B log [Cl^-], A = –1.026 ± 0.004 V, B = –0.204 ± 0.003 V, R^2 = 0.999.

4.5.2 The effect of PO_4^{3-} ions

It has been reported that phosphate ions act as inhibitors on the pit initiation of aluminium in neutral chloride solutions by forming insoluble precipitates [71, 72]. Shalaby *et al.* [73] investigated the corrosion behaviour of aluminium in 0.01 M NaCl containing different anions, including phosphates. They found that the phosphate ions play a dual role. At low concentrations they modify the rate of nucleation and growth of the passive oxide layer and at higher concentrations they become incorporated into this

layer and hence increase the protective nature of the film. As discussed earlier with the iron and stainless steels (Sections 4.2.3, 4.3.3, and 4.4.3), phosphate ions act as inhibitors towards the corrosion of aluminium. The potentiodynamic polarisation tests carried out on the pure aluminium electrode in 6.5×10^{-3} M KH_2PO_4 solutions with and without 5.0×10^{-4} M NaCl are shown in Figure 4.26 and confirm the inhibiting action of the phosphates. In these experiments, the aluminium electrode was polarised in the anodic direction from an initial potential of -1.000 V vs. SCE up to a final potential of 3.500 V vs. SCE. In the 6.5×10^{-3} M KH_2PO_4 solution the corrosion potential, E_{corr}, of pure aluminium is -0.869 V vs. SCE and the corresponding corrosion current, j_{corr}, is 1.4×10^{-7} A cm^{-2}. The electrode exhibits a wide passive region that extends from about -0.150 V vs. SCE up to 3.500 V vs. SCE. On addition of 5.0×10^{-4} M NaCl to the phosphate-containing solution, there is little variation in the corrosion potential, E_{corr}, or the corrosion current, j_{corr}, however the breakdown potential, E_{br}, occurs at 0.276 V vs. SCE. At higher applied potentials the current reaches a limiting value which corresponds to actively propagating pits that fail to repassivate at these high applied potentials.

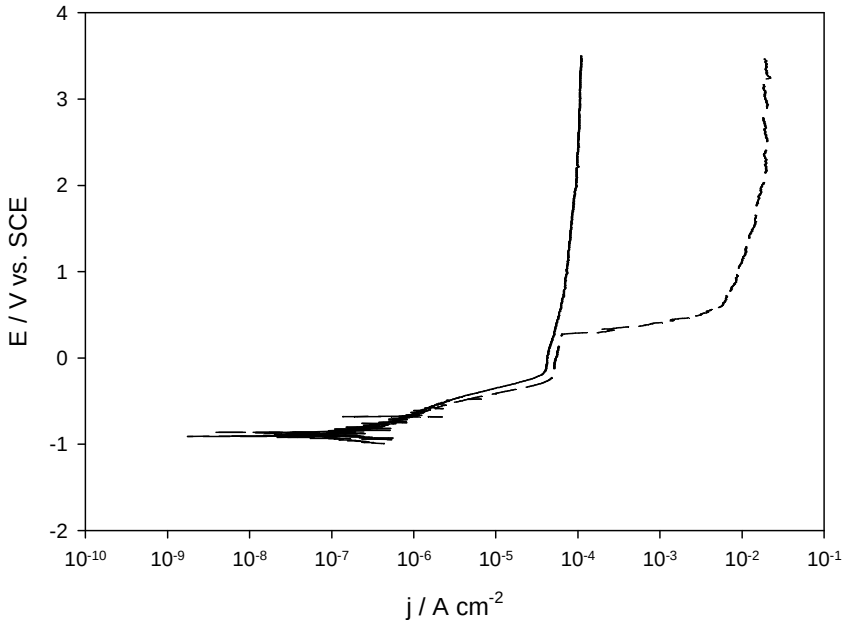

Figure 4.26: Potentiodynamic polarisation curves recorded for the pure aluminium electrode at a scan rate of 10 mV s^{-1} in 6.5×10^{-3} M KH_2PO_4 solutions with – – – 5.0×10^{-4} M NaCl and —— without NaCl, at a pH of 5.0.

The presence of chloride anions, even in small concentrations, certainly represents an advantage in terms of the energy needed to cause the breakdown of the passive film on pure aluminium. However, as outlined earlier, the concentration of chloride ions in real wastewater samples can drop to very low levels. Moreover, it is crucial to ascertain the grade of damage caused by pitting corrosion to avoid an uneven consumption of the electrodes and operational issues of the treatment plant.

4.6 Al-2Mg alloy

Pure aluminium exhibits good corrosion resistance due to the presence of a natural passive oxide layer. Generally, the addition of alloying elements decreases the corrosion resistance and, at the same time, modifies the solution-potential or corrosion potential of the metal [27]. As shown in Section 1.4.2.4, Fig. 1.13, in magnesium-containing alloys (5xxx series), the corrosion potential decreases slightly with the increasing content of magnesium [26, 27] and this feature can be beneficial in electrocoagulation from the perspective of the energy consumption. The 5xxx series also possesses an excellent resistance to pitting corrosion [31]. For this reason, an alloy belonging to this series, the EN-AW 5251 (Section 1.4.2.4), with 2% of magnesium, was selected for study.

The potentiodynamic polarisation tests were carried out by polarising the Al-2Mg electrodes with a geometric surface area of 0.58 cm^2 in the anodic direction, from -1.000 V vs. SCE up to the breakdown potential, E_{br}, at a scan rate of 1 mV s^{-1}. In the cases where the current density increased sharply above the corrosion potential, E_{corr}, the scan was stopped at 0.01 mA cm^{-2} and the potential corresponding to this value of current density was recorded as the breakdown potential, E_{br}. Cyclic potentiodynamic polarisation curves were recorded at 1 mV s^{-1} and again the Al-2Mg electrode was polarised in the anodic direction, but the scan was reversed when the current density reached a value of 1 mA cm^{-2}.

4.6.1 The effect of Cl^- ions

The potentiodynamic polarisations curves recorded for Al-2Mg electrode in 0.017 M and 0.170 M NaCl solutions are compared in Figure 4.27(a). It is clear that these data are very different to those obtained with pure aluminium and highlight the role of

magnesium in modifying the properties of the passive film. The corrosion potential, E_{corr}, in 0.170 M NaCl is -0.664 V vs. SCE, compared to a value of -0.554 V vs. SCE in 0.017 M NaCl. However, there is little variation in the corrosion currents, j_{corr}, which were computed at 1.20×10^{-6} A cm^{-2}. Above the corrosion potential the current density increases sharply. Consequently, the electrode does not exhibit any passive region regardless of the concentration of chloride ions and in electrocoagulation applications this feature would be advantageous for the energy supply to the system. The breakdown potential, E_{br}, was taken at a reasonably high current density of 0.01 mA cm^{-2}, and in 0.017 M NaCl it was found at -0.530 V vs. SCE while in 0.170 M NaCl it is observed at -0.636 V vs. SCE. Similar behaviour was recorded by other authors with Al-2.5Mg in 3.5 wt. % NaCl [74] and Al-3Mg in 3 wt. % NaCl [75]. In both studies the corrosion potential coincided with the breakdown potential and there was no evidence of any passive region.

In Figure 4.27(b) the breakdown potential, E_{br}, of the Al-2Mg electrode is plotted as a function of the logarithm of the chloride concentration to give a linear relationship. In 0.10 M NaCl an average breakdown potential of -0.590 V vs. SCE was found, which is in good agreement with the value of -0.640 V vs. SCE reported by Böhni and Uhlig [66] for an aluminium alloy containing 2.4% of magnesium polarised in 0.1 M NaCl solution. As displayed in Figure 4.27(b), a linear regression analysis of the experimental points provided a value of B as -0.108 V.

$$E_{br} = -0.712 - 0.108[\mathrm{Cl}^-] \qquad \textbf{Eq. 4.6}$$

By comparing this to the value obtained with pure aluminium, -0.204 V, in Section 4.5.1, Eq. 4.5, it is evident that the breakdown potential of the Al-2Mg electrode is less affected by the presence of chloride ions in solution.

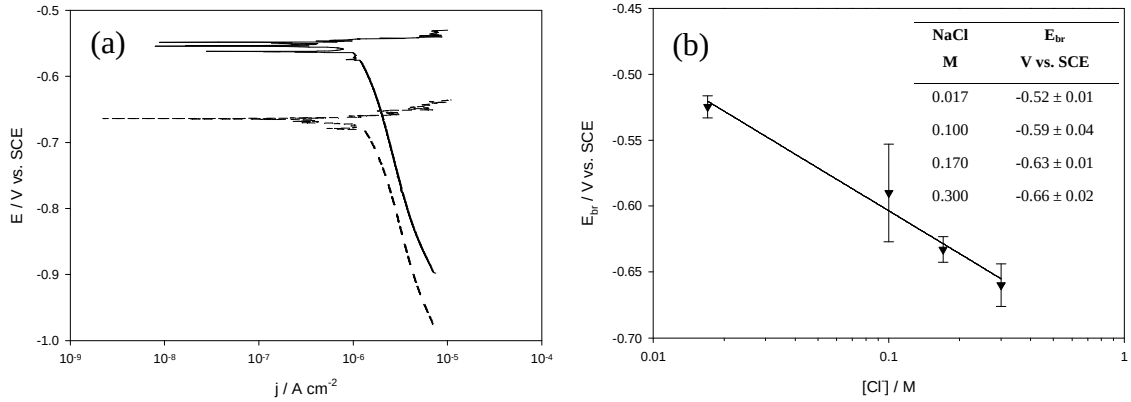

Figure 4.27: (a) Potentiodynamic polarisation curves for the Al-2Mg electrode in —— 0.017 M and – – – 0.170 M NaCl solutions at a pH of 5.0, recorded at a scan rate of 1 mV s^{-1}. (b) Breakdown potential, E_{br}, of the Al-2Mg electrode as a function of the logarithm of the chloride concentration. The breakdown potential, E_{br}, was obtained from potentiodynamic polarisation tests at a scan rate of 1 mV s^{-1}. Each experiment was performed in triplicate (n = 3). The experimental points were fitted by a linear regression analysis to E_{br} = A + B log [Cl^-], A = –0.712 ± 0.013 V, B = –0.108 ± 0.012 V, R^2 = 0.976.

The cyclic potentiodynamic polarisation curves recorded for the Al-2Mg alloy in 0.017 M and 0.170 M NaCl solutions are shown in Figure 4.28(a). As can be seen from the figure, both cyclic polarisation curves exhibit hysteresis. The size of the hysteresis loop is comparable in both 0.017 M and 0.170 M NaCl solutions, implying that the extent of the damage caused by pitting is not significantly different. Post-scan examinations of the specimens using light microscopy confirmed that the dimensions of the pits are similar regardless of the concentration of the chloride ions. In Figure 4.28(b) and (c) the micrographs recorded for the Al-2Mg electrode surface after the cyclic polarisation scan in 0.170 M NaCl are presented and these depict the nucleation of several, small pits. The diameter of the cluster, which comprises several pits, was calculated as 110 μm. Other small sites of attack are also visible in Figure 4.28(c), and these are probably at an earlier stage of nucleation or development. The small number of active sites appears to depend on the Mg content. Indeed, in studying the susceptibility to the electrochemical corrosion of Al-Mg alloys with low Mg content, Brillas *et al.* [76] concluded that the pitting attack was greater when the Mg content was increased. The active sites were attributed to the solubility of magnesium. Although magnesium is highly soluble in aluminium at high temperatures, it does not exceed 1% at room temperature. Therefore, it precipitates as soon as the temperature is decreased. It has been reported that magnesium precipitation starts at the grain boundaries as Al_3Mg_2 or

Al_8Mg_5, which is commonly called the β-phase [27]. As reported in Section 1.4.2.4, these intermetallics are anodic and therefore they represent a suitable site for localised attack in the form of intergranular or stress corrosion, if the precipitation is continuous at the grain boundaries. However, it has been reported that Al-Mg alloys containing less than 3% in magnesium are resistant to these types of localised corrosion [11]. The Al-Mg alloy used in this study contains 2% of Mg and as shown in Figure 4.28(b) and (c), there is no presence of intergranular or stress corrosion. However, it is likely that the peculiar form of pitting, a few sites made up of several pits, which was observed for the Al-2Mg alloy in NaCl solutions, is due to the preferential attack at the intermetallic compounds present on the electrode surface.

It is clear that the presence of a small concentration of chloride activates the surface of the Al-2Mg electrode, giving rise to dissolution. The electrode does not exhibit any passive region. However, the corrosion of the Al-2Mg alloy is predominantly in the form of clusters of small pits, distributed across the surface.

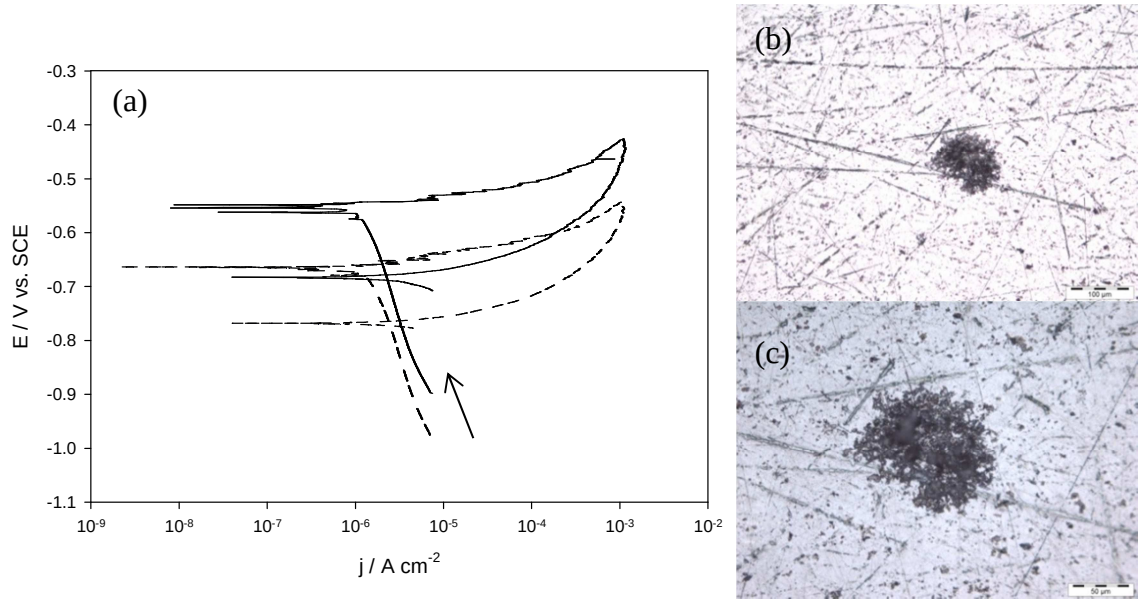

Figure 4.28: (a) Cyclic potentiodynamic polarisation curves for the Al-2Mg electrode in —— 0.017 M and – – – 0.170 M NaCl solutions at a pH of 5.0, at a scan rate of 1 mV s^{-1}; micrographs of the Al-2Mg electrode at the end of the cyclic potentiodynamic polarisation scan in 0.170 M NaCl solution (b) scale bar corresponding to 100 μm and (c) scale bar corresponding to 50 μm.

4.6.2 The effect of SO_4^{2-} ions

The potentiodynamic polarisation curves of Al-2Mg recorded in a 0.017 M NaCl and 8.1×10^{-4} M Na_2SO_4 solution and in 0.017 M NaCl are compared in Figure 4.29. Although sulfate is known to have an inhibiting activity towards aluminium [27, 66], there are no significant differences in the shape of the polarisation curves recorded in the absence and in the presence of sulfate ions. The addition of 8.1×10^{-4} M Na_2SO_4 to the 0.017 M NaCl solution gave rise to a 50 mV increase in the corrosion potential, E_{corr}, and a slight decrease in the corrosion current, from 1.09×10^{-6} A cm^{-2} to 7.13×10^{-7} A cm^{-2} in 0.017 M NaCl, and in 0.017 M NaCl and 8.1×10^{-4} M Na_2SO_4, respectively. Above the corrosion potential, E_{corr}, which occurs at -0.508 V vs. SCE, there is a large increase in current density without any passivity region. Similar behaviour was recorded in 0.017 M NaCl (Section 4.6.1, Figure 4.27). The breakdown potential, E_{br}, was determined at a current density of 0.01 mA cm^{-2}, and was found at -0.464 V vs. SCE. This corresponds to a 70 mV increase compared with the data recorded in 0.017 M NaCl, where the breakdown potential was -0.530 V vs. SCE. This is in good agreement with the extensive literature existing on the effect of sulfate ions on the pitting corrosion of pure aluminium [69-72, 77-82]. The earlier studies showed that in concentrated NaCl solutions the breakdown potential was shifted towards noble values by adding sulfate ions at concentrations above 0.3 M, and that sulfate retarded pit initiation due to its competitive adsorption with chloride [77, 78]. Later, Pyun and co-workers [69, 70, 81, 82] deduced that sulfate ion addition retards the incorporation of chloride ions into the oxide film on pure aluminium, impeding pit initiation. However, they also reported that sulfate ions enhance the growth of pre-existing pits. These findings are consistent with the results obtained in Figure 4.29. Here, with the addition of sulfate to NaCl solution the breakdown potential, E_{br}, is shifted in the anodic direction by about 70 mV, thus retarding the initiation of pitting attack. This small shift is compatible with the low concentration of sulfate used, 8.1×10^{-4} M Na_2SO_4. Böhni and Uhlig [66] have reported a similarity in the behaviour of inhibiting anions for aluminium and 18-8 stainless steel. It is reasonable to assume that in the case of the Al-2Mg alloy the ratio of the SO_4^{2-}/Cl^- concentrations has an important role in defining the extent of the sulfate effect (Sections 4.3.2 and 4.4.2).

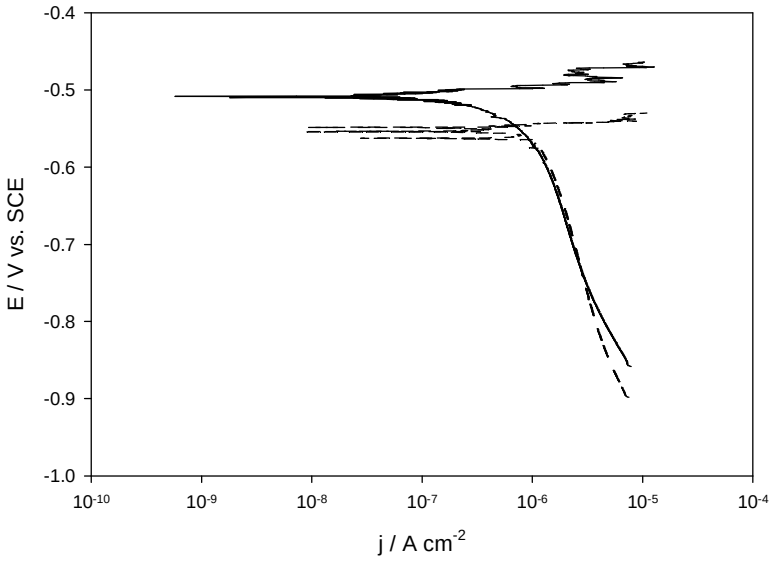

Figure 4.29: Potentiodynamic polarisation curves for the Al-2Mg electrode in —— 0.017 M NaCl and 8.1×10^{-4} M Na_2SO_4 solution at a pH of 5.0 and – – – 0.017 M NaCl solution at a pH of 5.0, recorded at a scan rate of 1 mV s^{-1}.

Pitting corrosion was confirmed by cyclic potentiodynamic polarisation tests carried out on the Al-2Mg electrode in 0.017 M NaCl and 8.1×10^{-4} M Na_2SO_4. A typical plot is shown in Figure 4.30(a) and it is clear that a hysteresis loop exists. Furthermore, as displayed in Figure 4.30(b) and (c), at the end of the scan the electrode surface shows the nucleation of several pits, similar to that found on the surface of the Al-2Mg electrode cycled in NaCl solutions (Section 4.6.1, Figure 4.28). The density of pits is also similar. However, in the presence of sulfates the size of the pit clusters are slightly smaller, about 80 μm, and the shape of some of the clusters are different. Indeed, as shown in Figure 4.30(b) and (c), circular-like clusters and irregular shaped clusters are present.

Clearly the sulfate ions have an important role in the pitting corrosion of the Al-2Mg electrode. At low concentrations, they impede the initiation of pits and introduce important changes in the morphology of the pit clusters. However, in the presence of chloride anions, the sulfate ions cannot prevent pitting corrosion of the Al-2Mg alloy.

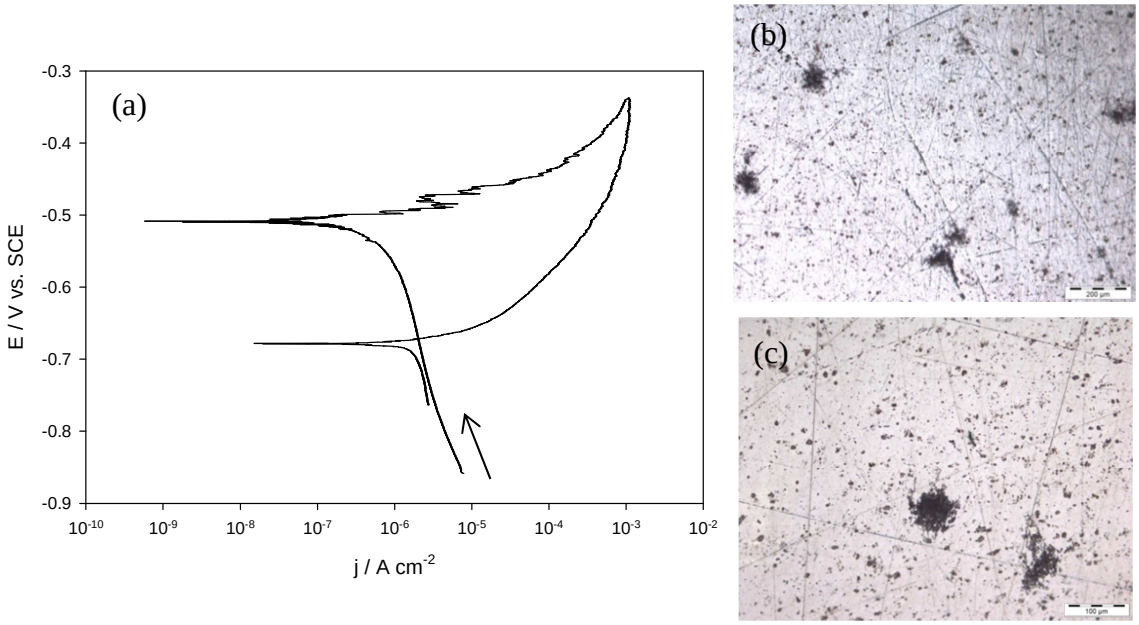

Figure 4.30: (a) Cyclic potentiodynamic polarisation curve for the Al-2Mg electrode in —— 0.017 M NaCl and 8.1 × 10^{-4} M Na_2SO_4 solution at a pH of 5.0, at a scan rate of 1 mV s^{-1}; micrograph of the Al-2Mg electrode at the end of the cyclic potentiodynamic polarisation scan (b) scale bar corresponding to 200 μm and (c) scale bar corresponding to 100 μm.

4.6.3 The effect of PO_4^{3-} ions

Phosphates are well known as inhibitors in the corrosion protection of aluminium in water [27]. For this reason, they are used in chemical conversion treatments to protect aluminium against corrosion. As there are no reports on the influence of phosphate anions on the electrochemical properties of Al-Mg alloys, polarisation curves were recorded in a 0.016 M KH_2PO_4 solution. A representative potentiodynamic polarisation curve for Al-2Mg electrode is shown in Figure 4.31(a) and it is clear that the polarisation behaviour is very different to that observed in the chloride-containing solutions. Above the corrosion potential, E_{corr}, which occurs at -0.484 V vs. SCE, the electrode is passivated and the passive region spans about 600 mV. As can be seen from the figure, the breakdown potential, E_{br}, is 0.103 V vs. SCE, significantly higher than that observed in the chloride-containing solutions. However, the onset of metastable pits is present well below this value, as evident from the fluctuations of the current density. After the breakdown potential, E_{br}, the current density increases rapidly suggesting a fast growth of pits on the electrode surface. The cyclic polarisation scan, shown in Figure 4.31(b), reveals the presence of a large hysteresis which is consistent with pitting corrosion. Indeed, this was confirmed upon examining the specimen using light

microscopy. The inset in Figure 4.31(b) provides a representative micrograph obtained at the end of the scan. The pits developed on the electrode surface are very different from those grown in chloride solutions (Section 4.6.1, Figure 4.30). The pits are not gathered in clusters, have an average diameter of 60 μm, and have a irregular shape.

Although the phosphate ions act as inhibitors towards the Al-2Mg alloy giving a wide passive region, the alloy corrodes at higher potentials and exhibits pitting corrosion. As discussed in Section 4.1, the presence of a region of passivity represents a potential disadvantage for the energy consumption in the electrocoagulation process to remove phosphates.

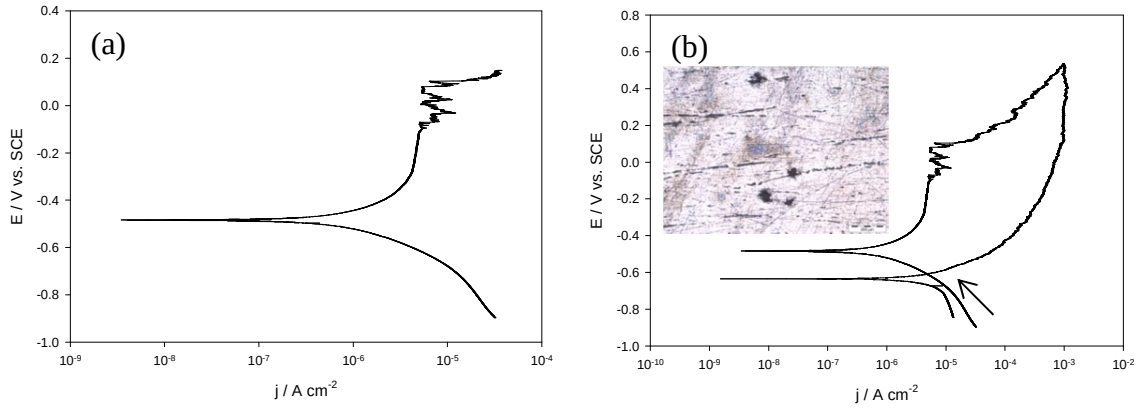

Figure 4.31: (a) Potentiodynamic polarisation curve and (b) cyclic potentiodynamic polarisation curve for the Al-2Mg electrode in —— 0.016 M KH_2PO_4 solution at a pH of 5.0 recorded at a scan rate of 1 mV s^{-1}. The inset shows a micrograph of the Al-2Mg electrode at the end of the cyclic potentiodynamic polarisation scan, scale bar corresponds to 200 μm.

4.6.4 The effect of co-existing anions in sww 1 and sww 2

The two synthetic wastewaters, sww 1 and sww 2, were formulated to investigate the dissolution behaviour of the electrode in a multicomponent environment in the presence of several co-existing ions. Again, potentiodynamic polarisation curves and cyclic polarisation curves were recorded in sww 1 and sww 2. In Figure 4.32 the potentiodynamic polarisation curves recorded for the Al-2Mg electrode in sww 1 and sww 2 are compared. The cathodic branches are similar and above the corrosion potential, E_{corr}, the current density shows a sharp increase. This behaviour is similar to

that observed for the Al-2Mg alloy in NaCl solutions (Section 4.6.1) and indicates that, above the corrosion potential, the electrode exhibits pitting corrosion. It is also evident from the figure that the concentration of chloride ions, which varies from 0.170 M in sww 2 to 0.017 M in sww 1, has a significant effect on the corrosion potential, E_{corr}, and the breakdown potential, E_{br}. The corrosion potential, E_{corr}, is shifted some 80 mV in the cathodic direction in the sww 2, (from -0.598 V vs. SCE in sww 1 to -0.670 V vs. SCE in sww 2). As can be observed in Section 4.6.1, Figure 4.27, a comparable shift of 100 mV was observed between the corrosion potentials recorded in 0.017 M and 0.170 M NaCl solutions. The breakdown potentials, E_{br}, were taken at 0.01 mA cm^{-2} and were calculated as -0.587 V and -0.661 V vs. SCE in sww 1 and sww 2 solutions, respectively. As shown in Section 4.6.1, Figure 4.27 a shift of about 100 mV in the breakdown potential was observed with the 0.017 M and 0.170 M NaCl solutions. In the two synthetic wastewaters the magnitude of the shift is somewhat smaller; in the sww 2 solution the breakdown potential, E_{br}, is about 70 mV lower than in the sww 1 solution. This smaller shift is likely due to the presence of the sulfate and phosphate anions, which possess an inhibiting effect on the corrosion of the Al-2Mg electrode, as shown in Sections 4.6.2 and 4.6.3.

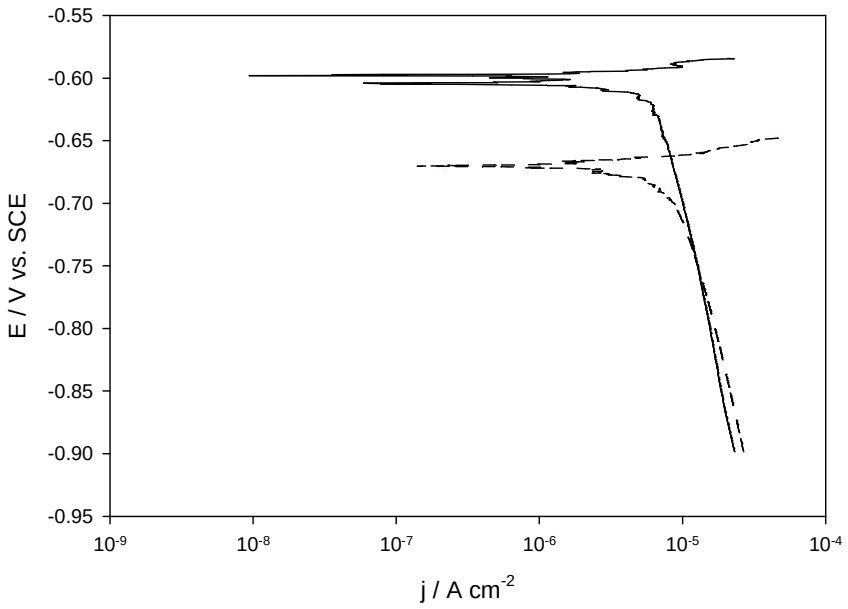

Figure 4.32: Potentiodynamic polarisation curves for the Al-2Mg electrode in —— sww 1 and – – – sww 2 solutions at a pH of 5.0 recorded at a scan rate of 1 mV s^{-1}.

The cyclic potentiodynamic polarisation curves recorded for Al-2Mg in sww 1 and sww 2 solutions are shown in Figure 4.33(a). In both scans the forward and the reverse traces are different, generating hysteresis. The hysteresis loop is somewhat smaller in the sww 2 solution. However, there was no significant difference in the distribution and morphology of pits between the sww 1 and sww 2 solutions. The micrographs recorded in the sww 2 solution are presented in Figure 4.33(b) and (c) and these depict the electrode surface at the end of the cyclic scan. Pits with different diameters are visible on the electrode surface and their dimensions range from 20 to 80 μm. This morphology is very different to that observed in the chloride-containing solutions where circular-shaped clusters of pits were observed (Section 4.6.1, Figure 4.28(b)). It is obvious that a different process leads to pitting attack in the presence of co-existing ions. The effects of the aggressive chloride actions may be mitigated in the presence of phosphate ions, which exert an inhibiting role, as discussed in Section 4.6.3. In addition, both synthetic wastewaters contain sulfate, 8.1×10^{-4} M. Since it was shown in Section 4.6.2 that sulfate ions retard the growth of pits on Al-2Mg electrode, it seems plausible that their presence in the sww 1 and sww 2 solutions may also have a role in the pitting attack, giving rise to pits with different sizes and distribution.

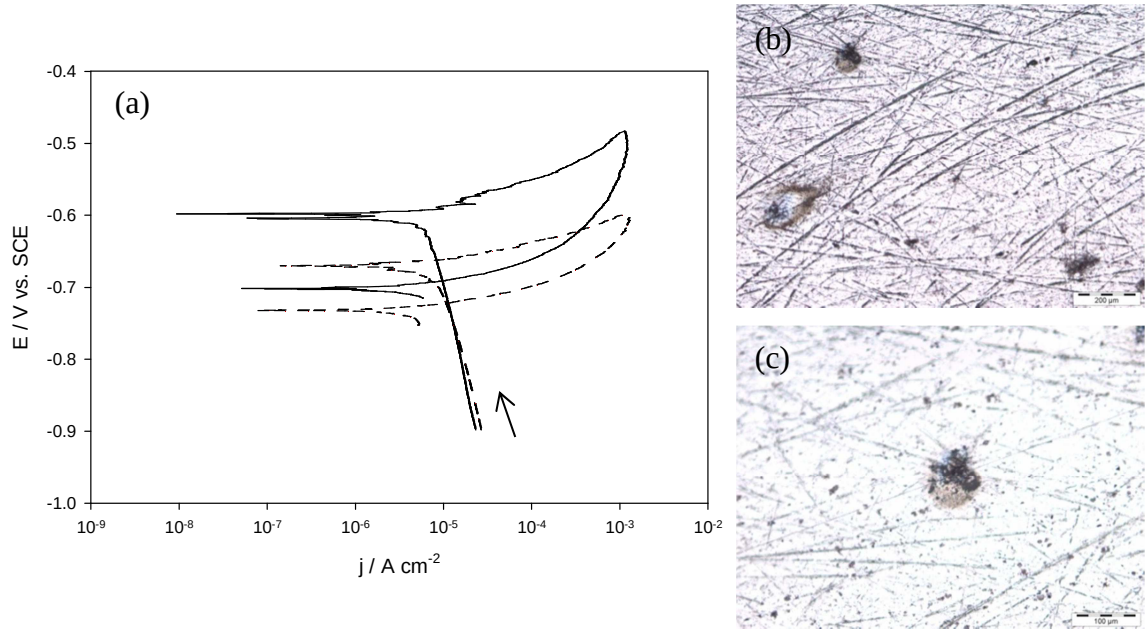

Figure 4.33: (a) Cyclic potentiodynamic polarisation curves for the Al-2Mg electrode in —— sww 1 and – – – sww 2 solutions at a pH of 5.0 recorded at a scan rate of 1 mV s^{-1}; micrographs of the Al-2Mg electrode at the end of the cyclic potentiodynamic polarisation scan in sww 2 solution with (b) scale bar corresponding to 200 μm and (c) scale bar corresponding to 100 μm.

In a multicomponent system, such as sww 1 and sww 2, which contains both activators and inhibitors, the corrosion behaviour of Al-2Mg is affected by the presence of both categories of anions. However, the presence of chloride ions, even in small concentration, determines the electrochemical behaviour of the alloy, since the polarisation curves obtained in the two synthetic wastewaters are similar to that obtained in chloride solutions. Chloride has a positive influence on the dissolution of the alloy which does not exhibit any passive region. The inhibiting phosphate and sulfate anions exert some influence with a shift of the breakdown potentials, E_{br}, towards more noble values. However, more significant differences in the size, shape and distribution of the pits are evident in the presence of the sulfate and phosphate anions.

4.7 Al-Zn-In alloy

Binary and ternary aluminium alloys have been recently investigated as materials for Al batteries or cathodic protection systems [83-88]. Although pure aluminium is a very attractive metal for its mechanical properties, the spontaneously formed oxide film on its surface leads to a significant loss of available energy and does not allow the active dissolution of the electrode as it is required in industrial applications. Numerous investigations have been reported on the addition of alloying components, such as Zn, In, Hg, Sn, Ga, Mg and Ti, to aluminium and these alloys give an active surface that corrodes in a nearly uniform manner [28, 29, 83, 89-96]. Also in electrocoagulation the passivation of the electrode surface has been identified as a primary disadvantage on employing aluminium as the anode material [5, 6, 8, 25]. However, only a few studies have been carried out on the electrocoagulation performances of Al-alloys [12, 97-100] whereas the majority are focused on the use of the pure aluminium. For this reason, an Al-Zn-In alloy was used as the anode material for electrocoagulation applications. This alloy contained 3% zinc and 0.02% indium. The potentiodynamic polarisation tests were carried out by polarising the Al-Zn-In electrode with an area of 0.38 cm^2 in the anodic direction, from -1.400 V vs. SCE up to the breakdown potential, E_{br}, or up to a current density value of 0.01 mA cm^{-2}. A scan rate of 1 mV s^{-1} was employed. The cyclic potentiodynamic polarisation curves were performed in a similar manner, but the scan was reversed when the current density reached a value of 1 mA cm^{-2}.

4.7.1 The effect of Cl^- ions

The potentiodynamic polarisation curves of Al-3Zn-0.02In in 0.017 M and 0.170 M NaCl solutions are shown in Figure 4.34(a). The corrosion potentials, E_{corr}, are -0.912 V vs. SCE in 0.017 M NaCl and -1.07 V vs. SCE in 0.170 M NaCl. The shape of the anodic curve is very similar in both solutions and presents an active dissolution without any passivity with the breakdown potential, E_{br}, occurring at -0.879 V vs. SCE and -1.05 V vs. SCE in 0.017 M and 0.170 M NaCl solutions, respectively. It is clear that the breakdown potentials, E_{br}, have values very similar to the corrosion potentials, E_{corr}. Moreover, in 0.170 M NaCl the corrosion potential, E_{corr}, and the breakdown potential, E_{br}, are shifted about 170 mV towards more negative values. The same behaviour was found with the Al-2Mg electrode in NaCl solutions (Section 4.6.1), although more positive values of both the corrosion potential and breakdown potential were observed. These data are in good agreement with the results presented by Muňoz *et al.* [29], where active behaviour above the corrosion potential was observed with Al-5Zn-0.02In and Al-4Zn-0.015In-0.1Si in deaerated 0.5 M NaCl solutions. Breslin *et al.* [28] have also studied the electrochemical behaviour of an Al-3.5Zn-0.02In alloy. In this case a passive region, although with higher passive currents, was evident before the breakdown of the film. However, the electrode was pre-polarised at -1.800 V vs. SCE for 1 min generating an oxide-free surface.

The influence of the chloride concentration on the breakdown potential, E_{br}, is illustrated in Figure 4.34(b), where a linear relationship is obtained between the breakdown potential, E_{br}, and the logarithm of the concentration of chloride ions. The value of the slope of the regression equation, which corresponds to B, is -0.123 V, as shown in Eq. 4.7. This value is smaller than that obtained with pure aluminium, -0.204 V (Section 4.5.1, Eq. 4.5), but higher than that calculated with the Al-2Mg alloy, -0.108 V (Section 4.6.1, Eq. 4.6).

$$E_{br} = -1.115 - 0.123[Cl^-] \qquad \textbf{Eq. 4.7}$$

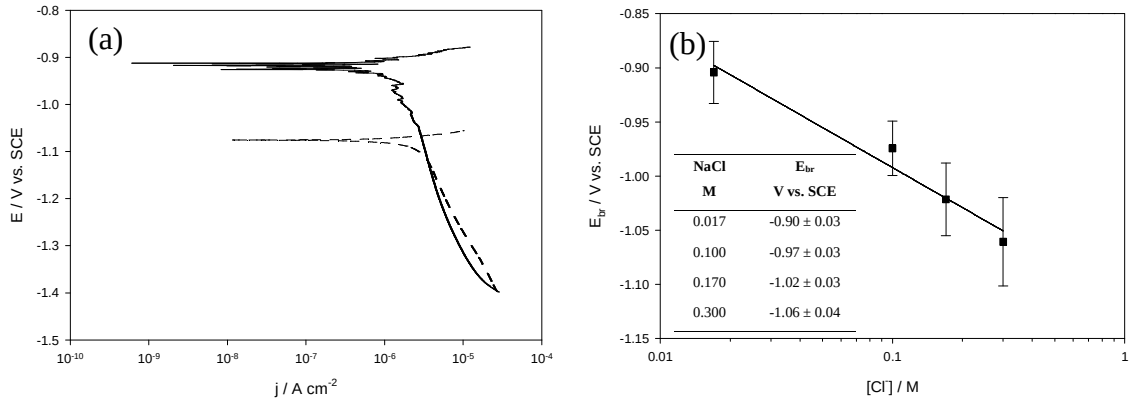

Figure 4.34: (a) Potentiodynamic polarisation curves for Al-3Zn-0.02In electrode in —— 0.017 M and – – – 0.170 M NaCl solutions at a pH of 5.0 recorded at a scan rate of 1 mV s^{-1}. **(**b) Breakdown potential, E_{br}, of the Al-3Zn-0.02In electrode as a function of the logarithm of the chloride concentration. The breakdown potential, E_{br}, was obtained from potentiodynamic polarisation tests. Each experiment was performed in triplicate (n = 3). The experimental points were fitted by a linear regression analysis to E = A + B log [Cl^-], A = –1.115 ± 0.018 V, B = –0.123 ± 0.016 V, R^2 = 0.966.

Figure 4.35 provides a comparison of the data fitted by linear regression analysis for pure aluminium (B = -0.204 V, Section 4.5.1, Eq. 4.5), Al-2Mg alloy (B = -0.108 V, Section 4.6.1, Eq. 4.6), and Al-3Zn-0.02In alloy (B = -0.123 V, Section 4.7.1, Eq. 4.7). As already outlined in the introduction (Section 4.1), an anode material with a low sensitivity to the chloride concentration is preferred in the electrocoagulation of wastewaters, since in treatment facilities the levels of chloride ions may vary considerably and occasionally drop to very low concentrations. According to Figure 4.35, the Al-2Mg electrode is the less susceptible material to the chloride concentration, since the B value is small, at -0.108 V. However, the Al-2Mg electrode also shows resistance to corrosion, as highlighted from the relatively high values of the breakdown potential, E_{br}, in Figure 4.35. Although the values of the breakdown potentials for pure aluminium are lower than the Al-2Mg electrode, pure aluminium is very sensitive to the concentration of chloride ions, as shown in Figure 4.35. The value of B is high at -0.204 V. The Al-3Zn-0.02In electrode shows a good compromise between the sensitivity to chloride ions, with a B value of -0.123 V, and the values of the breakdown potential.

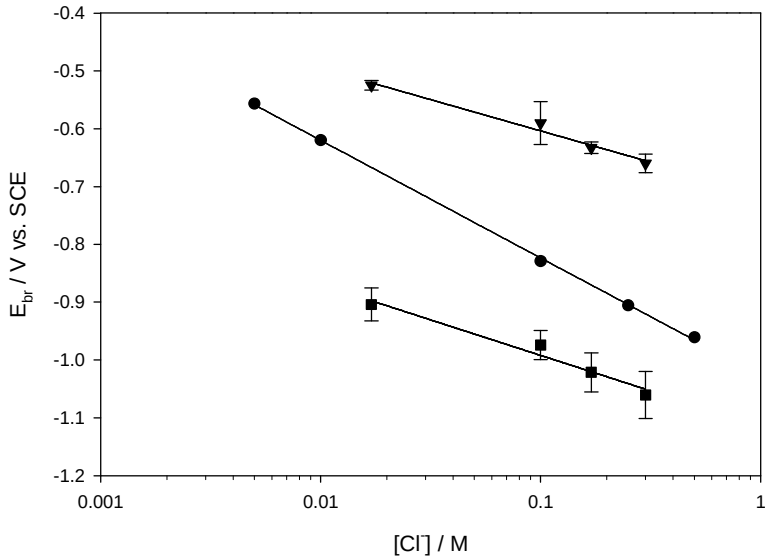

Figure 4.35: Breakdown potentials, E_{br}, of ▼ Al-2Mg, ● pure aluminium, and ■ Al-3Zn-0.02In electrodes plotted as a function of the logarithm of the chloride concentration.

The cyclic potentiodynamic polarisation curves recorded for the Al-3Zn-0.02In in 0.017 M and 0.170 M NaCl solutions are shown in Figure 4.36(a). Hysteresis is evident in both plots. However, the area of the hysteresis loop is smaller in 0.017 M NaCl. The morphology of the electrodes recorded following the cyclic polarisation measurements are presented in Figure 4.36(b) and (c), and it is clear that localised sites of dissolution are uniformly dispersed over the entire surface of the electrode. It was not possible to establish an average diameter of the pits as they tend to grow and propagate along the grain boundaries of the alloy with a dendritic shape. The density of the pits is considerably higher in comparison with the number of pits developed on the surface of Al-2Mg in NaCl solutions (Figure 4.28). Similar findings were found by Muňoz *et al.* [29], who observed that the attack of Al-5Zn-0.02In alloy in 0.5 M NaCl solution initiates at the grain boundaries and propagates into the bulk of the grain through interdendritic zones. The sites of initiation and growth of pits are preferentially located at areas enriched in In and Zn during the solidification process of the alloy due to the low solubility of Zn and In at ambient temperatures [101].

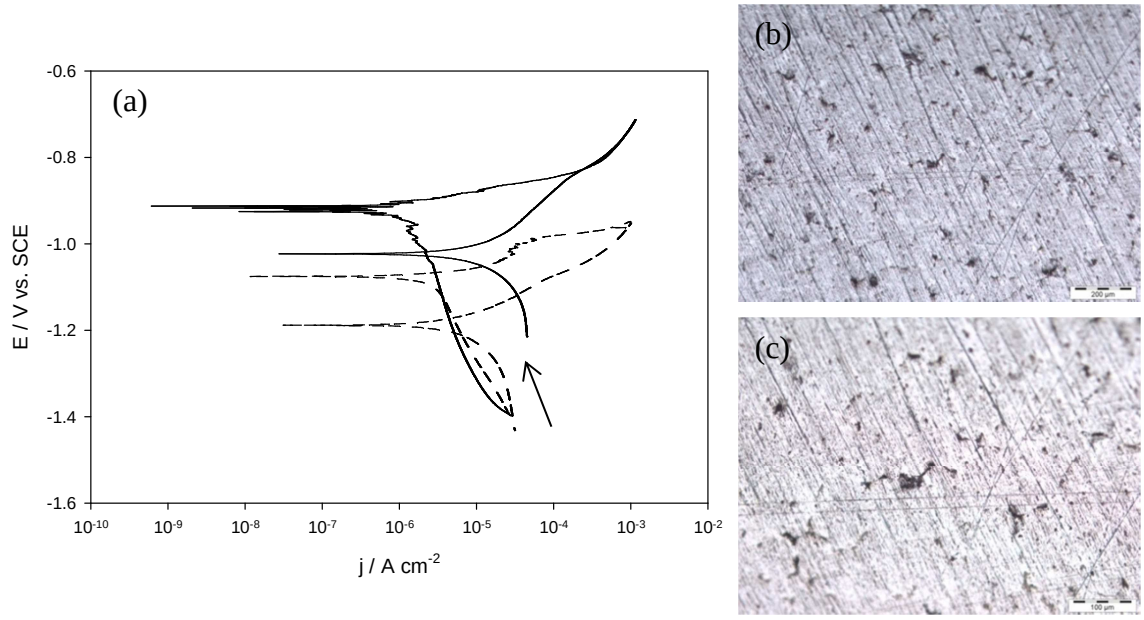

Figure 4.36: (a) Cyclic potentiodynamic polarisation curves for the Al-3Zn-0.02In electrode in —— 0.017 M and – – – 0.170 M NaCl solutions at a pH of 5.0 recorded at a scan rate of 1 mV s^{-1}; micrographs of the Al-3Zn-0.02In electrode at the end of the cyclic potentiodynamic polarisation scan in 0.017 M NaCl solution (b) scale bar corresponding to 200 μm and (c) scale bar corresponding to 100 μm.

The electrochemical behaviour of the Al-3Zn-0.02In electrode in NaCl solutions is characterised by low corrosion potentials, even in low chloride concentrations. The electrode corrodes mainly in the form of pitting. However, the extent of the damage is low since the growth of the pits on the specimen surface is limited. In addition, an even dispersion of the pits can be observed. A very low corrosion potential, the absence of any passive region, and general/uniform corrosion are positive characteristics for a material in electrocoagulation process.

4.7.2 The effect of SO_4^{2-} ions

The effect of small additions of sulfate to the chloride solution on the electrochemical behaviour of the Al-3Zn-0.02In alloy was investigated by polarising the electrode in a solution of 0.017 M NaCl and 8.1×10^{-4} M Na_2SO_4. The resulting potentiodynamic polarisation curve recorded in this solution is presented in Figure 4.37. The polarisation curve recorded in 0.017 M NaCl is also shown for comparison. In the presence of sulfate ions the corrosion potential, E_{corr}, of the Al-3Zn-0.02In electrode is shifted by about 100 mV towards more cathodic values, adopting a value of -1.015 V vs. SCE. This is somewhat different to that obtained for Al-2Mg alloy (Section 4.6.2). However,

at potentials slightly higher than the corrosion potential there was no sharp increase in the current. All three replications of the polarisation scan, which were performed in the 0.017 M NaCl and 8.1 × 10^{-4} M Na_2SO_4 solution, exhibited a decrease in the current density above the corrosion potential. This is probably due to repassivation of the electrode surface in the presence of sulfate ions. The breakdown potential, E_{br}, was read at a current density of 0.01 mA cm^{-2} and was found at -0.858 V vs. SCE, which is similar to that recorded in the 0.017 M NaCl solution, -0.912 V vs. SCE. As shown for the Al-2Mg system, in Section 4.6.2, the addition of sulfate ions to the chloride solution resulted in a 66 mV shift in the breakdown potential, which again is different to that observed with the Al-3Zn-0.02In electrode.

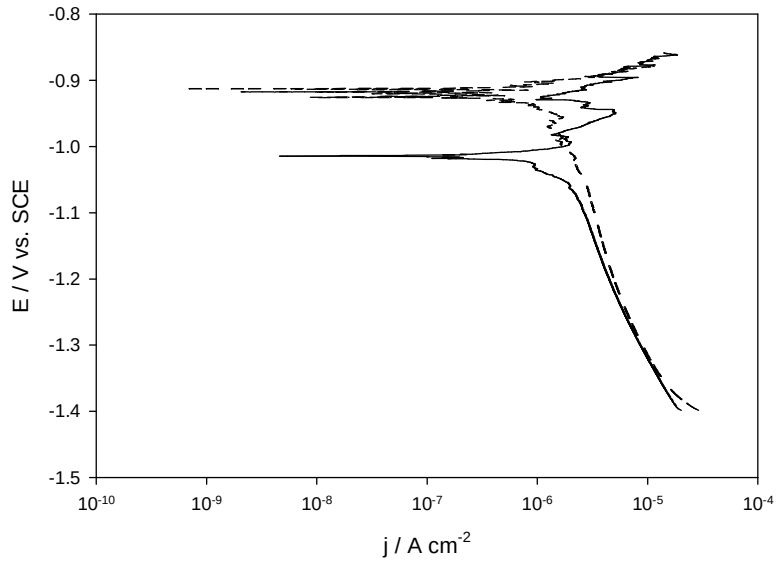

Figure 4.37: Potentiodynamic polarisation curves for the Al-3Zn-0.02In electrode in —— 0.017 M NaCl and 8.1 × 10^{-4} M Na_2SO_4 solution at a pH of 5.0 and – – – 0.017 M NaCl solution at a pH of 5.0 recorded at a scan rate of 1 mV s^{-1}.

The cyclic potentiodynamic polarisation curve recorded for Al-3Zn-0.02In in the 0.017 M NaCl and 8.1 × 10^{-4} M Na_2SO_4 solution is shown in Figure 4.38(a). The data exhibits a small hysteresis effect, which may indicate localised dissolution. The surface morphology of the electrode at the end of the cyclic scan is shown in Figure 4.38(b) and (c). Pits very similar to that observed on the surface of the electrode in NaCl solutions (Section 4.7.1, Figure 4.36) are present on the surface. As seen previously with the NaCl solutions, the pits do not have a circular or semi-circular shape. Instead they begin to

grow and develop along the grain boundaries of the alloy. By comparing Figure 4.36(c) and Figure 4.38(c) it appears that the pits formed in the 0.017 M NaCl and 8.1×10^{-4} M Na_2SO_4 solution are larger, but a lower number of active sites are generated. These results indicate that the sulfate ions inhibit the pit initiation, since the breakdown potential, E_{br}, is shifted towards slightly more noble values and fewer sites of attack are found on the electrode surface. However, once the pits occur, the sulfate anions enhance and increase the rate of propagation, as larger sized pits are now evident on the surface. Indeed, this is consistent with several reports on the influence of sulfate anions on pure aluminium [69, 70, 81, 82].

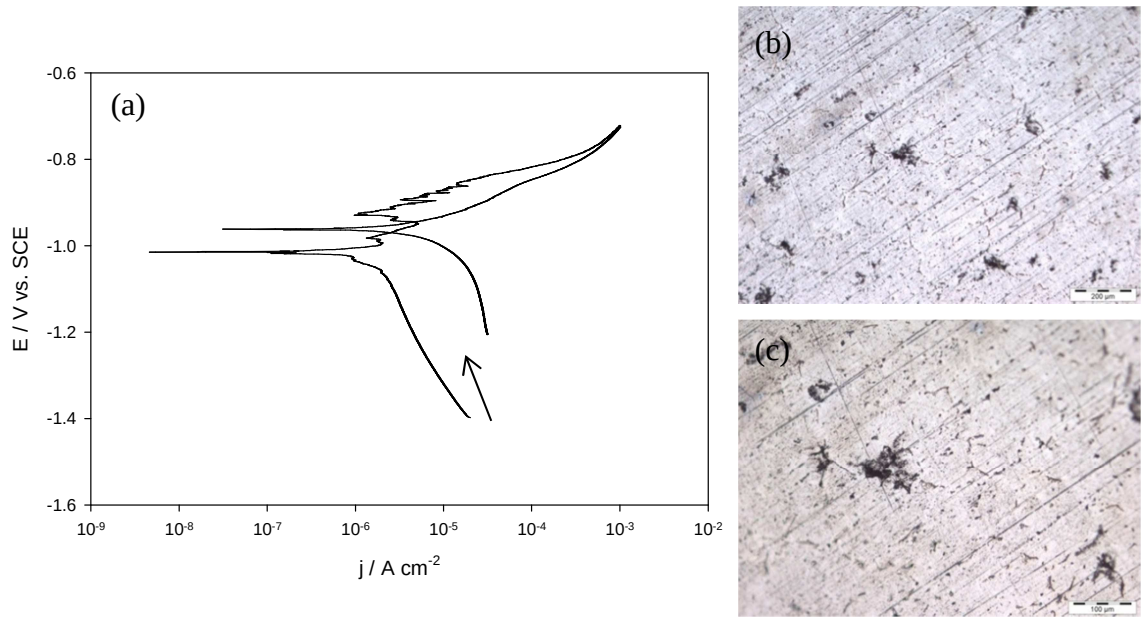

Figure 4.38: (a) Cyclic potentiodynamic polarisation curve for the Al-3Zn-0.02In electrode in —— 0.017 M NaCl and 8.1×10^{-4} M Na_2SO_4 solution at a pH of 5.0 recorded at a scan rate of 1 mV s^{-1}; micrograph of the Al-3Zn-0.02In electrode at the end of the cyclic potentiodynamic polarisation scan with (b) scale bar corresponding to 200 μm and (c) scale bar corresponding to 100 μm.

It is clear that the presence of small concentrations of sulfate ions in the NaCl solution is responsible for two contrasting effects. The corrosion potential, E_{corr}, is shifted to less noble values. On the other hand, the breakdown potential, E_{br}, occurs at more positive values, although the potential shift is small. Moreover, the growth of the pits on the electrode surface is limited to a few sites, however it was observed that pits grow larger in size in the presence of sulfates. This result may indicate the role of sulfate in hindering the pit attack but facilitating the growth and propagation of existing pits.

4.7.3 The effect of PO_4^{3-} ions

The influence of phosphate anions on the properties of Al-3Zn-0.02In alloy was studied by recording the potentiodynamic polarisation curves in a slightly acidic, pH 5.0, 0.016 M KH_2PO_4 solution. A typical polarisation curve is shown in Figure 4.39(a). The corrosion potential, E_{corr}, is -0.680 V vs. SCE, while the corrosion current, j_{corr}, is relatively low at 1.41×10^{-6} A cm^{-2}. The shape of the curve is characterised by a broad passive region, about 400 mV, which extends from -0.680 V vs. SCE to -0.232 V vs. SCE. As evident from the figure, current fluctuations are present before the onset of pit growth. Similar behaviour was found for the Al-2Mg alloy in phosphate solution, as shown in Figure 4.31(a). Phosphate ions are well-known inhibiting agents in industrial applications, and alter the behaviour of the Al-3Zn-0.02In electrode from active dissolution to more passive behaviour. The cyclic potentiodynamic polarisation curve, which is presented in Figure 4.39(b), shows significant hysteresis. This indicates considerable dissolution and modification of the surface. The inset in the figure depicts the morphology of the electrode surface at the end of the cyclic scan and it is clear that the surface is covered by several pits with different forms. The majority of the pits are non-circular in shape with a length of about 80 μm. This suggests that once the breakdown of the passive film occurs, the damage of the specimen by pits and localised dissolution sites is extensive.

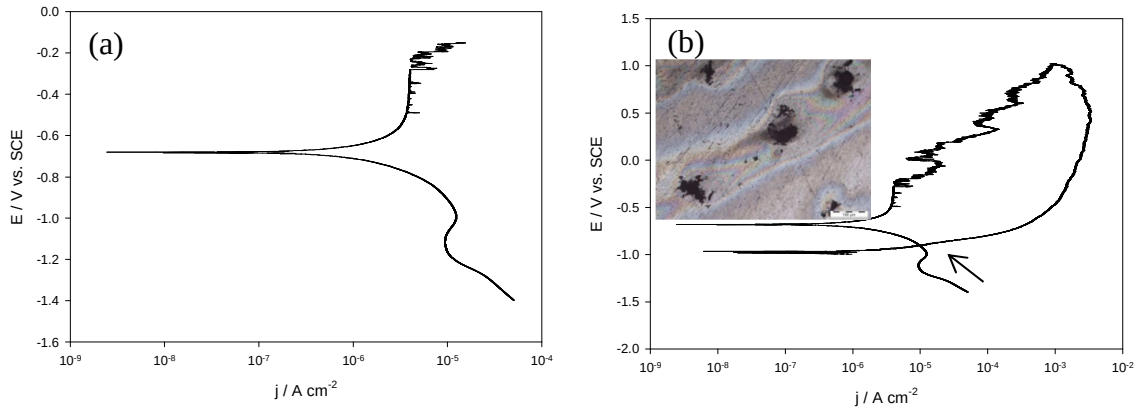

Figure 4.39: (a) Potentiodynamic polarisation curve and (b) cyclic potentiodynamic polarisation curve for Al-3Zn-0.02In electrode in —— 0.016 M KH_2PO_4 solution at a pH of 5.0 recorded at a scan rate of 1 mV s^{-1}. The inset shows a micrograph of the Al-3Zn-0.02In electrode at the end of the cyclic potentiodynamic polarisation scan, with the scale bar corresponding to 100 μm.

The potentiodynamic polarisation tests for the Al-3Zn-0.02In electrode were also performed in 6.5×10^{-3} M KH_2PO_4 solution with and without the presence of 5.0×10^{-4} M NaCl. They were carried out by polarising the electrode from -0.500 V vs. SCE at a scan rate of 10 mV s^{-1}. Although not shown, the addition of chloride had a significant effect on increasing the dissolution rate of the Al-Zn-In alloy. This is significant given the low concentration of the chloride anions, 5.0×10^{-4} M.

4.7.4 The effect of co-existing anions in sww 1 and sww 2

In Figure 4.40 the potentiodynamic polarisation curves recorded for Al-3Zn-0.02In in sww 1 and sww 2 solutions are displayed. The corrosion potential, E_{corr}, is -0.798 V vs. SCE and -0.857 V vs. SCE in sww 1 and sww 2, respectively. On comparing these values with the data obtained in 0.017 M and 0.170 M NaCl solutions in Section 4.7.1 and Figure 4.34, it is evident that the corrosion potential is shifted to more noble values by 100 mV in sww 1 and 200 mV in sww 2. This shift is probably connected with the presence of the phosphate anions. As shown in Section 4.7.2, the addition of sulfate ions to the NaCl solution gave rise to a decrease in the corrosion potential, whereas phosphate ions greatly shifted the corrosion potential to the anodic direction (Section 4.7.3). Consequently, the shift in the corrosion potential towards more positive values in sww 1 and sww 2 solutions is due to the presence of phosphate ions. Above the corrosion potential, active dissolution is observed and there is no evidence of any passive region. This behaviour is similar to that observed in NaCl solutions (Section 4.7.1, Figure 4.34). The influence of the chloride concentration can be seen by the difference in the gradients of the anodic current for the two synthetic wastewaters. In sww 2 solution, which contains a higher concentration of chloride, the increase in current above the corrosion potential is more rapid, giving a higher gradient. On the other hand, in sww 1 solution the gradient of the current increase is lower.

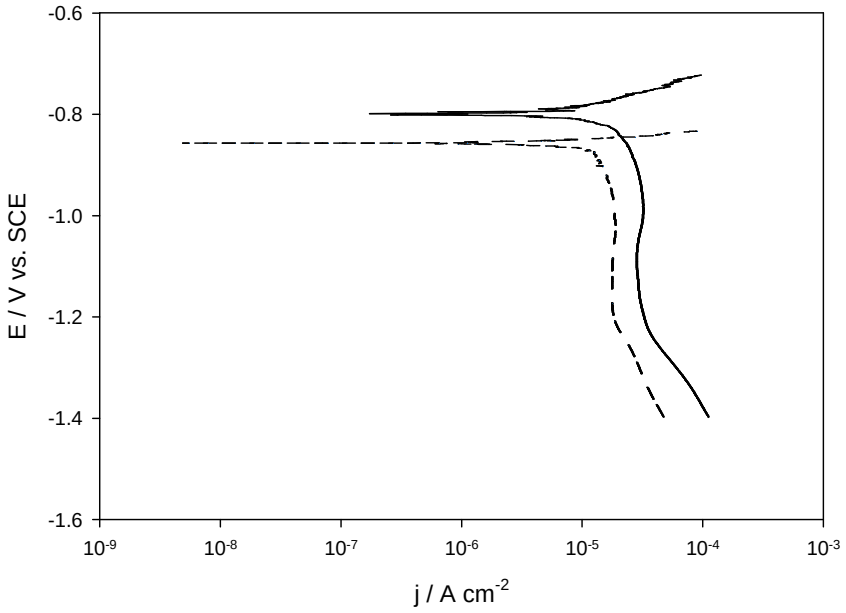

Figure 4.40: Potentiodynamic polarisation curves for the Al-3Zn-0.02In electrode in —— sww 1 and – – – sww 2 solutions at a pH of 5.0 recorded at a scan rate of 1 mV s^{-1}.

The cyclic potentiodynamic polarisation curves recorded for the Al-3Zn-0.02In electrode in sww 1 and sww 2 solutions are shown in Figure 4.41(a). Both cyclic curves show evidence of hysteresis, which is more significant in the case of sww 1. The corresponding micrographs of the electrode surfaces, recorded after the cyclic scans in sww 1 and sww 2 solutions, are shown in Figure 4.41(b) and (c), and reveal the existence of pitting corrosion. However the morphology of the electrode surface in the two solutions is quite different. In sww 1 the density of the attack is high and the pits are relatively small. In the sww 2 solution the attack occurs preferentially at a limited number of sites, but the extent of the pitting attack is more severe, as the pits are considerably larger in size.

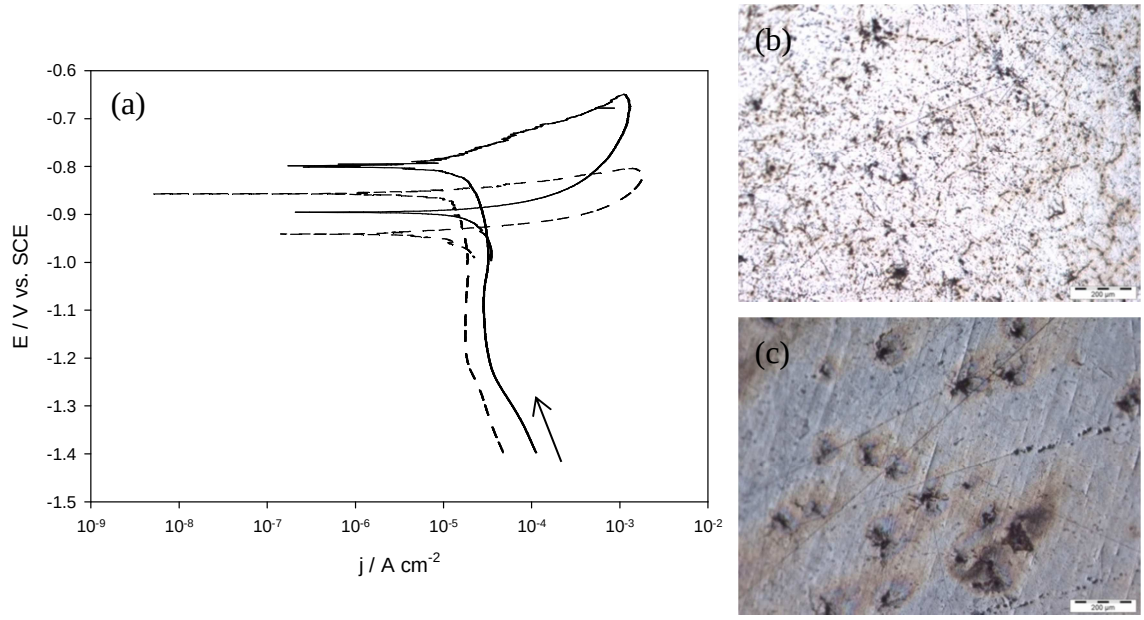

Figure 4.41: (a) Cyclic potentiodynamic polarisation curves for the Al-3Zn-0.02In electrode in —— sww 1 and – – – sww 2 solutions at a pH of 5.0 recorded at a scan rate of 1 mV s^{-1}; micrographs of the Al-3Zn-0.02In electrode at the end of the cyclic potentiodynamic polarisation scan in (b) sww 1, with the scale bar corresponding to 200 μm and (c) sww 2, with the scale bar corresponding to 200 μm.

The corrosion behaviour of the Al-3Zn-0.02In electrode in a multicomponent system is clearly affected by the different ions present in the solutions. The activation of the electrode, manifest by low corrosion potentials and the absence of a passive region, is weakened by the inhibiting effects of the phosphate ions, which raise the value of the corrosion potential. Higher concentrations of chloride anions seem to minimise this passivation effect. However, more severe pitting attack, probably due to the role of sulfate ions in enhancing the growth of existing pits is observed. It is clear that the Al-3Zn-0.02In alloy has the lowest corrosion potential, which in turn denotes ease in the dissolution process and makes this alloy interesting in electrocoagulation applications.

4.8 Summary

In this chapter the electrochemistry of several iron and aluminium alloys in synthetic wastewaters was investigated. Corrosion parameters, such as the corrosion potential, E_{corr}, and the breakdown potential, E_{br}, are computed and used to outline the dissolution of the electrode and the occurrence of localised forms of corrosion. Low E_{corr} values the absence of passivity, and a uniform dissolution of the metal are considered advantageous in the electrocoagulation process in terms of energy consumption and

operational perspective. Furthermore, the susceptibility of the various alloys to the concentration of chloride was determined. In wastewater treatment plants, the level of chlorides may vary considerably. Consequently, a great sensitivity of the metal dissolution to the chloride concentration is considered an important drawback in electrocoagulation.

The electrochemical behaviour of the pure iron electrode is highly dependent on the chloride content of the test solution. In NaCl solutions, the corrosion potential, E_{corr}, and the breakdown potential, E_{br}, decrease with increasing concentrations of chloride. On the other hand, the corrosion current, j_{corr}, increases suggesting an enhanced dissolution. In addition, the morphology of the attack is consistent with pitting corrosion. The presence of sulfate ions, even in small concentration, mitigates the effect of chlorides. This was most probably ascribed to the competitive adsorption of anions on the electrode surface. Consequently, the mitigation effect depends on the ratio of the sulfate to chloride concentration. The dissolution of the pure iron electrode is strongly facilitated in the presence of phosphate ions. Indeed, the electrode exhibits active dissolution and high corrosion currents. This behaviour is consistent with a solution pH in the range of 4.5-7.0. In the two synthetic wastewaters, sww 1 and sww 2, a general dissolution with no sign of passivity is observed. The pitting attack by chloride ions is minimised by the presence of inhibiting anions, such as sulfates and phosphates. Moreover, the variation in the chloride concentration has little influence on the dissolution of the iron electrode.

The AISI 310 electrode is characterised by a passive nature because of the high content of chromium. This feature has some implications in its electrochemical behaviour. Indeed, the electrode remains passive for an extended region even in high concentrations of chloride ions. When the breakdown occurs, isolated, large pits are observed on the electrode surface. Sulfate ions inhibit the onset of pitting, shifting the breakdown potential, E_{br}, towards more noble values and lowering the corrosion current, j_{corr}. A similar effect is observed in the presence of phosphate ions, which passivate the electrode. The concentration of chloride gains relevance in the synthetic wastewaters, which contain several anions. The electrode remains passive for a large potential region and then eventually it suffers severe pitting corrosion at potentials

dependent on the concentration of chlorides. The breakdown of the passive film and the subsequent dissolution occur at high potentials, where the electrochemistry of chromium might be involved with its dissolution in the test solution.

The low content in chromium greatly influences the electrochemical behaviour of the AISI 420 electrode. Indeed, in NaCl solutions, the breakdown of the passive film occurs at potential values lower than those observed with the AISI 310. In addition, the AISI 420 is susceptible to a severe form of localised corrosion which gives rise to large, deep pits on the electrode surface. Again, the presence of inhibiting anions, such as sulfates and phosphates, passivates the electrode. For example, in the sulfate-containing solution a larger passive region and smaller pits are observed in comparison to the chloride-containing solution. On the other hand, the electrode surface does not show any evidence of pits in the presence of phosphate ions. The effect of these inhibiting ions is evident in the synthetic wastewaters, which also contain chlorides. The breakdown potential, E_{br}, occurs at lower values due to the competitive action of the anions. Consequently, smaller pits develop on the electrode surface.

The pure aluminium electrode is highly susceptible to pitting corrosion and the occurrence of the breakdown of the passive film shows a significant dependence on the concentration of chloride ions. For example, in phosphate-containing solutions, the electrode remains in a passive state. However, when chloride ions are also present in the solution, pitting occurs.

The dependence on the chloride concentration is minimised for the Al-2Mg electrode. Indeed, in chloride solutions it shows active dissolution. Also in the presence of sulfate ions, the electrode exhibits corrosion, although the onset of the pit initiation is retarded. However, the inhibiting action of phosphate ions is clearly evident in the form of a large passive region. The corrosion of the Al-2Mg electrode in the synthetic wastewaters is very similar to that observed in chloride-containing solutions. The electrode does not exhibit any passive region, although the presence of the inhibiting anions causes a shift of the breakdown potential towards more noble values and changes the morphology of the pitting attack on the electrode surface.

The electrochemical behaviour of the Al-3Zn-0.02In in chloride solutions is characterised by active dissolution with a uniform dispersion of the dissolution sites. The dissolution of this alloy shows a low dependence on the chloride concentration and a significant low corrosion potential, E_{corr}, even in low concentrated solutions. While in the presence of sulfate ions the electrode exhibits some signs of repassivation of its surface, the inhibiting effect of phosphate ions is remarkably more evident. Indeed, a broad passive region is observed. However, when the breakdown of the passive film occurs, the damage on the electrode surface by localised dissolution is extensive. The presence of a small concentration of chloride ions seems to have a positive effect on the passivity in phosphate-containing solutions. An active dissolution is also exhibited in the synthetic wastewaters, although the corrosion potentials, E_{corr}, are shift towards more noble values in the presence of the inhibiting sulfate and phosphate anions. However, this alloy has the lowest corrosion potential, which denotes ease in the dissolution process. The morphology of the attack is in the form of small, evenly dispersed pits in low content chloride solutions. The electrode suffers a more severe attack in highly concentrated chloride solutions.

4.9 References

[1] Chen, X.M., Chen, G.H., Yue, P.L., *Sep. Purif. Technol.*, **19** (2000) 65-76.
[2] Canizares, P., Jimenez, C., Martinez, F., Saez, C., Rodrigo, M.A., *Ind. Eng. Chem. Res.*, **46** (2007) 6189-6195.
[3] Holt, P., Barton, G., Mitchell, C., *Electrocoagulation as a Wastewater Treatment*, in: The Third Annual Australian Environmental Engineering Research Event, Castlemaine, Victoria, 1999.
[4] Baklan, V.Y., Kolesnikova, I.P., *J. Aerosol Sci.*, **27** (1996) S209-S210.
[5] Chen, G.H., *Sep. Purif. Technol.*, **38** (2004) 11-41.
[6] Vik, E.A., Carlson, D.A., Eikum, A.S., Gjessing, E.T., *Water Res.*, **18** (1984) 1355-1360.
[7] Novikova, S.P., Shkorbatova, T.L., Sokol, E.Y., *Sov. J. Water Chem. Tech.*, **4** (1982) 353-357.
[8] Mollah, M.Y.A., Schennach, R., Parga, J.R., Cocke, D.L., *J. Hazard. Mater.*, **84** (2001) 29-41.
[9] Do, J.S., Chen, M.L., *J. Appl. Electrochem.*, **24** (1994) 785-790.
[10] Hülser, P., Krüger, U.A., Beck, F., *Corros. Sci.*, **38** (1996) 47-57.
[11] Uhlig, H.H., Revie, R.W., *Uhlig's Corrosion Handbook*, 2nd ed., John Wiley & Sons, New York, 2000.
[12] Emamjomeh, M.M., Sivakumar, M., *J. Environ. Manage.*, **90** (2009) 1663-1679.
[13] Amani-Ghadim, A.R., Aber, S., Olad, A., Ashassi-Sorkhabi, H., *Electrochim. Acta*, **56** (2011) 1373-1380.
[14] Mameri, N., Yeddou, A.R., Lounici, H., Belhocine, D., Grib, H., Bariou, B., *Water Res.*, **32** (1998) 1604-1612.

[15] Kuan, W.H., Hu, C.Y., Chiang, M.C., *Water Sci. Technol.*, **60** (2009) 1341-1346.
[16] Gadd, A., Ryan, D., Kavanagh, J., Beaurain, A.-L., Luxem, S., Barton, G., *J. Appl. Electrochem.*, **40** (2010) 1511-1517.
[17] Hutnan, M., Drtil, M., Kalina, A., *J. Hazard. Mater.*, **131** (2006) 163-169.
[18] Kobya, M., Hiz, H., Senturk, E., Aydiner, C., Demirbas, E., *Desalination*, **190** (2006) 201-211.
[19] Buzzini, A.P., Patrizzi, L.J., Motheo, A.J., Pires, E.C., *J. Environ. Manage.*, **85** (2007) 847-857.
[20] Kobya, M., Delipinar, S., *J. Hazard. Mater.*, **154** (2008) 1133-1140.
[21] Yetilmezsoy, K., Ilhan, F., Sapci-Zengin, Z., Sakar, S., Gonullu, M.T., *J. Hazard. Mater.*, **162** (2009) 120-132.
[22] Bouhezila, F., Hariti, M., Lounici, H., Mameri, N., *Desalination*, **280** (2011) 347-353.
[23] Secula, M.S., Cretescu, I., Petrescu, S., *Desalination*, **277** (2011) 227-235.
[24] Baboian, R., *Corrosion Tests and Standards: Application and Interpretation*, 2nd Edition ed., ASTM, Baltimore, 2005.
[25] Mouedhen, G., Feki, M., Wery, M.D.P., Ayedi, H.F., *J. Hazard. Mater.*, **150** (2008) 124-135.
[26] Vargel, C., *Corrosion of Aluminium*, Elsevier, 2001.
[27] Davis, J.R., *Corrosion of Aluminum and Aluminum Alloys*, ASM International, 1999.
[28] Breslin, C.B., Friery, L.P., Carroll, W.M., *Corros. Sci.*, **36** (1994) 85-97.
[29] Munoz, A.G., Saidman, S.B., Bessone, J.B., *Corros. Sci.*, **44** (2002) 2171-2182.
[30] Venugopal, A., Angal, R.D., Raja, V.S., *Corrosion*, **52** (1996) 138-142.
[31] Ahmad, Z., *Principles of Corrosion Engineering and Corrosion Control*, Butterworth-Heinemann, Oxford, 2006.
[32] OECD, Test No. 303: Simulation Test - Aerobic Sewage Treatment - A: Activated Sludge Units; B: Biofilms, in: OECD Guidelines for the Testing of Chemicals, Adopted 22 January 2011.
[33] Galvele, J.R., *J. Electrochem. Soc.*, **123** (1976) 464-474.
[34] Galvele, J.R., in: R.P. Frankenthal, J. Kruger (Eds.) Passivity of Metals, The Electrochemical Society, Princeton, NJ, 1978, pp. 285-327.
[35] Pletcher, D., *Electrochemistry*, The Royal Society of Chemistry, London, 1983.
[36] Laycock, N.J., Newman, R.C., *Corros. Sci.*, **39** (1997) 1771-1790.
[37] Laycock, N.J., Newman, R.C., *Corros. Sci.*, **40** (1998) 887-902.
[38] Alvarez, M.G., Galvele, J.R., *Corros. Sci.*, **24** (1984) 27-48.
[39] Beavers, J.A., Durr, C.L., Thompson, N.G., *Unique Interpretation of Potentiodynamic Polarization Technique*, in: Corrosion 98, March 22 - 27, San Diego CA, 1998, NACE International.
[40] Vatankhah, G., Drogowska, M., Menard, H., Brossard, L., *J. Appl. Electrochem.*, **28** (1998) 173-183.
[41] MacDougall, B., Bardwell, J.A., *J. Electrochem. Soc.*, **135** (1988) 2437-2441.
[42] Bird, H.E.H., Pearson, B.R., Brook, P.A., *Corros. Sci.*, **28** (1988) 81-86.
[43] Nobe, K., Tobias, R.F., *Corrosion*, **20** (1964) 263.
[44] Roberge, P.R., *Handbook of Corrosion Engineering*, McGraw-Hill, New York, 1999.
[45] McCaffrey, E., *Introduction to Corrosion Science*, Springer, 2010.
[46] Cohen, S.M., *Corrosion*, **51** (1995) 71-78.
[47] Vetere, V.F., Romagnoli, R., *Br. Corros. J.*, **29** (1994) 115-119.
[48] Sastri, V.S., *Green Corrosion Inhibitors: Theory and Practice*, John Wiley & Sons, 2011.
[49] Szklarska-Smialowska, Z., Staehle, R.W., *J. Electrochem. Soc.*, **121** (1974) 1393-1401.
[50] Pryor, M.J., Cohen, M., *J. Electrochem. Soc.*, **98** (1951) 263-272.
[51] İrdemez, Ş., Demircioğlu, N., Yildiz, Y.Ş., *J. Hazard. Mater.*, **137** (2006) 1231-1235.

[52] Silverman, D.C., *Tutorial on Cyclic Potentiodynamic Polarization Technique*, in: Corrosion 98, March 22 - 27, San Diego CA, 1998, NACE International.
[53] Sedriks, A.J., *Corrosion of Stainless Steel*, John Wiley and Sons, New York, USA, 1979.
[54] Kamachi Mudali, U., Pujar, M.G., *Pitting Corrosion of Austenitic Stainless Steel and Their Weldments*, in: H.S. Khatak, B. Ray (Eds.) Corrosion of Austenitic Stainless Steel - Mechanism, Mitigation and Monitoring, Woodhead Publishing Limited, 2002.
[55] Cramer, S.D., Covino, B.S., *ASM Handbook Volume 13A: Corrosion: Fundamentals, testing, and Protection*, ASM International, 2003.
[56] Leckie, H.P., Uhlig, H.H., *J. Electrochem. Soc.*, **113** (1966) 1262-1267.
[57] Horvath, J., Uhlig, H.H., *J. Electrochem. Soc.*, **115** (1968) 791-795.
[58] Revie, R.W., Uhlig, H.H., *Corrosion and Corrosion Control - An introduction to Corrosion Science and Engineering*, 4th ed., John Wiley and Sons, 2008.
[59] Brauns, E., Schwenk, W., *Archiv. Eisenhuttenw.*, **32** (1961).
[60] Lakatos-Varsányi, M., Falkenberg, F., Olefjord, I., *Electrochim. Acta*, **43** (1998) 187-197.
[61] Uhlig, H., Gilman, G., *Corrosion*, **20** (1964).
[62] de Cristofaro, N., *Passivity and Passivity Breakdown of 13%Cr, 15%Cr and 13Cr5Ni2MoN Stainless Steel in Chloride-Containing Solutions*, in: EUCORR '97 and EUCORR '98, 1999, IOM Communications Ltd.
[63] Van Gheem, E., Vereecken, J., Le Pen, C., *J. Appl. Electrochem.*, **32** (2002) 1193-1200.
[64] Pyun, S.I., Lee, W.J., *Corros. Sci.*, **43** (2001) 353-363.
[65] Frankel, G.S., *J. Electrochem. Soc.*, **145** (1998) 2970-2970.
[66] Bohni, H., Uhlig, H.H., *J. Electrochem. Soc.*, **116** (1969) 906-910.
[67] Broli, A., Holtan, H., *Corros. Sci.*, **13** (1973) 237-246.
[68] McCafferty, E., *Corros. Sci.*, **37** (1995) 481-492.
[69] Pyun, S.I., Moon, S.M., *J. Solid State Electrochem.*, **3** (1999) 331-336.
[70] Pyun, S.I., Na, K.H., Lee, W.J., Park, J.J., *Corrosion*, **56** (2000) 1015-1021.
[71] Na, K.-H., Pyun, S.-I., *Corros. Sci.*, **49** (2007) 2663-2675.
[72] Rudd, W.J., Scully, J.C., *Corros. Sci.*, **20** (1980) 611-631.
[73] Shalaby, L.A., El Sobki, K.M., Abdul Azim, A.A., *Corros. Sci.*, **16** (1976) 637-643.
[74] Ahmad, Z., Ul-Hamid, A., Bj, A.A., *Corros. Sci.*, **43** (2001) 1227-1243.
[75] Halambek, J., Berkovic, K., Vorkapic-Furac, J., *Corros. Sci.*, **52** (2010) 3978-3983.
[76] Brillas, E., Cabot, P.L., Centellas, F., Garrido, J.A., Perez, E., Rodriguez, R.M., *Electrochim. Acta*, **43** (1998) 799-812.
[77] Flis, J., Kowalczyk, L., *J. Appl. Electrochem.*, **25** (1995) 501-507.
[78] Hampson, N.A., Jackson, N., Stirrup, B.N., *Surf. Technol.*, **5** (1977) 277-289.
[79] Hunkeler, F., Bohni, H., *Werkst. Korros.-Mater. Corros.*, **34** (1983) 68-77.
[80] Kolics, A., Polkinghorne, J.C., Wieckowski, A., *Electrochim. Acta*, **43** (1998) 2605-2618.
[81] Lee, W.J., Pyun, S.I., *Electrochim. Acta*, **45** (2000) 1901-1910.
[82] Pyun, S.I., Moon, S.M., Ahn, S.H., Kim, S.S., *Corros. Sci.*, **41** (1999) 653-667.
[83] El Shayeb, H.A., Abd El Wahab, F.M., El Abedin, S.Z., *J. Appl. Electrochem.*, **29** (1999) 473-480.
[84] Gudic, S., Smoljko, I., Kliskic, M., *J. Alloys Compd.*, **505** (2010) 54-63.
[85] Gudic, S., Smoljko, I., Kliskic, M., *Mater. Chem. Phys.*, **121** (2010) 561-566.
[86] Zecevic, S., Gajic, L., Despic, A.R., Drazic, D.M., *Electrochim. Acta*, **26** (1981) 1625-1631.
[87] Zhuk, A.Z., Sheindlin, A.E., Kleymenov, B.V., Shkolnikov, E.I., Lopatin, M.Y., *J. Power Sources*, **157** (2006) 921-926.
[88] Nestoridi, M., Pletcher, D., Wood, R.J.K., Wang, S., Jones, R.L., Stokes, K.R., Wilcock, I., *J. Power Sources*, **178** (2008) 445-455.
[89] Bruzzone, G., Barbucci, A., Cerisola, G., *J. Alloys Compd.*, **247** (1997) 210-216.
[90] Burri, G., Luedi, W., Haas, O., *J. Electrochem. Soc.*, **136** (1989) 2167-2171.

[91] Keir, D.S., Pryor, M.J., Sperry, P.R., *J. Electrochem. Soc.*, **116** (1969) 319-322.
[92] Reding, J.T., Newport, J.J., *Materials Protection*, **5** (1966) 15-&.
[93] Saidman, S.B., Garcia, S.G., Bessone, J.B., *J. Appl. Electrochem.*, **25** (1995) 252-258.
[94] Sakano, T., Toda, K., Hanada, M., *Materials Protection*, **5** (1966) 45-50.
[95] Tuck, C.D.S., Hunter, J.A., Scamans, G.M., *J. Electrochem. Soc.*, **134** (1987) 2970-2981.
[96] Reboul, M.C., Gimenez, P., Rameau, J.J., *Corrosion*, **40** (1984) 366-371.
[97] Vasudevan, S., Lakshmi, J., Sozhan, G., *Clean-Soil Air Water*, **38** (2010) 506-515.
[98] Vasudevan, S., Lakshmi, J., Sozhan, G., *Desalination*, **275** (2011) 260-268.
[99] Vasudevan, S., Lakshmi, J., Jayaraj, J., Sozhan, G., *J. Hazard. Mater.*, **164** (2009) 1480-1486.
[100] Khemis, M., Tanguy, G., Leclerc, J.P., Valentin, G., Lapicque, F., *Process Saf. Environ. Protect.*, **83** (2005) 50-57.
[101] Yan, H., Downes, J., Boden, P.J., Harris, S.J., *J. Electrochem. Soc.*, **143** (1996) 1577-1583.

5 Performance of the Electrodes in Synthetic Wastewaters and a Screening Chemometric Study on the Removal of Phosphates by AISI 420 Electrode

5.1 Introduction

In Chapter 3 results on the removal of phosphates using Al-2Mg and AISI 420 electrodes were presented. The removal efficiency of these two electrodes was investigated by varying several operating parameters, such as the initial concentration of phosphates, current density, initial pH and the concentration of sodium chloride. A simplified model for the removal mechanism and the kinetics of the phosphate removal were discussed. In addition, the two alloys were tested to treat real samples from two wastewater facilities in Co. Longford. The use of these real samples revealed that the removal efficiency depends on the electrochemistry of each electrode and the physico-chemical properties of the solution. As a consequence, the electrochemical behaviour and the corrosion properties of several electrode materials were studied and these results were presented in Chapter 4. The study was carried out in synthetic wastewaters in order to obtain more realistic results in terms of the electrode behaviour for potential applications in wastewater treatment plants.

An extensive literature exists on the use of iron and aluminium as electrode materials in electrocoagulation processes [1]. Conversely, few studies have been reported on iron and aluminium alloys. As shown in Chapter 4, alloying elements can enhance the rate of dissolution of the electrodes or alter the nature of ferrous and non-ferrous alloys. These

features may result in better performances from the perspectives of the removal efficiency and the energy consumption.

In this chapter, results are presented and discussed on the performance of ferrous and non-ferrous electrode materials in removing three different types of pollutants. The efficiency of the electrodes, which is studied in the synthetic wastewaters, is compared and correlated to the electrochemistry of the electrodes studied in the same test solutions, Chapter 4. As shown in Chapter 4, the solution conductivity and the concentration of chloride ions play a key role in the electrocoagulation performance of the electrodes. Moreover, the composition of the wastewater in treatment plants is typically complex and involves various ions. As shown in Chapter 4, these ions can act as inhibitors or activators in electrocoagulation, thus affecting the removal performance and the energy demand. In the present study, in order to investigate the effect of co-existing ions, electrocoagulation tests were carried out in two synthetic wastewaters, sww 1 and sww 2, which were formulated from the OECD synthetic sewage [2] and contained some of the ions most commonly present in wastewater. The composition of the two solutions is shown in Table 5.1 and differs in the chloride ion concentration, 0.017 M in sww 1 and 0.170 M in sww 2.

Three different pollutants were then added to the test solutions. Phosphate anions were selected as a model of inorganic pollutants. These inorganic pollutants are not particularly toxic, however they are still a danger to the environment because they are used extensively as fertilisers [3] and are responsible for the phenomenon of eutrophication. A dye was used as a model of soluble organic pollutants. Although there are a lot of soluble organic compounds, special attention is paid to dyes because of the great amount discharged from industries [4]. These compounds usually have functional groups and a high molecular weight. Furthermore, they are highly soluble in water and persistent once discharged into the natural environment [5]. An azo dye, *C.I. Acid Orange 7* or Orange II, was used. Its structure is shown in Section 2.3.3.1. This dye is widely used in textile industries for dyeing [5] and several studies on its removal by electrocoagulation have already been reported in the literature [6-10]. Finally, Zn^{2+} ions were selected as a model of metallic pollutants. Zinc is used mainly for galvanising iron but it is also important in the preparation of certain alloys, i.e. brass, and as a pigment, i.e. ZnO [11].

Table 5.1: Composition of the electrolyte solutions, sww 1 and sww 2, used in the electrocoagulation tests. The pH was maintained at 5.0.

	$CaCl_2.2H_2O$ / g L^{-1}	$MgSO_4.7H_2O$ / g L^{-1}	NaCl / g L^{-1}	PO_4-P / mg L^{-1}	Orange II / mg L^{-1}	Zn^{2+} / mg L^{-1}	κ / mS m^{-1}
sww 1	0.4	0.2	0.7	500.0	50.0	100.0	3.7
sww 2	0.4	0.2	7.0	500.0	50.0	100.0	14.4

The energy consumption of the electrocoagulation process is also presented and discussed in this chapter. Although quite attractive, few companies use electrocoagulation for treating wastewater, which is mainly due to the energy costs. Some examples of companies involved in electrocoagulation include Watertectonics Inc., Kaselco Inc., Powell Water Systems Inc., Ecolotron Inc. and OilTrap Environmental Products Inc. The major impediment to the more widespread use of electrocoagulation over conventional methods is the uncertainty about the energy costs. Therefore, a study on the energy consumption is one of the most important steps in developing a successful electrocoagulation unit.

In electrocoagulation many factors, such as the pH, current density, composition and concentration of the solution and conductivity, affect the efficiency of the process. The efficiency of a specific process may be increased upon optimisation of these factors. As mentioned in Section 2.3.7, the classical approach to optimise a process involves varying a single factor while keeping the other factors fixed at a specific set of conditions, 'one-factor-a-time' or OFAT [12]. However, this method is time consuming and may give rise to optimisation conditions that are far from reality [12-14].

Recently, the use and the importance of the Design of Experiments, DoE, in agricultural [15-17], industrial [12, 13, 18] and other scientific applications [19, 20] have been well documented. These techniques are an efficient method of developing, improving and optimising a process and can be used to determine the relative significance of a number of factors and their interactions [21]. In the present study, the DoE was used as a preliminary screening step in order to identify the non-relevant factors affecting the efficiency of electrocoagulation in removing phosphates. Indeed, several studies have reported that the current density and time are the most important factors in the electrocoagulation efficiency. However, other factors that might be relevant have not

been considered or investigated. In this chapter, the results of a DoE screening experiment are presented and discussed. The factors, which were likely to affect the efficiency of the electrocoagulation removal of phosphates using stainless steel AISI 420 electrode, were selected in order to determine which were relevant for the process.

5.2 Iron system

Three iron-based alloys, namely pure iron, stainless steel AISI 310 and stainless steel AISI 420, were investigated as anodes in the electrocoagulation tests. As outlined in Section 4.1, the two stainless steel grades were selected as alternatives to the pure iron electrode. Indeed, several authors [4, 22-32] reported some limitations to the use of iron electrodes in electrocoagulation, for example a yellowish colour of the effluent owing to rust formation (Fe_2O_3). The presence of chromium in the stainless steels prevents the formation of rust on the electrode surface.

Results are presented and discussed on the electrocoagulation performance of the three anode materials for removing phosphates, Orange II dye and zinc from the two synthetic wastewaters. The compositions of the two test solutions used are given in Table 5.1. A comparison of the electrodes is shown and the results are correlated to the electrochemical behaviour that has been presented in Chapter 4. Moreover, the energy requirement for the process was calculated for the three electrode materials. For all the electrocoagulation experiments, the current density was 11.7 mA cm^{-2}, the ratio of the surface area of the anode to the volume of solution, SA/V, was 19.4 m^{-1} and the electrocoagulation time was 30 min. A plate of stainless steel AISI 310 was used as the cathode. The composition of the electrode materials and the full experimental details are given in Sections 2.2.2 and 2.3.1.2.

5.2.1 The electrode performance in removing three representative pollutants from synthetic wastewaters

5.2.1.1 The removal of phosphates

Iron is widely used as an electrode material in electrocoagulation applications [33]. In particular, several studies have been reported on the electrocoagulation removal of phosphates using iron as the anode material [34-37]. As outlined in Section 3.3, it is believed that the removal of phosphates is mainly accomplished through the adsorption of phosphates on Fe^{3+} hydrolysis products. As a result, iron is a promising electrode material for the removal of phosphates. Indeed, İrdemez *et al.* [35] obtained the complete removal of phosphates using iron plate electrodes with initial concentrations of 25 and 50 mg L^{-1} PO_4-P after 20 min and a removal efficiency of 95% and 75% was reached with 100 and 150 mg L^{-1} PO_4-P, respectively. On the other hand, there are no studies carried out on the electrocoagulation removal of phosphates using stainless steel electrodes. As detailed in Section 3.3, AISI 420 exhibits very good removal efficiencies for the removal of phosphates. As a consequence, the removal efficiencies of phosphates are compared in this section for three iron-based electrodes, pure iron, AISI 310 and AISI 420.

The residual concentrations of PO_4-P in the sww 1 solution, plotted as a function of the electrocoagulation period, are compared for pure iron, AISI 310 and AISI 420 electrodes in Figure 5.1. The corresponding data are presented in Table 5.2. It is clearly apparent from these data that, at the end of the electrocoagulation period, the removal efficiency of the pure iron electrode is considerably higher than that observed with the other two materials. Indeed, the final concentration of phosphates is 40.7 mg L^{-1} for pure iron, which corresponds to a removal efficiency of 92%. A lower removal efficiency of 86% was obtained with AISI 420, while the removal efficiency of 38% for AISI 310 was very poor. The results obtained for pure iron and AISI 420 compare well with the findings reported in Section 3.3. However, it is evident from the data presented that the performance of AISI 310 is poor in terms of the removal of phosphates.

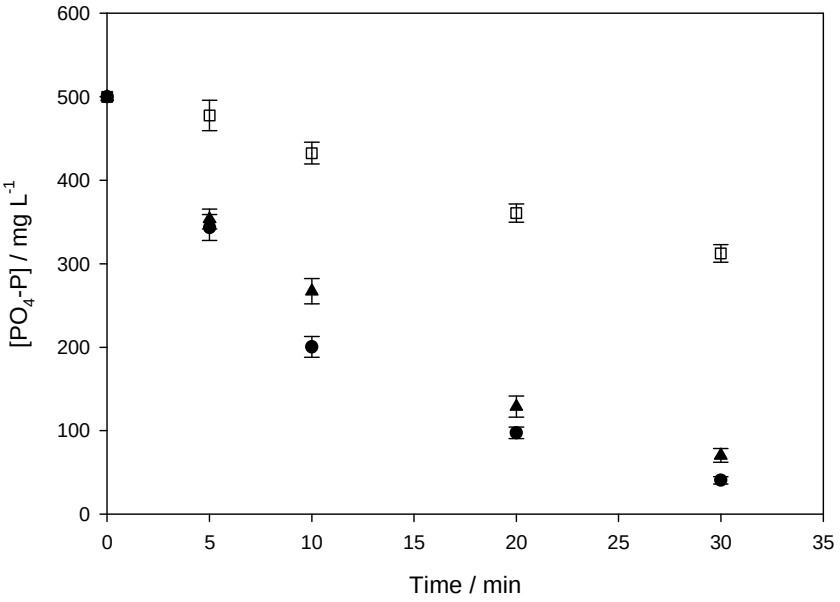

Figure 5.1: Residual concentrations of PO_4-P for ● pure iron, □ AISI 310 and ▲ AISI 420 electrodes plotted as a function of the electrocoagulation time in sww 1 solution (Table 5.1). (Cathode = AISI 310, pH = 5.0, κ = 3.7 mS m^{-1}, j = 11.7 mA cm^{-2}, SA/V = 19.4 m^{-1}).

Table 5.2: Residual concentrations of PO_4-P and removal efficiency for pure iron, AISI 310 and AISI 420 electrodes in sww 1 solution. Each experiment was performed in triplicate (n = 3).

Time / min	**[PO_4-P] / mg L^{-1}**			**η / %**		
	Iron	**AISI 420**	**AISI 310**	**Iron**	**AISI 310**	**AISI 420**
0	500.0	500.0	500.0	0	0	0
5	343 ± 15	477 ± 18	354 ± 12	31 ± 3	4 ± 4	29 ± 4
10	200 ± 12	433 ± 13	267 ± 15	60 ± 2	13 ± 3	47 ± 3
20	98 ± 7	361 ± 11	129 ± 13	80 ± 1	28 ± 2	74 ± 3
30	40.7 ± 4.4	313 ± 11	70 ± 8	91.9 ± 0.9	37 ± 2	86 ± 2

Figure 5.2 shows the residual concentrations of PO_4-P in the sww 2 solution, plotted as a function of the electrocoagulation time, for pure iron, AISI 310 and AISI 420. The corresponding data are given in Table 5.3. As can be seen, at the end of the 30 min period, the concentrations recorded are 37, 292 and 68 mg L^{-1}, giving removal efficiencies of 93%, 42% and 87%, for pure iron, AISI 310 and AISI 420, respectively. Again, the highest removal efficiency is observed with pure iron and the AISI 420 electrodes. Clearly, the removal efficiencies for the electrodes are very similar to that

observed in the sww 1 solution (Table 5.2). This similarity observed in both solutions, sww 1 and sww 2, which differ in the conductivity level, suggests that, in removing phosphates, the performance of the iron system is not affected by the conductivity or the chloride content of the solution. However, it is worth noting that the removal efficiencies of AISI 310, recorded in sww 1 and sww 2, do not entirely fall within the limits of the experimental errors. This may indicate a slight increase of the electrode performance when the process is carried out in the more conducting solution, sww 2.

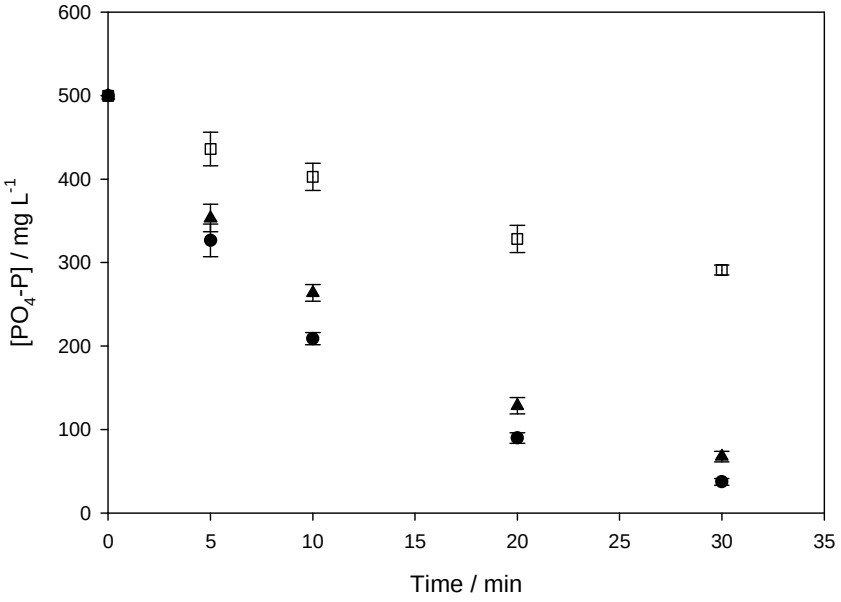

Figure 5.2: Residual concentrations of PO_4-P for ● iron, □ AISI 310 and ▲ AISI 420 electrodes plotted as a function of the electrocoagulation time in sww 2 solution (Table 5.1). (Cathode = AISI 310, pH = 5.0, κ = 14.4 mS m^{-1}, j = 11.7 mA cm^{-2}, SA/V = 19.4 m^{-1}).

Table 5.3: Residual concentrations of PO_4-P and removal efficiency for pure iron, AISI 310 and AISI 420 electrodes in sww 2 solution. Each experiment was performed in triplicate (n = 3).

Time / min	**[PO_4-P] / mg L^{-1}**			**η / %**		
	Iron	**AISI 420**	**AISI 310**	**Iron**	**AISI 310**	**AISI 420**
0	500.0	500.0	500.0	0	0	0
5	327 ± 20	436 ± 20	353 ± 16	35 ± 4	13 ± 4	29 ± 3
10	209 ± 7	403 ± 16	264 ± 10	58 ± 1	19 ± 3	47 ± 2
20	90 ± 6	328 ± 16	128 ± 10	82 ± 1	34 ± 3	74 ± 2
30	37 ± 4	292 ± 6	68 ± 6	92.6 ± 0.8	42 ± 1	86 ± 1

5.2.1.2 The removal of Orange II dye

The treatment of textile dyes using the electrocoagulation technique has been reported by a number of authors [1]. Two mechanisms, involving iron flocs, have been proposed. These two mechanisms focus on either surface complexation or electrostatic attraction, although secondary reactions may occur if the anode potential is sufficiently high [38]. These reactions include direct oxidation of organic compounds present in the wastewater. Rajeshwar and Ibanez [39] have concluded that iron anodes remove azo dyes by the additional mechanism of degradation, possibly due to the action of reducing Fe^{2+} ions [40], other than adsorption. However, there is no general agreement on how azo dyes are removed from wastewaters and only limited information about the by-products formed in the decolourisation process. For example, Daneshvar *et al.* [7] claimed that, in the electrocoagulation process with iron electrodes, Orange II dye molecules can also be removed by a degradation reaction. This theory was supported by the UV, FT-IR and NMR spectra of the desorbed samples, which show the presence of sulfanilic acid and 1-amino-2-naphtol. The degradation and the cleavage of the azo bond is probably facilitated by the oxidation of electrogenerated Fe^{2+} and/or hypochlorite ions [41]. In contrast, Chafi *et al.* [6] have shown that adsorption or entrapment of the Orange II dye molecules is the prevailing mechanism when iron electrodes are used in electrocoagulation. However, interactions between the iron flocs and the dye molecules [9], could not be observed by comparing X-ray diffractograms of blank samples and dye-containing residues. Regardless of the main mechanism involved in the removal of the dye, the studies reported in the literature [6, 7, 9] show the effectiveness of iron electrodes in the treatment of Orange II dye. On the other hand, only a few studies have been focused on the electrocoagulation removal of azo dyes with stainless steel electrodes [42, 43]. These studies showed excellent performances of stainless steel electrodes. For example, Arsalan-Alaton *et al.* [42] reported complete and fast colour removal in just 5 min during electrocoagulation of simulated reactive dye bath effluent. It appears that the iron-based electrodes are promising in the removal of Orange II.

In Figure 5.3 the residual concentrations of Orange II dye recorded in the sww 1 solution as a function of the electrocoagulation period for pure iron, AISI 310 and AISI 420 are presented. The corresponding data are shown in Table 5.4. As evident from Figure 5.3, after the electrocoagulation period of 30 min, the removal efficiencies for

pure iron and AISI 420 are similar, 98% and 99% and the dye was completely removed at the end of the process. These results confirm high efficiencies of iron and stainless steel electrodes in the treatment of Orange II. However, in contrast with the expected results, the removal of the azo dye by the AISI 310 electrode is negligible, with an efficiency of just 28%.

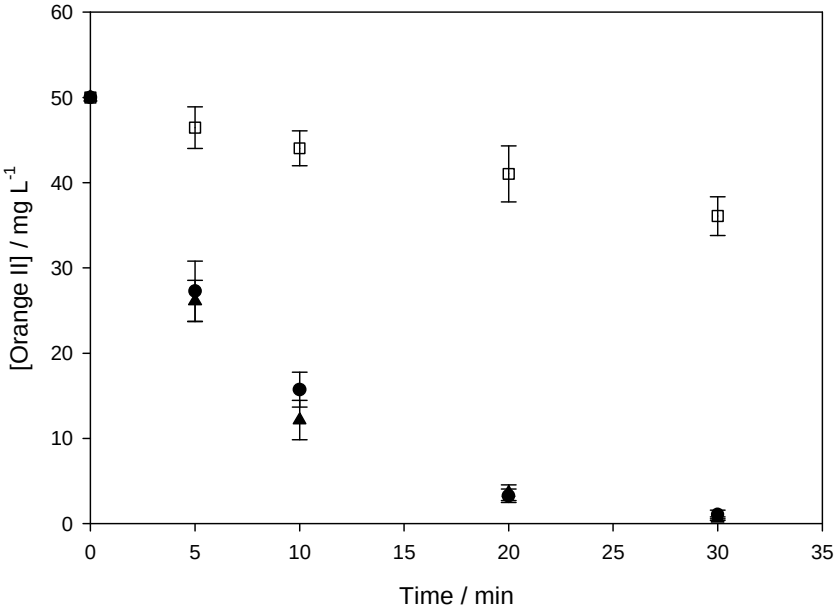

Figure 5.3: Residual concentrations of Orange II for ● iron, □ AISI 310 and ▲ AISI 420 electrodes plotted as a function of the electrocoagulation time in sww 1 solution (Table 5.1). (Cathode = AISI 310, pH = 5.0, κ = 3.7 mS m^{-1}, j = 11.7 mA cm^{-2}, SA/V = 19.4 m^{-1}).

Table 5.4: Residual concentrations of Orange II and removal efficiency for pure iron, AISI 310 and AISI 420 electrodes in sww 1 solution. Each experiment was performed in triplicate (n = 3).

Time / min	**[Orange II] / mg L^{-1}**			**η / %**		
	Iron	**AISI 420**	**AISI 310**	**Iron**	**AISI 310**	**AISI 420**
0	50.0	50.0	50.0	0	0	0
5	27 ± 4	47 ± 3	26 ± 3	45 ± 7	7 ± 5	48 ± 5
10	16 ± 2	44 ± 2	12 ± 2	68 ± 4	12 ± 4	76 ± 5
20	3.3 ± 0.8	41 ± 3	3.6 ± 0.9	93 ± 2	18 ± 7	93 ± 2
30	1.1 ± 0.5	36 ± 2	0.6 ± 0.2	98 ± 1	28 ± 5	98.8 ± 0.4

The residual concentrations of Orange II dye in the sww 2 solution, plotted as a function of the electrocoagulation time, are shown in Figure 5.4 for pure iron, AISI 310 and AISI 420 electrodes. The corresponding data are displayed in Table 5.5. After 30 min, the observed concentrations are 0.5, 34 and 0.7 mg L^{-1} of Orange II for pure iron, AISI 310 and AISI 420, respectively. It is clearly evident from these data that excellent performances are achieved with pure iron and AISI 420 as the anode materials for removing the dye. Conversely, the effectiveness of AISI 310 is quite low. Similar results were observed for the electrocoagulation tests carried out in the sww 1 solution, which contains a lower concentration of chloride ions. Indeed, on comparing the data displayed in Table 5.4 for sww 1 and Table 5.5 for sww 2, it is apparent that the values of the residual concentrations of Orange II using the three iron-based alloys are similar in both sww 1 and sww 2.

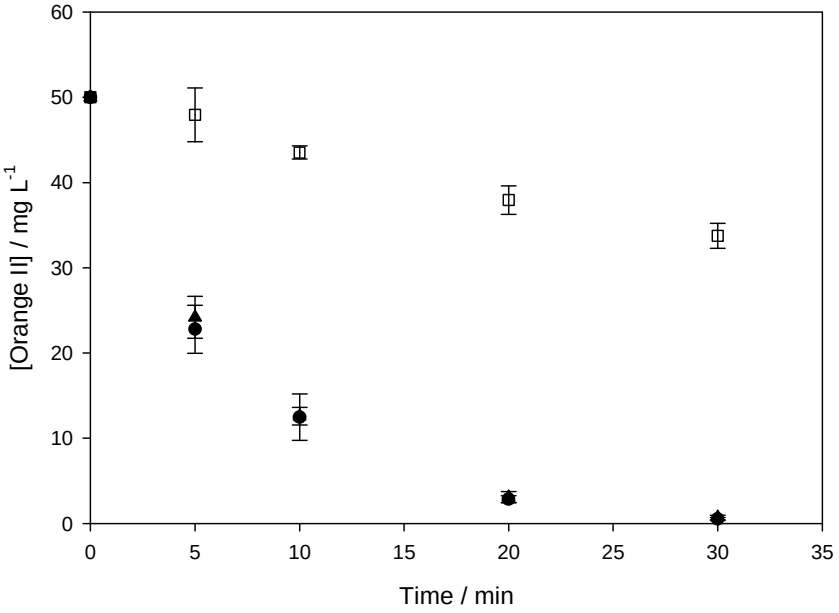

Figure 5.4: Residual concentrations of Orange II for ● iron, □ AISI 310 and ▲ AISI 420 electrodes plotted as a function of the electrocoagulation time in sww 2 solution (Table 5.1). (Cathode = AISI 310, pH = 5.0, κ = 14.4 mS m^{-1}, j = 11.7 mA cm^{-2}, SA/V = 19.4 m^{-1}).

Table 5.5: Residual concentrations of Orange II and removal efficiency for pure iron, AISI 310 and AISI 420 electrodes in sww 2 solution. Each experiment was performed in triplicate (n = 3).

Time / min	**[Orange II] / mg L^{-1}**			***η*** **/ %**		
	Iron	**AISI 420**	**AISI 310**	**Iron**	**AISI 310**	**AISI 420**
0	50.0	50.0	50.0	0	0	0
5	23 ± 3	48 ± 3	24 ± 3	54 ± 6	4 ± 6	52 ± 5
10	13 ± 3	43.5 ± 0.8	13 ± 1	75 ± 5	13 ± 2	75 ± 2
20	2.9 ± 0.4	38 ± 2	3.1 ± 0.7	93.6 ± 0.8	24 ± 3	94 ± 1
30	0.5 ± 0.2	34 ± 2	0.7 ± 0.3	98.9 ± 0.3	32 ± 3	98.6 ± 0.5

5.2.1.3 The removal of zinc ions

In electrocoagulation applications for the removal of metal ions, according to Adhoum *et al.* [44], the formed flocs act as adsorbents or traps for the metal ions, which are subsequently removed from the solution. These mechanisms have been already described in Chapter 3. However, the authors pointed out that the increase in the solution pH, which occurs during the electrocoagulation period and reported by several other authors and in Chapter 3, may induce the coprecipitation of Zn^{2+} in the form of its corresponding hydroxide species [45-47]. This precipitation acts synergistically to remove the metal ions from the solution. Although few studies have been reported in the literature on the electrocoagulation removal of Zn^{2+} ions using iron electrodes [48-50], they all support the synergistic effect of the hydroxide precipitation. In particular, Al Aji *et al.* [48] studied the effect of the initial pH on the removal of some metal ions, including zinc, with iron plate electrodes. For Zn^{2+} ions, they found the maximum removal at an initial pH of 9.0. The precipitation of $Zn(OH)_2$ begins at pH values between 7.0 and 8.0 [51]. On the other hand, there are very few reports in the literature on the removal of zinc ions by stainless steel electrodes. Kabdaşlı *et al.* [52] investigated the treatability of metal plating wastewater containing complexed nickel and zinc using stainless steel electrodes. According to their results, the organic complexing reagent used in the metal plating bath did not form complex species with zinc. Consequently, their results can be extrapolated to zinc solutions which do not contain any complexing agents. The Zn^{2+} ions were completely and rapidly removed at different current densities [52]. This was ascribed to the hydroxide precipitation in the pH range of 7.0 to 12.0 [52].

The removal of zinc ions was studied using the three iron electrodes in both the sww 1 and sww 2 solutions. The residual concentrations of Zn^{2+} ions at the end of the electrocoagulation period in the sww 1 solution for pure iron, AISI 310 and AISI 420 are presented in Figure 5.5 and the corresponding data are displayed in Table 5.6. It is clearly evident that the removal of Zn^{2+} ions is fully attained in 30 min for all the three electrode materials. This result is in very good agreement with the studies reported on the electrocoagulation removal of zinc ions with iron [44-48] or stainless steel electrodes [52]. However, Figure 5.5 shows that the removal proceeds faster with pure iron and AISI 420, while it is somewhat slower for AISI 310. Indeed, after 20 min the measured concentrations were 0.4 and 2 mg L^{-1} for pure iron and AISI 420, respectively, while for AISI 310 the concentration of zinc was 8 mg L^{-1}.

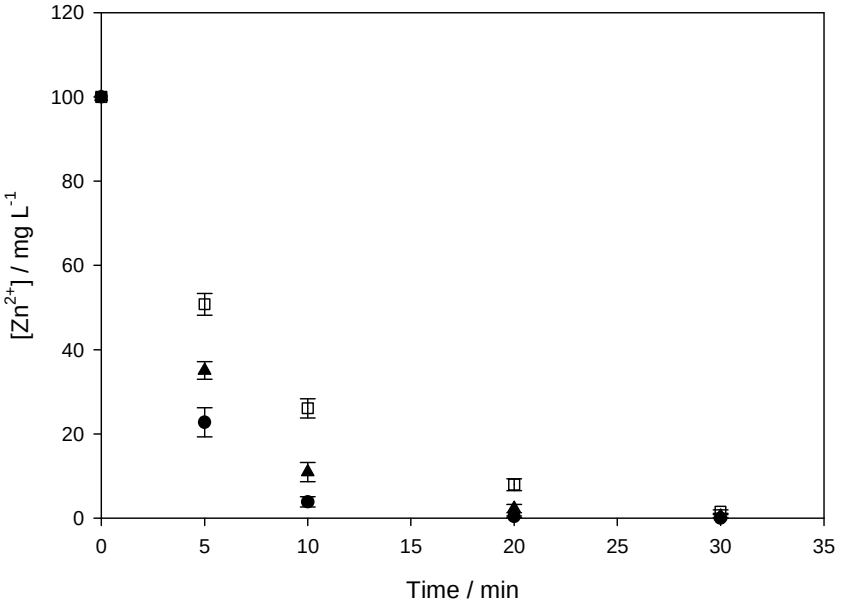

Figure 5.5: Residual concentrations of Zn^{2+} ions for ● iron, □ AISI 310 and ▲ AISI 420 electrodes plotted as a function of the electrocoagulation time in sww 1 solution (Table 5.1). (Cathode = AISI 310, pH = 5.0, κ = 3.7 mS m^{-1}, j = 11.7 mA cm^{-2}, SA/V = 19.4 m^{-1}).

Table 5.6: Residual concentrations of Zn^{2+} ions and removal efficiency for pure iron, AISI 310 and AISI 420 electrodes in sww 1 solution. Each experiment was performed in triplicate (n = 3).

Time / min	**[Zn^{2+}] / mg L^{-1}**			***η*** **/ %**		
	Iron	**AISI 420**	**AISI 310**	**Iron**	**AISI 310**	**AISI 420**
0	100.0	100.0	100.0	0	0	0
5	23 ± 3	51 ± 3	35 ± 1	77 ± 3	49 ± 3	65 ± 2
10	4.0 ± 1	26 ± 2	11 ± 2	96 ± 1	74 ± 2	89 ± 2
20	0.4 ± 0.2	8 ± 1	2 ± 1	99.6 ± 0.2	92 ± 1	98 ± 1
30	BDL*	1.5 ± 0.4	0.5 ± 0.4	BDL*	98.5 ± 0.4	99.5 ± 0.4

*BDL = Below Detection Limit (Section 2.3.3).

Figure 5.6 provides the residual concentrations of Zn^{2+} ions recorded in the sww 2 solution as a function of the electrocoagulation period for pure iron, AISI 310 and AISI 420 electrodes. The corresponding data are shown in **Error! Reference source not found.**. According to these data, Zn^{2+} ions are readily removed from the solution using pure iron and the AISI 420 electrodes, with an efficiency of 100% after 30 min. Although somewhat lower, the AISI 310 electrode also shows a good removal performance, with a final concentration of 1.8 mg L^{-1} Zn^{2+}. By comparing the data presented in Table 5.6 and **Error! Reference source not found.**, it is clear that the removal performances of the three iron-based electrodes are very similar in the sww 1 and sww 2 test solutions. It appears that the concentration of chloride anions and the conductivity of the solution have little effect on the removal of the Zn^{2+} ions.

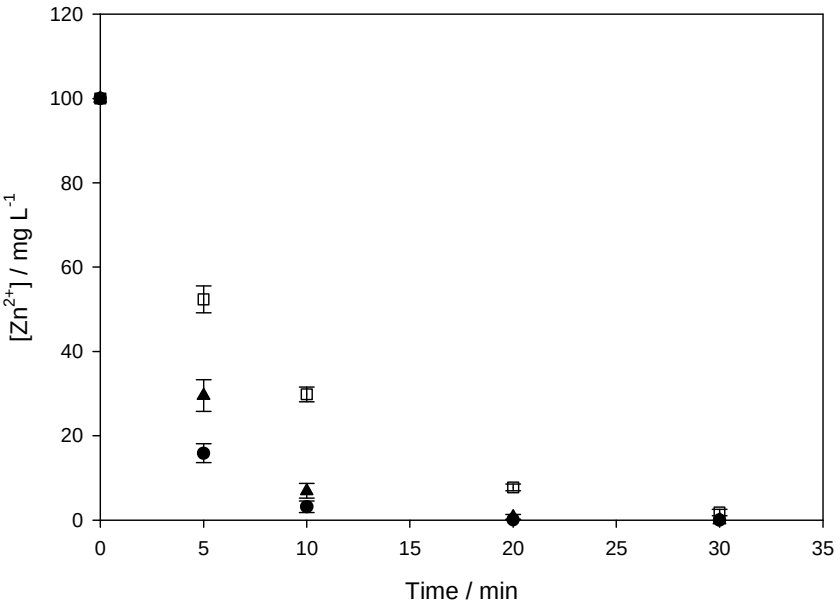

Figure 5.6: Residual concentrations of Zn^{2+} ions for ● iron, □ AISI 310 and ▲ AISI 420 electrodes plotted as a function of the electrocoagulation time in sww 2 solution (Table 5.1). (Cathode = AISI 310, pH = 5.0, κ = 14.4 mS m^{-1}, j = 11.7 mA cm^{-2}, SA/V = 19.4 m^{-1}).

Table 5.7: Residual concentrations of Zn^{2+} ions and removal efficiency for pure iron, AISI 310 and AISI 420 electrodes in sww 2 solution. Each experiment was performed in triplicate (n = 3).

Time / min	**[Zn^{2+}] / mg L^{-1}**			**η / %**		
	Iron	**AISI 420**	**AISI 310**	**Iron**	**AISI 310**	**AISI 420**
0	100.0	100.0	100.0	0	0	0
5	16 ± 2	52 ± 3	30 ± 4	84 ± 2	48 ± 3	71 ± 4
10	3 ± 1	30 ± 2	7 ± 2	97 ± 1	70 ± 2	93 ± 2
20	0.1 ± 0.1	7.7 ± 0.8	0.7 ± 0.6	99.9 ± 0.1	92.3 ± 0.8	99.3 ± 0.6
30	BDL*	1.8 ± 0.8	BDL*	BDL*	98.2 ± 0.8	BDL*

*BDL = Below Detection Limit (Section 2.3.3).

5.2.2 The electrochemistry and the removal performance of the iron system

As shown in Section 5.2.1, the pure iron electrode is the most efficient iron-based material for removing the three pollutants from the synthetic test solutions. The AISI 420 grade exhibits removal efficiencies similar to those observed with the pure iron, although they are slightly lower in the case of phosphates removal. On the other hand,

the high Cr content steel grade, AISI 310, results in poor removal efficiencies for phosphates and Orange II dye. Good performance is instead achieved for the removal of Zn^{2+} ions. However, it is worth noting that the removal of the three pollutants is brought about through different mechanisms, as outlined in Section 5.2.1. The phosphate anions are mainly removed by charge neutralisation and adsorption/sweep coagulation (Section 3.3), while the removal of Orange II dye and zinc ions has been ascribed to chemical reactions involving the degradation of the molecule [39, 53] and to hydroxide precipitation [44], respectively.

According to the results obtained in Section 4.2.4, the pure iron electrode shows no passive behaviour and general dissolution or corrosion occurs. Consequently, secondary reactions at the anode are minimised as only low potentials are required to facilitate dissolution. These findings are in very good agreement with the high removal efficiencies obtained in the treatment of the two synthetic wastewaters. In addition, similar removal efficiencies for the three pollutants were measured in both sww 1 and sww 2 solutions. This suggests that the pure iron anode behaves equally well in low and high conductivity solutions. Indeed, the 10-fold increase in the chloride concentration, from sww 1 to sww 2, shows little influence on the potentiodynamic polarisation curves, as shown in Section 4.2.4.

On the other hand, the AISI 310 stainless steel electrode exhibits poor removal efficiencies in the treatment of phosphates and Orange II dye in both the sww 1 and sww 2 solutions. This is not consistent with the existing literature reported in Section 5.2. It is likely that the electrochemistry of this stainless steel is somehow involved. Corrosion studies, performed in the sww 1 and sww 2 solutions and presented in Section 4.3.4, have shown that the AISI 310 electrode remains passive in both electrolytes over a wide range of potentials. The passive nature of this steel could account for the results obtained in Section 5.2.1. When a constant current is applied in the electrocoagulation tests, the anode potential may assume high values to overcome this passivity. This may give rise to secondary reactions at the anode and to the dissolution of chromium from steel. Secondary reactions that do not result in the dissolution of Fe^{2+} ions may decrease the current efficiency of the process and be responsible for less electrogenerated Fe^{2+} ions and, consequently, lower amounts of the iron flocs in the solution. The poor removal of phosphates may be due to the low

production of flocs. Indeed, at the end of the electrocoagulation tests performed with the AISI 310, a relatively small number of flocs were observed in the solution compared with the pure iron electrode. The low amount of electrogenerated Fe^{2+} ions is also likely to be involved in the poor efficiency recorded for the removal of Orange II dye. Indeed, as reported by Wilcock *et al.* [40] the removal of azo dyes is also carried out by chemical reactions resulting in the cleavage of the azo bond. The Fe^{2+} ions released from the electrode may act as a reducing agent to degrade the dye. The occurrence of concurrent reactions that compete with the electrodissolution of the anode results in less Fe^{2+} ions and, consequently, a lower rate of cleavage of the azo bonds. These concurrent reactions may also involve the release of Cr(VI), as already postulated in Section 4.3.4. Indeed, the presence of Cr(VI) was detected in the sample treated with the AISI 310 grade steel. Figure 5.7 shows the UV-Vis spectrum of a representative sample. The two characteristic absorption peaks for Cr(VI) at an acidic pH at around 260 nm and 370 nm and a peak minimum at around 313 nm are clearly evident from the spectrum [54-57]. The presence of chromium at the end of the electrocoagulation tests is quite surprising, since several studies have been reported on the treatment of wastewater containing hexavalent chromium by electrocoagulation [58-66]. The reduction of Cr(VI) to Cr(III) is facilitated by the electrolytically generated ferrous ions, Eq. 5.1:

$$CrO_4^{2-} + 8H^+ + 3Fe^{2+} \rightarrow Cr^{3+} + 3Fe^{3+} + 4H_2O \qquad \textbf{Eq. 5.1}$$

Due to the low concentration of Fe^{2+} ions dissolved from the AISI 310 anode, the hexavalent chromium, Cr(VI), was not removed from the solution and was detected in both synthetic wastewaters.

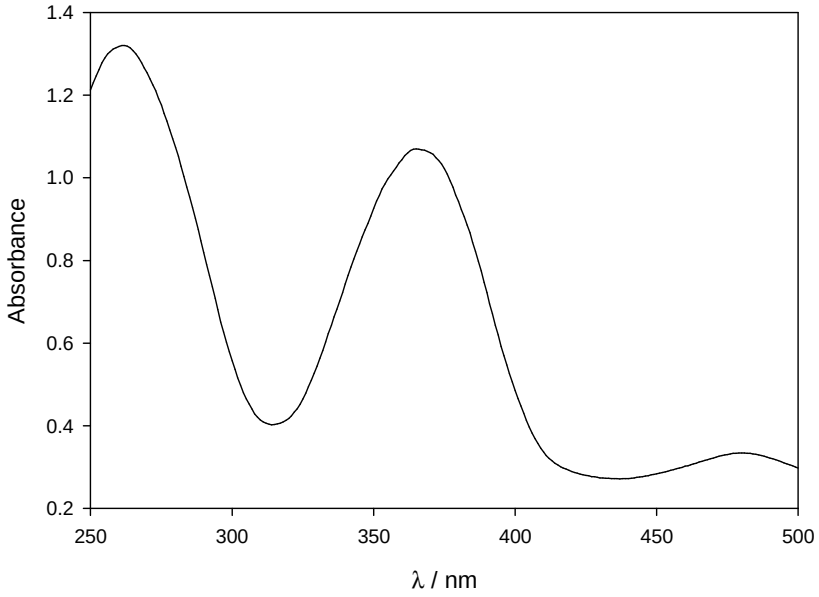

Figure 5.7: UV-Vis spectrum of a representative sample at the end of the electrocoagulation experiment in sww 2 solution with the AISI 310 anode, where the solution pH was acidified. (Anode/cathode = AISI 310/AISI 310, pH = 5.0, κ = 14.4 mS m^{-1}, j = 11.7 mA cm^{-2}, SA/V = 19.4 m^{-1}).

The slight increase in the efficiency for the removal of phosphates and Orange II in the sww 2 solution may indicate that the side reactions at the anode are diminished and, consequently, more Fe^{2+} ions are generated in the solution. This is supported by the findings from Section 4.3.4, where the breakdown potential was observed at lower potentials in the sww 2 solutions. On the other hand, the electrocoagulation removal of Zn^{2+} ions with the AISI 310 electrode as the anode material is fully attained in 30 min in both test solutions. As mentioned previously, these results are associated with the alkaline pH values that the solutions exhibit during the electrocoagulation process and that can result in the precipitation of zinc hydroxide.

The performance of the AISI 420 electrode in the removal of the Orange II dye and Zn^{2+} ions is similar to that observed with the pure iron electrode. However, slightly lower removal efficiencies were obtained in the removal of phosphates. As mentioned earlier, the removal of Orange II and zinc is mainly attained through other mechanisms other than coagulation-flocculation. Consequently, the result observed for phosphates is likely to be connected with the coagulant to pollutant ratio, which is a key factor in the coagulation processes, as outlined in Chapter 3. Indeed, as reported in Section 3.3.5, the occurrence at the anode of secondary reactions, which compete with the dissolution of

iron, may result in lower coagulant dosage and, in turn, lower removal efficiency. These reactions occur at high anode potentials, where chromium dissolution may take place in a similar manner to that observed with the AISI 310 electrode. However, UV-Vis spectra at a neutral pH, recorded on the samples at the end of the electrocoagulation tests, did not detect any absorption peaks characteristic for Cr(VI). Figure 5.8 shows the spectrum of a representative sample in the sww 2 solution. Moreover, similarly to the pure iron electrode, the removal efficiencies of the three pollutants were similar in both test solutions using the AISI 420 grade as the anode material. Clearly, the solution conductivity does not affect the removal mechanism using the AISI 420 stainless steel electrode. This is in good agreement with the potentiodynamic polarisation tests and the corrosion parameters reported in Section 4.4.4, which are similar in both the sww 1 and sww 2 solutions.

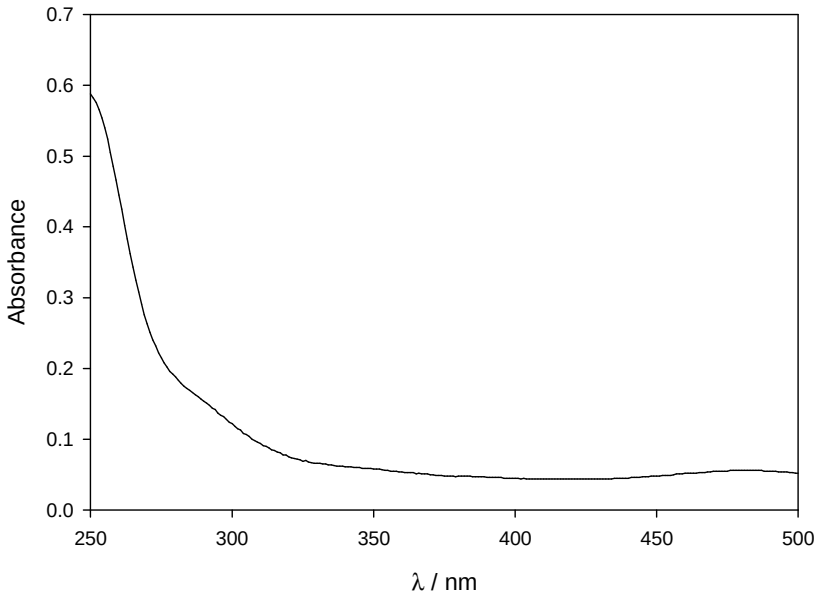

Figure 5.8: UV-Vis spectrum of a representative sample at the end of the electrocoagulation experiment in sww 2 solution with the AISI 420 anode, where the solution was acidified. (Anode/cathode = AISI 420/AISI 310, pH = 5.0, κ = 14.4 mS m^{-1}, j = 11.7 mA cm^{-2}, SA/V = 19.4 m^{-1}).

5.2.3 Energy efficiency

It is widely recognised that the energy cost is the main drawback when electrochemical processes are applied to wastewater treatment processes. Therefore, the costs of the electrocoagulation systems are critical before this technique can be used and applied to environmental problems [67]. The costs of an electrocoagulation system include the operating costs due to the electrode materials, the electrical energy, as well as labour, maintenance and other fixed costs [68]. In the present study, the energy consumption of the iron-based anodes used in Section 5.2.1 to treat the two synthetic wastewaters is taken into account.

When a current is applied between the anode and the cathode of the cell, the cell potential depends on four main terms, the equilibrium potential difference, E_{eq}, the anode overpotential, E_a, the cathode overpotential, E_c, and the ohmic potential drop of the solution, E_{IR} [69]. The anode overpotential includes the activation overpotential, $\eta_{a,a}$ and the concentration overpotential, $\eta_{a,c}$, as well as the possible passive overpotential, $\eta_{a,p}$, due to the presence of a passive film at the anode surface, while the cathode overpotential is mainly composed of the activation overpotential, $\eta_{c,a}$ and concentration overpotentials, $\eta_{c,c}$.

$$E_{cell} = E_{eq} + \eta_{a,a} + \eta_{a,c} + \eta_{a,p} + \left|\eta_{c,a}\right| + \left|\eta_{c,c}\right| + E_{IR} \qquad \textbf{Eq. 5.2}$$

The equilibrium potential difference, E_{eq}, depends on the anode and cathode used in the process and is related to the corrosion potential, E_{corr}. Consequently, anodes with low E_{corr} in a given solution require less electrical energy for electrocoagulation. The activation and concentration overpotentials increase with the current density. However, the concentration overpotential is mainly related to the mixing conditions, consequently, it can be considered negligible if good mixing is maintained during the process [70]. The ohmic potential drop of the solution, E_{IR}, is directly proportional to the electrode spacing, d, and inversely proportional to the solution conductivity, κ [38].

The energy supplied to the system is usually expressed in terms of specific electrical energy consumption, SEEC, in Wh m^{-3}, according to Eq. 5.3.

$$\text{SEEC}\left(\text{Wh m}^{-3}\right) = \frac{E_{cell}It}{V} \qquad \textbf{Eq. 5.3}$$

Here, E_{cell} is the cell voltage in V vs. SCE, I is the current in A, t is the electrocoagulation time in h and V is the volume of the solution treated in m^3. In the present study a constant current density was applied, while the average potential of the cell, $\overline{E}_{cell}$, recorded during each experiment was used in Eq. 5.3. Furthermore, the energy consumption can be expressed simply as the electrical energy consumption, EEC, in Wh, since the volume of the treated solutions was constant in each experiment, 200 mL.

$$\text{EEC}\left(\text{Wh}\right) = \overline{E}_{cell}It \qquad \textbf{Eq. 5.4}$$

Figure 5.9 shows the energy consumption, in Wh, of the three iron-based anode materials required to treat the sww 1 and sww 2 solutions. It is clear from the figure that the energy requirements of pure iron and the AISI 420 electrodes in sww 1 are similar, at 1.35 and 1.41 Wh, respectively. The same trend is observed in the sww 2 solution, where 0.52 and 0.62 Wh are required for pure iron and the AISI 420 system, respectively. On the other hand, considerably higher consumption is exhibited by the AISI 310 grade in both test solutions, with 2.17 and 0.97 Wh in the sww 1 and sww 2 solutions, respectively. The lower energy observed in the electrocoagulation tests carried out in the sww 2 solution is due to the higher conductivity of this solution, as displayed in Table 5.1. Indeed, Eq. 5.2 shows that the IR drop can be easily minimised by increasing the conductivity of the solution. A decrease of the IR drop term results in a lower cell potential, E_{cell} and, consequently, a lower energy consumption, EEC (Eq. 5.4).

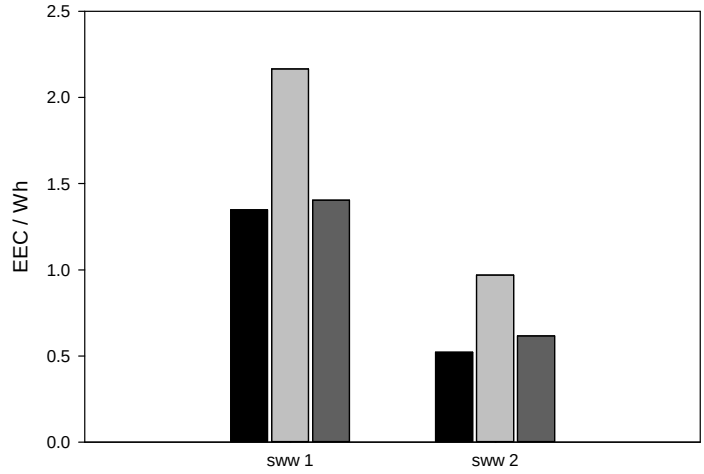

Electrode	EEC / Wh	
	sww 1	**sww 2**
Fe	1.35	0.52
AISI 310	2.17	0.97
AISI 420	1.41	0.62

Figure 5.9: Effect of anode material on the electrical energy consumption, EEC, for ■ pure iron, ■ stainless steel AISI 310 and ■ stainless steel AISI 420 in sww 1 and sww 2 solutions (Table 5.1). (Cathode = AISI 310, pH = 5.0, j = 11.7 mA cm^{-2}, SA/V = 19.4 m^{-1}).

As mentioned earlier, the cell potential, E_{cell}, which determines the energy efficiency of the electrocoagulation process, is connected to the corrosion potential, E_{corr}, of the anode/cathode used. Provided that the same type of cathode is used, anodes with low E_{corr} in a given solution are more efficient in terms of energy consumption. Table 5.8 shows the E_{corr} values recorded in the potentiodynamic polarisation tests reported in Section 4.10 for pure iron, stainless steel AISI 310 and stainless steel AISI 420 electrodes in the sww 1 and sww 2 solutions. It is clearly evident that the negative values of E_{corr} exhibited by the pure iron electrode result in high energy efficiency for the electrocoagulation process. In addition, the values of E_{corr} for AISI 420 are only about 60 mV higher giving similar energy consumption of these two systems, as shown in Figure 5.9. However, the E_{corr} values recorded for the AISI 310 electrode are significantly higher. As a consequence, the energy demand of this alloy for the electrocoagulation tests is much higher.

Table 5.8: Corrosion potentials, E_{corr}, for pure iron, AISI 310 and AISI 420 electrodes measured in sww 1 and sww 2 solutions (Section 4.10).

Electrode	E_{corr} / V vs. SCE	
	sww 1	**sww 2**
Pure iron	-0.704	-0.724
AISI 310	-0.448	-0.525
AISI 420	-0.641	-0.659

5.3 Aluminium system

In this section results are presented on the electrocoagulation removal and energy efficiency performances of two aluminium-based alloys. Aluminium-magnesium, Al-2Mg, and aluminium-zinc-indium, Al-3Zn-0.02In, alloys were chosen in order to minimise both the effects of passivation and pitting corrosion of pure aluminium, which are well-known drawbacks of the aluminium electrode in electrocoagulation [25, 33, 47, 71, 72], as already outlined in Section 4.1.

The same synthetic test solutions, which were presented in Table 5.1 and used for the iron system, were employed to investigate the performance of the two aluminium alloys for the treatment of phosphates, Orange II dye and zinc ions. The removal and the energy efficiencies of the two alloys were compared. The electrocoagulation tests were carried out with a current density of 11.7 mA cm^{-2}, a ratio of the surface area of the anode to the volume of solution, SA/V, of 19.4 m^{-1} and the electrocoagulation time was maintained at 30 min. A plate of stainless steel AISI 310 was used as the cathode. The composition of the electrode materials and the full experimental details are given in Sections 2.2.2 and 2.3.1.2.

5.3.1 The electrode performance in removing three representative pollutants from synthetic wastewaters

5.3.1.1 The removal of phosphates

Aluminium and aluminium alloys have been used as anode materials in the electrocoagulation removal of phosphates from solutions [35, 73-77]. In Section 3.2, results were presented on the removal of phosphates using the Al-2Mg electrode and good removal efficiencies, which are consistent with the existing literature, were observed. For example, after 20 min the removal efficiency was 75%, 57% and 40.5% for initial concentrations of phosphates of 20.0, 60.0 and 150.0 mg L^{-1}, respectively. Similarly to the electrocoagulation with iron electrodes, the removal of phosphates with aluminium electrodes is attained mainly through the mechanism of adsorption on aluminium flocs.

In this section the performance of the Al-2Mg and Al-3Zn-0.02In electrodes in removing phosphates from the sww 1 and sww 2 solutions are compared. Figure 5.10 shows the residual concentrations of PO_4-P in the sww 1 solution plotted as a function of the electrocoagulation time for the Al-2Mg and Al-3Zn-0.02In electrodes. In Table 5.9 the corresponding data are reported. At the end of 30 min, the concentration of PO_4-P is 53 mg L^{-1} using the Al-2Mg electrode and 36 mg L^{-1} for the Al-3Zn-0.02In system. It is apparent that the Al-3Zn-0.02In exhibits a better removal performance than the Al-2Mg anode.

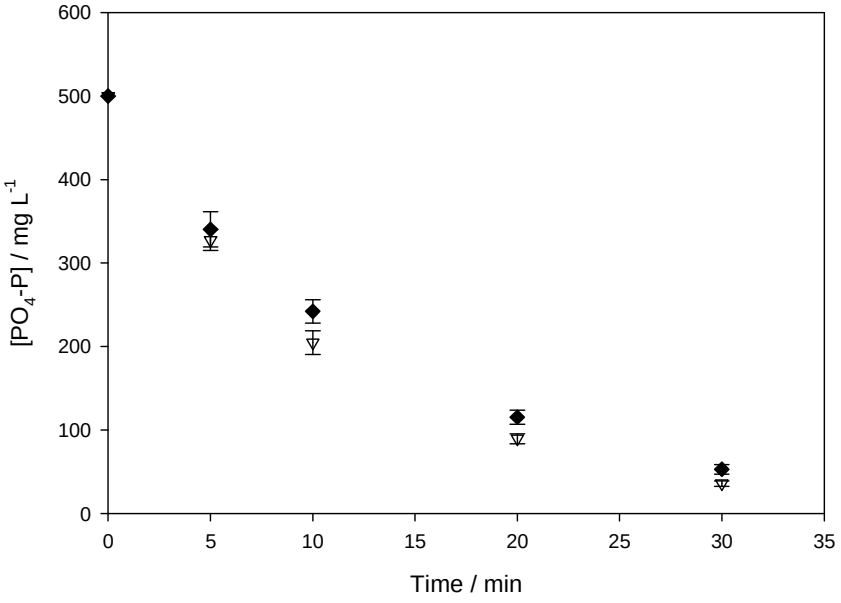

Figure 5.10: Residual concentrations of PO_4-P for ◆ Al-2Mg and ▽ Al-3Zn-0.02In electrodes plotted as a function of the electrocoagulation time in sww 1 solution (Table 5.1). (Cathode = AISI 310, pH = 5.0, κ = 3.7 mS m^{-1}, j = 11.7 mA cm^{-2}, SA/V = 19.4 m^{-1}).

Table 5.9: Residual concentrations of PO_4-P and removal efficiency for Al-2Mg and Al-3Zn-0.02In electrodes in sww 1 solution. Each experiment was performed in triplicate (n = 3).

Time / min	**[PO_4-P] / mg L^{-1}**		**η / %**	
	Al-2Mg	**Al-3Zn-0.02In**	**Al-2Mg**	**Al-3Zn-0.02In**
0	500.0	500.0	0	0
5	340 ± 21	328 ± 12	32 ± 4	34 ± 2
10	242 ± 14	205 ± 14	52 ± 3	59 ± 3
20	115 ± 9	90 ± 6	77 ± 2	82 ± 1
30	53 ± 6	36 ± 3	89 ± 1	92.8 ± 0.7

A 10-fold increase in the conductivity of the test solution results in improved removal efficiencies for both aluminium alloys. This is shown in Figure 5.11, where the residual concentrations of PO_4-P recorded in the sww 2 solution are plotted as a function of the electrocoagulation period. The corresponding data, which are displayed in Table 5.10, show final concentrations of 35 mg L^{-1} for Al-2Mg and 24 mg L^{-1} for the Al-3Zn-0.02In electrode. Clearly, better performances were achieved in the sww 2 solution. This improvement is probably due to the higher concentration of chloride ions in the sww 2 solution. Indeed, as reported in Section 3.2.4, the presence of NaCl in solution promotes the coagulation of phosphates.

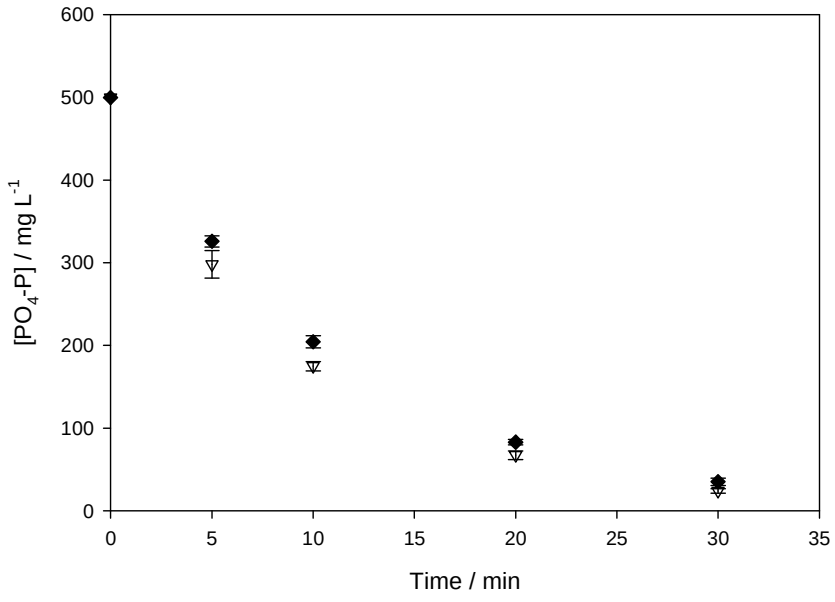

Figure 5.11: Residual concentrations of PO_4-P for ◆ Al-2Mg and ▽ Al-3Zn-0.02In electrodes plotted as a function of the electrocoagulation time in sww 2 solution (Table 5.1). (Cathode = AISI 310, pH = 5.0, κ = 3.7 mS m^{-1}, j = 11.7 mA cm^{-2}, SA/V = 19.4 m^{-1}).

Table 5.10: Residual concentrations of PO_4-P and removal efficiency for Al-2Mg and Al-3Zn-0.02In electrodes in sww 2 solution. Each experiment was performed in triplicate (n = 3).

Time / min	**[PO_4-P] / mg L^{-1}**		**η / %**	
	Al-2Mg	**Al-3Zn-0.02In**	**Al-2Mg**	**Al-3Zn-0.02In**
0	500.0	500.0	0	0
5	325 ± 7	298 ± 17	35 ± 1	40 ± 4
10	205 ± 7	175 ± 6	59 ± 1	65 ± 1
20	83 ± 3	67 ± 5	83.4 ± 0.7	86 ± 1
30	35 ± 4	24 ± 3	93.0 ± 0.9	95.2 ± 0.5

5.3.1.2 The removal of Orange II dye

It has been shown that the iron system is more efficient for the removal of azo dyes compared to the aluminium system, ascribing this difference to the removal mechanisms involved in the two systems [4, 24, 39, 40, 46, 50]. For example, Chafi *et al.* [6] reported that higher currents are required by the Al system to achieve the same efficiency as the Fe system. Adsorption was identified as the main removal mechanism for the Fe system, while the degradation of the dye into 2-naphtol was observed with the Al system, suggesting a mechanism of electroreduction of the azo bond. Mollah *et al.* [9] found an absorption band at 250 nm, which increased with the electrocoagulation period using aluminium electrodes. They attributed the band to possible by-products of Orange II dye degradation. In addition, FT-IR spectra did not reveal any trace of the dye, suggesting a partial destruction of the dye molecule. However, the authors pointed out that more research is needed in this direction since the detection of the dye in the flocs is quite difficult due to dilution factors and to the sensitivity constraint of the FT-IR instrument. In contrast with these findings, other studies [39, 40, 53] indicate that the removal mechanism of azo dyes with aluminium electrodes is physical adsorption rather than dye degradation.

In Figure 5.12 the residual concentrations of Orange II dye plotted as a function of the electrocoagulation period for Al-2Mg and Al-3Zn-0.02In electrodes are shown. It is clearly evident from this figure and from the corresponding data displayed in Table 5.11 that the removal is not complete in 30 min. The measured concentrations are 30 and 11 mg L^{-1} for Al-2Mg and Al-3Zn-0.02In, respectively, corresponding to removal efficiencies of

40% and 78%. Clearly, the removal performance of the aluminium-zinc alloy is somewhat better at 78%, but these efficiencies are considerably lower than the values calculated with the AISI 420 and pure iron electrodes. These results are in good agreement with a better performance of the iron system in removing azo dyes.

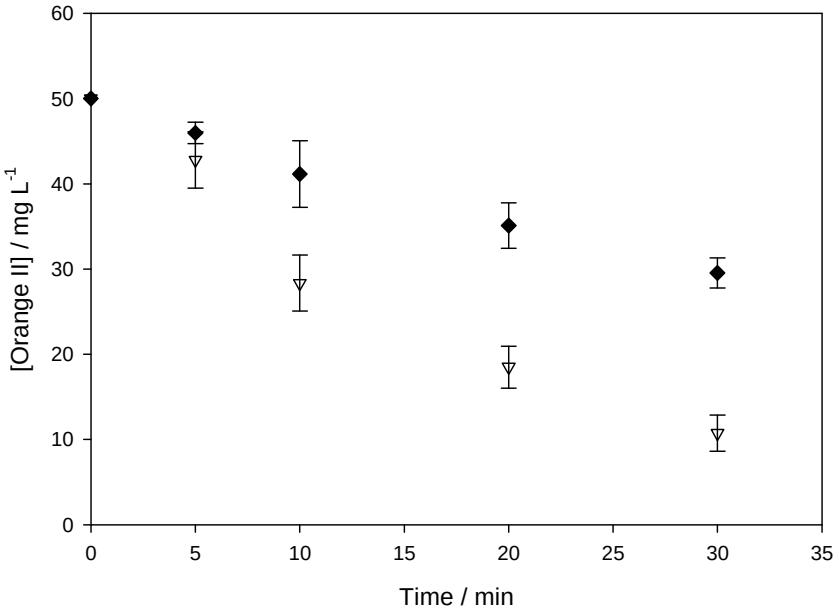

Figure 5.12: Residual concentrations of Orange II for ◆ Al-2Mg and ▽ Al-3Zn-0.02In electrodes plotted as a function of the electrocoagulation time in sww 1 solution (Table 5.1). (Cathode = AISI 310, pH = 5.0, κ = 3.7 mS m^{-1}, j = 11.7 mA cm^{-2}, SA/V = 19.4 m^{-1}).

Table 5.11: Residual concentrations of Orange II and removal efficiency for Al-2Mg and Al-3Zn-0.02In electrodes in sww 1 solution. Each experiment was performed in triplicate (n = 3).

Time / min	**[Orange II] / mg L^{-1}**		**η / %**	
	Al-2Mg	**Al-3Zn-0.02In**	**Al-2Mg**	**Al-3Zn-0.02In**
0	50.0	50.0	0	0
5	46 ± 1	43 ± 3	8 ± 3	14 ± 7
10	41 ± 4	28 ± 3	18 ± 8	43 ± 7
20	35 ± 3	19 ± 3	30 ± 5	63 ± 5
30	30 ± 2	11 ± 2	41 ± 4	78 ± 4

The results obtained in the sww 2 solution are shown in Figure 5.13 and Table 5.12. In particular, Figure 5.13 illustrates the residual concentrations of Orange II dye plotted as a function of the electrocoagulation period for Al-2Mg and Al-3Zn-0.02In. Again it is evident that the Al-3Zn-0.02In electrode is more efficient in removing the dye, particularly at longer electrocoagulation times. The removal of the dye appears to reach a limiting value after about 15-20 min min for the Al-2Mg electrode. The corresponding data are displayed in Table 5.12. As can be observed from these data, the final concentration of Orange II is 29 and 9 mg L^{-1} using the Al-2Mg and Al-3Zn-0.02In electrodes, respectively. On comparing these values to those obtained in the sww 1 solution (Table 5.11), it is evident that the removal efficiencies are similar in both solutions. Clearly, there is no evidence of any increase in the removal efficiency on increasing the chloride concentration or the conductivity of the solution.

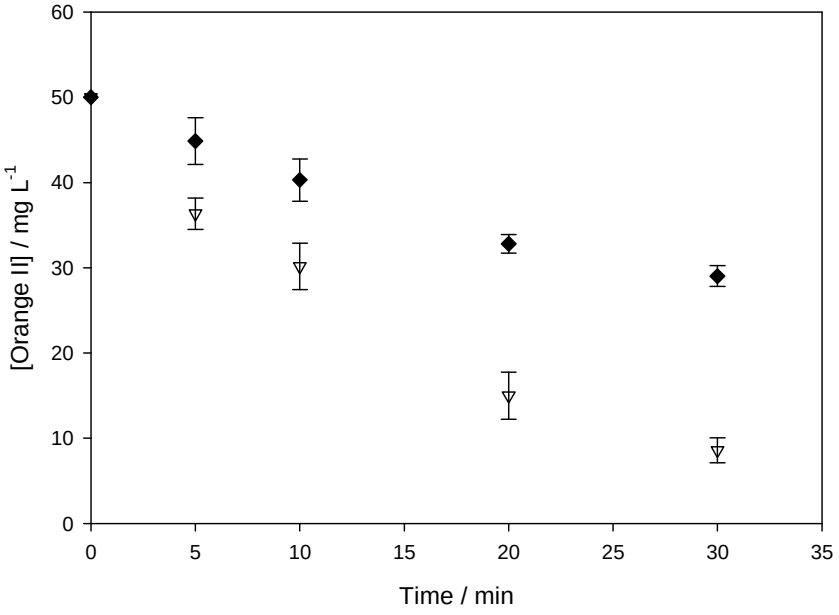

Figure 5.13: Residual concentrations of Orange II for ◆ Al-2Mg and ▽ Al-3Zn-0.02In electrodes plotted as a function of the electrocoagulation time in sww 2 solution (Table 5.1). (Cathode = AISI 310, pH = 5.0, κ = 3.7 mS m^{-1}, j = 11.7 mA cm^{-2}, SA/V = 19.4 m^{-1}).

Table 5.12: Residual concentrations of Orange II and removal efficiency for Al-2Mg and Al-3Zn-0.02In electrodes in sww 2 solution. Each experiment was performed in triplicate (n = 3).

Time / min	**[Orange II] / mg L^{-1}**		***η*** **/ %**	
	Al-2Mg	**Al-3Zn-0.02In**	**Al-2Mg**	**Al-3Zn-0.02In**
0	50.0	50.0	0	0
5	45 ± 3	36 ± 2	10 ± 5	27 ± 4
10	40 ± 3	30 ± 3	19 ± 5	40 ± 5
20	33 ± 1	15 ± 3	34 ± 2	70 ± 6
30	29 ± 1	9 ± 1	42 ± 2	83 ± 3

5.3.1.3 The removal of zinc ions

Several studies have been reported in the literature on the removal of zinc ions from solution using aluminium electrodes [38, 44, 78, 79]. Again in these studies, similar to that found with the iron system (Section 5.2.1.3), the coprecipitation of $Zn(OH)_2$ species plays a dominant role in the removal mechanism. In particular, an extensive study on the electrocoagulation removal of Zn(II), Cu(II), Ni(II), Ag(I) and Cr(VI) was presented by Heidmann and Calmano [79]. The authors concluded that metallic cations are removed through several mechanisms. However, the main mechanism for the removal of Zn^{2+} ions is the precipitation as hydroxide species. The removal rate for zinc was independent of its initial concentrations and was lowered by the presence of other metal ions, which were removed similarly, because of the competition for OH^- ions produced at the cathode. According to these studies, it is then expected that the use of an aluminium alloy, such as the Al-2Mg or Al-3Zn-0.02In electrodes, may result in an efficient removal of zinc ions from the solution.

Figure 5.14 shows the residual concentrations of Zn^{2+} ions plotted as a function of the electrocoagulation time for Al-2Mg and Al-3Zn-0.02In electrodes in the sww 1 solution. The corresponding data are given in Table 5.13. These data show very good efficiencies in removing zinc ions, although the performance of Al-2Mg is somewhat lower. In 30 min the residual concentration of Zn^{2+} ions is reduced to 1.4 mg L^{-1} for the Al-2Mg electrode, while complete removal is achieved with Al-3Zn-0.02In.

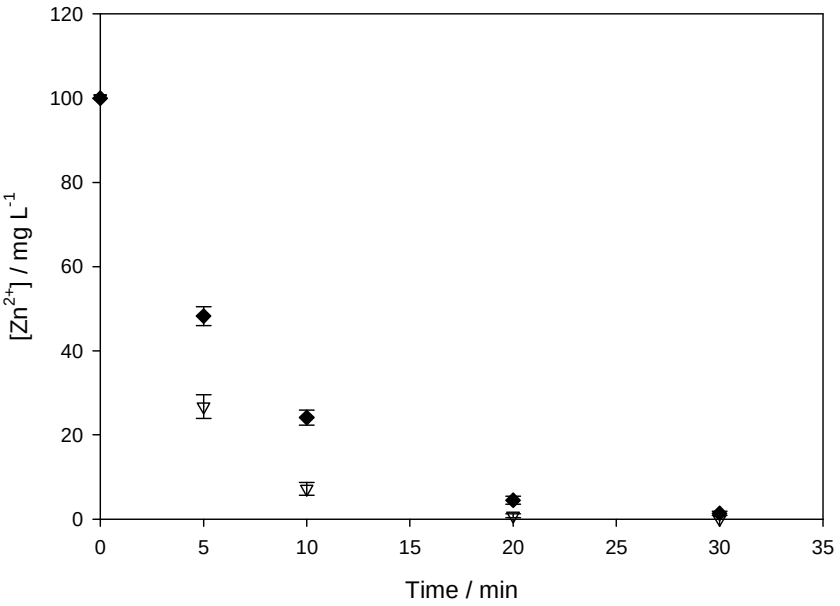

Figure 5.14: Residual concentrations of Zn^{2+} ions for ◆ Al-2Mg and ▽ Al-3Zn-0.02In electrodes plotted as a function of the electrocoagulation time in sww 1 solution (Table 5.1). (Cathode = AISI 310, pH = 5.0, κ = 3.7 mS m^{-1}, j = 11.7 mA cm^{-2}, SA/V = 19.4 m^{-1}).

Table 5.13: Residual concentrations of Zn^{2+} ions and removal efficiency for Al-2Mg and Al-3Zn-0.02In electrodes in sww 1 solution. Each experiment was performed in triplicate (n = 3).

Time / min	**[Zn^{2+}] / mg L^{-1}**		**η / %**	
	Al-2Mg	**Al-3Zn-0.02In**	**Al-2Mg**	**Al-3Zn-0.02In**
0	100.0	100.0	0	0
5	48 ± 2	27 ± 3	52 ± 2	73 ± 3
10	24 ± 2	7 ± 2	76 ± 2	93 ± 2
20	4 ± 2	0.8 ± 0.5	96 ± 1	99.2 ± 0.5
30	1.4 ± 0.5	BDL*	98.6 ± 0.5	BDL*

*BDL = Below Detection Limit (Section 2.3.3).

The removal performances of Al-2Mg and Al-3Zn-0.02In electrodes in the sww 2 solutions are similar to those observed in the sww 1 solution. In Figure 5.15 the residual concentrations of Zn^{2+} ions in the sww 2 solution are presented as a function of the electrocoagulation period for the two aluminium alloys. Table 5.14 provides the corresponding data. The efficiency measured in the sww 2 solution (Table 5.14) is similar to that observed in the sww 1 solution (Table 5.13). This is particularly

noticeable in the case of Al-2Mg. The concentration of Zn^{2+} ions at the end of the electrocoagulation period is 0.9 mg L^{-1}, which is within the experimental error if compared with the value of 1.4 mg L^{-1} observed in the sww 1 solution. However, it is clear from the data presented in Table 5.14 that a moderate increase of the removal performance occurs in the sww 2 solution for the Al-3Zn-0.02In electrode. Although at the end of the process Zn^{2+} ions are completely removed from both solutions, after 10 min of the electrocoagulation time the residual concentrations of zinc ions are 7.0 and 3.2 mg L^{-1} in the sww 1 and sww 2 solutions, respectively.

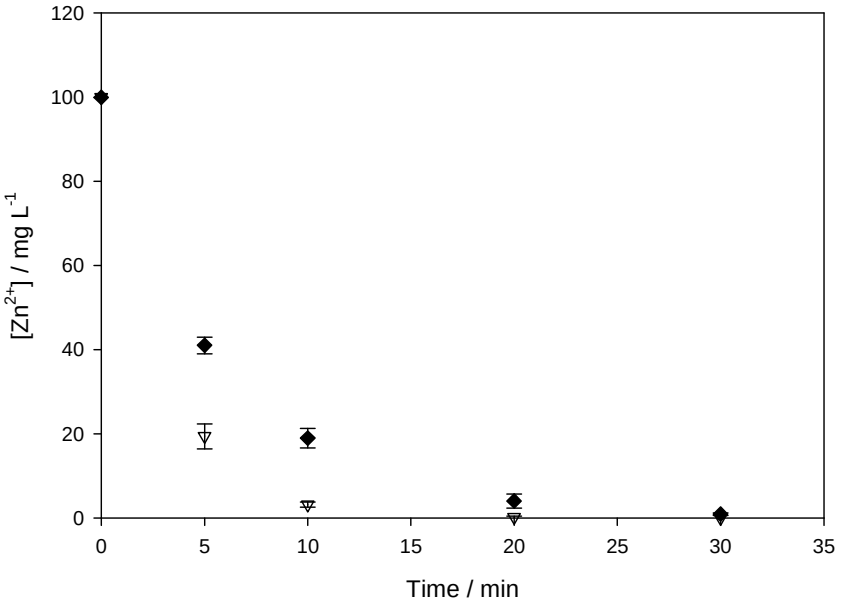

Figure 5.15: Residual concentrations of Zn^{2+} ions for ◆ Al-2Mg and ▽ Al-3Zn-0.02In electrodes plotted as a function of the electrocoagulation time in sww 2 solution (Table 5.1). (Cathode = AISI 310, pH = 5.0, κ = 3.7 mS m^{-1}, j = 11.7 mA cm^{-2}, SA/V = 19.4 m^{-1}).

Table 5.14: Residual concentrations of Zn^{2+} ions and removal efficiency for Al-2Mg and Al-3Zn-0.02In electrodes in sww 2 solution. Each experiment was performed in triplicate (n = 3).

Time / min	**[Zn^{2+}] / mg L^{-1}**		***η*** **/ %**	
	Al-2Mg	**Al-3Zn-0.02In**	**Al-2Mg**	**Al-3Zn-0.02In**
0	100.0	100.0	0	0
5	41 ± 2	19 ± 3	59 ± 2	81 ± 3
10	19 ± 2	3.2 ± 0.6	81 ± 2	96.8 ± 0.6
20	4 ± 2	0.2 ± 0.3	96 ± 2	99.8 ± 0.3
30	0.9 ± 0.3	BDL*	99.8 ± 0.3	BDL*

*BDL = Below Detection Limit (Section 2.3.3).

As reported in the literature on the electrocoagulation removal of Zn^{2+} ions with Al electrodes [38, 44, 78, 79], these results are in agreement with a removal attained mainly through precipitation of zinc hydroxide species owing to the alkaline pH of the solution treated by electrocoagulation. In Section 3.2.3, it was shown that the final pH of the solutions treated with Al-2Mg electrode was in the range of 9.0 to 10.0, when the initial pH was 5.0. At these pH values, *i.e.* 9.0 to 10.0, the aluminium hydroxide precipitate dissolves to form the monomeric anionic hydroxyaluminium species, $Al(OH)_4^-$, as reported in Section 3.2.3, and in the speciation diagrams of aluminium in Section 1.3.2.2, Fig. 1.5(a). The anionic hydroxyaluminium species is soluble in solution. Consequently, the high removal efficiencies of Zn^{2+} ions observed for Al-2Mg and Al-3Zn-0.02In is due to a mechanism different from adsorption. The speciation diagram for aqueous zinc solutions, displayed in Figure 5.16, shows that the predominant species in the pH range of 8.5 to 10.5 is $Zn(OH)_2$ [38, 44, 78, 79], therefore its removal is accomplished primarily through hydroxide precipitation due to the alkaline pH of the solution during the electrocoagulation process.

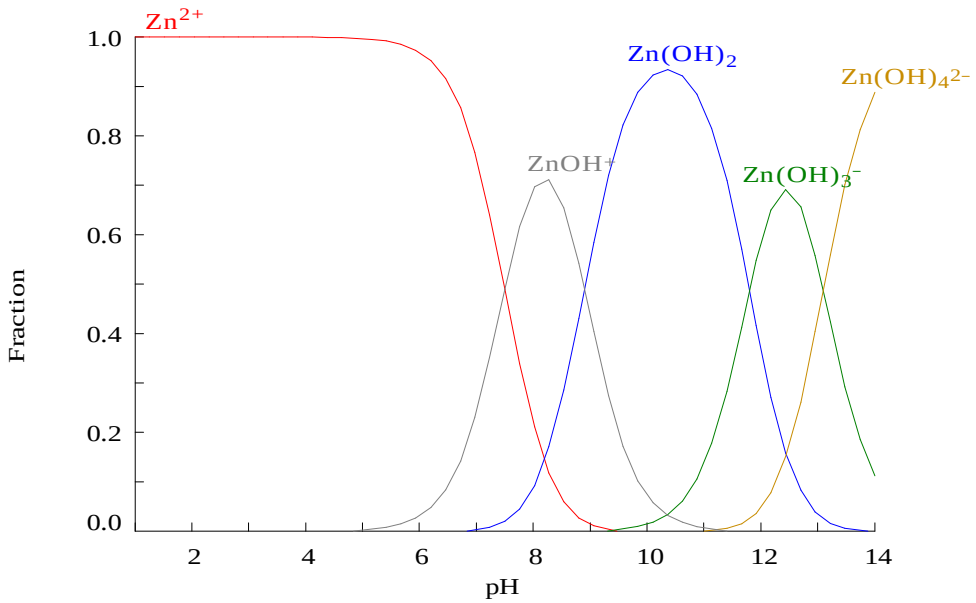

Figure 5.16: Speciation diagram of zinc in aqueous solutions. The diagram was calculated with the MEDUSA software developed by Puigdomenech [80] at the KTH Royal Institute of Technology, Sweden and based on the SOLGASWATER algorithm [81].

5.3.2 The electrochemistry and the removal performance of the aluminium system

According to the results presented in Section 5.3.1, the Al-3Zn-0.02In electrode shows better removal performance than the Al-2Mg electrode for the three pollutants contained in the synthetic wastewaters. However, both alloys exhibit moderately good efficiency for the removal of the Orange II dye. As in the case of the iron system, it is worth noting that the three pollutants are removed through different mechanisms, with the removal of phosphates depending mainly on the floc production and Zn^{2+} ions on the alkaline pH of the solution and the formation and precipitation of the hydroxide species. On the other hand, the removal of the Orange II dye in the aluminium system is attained by adsorption or degradation, as outlined in Section 5.3.1.2.

As reported in Section 4.6.4, the electrochemical behaviour of the Al-2Mg electrode in the sww 1 and sww 2 solutions is determined by the presence of chloride, which, even in small concentration, has a positive influence on the dissolution of the alloy. The potentiodynamic polarisation curves, do not exhibit any passive region. This behaviour is connected to the good removal performance observed for phosphates, which are removed through a mechanism involving the generation of Al^{3+}, as shown in Section 3.2.

On the other hand, the Orange II dye is not removed as efficiently as the phosphate anions. In some studies carried out with aluminium electrodes, the removal of dyes is attributed to the electroreduction of the azo bond [6, 9] as higher currents are required to obtain the same decolourisation efficiency observed in the iron system [6]. In contrast, other studies have shown that the lower efficiency observed with the aluminium electrodes for removing azo dyes is due to the occurrence of a single removal mechanism, based on adsorption on the flocs, rather than a combination of adsorption and molecule degradation which occurs with the iron system [39, 40, 53]. The results presented in Section 5.3.1.2 show similar removal efficiencies in the sww 1 and sww 2 solutions, which have different conductivities. As reported in Section 3.3.5, the coagulant dosage, Al^{3+} ions, is higher in more conducting solutions because the low potentials exhibited by the anode do not promote the occurrence of secondary reactions, which compete with the dissolution of aluminium. Consequently, a removal mechanism of Orange II, which involves only the Al^{3+} ions and, in turn, adsorption on the flocs, is unlikely as the removal efficiency is similar in the sww 1 and sww 2 solutions. It seems that the removal of the Orange II dye using the Al-2Mg electrode as the anode material is more complex and depends on a combination of adsorption and molecule degradation.

As shown in Section 4.7.4, the electrochemical behaviour of Al-3Zn-0.02In is consistent with active dissolution with an absence of a passive region and low corrosion potentials, even in solutions containing low concentrations of chloride anions. As a result, the removal performance of this alloy is considerably higher than the Al-2Mg, as shown in Section 5.3.1. The excellent results obtained for the removal of phosphates are probably due to the ease of the dissolution process of the Al-3Zn-0.02In electrode. Higher efficiencies are obtained in the more conducting solution, sww 2, suggesting a higher rate of Al^{3+} dissolution, in good agreement with the polarisation curves shown in Section 4.7.4. On the other hand, the similar removal efficiency recorded in the sww 1 and sww 2 solutions for the Orange II dye suggests that mechanisms other than adsorption, probably concerning the degradation of the dye, are involved in the removal of the Orange II dye.

5.3.3 Energy efficiency

As detailed earlier, the energy consumption is important in the development and applications of the electrocoagulation systems. In this section, results are presented on the energy consumption of the Al-2Mg and Al-3Zn-0.02In electrodes in the electrocoagulation tests described in Section 5.3.1 for treating the two synthetic wastewaters. The energy requirements for each electrode were expressed as the electrical energy consumption, EEC, in Wh, and computed according to Eq. 5.4.

Figure 5.17 shows the energy consumption, in Wh, of the two aluminium alloys required in the treatment of the sww 1 and sww 2 solutions. It is apparent from this figure that the Al-3Zn-0.02In electrode is consistently more efficient in terms of energy in both test solutions. Indeed, the energy consumption is 0.51 and 0.26 Wh in the sww 1 and sww 2 solutions, respectively. On the other hand, higher energy consumption is exhibited by the Al-2Mg electrode, with 1.53 Wh in sww 1 and 0.61 Wh in the sww 2 solution. As already observed for the iron system (Section 5.2.3), the energy demand diminishes considerably in the sww 2 solution, which has a higher conductivity. This effect is expected since the solution conductivity, κ, is one of the terms affecting the cell voltage, E_{cell}, as indicated in Eq. 5.2.

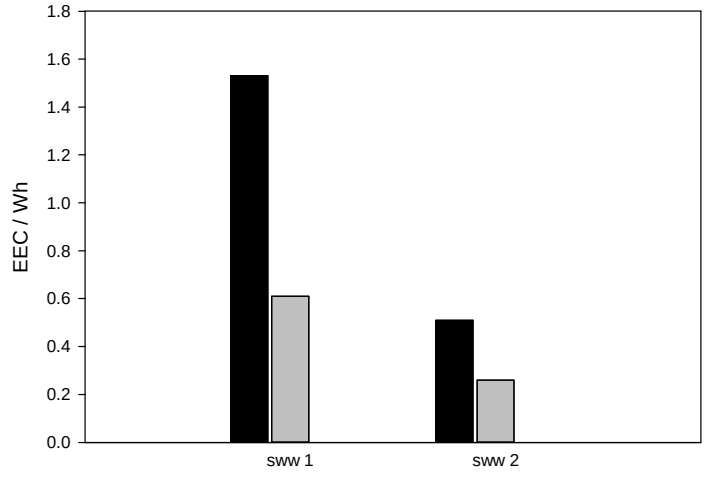

Electrode	EEC / Wh	
	sww 1	**sww 2**
Al-2Mg	1.53	0.51
Al-3Zn-0.02In	0.61	0.26

Figure 5.17: Effect of anode material on the electrical energy consumption, EEC, for ■ Al-2Mg and ■ Al-3Zn-0.02In in sww 1 and sww 2 solutions (Table 5.1).
(Cathode = AISI 310, pH = 5.0, j = 11.7 mA cm^{-2}, SA/V = 19.4 m^{-1}).

The cell potential, E_{cell}, depends on the type of electrodes employed in the electrocoagulation tests. In addition, it is connected to the corrosion potential, E_{corr}, of the anode, as mentioned in Section 5.2.3. Consequently, materials which adopt low values of E_{corr} result in greater energy efficiency for the electrocoagulation process. The E_{corr} values for the Al-2Mg and Al-3Zn-0.02In electrodes are shown in Table 5.15. They were measured from the potentiodynamic polarisation tests carried out in the sww 1 and sww 2 solutions and are presented in Section 4.10. As expected, the Al-3Zn-0.02In electrode exhibits more negative values of E_{corr} and, as a result, requires lower energy, as shown in Figure 5.17.

Table 5.15: Corrosion potentials, E_{corr}, for Al-2Mg and Al-3Zn-0.02In electrodes measured in sww 1 and sww 2 solutions (Section 4.10).

Electrode	**E_{corr} / V vs. SCE**	
	sww 1	**sww 2**
Al-2Mg	-0.598	-0.670
Al-3Zn-0.02In	-0.798	-0.857

5.4 Screening chemometric study

The two main applications of the Design of Experiments, DoE, are screening and optimisation [13]. In screening, the factors that most affect the process are identified, while optimisation consists in determining the optimal settings or conditions for the process. Firstly, a screening design is used and includes all the controllable factors that may possibly influence the experiment. Once the most important factors have been identified, an experimental optimisation design is carried out.

As described in Section 2.3.7, full factorial designs are usually used as screening designs. They are indicated as 2^n designs, where the base 2 stands for the number of factor levels and n the number of factors, each with a high and low values. The lower level is indicated with a '-' sign, while the higher level with a '+' sign. Fractional factorial designs are good alternatives to a full factorial design. Indeed, if the number of factors is considerably high, the number of experiments to be performed in a full factorial design becomes prohibitive. A fractional design is a representative subset of a

full factorial design, where the number of experiments is reduced by a number p, according to a 2^{k-p} design, where *k* is the number of factors investigated.

In the present study, a 2^{5-1} fractional factorial design with two replicates and blocking was employed as a screening design for the electrocoagulation removal of phosphates using stainless steel AISI 420 as the anode material. Each block was performed on a different day. In total, 32 experiments were carried out in four days. Five factors were studied: current density (A), electrocoagulation time or EC time (B), surface area of the electrode to the volume of the solution ratio or SA/V (C), flocculation time or floc time (D) and settlement time or settl time (E). As detailed in Chapter 3, the current density and the electrocoagulation time are important variables in the electrocoagulation process. The electrode surface area to the volume solution ratio has been reported by Holt *et al.* [82] as a key factor in electrocoagulation experiments. In addition, the flocculation time and settlement time were included in the study. The flocculation time was taken as the time period between the end of the experiment and the cessation of the solution stirring, and the settlement time was determined as the time between the stop of the solution stirring and the analysis of the sample. Table 5.16 shows the investigated factors and the corresponding levels that were studied. Full experimental details, including the design matrix, are given in Sections 2.3.1.4 and 2.3.7.

The choice of blocking the fractional factorial design came from the observation that it was not possible to perform all the 32 experiments under homogeneous conditions. For example, fresh solutions of phosphates and sodium chloride were prepared every day. Moreover, although carefully cleaned before each experiment and every day, the state of the electrode surface was not exactly reproducible. Blocking is a design technique used to reduce or eliminate the variability that arises from nuisance factors, that is factors that may influence the process but that are not the objectives of the investigation [12]. In the present study, blocking was used to test the robustness of the electrocoagulation process and assess whether blocking or not is necessary for future designs. The implications of blocking on the fractional factorial design and the corresponding design matrix are given in Section 2.3.7.

Table 5.16: Factors investigated in the 2^{5-1} fractional factorial design and their corresponding levels (Anode/Cathode = AISI 420/AISI 310, [PO_4-P] = 15.0 mg L^{-1}, pH = 5.0).

Factors		**Levels**	
		(-) low	(+) high
current density / mA cm^{-2}	A	2	5.5
EC time / min	B	5	60
SA/V / m^{-1}	C	9.1	13.7
floc time / min	D	2	30
settl time / min	E	10	60

5.4.1 Estimating factor effects and forming the initial model

As reported in Section 2.3.7, the first step in a DoE analysis is to determine the significance of the coefficients. The simplest approach is to consider the magnitude of the coefficients. However, a statistical indicator is usually employed. For example, Student's t-test and F-test can be performed. It is also convenient to present the coefficients graphically and a classical approach is to plot the effects on a normal probability plot [12]. In this case, the effects that are negligible are normally distributed and fall along a straight line on the plot, while significant effects do not lie along the straight line.

The normal probability plot of the effects obtained for the 2^{5-1} fractional design is displayed in Figure 5.18. All the effects that lie along the line are negligible, whereas the large effects are far from the line. The important effects that emerge from this analysis are the current density (A), electrocoagulation time (B), SA/V (C), settlement time (E) and the interaction current density-SA/V (AC).

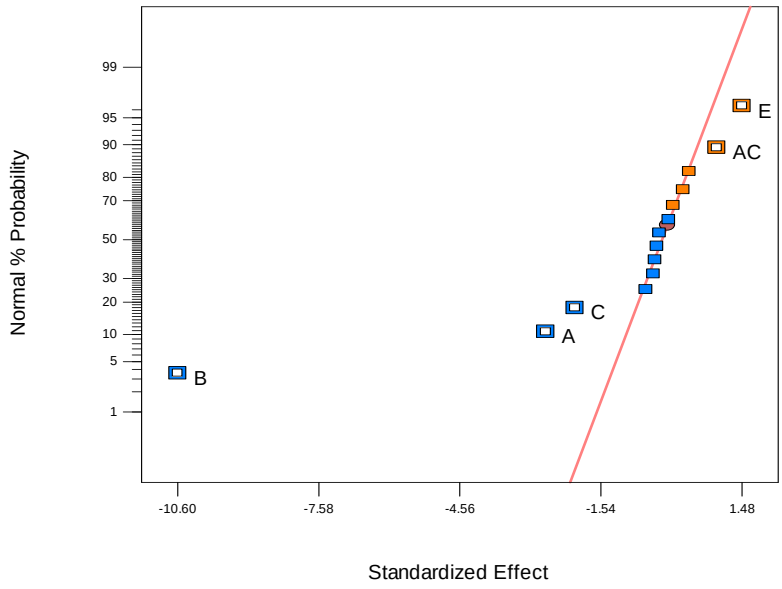

Figure 5.18: Normal probability plot of the effects for the 2^{5-1} fractional factorial design.

The main effects of A (current density), B (electrocoagulation time), C (SA/V) and E (settlement time) are plotted in Figure 5.19. The effects of A, B and C are negative. Consequently, considering only these main effects, the electrocoagulation tests would be run at the high level to minimise the residual concentration of phosphates. On the other hand, the main effect E is positive indicating that the residual concentration of phosphates increases on increasing the settlement time. This may be due to a desorption process of phosphates from the flocs. The main effects A and C are involved in interactions. This interaction is plotted in Figure 5.20. From the figure it is apparent that the current density effect is negligible when the SA/V ratio is at the high level, whereas it is larger when the ratio is at the low level, with the best results obtained with low SA/V and high current density. Consequently, when small SA/V ratios are used in electrocoagulation tests, a higher current density would give better results in terms of removal efficiencies.

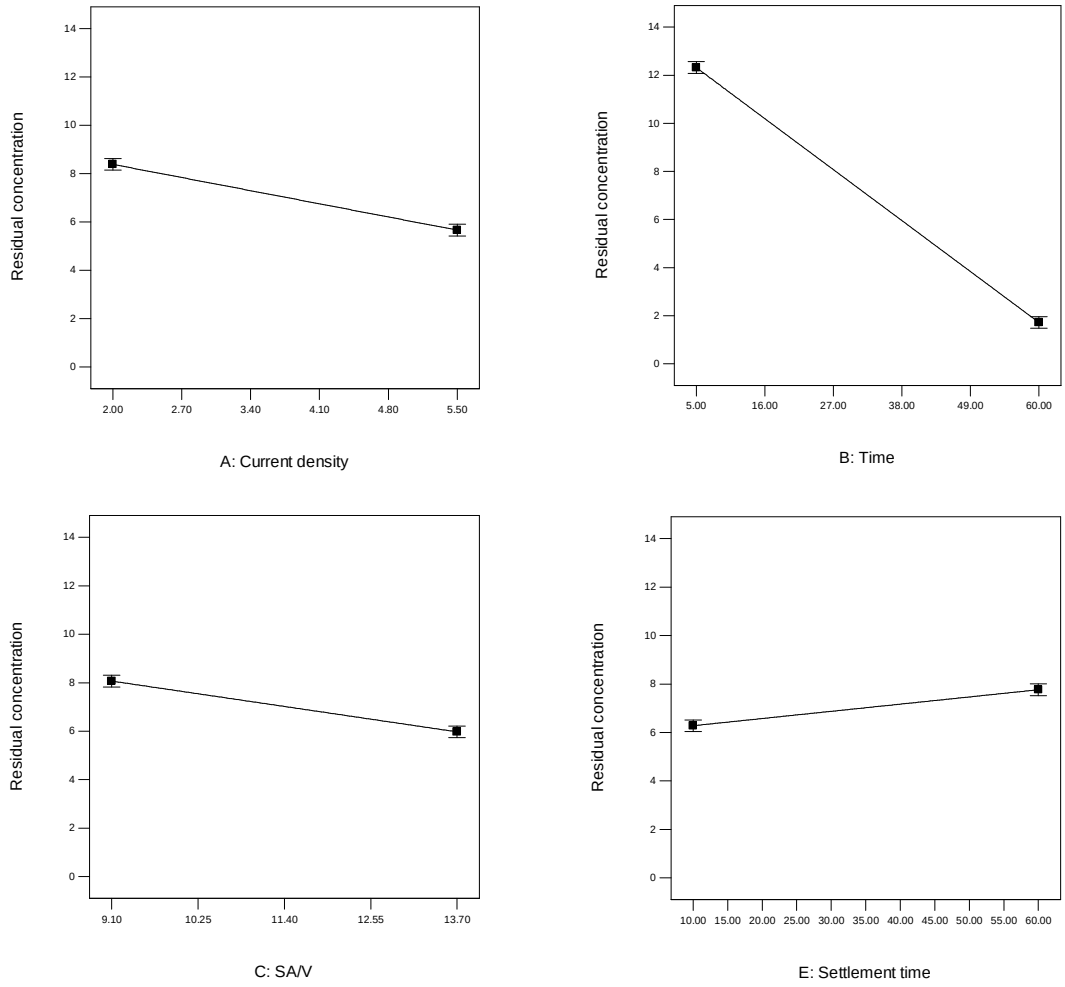

Figure 5.19: Main effects plot for the 2^{5-1} fractional factorial design.

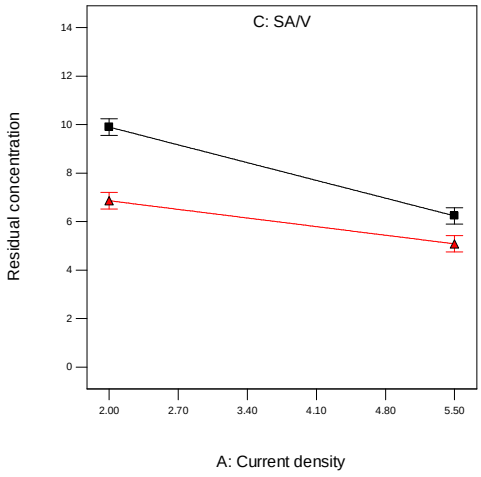

Figure 5.20: Interaction plot for the 2^{5-1} fractional factorial design. ■ C = 9.1 m^{-1}, ▲ C = 13.7 m^{-1}.

The parameters in the effect model were estimated by the least square method using Design-Expert® Version 8.0.7.1 by Stat-Ease, Inc. and are shown in Eq. 5.5:

$$[PO_4\text{-P}] = 25.36 - 2.11 \text{ current density} - 0.19 \text{ EC time} - 0.89 \text{ SA/V} + 0.03 \text{ floc time} + 0.12 \text{ current density-SA/V} \quad \textbf{Eq. 5.5}$$

Again, this equation shows that the coefficient of the current density is the largest at 2.11, while the SA/V ratio is also significant.

5.4.2 Performing statistical tests

The significance and the adequacy of the model were evaluated by analysis of variance, ANOVA, and the corresponding data are presented in Table 5.17. The Fisher's variance test (F-test) and the coefficient of determination between the experimental and predicted values were used to test the significance. According to the data in Table 5.17, F_0, which is defined as the mean of squares of the model to the mean of squares of the error ratio, MS_{Model}/MS_{error}, is higher than the tabulated F-value (2.640 at 95% significance). In addition, the *p*-value, which is lower than 0.0001 confirms that the regression model is statistically significant. Furthermore, a value of 0.9813 was obtained as the adjusted R^2 value. This indicates that the model explains about 98% of the variability observed in the data.

It is also interesting to determine if blocking is necessary in future experiments. For this purpose, the ratio of MS_{Block} to MS_{error} is considered. From Table 5.17, this ratio can be computed as 2.33. This value is relatively low and indicates that the blocking factor does not have a significant effect. This also highlights the robustness of the electrocoagulation process carried out on different days. As a consequence, blocking is not necessary in future DoE analyses.

Table 5.17: Analysis of variance for the model presented in Eq. 5.5.

Source	Analysis of variance				
	SS[a]	**dof**[b]	**MS**[c]	F_0	***p*-value**
Model	1018.54	5	203.71	470.56	< 0.0001
Block	3.00	3	1.00		
Error	9.96	23	0.43		

[a] Sum of squares.
[b] Degrees of freedom.
[c] Mean square.

Before conclusions from the analysis of variance are adopted, the adequacy of the model should be checked. An important diagnostic tool is the residual analysis [83]. Residuals, the difference between experimental and predicted responses, are considered as unexplained variations in the model and occur based on a normal distribution, if the model is a good predictor. The normal probability plot of the residuals for the present 2^{5-1} fractional factorial design is shown in Figure 5.21(a). A moderate departure from normality is evident from both sides of the plot, indicating the tendency of the normal probability plot to bend down slightly on both right and left sides. However, it can be concluded that the points lie reasonably close to a straight line. Figure 5.21(b) presents the residuals plotted as a function of the predicted values. The residuals are distributed well and randomly on both sides of the plot. However, this plot indicates a tendency for the variance of the residuals to increase as the concentration of phosphates is halfway. The residual analysis supports the conclusion that A (current density), B (electrocoagulation time), C (SA/V ratio), E (settlement time) and AC (the current density-SA/V ratio) are the only significant effects and that the underlying assumptions of the analysis are satisfied.

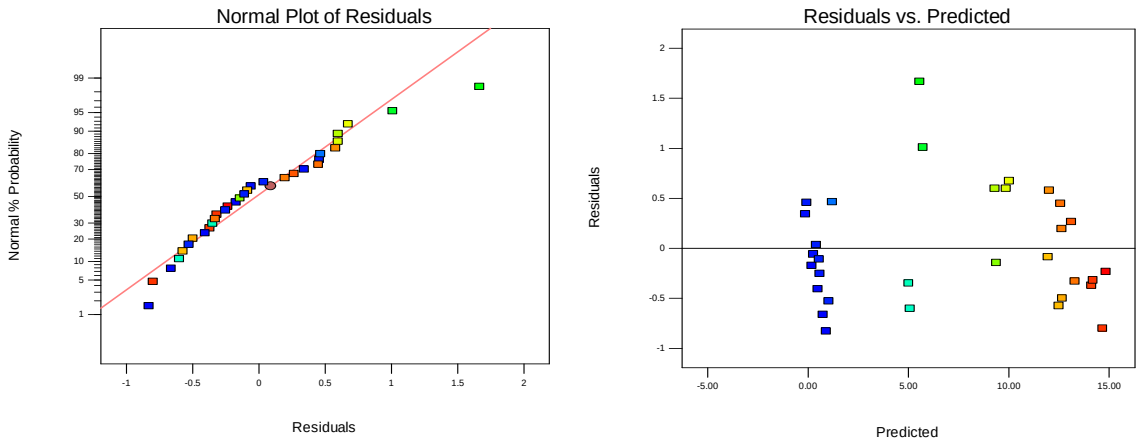

(a) (b)

Figure 5.21: (a) Normal probability plot of residuals and (b) plot of residuals versus predicted values.

5.5 Summary

The subject of the present chapter is the performance of iron and aluminium electrode materials in removing three different types of pollutants from synthetic wastewaters. Pure iron and Al-3Zn-0.02In electrodes appear as promising, effective materials in terms of both removal efficiency and energy consumption.

It has been reported in the literature that the three pollutants, which were added to the test solutions, are removed through different mechanisms. The removal of phosphates depends mainly on adsorption, while the removal of Zn^{2+} ions depends on the alkaline pH of the solution and the consequent precipitation of the hydroxide species. On the other hand, the removal of the Orange II dye is attained by chemical degradation of the molecule in the iron system and by a more complex process, probably involving adsorption or degradation, in the aluminium system.

For the iron system, the pure iron is the most efficient material for removing phosphates, Orange II and zinc ions. Moreover, its performance is not affected by the conductivity of the solutions. The absence of passivity and the general-like corrosion of the pure iron electrode, observed in the polarisation tests in Section 4.2 account for these results. Stainless steel AISI 420 shows similar performance to that observed with the pure iron electrodes. However, slightly lower removal efficiencies are obtained in the removal of phosphates and are attributed to a lower coagulant dosage due to higher

potentials exhibited by the anode, as shown in Section 3.3.5. The very good removal efficiencies exhibited by AISI 420, however, contrast with the extensive and severe damage of the electrode surface caused by pitting, as shown in Section 4.4.4. It has been reported in Section 4.1 that an uneven consumption of the electrode might adversely affect the electrocoagulation process. The poor removal efficiency and, above all, the leaching of hexavalent chromium, Cr(VI), from the stainless steel AISI 310 make this material not suitable for electrocoagulation applications.

As regards the aluminium system, the Al-3Zn-0.02In shows better removal performance than the Al-2Mg electrode. It would appear that the good results obtained with the Al-3Zn-0.02In are related to the ease of the electrode dissolution, as highlighted in Section 4.7.4. However, both alloys exhibit moderately good efficiency for the removal of the Orange II dye. This is associated with the removal mechanism of the azo dye, which, in the case of the aluminium system, appears as a complex process depending on a combination of adsorption and molecule degradation.

The energy consumption in electrocoagulation is dependent on the potential of the cell, E_{cell}, which, in turn, is related to the corrosion potential, E_{corr}, of the anode. By comparing the E_{corr} values measured in the potentiodynamic polarisation tests, reported in Chapter 4 for the iron and aluminium alloys, it has been observed that materials which adopt low values of E_{corr} result in greater energy efficiency for the electrocoagulation process. As a result, pure iron and Al-3Zn-0.02In are more efficient in terms of energy in the electrocoagulation process.

A chemometric technique, Design of Experiments or DoE, was used to identify the most relevant factors affecting the electrocoagulation removal of phosphates using stainless steel AISI 420 as the anode. According to this screening experimental design, the current density and the ratio of the surface area of the electrode to the volume of the solution, SA/V, are the most relevant variables influencing the removal efficiency of the process. On the other hand, the effect of performing the electrocoagulation tests under non homogeneous conditions, e.g., test solutions made up daily or non reproducible electrode surfaces, was negligible.

5.6 References

[1] Emamjomeh, M.M., Sivakumar, M., *J. Environ. Manage.*, **90** (2009) 1663-1679.
[2] OECD, Test No. 303: Simulation Test - Aerobic Sewage Treatment - A: Activated Sludge Units; B: Biofilms, in: OECD Guidelines for the Testing of Chemicals, Adopted 22 January 2011.
[3] Valsami-Jones, E., *Phosphorus in Environmental Technologies: Principles and Applications*, IWA Publishing, Cornwall, UK, 2004.
[4] Canizares, P., Jimenez, C., Martinez, F., Saez, C., Rodrigo, M.A., *Ind. Eng. Chem. Res.*, **46** (2007) 6189-6195.
[5] Hunger, K., *Industrial Dyes - Chemistry, Properties, Applications*, Wiley-VCH, Weinheim, 2003.
[6] Chafi, M., Gourich, B., Essadki, A.H., Vial, C., Fabregat, A., *Desalination*, **281** (2011) 285-292.
[7] Daneshvar, N., Ashassi-Sorkhabi, H., Tizpar, A., *Sep. Purif. Technol.*, **31** (2003) 153-162.
[8] Mollah, M.Y.A., Gomes, J.A.G., Das, K.K., Cocke, D.L., *J. Hazard. Mater.*, **174** (2010) 851-858.
[9] Mollah, M.Y.A., Pathak, S.R., Patil, P.K., Vayuvegula, M., Agrawal, T.S., Gomes, J.A.G., Kesmez, M., Cocke, D.L., *J. Hazard. Mater.*, **109** (2004) 165-171.
[10] Gomes, J.A., Cocke, D.L., Mahmud, M.A., Moreno, H., Peterson, E., Mollah, M.Y., Parga, J.R., *ECS Transaction*, **6** (2008) 29-41.
[11] Ayres, D.C., Hellier, D., *Dictionary of Environmentally Important Chemicals*, 1st ed., Blackie Academic & Professional, London and New York, 1998.
[12] Montgomery, D.C., *Design and Analysis of Experiments*, 7th ed., John Wiley & Sons, 2009.
[13] Box, G.E.P., Hunter, J.S., Hunter, W.G., *Statistics for experimenters: design, discovery, and innovation*, 2nd ed., Wiley, Hoboken, NJ, 2005.
[14] Fisher, R.A., *The Design of Experiments*, Halfner press, New York, 1935.
[15] Yates, F., *J. R. Stat. Soc.*, **2** (1935) 181-247.
[16] Kempthorne, O., *The Design and Analysis of Experiments*, Wiley, New York, 1952.
[17] Fisher, R.A., *The Design of Experiments*, Hafner Press, New York, 1960.
[18] Wu, C.F.J., Hamada, M., *Experiments: planning, analysis, and parameter design optimization*, Wiley, New York, 2000.
[19] Lindquist, E.F., *Design and Analysis of Experiments in Psychology and Education*, Houghton Mifflin Company, 1953.
[20] Kirk, R.E., *Experimental Design: Procedures for the Behavioral Sciences*, Brooks/Cole Publishing Company, Monterey, CA, 1968.
[21] Morgenthaler, S., Schumacher, M.M., *Chemom. Intell. Lab. Syst.*, **47** (1999) 127-141.
[22] Baklan, V.Y., Kolesnikova, I.P., *J. Aerosol Sci*, **27,** (1996) S209-S210.
[23] Bouhezila, F., Hariti, M., Lounici, H., Mameri, N., *Desalination*, **280** (2011) 347-353.
[24] Buzzini, A.P., Patrizzi, L.J., Motheo, A.J., Pires, E.C., *J. Environ. Manage.*, **85** (2007) 847-857.
[25] Chen, G.H., *Sep. Purif. Technol.*, **38** (2004) 11-41.
[26] Chen, X.M., Chen, G.H., Yue, P.L., *Sep. Purif. Technol.*, **19** (2000) 65-76.
[27] Holt, P., Barton, G., Mitchell, C., *Electrocoagulation as a Wastewater Treatment*, in: The Third Annual Australian Environmental Engineering Research Event, Castlemaine, Victoria, 1999.
[28] Hutnan, M., Drtil, M., Kalina, A., *J. Hazard. Mater.*, **131** (2006) 163-169.
[29] Kobya, M., Delipinar, S., *J. Hazard. Mater.*, **154** (2008) 1133-1140.
[30] Kobya, M., Hiz, H., Senturk, E., Aydiner, C., Demirbas, E., *Desalination*, **190** (2006) 201-211.
[31] Secula, M.S., Cretescu, I., Petrescu, S., *Desalination*, **277** (2011) 227-235.

[32] Yetilmezsoy, K., Ilhan, F., Sapci-Zengin, Z., Sakar, S., Gonullu, M.T., *J. Hazard. Mater.*, **162** (2009) 120-132.
[33] Mollah, M.Y.A., Schennach, R., Parga, J.R., Cocke, D.L., *J. Hazard. Mater.*, **84** (2001) 29-41.
[34] Irdemez, S., Demircioglu, N., Yildiz, Y.S., *J Hazard Mater*, **137** (2006) 1231-1235.
[35] Irdemez, S., Demircioglu, N., Yildiz, Y.S., Bingul, Z., *Sep. Purif. Technol.*, **52** (2006) 218-223.
[36] Zheng, X.Y., Kong, H.N., Wu, D.Y., Wang, C., Li, Y., Ye, H.R., *Water Sci. Technol.*, **60** (2009) 2929-2938.
[37] Behbahani, M., Moghaddam, A.M.R., Arami, M., *Int. J. Environ. Res.*, **5** (2011) 403-412.
[38] Comninellis, C., Chen, G.E., *Electrochemistry for the Environment*, Springer, New York, 2010.
[39] Rajeshwar, K., Ibanez, J., *Environmental Electrochemistry: Fundamentals and Applications in Pollution Abatement*, Academic Press, 1997.
[40] Wilcock, A., Tebbens, J., Fuss, F., Wagner, J., Brewster, M., *Text. Chem. Color.*, **24** (1992) 29-37.
[41] Martinez-Huitle, C.A., Brillas, E., *Appl. Catal., B*, **87** (2009) 105-145.
[42] Arslan-Alaton, I., Kabdasli, I., Vardar, B., Tuenay, O., *J. Hazard. Mater.*, **164** (2009) 1586-1594.
[43] Kabdasli, I., Vardar, B., Arslan-Alaton, I., Tuenay, O., *Chem. Eng. J.*, **148** (2009) 89-96.
[44] Adhoum, N., Monser, L., Bellakhal, N., Belgaied, J.E., *J. Hazard. Mater.*, **112** (2004) 207-213.
[45] Cenkin, V.E., Belevstev, A.N., *Eff. Water Treat. J.*, **25** (1985) 243-249.
[46] Biswas, N., Lazarescu, G., *Int. J. Environ. Studies*, **38** (1991) 65-72.
[47] Vik, E.A., Carlson, D.A., Eikum, A.S., Gjessing, E.T., *Water Res.*, **18** (1984) 1355-1360.
[48] Al Aji, B., Yavuz, Y., Koparal, A.S., *Sep. Purif. Technol.*, **86** (2012) 248-254.
[49] Anbari, R.H.A., Alfatlawi, S.M., Albaidhani, J.H., *Adv. Mater. Res.*, **468-471** (2012) 2882-2890.
[50] Yadav, A.K., Singh, L., Mohanty, A., Satya, S., Sreekrishnan, T.R., *Desalin. Water Treat.*, **46** (2012) 352-358.
[51] Cotton, F.A., Wilkinson, G., *Advanced Inorganic Chemistry - A Comprehensive Text*, 4th ed., Wiley-Interscience, New York, 1980.
[52] Kabdasli, I., Arslan, T., Oelmez-Hanci, T., Arslan-Alaton, I., Tuenay, O., *J. Hazard. Mater.*, **165** (2009) 838-845.
[53] Yang, C.L., McGarrahan, J., *J. Hazard. Mater.*, **127** (2005) 40-47.
[54] Cruywagen, J.J., Heyns, J.B.B., Rohwer, E.A., *Polyhedron*, **17** (1998) 1741-1746.
[55] Poulopoulou, V.G., Vrachnou, E., Koinis, S., Katakis, D., *Polyhedron*, **16** (1997) 521-524.
[56] Shenyang, T., Kean, L., *Talanta*, **33** (1986) 775-777.
[57] Tandon, R.K., Crisp, P.T., Ellis, J., Baker, R.S., *Talanta*, **31** (1984) 227-228.
[58] Akbal, F., Camci, S., *Desalination*, **269** (2011) 214-222.
[59] Arroyo, M.G., Perez-Herranz, V., Montanes, M.T., Garcia-Anton, J., Guinon, J.L., *J. Hazard. Mater.*, **169** (2009) 1127-1133.
[60] Bazrafshan, E., Mahvi, A.H., Naseri, S., Mesdaghinia, A.R., *Turk. J. Eng. Envir. Sci.*, **32** (2008) 59-66.
[61] Gao, P., Chen, X.M., Shen, F., Chen, G.H., *Sep. Purif. Technol.*, **43** (2005) 117-123.
[62] Golder, A.K., Samanta, A.N., Ray, S., *Sep. Purif. Technol.*, **53** (2007) 33-41.
[63] Parga, J.R., Cocke, D.L., Valverde, V., Gomes, J.A.G., Kesmez, M., Moreno, H., Weir, M., Mencer, D., *Chem. Eng. Technol.*, **28** (2005) 605-612.
[64] Thella, K., Verma, B., Srivastava, V.C., Srivastava, K.K., *J. Environ. Sci. Health., Part A*, **43** (2008) 554-562.
[65] Zaroual, Z., Chaair, H., Essadki, A.H., El Ass, K., Azzi, M., *Chem. Eng. J.*, **148** (2009) 488-495.

[66] Zongo, I., Leclerc, J., Maiga, H.A., Wethe, J., Lapicque, F., *Sep. Purif. Technol.*, **66** (2009) 159-166.
[67] Donini, J.C., Kan, J., Szynkarczuk, J., Hassan, T.A., Kar, K.L., *Can. J. Chem. Eng.*, **72** (1994) 1007-1012.
[68] Bayramoglu, M., Kobya, M., Can, O.T., Sozbir, M., *Sep. Purif. Technol.*, **37** (2004) 117-125.
[69] Chen, X.M., Chen, G.H., Yue, P.L., *Chem. Eng. Sci.*, **57** (2002) 2449-2455.
[70] Essadki, A.H., Bennajah, M., Gourich, B., Vial, C., Azzi, M., Delmas, H., *Chem. Eng. Process.*, **47** (2008) 1211-1223.
[71] Gadd, A., Ryan, D., Kavanagh, J., Beaurain, A.-L., Luxem, S., Barton, G., *J. Appl. Electrochem.*, **40** (2010) 1511-1517.
[72] Mouedhen, G., Feki, M., Wery, M.D.P., Ayedi, H.F., *J. Hazard. Mater.*, **150** (2008) 124-135.
[73] Bektas, N., Akbulut, H., Inan, H., Dimoglo, A., *J. Hazard. Mater.*, **106** (2004) 101-105.
[74] Irdemez, S., Yildiz, Y.S., Tosunoglu, V., *Sep. Purif. Technol.*, **52** (2006) 394-401.
[75] Lacasa, E., Canizares, P., Saez, C., Fernandez, F.J., Rodrigo, M.A., *Chem. Eng. J.*, **172** (2011) 137-143.
[76] Vasudevan, S., Lakshmi, J., Jayaraj, J., Sozhan, G., *J. Hazard. Mater.*, **164** (2009) 1480-1486.
[77] Vasudevan, S., Sozhan, G., Ravichandran, S., Jayaraj, J., Lakshmi, J., Sheela, S.M., *Ind. Eng. Chem. Res.*, **47** (2008) 2018-2023.
[78] Merzouk, B., Gourich, B., Sekki, A., Madani, K., Chibane, M., *J. Hazard. Mater.*, **164** (2009) 215-222.
[79] Heidmann, I., Calmano, W., *Sep. Purif. Technol.*, **71** (2010) 308-314.
[80] Puigdomenech, I., *Windows software for the graphical presentation of chemical speciation, March 26-30*, in: 219th ACS National Meeting, San Francisco, CA, 2000, Am. Chem. Soc.
[81] Eriksson, G., *Anal. Chim. Acta*, **112** (1979) 375-383.
[82] Holt, P., Barton, G., Mitchell, C., *Electrocoagulation as a Wastewater Treatment*, in: The Third Annual Australian Environmental Engineering Research Event, 23-26 November, Castlemaine, Victoria, 1999.
[83] Brereton, R.G., *Chemometrics: Data Analysis for the Laboratory and Chemical Plant*, Wiley, Chichester, UK, 2003.

6 Conclusions

6.1 General conclusions

In this work, electrocoagulation was shown to be a robust, effective and reliable technology as a wastewater treatment. As a first step, it was used for the removal of phosphates using an iron and an aluminium alloy as the anode material. Since electrocoagulation involves the electrolytic oxidation of the anode, it was important to understand how the electrode corroded. Consequently, several materials were investigated in terms of their electrochemical behaviour and corrosion properties, which were then correlated to the efficiency and energy performance for the electrocoagulation removal of three pollutants from synthetic wastewaters.

The feasibility of the electrocoagulation technique in removing phosphates was studied using an aluminium-magnesium and a stainless steel electrode, namely Al-2Mg and AISI 420, under different operating conditions. Both alloys showed excellent removal efficiencies. However, the Al-2Mg electrode was more efficient than the AISI 420 electrode. Indeed, using the same settings, efficiencies of 95.9% and 79.7% were observed for the Al-2Mg and the AISI 420, respectively, with an initial concentration of phosphates of 150 mg L^{-1} and an initial pH of 5.0. Other initial concentrations were used and, for both the Al and Fe systems, a decrease in the removal efficiency was found on increasing the initial concentration of phosphates.

As expected, the efficiency of the process was enhanced on increasing the current density applied to the electrodes. For the Al-2Mg electrode, as the current density increased from 5.3 to 11.0 mA cm^{-2}, the removal efficiency increased accordingly from 77% to 91%. On the other hand, an increase from 46% to 69% was observed with current densities of 2.6 and 11.0 mA cm^{-2} using the AISI 420 electrode.

The electrocoagulation process was highly dependent on the initial pH values of the solution, in good agreement with several studies reported in the literature [1-3]. In the present study, the highest efficiency for phosphate removal was achieved at an acidic initial pH of 3.0, for both Al and Fe systems. These results are consistent with the findings of İrdemez *et al.* [4, 5] on the removal of phosphates using aluminium and iron electrodes. However, there is no general agreement in the literature on the optimal initial pH for the electrocoagulation removal of phosphates. This is probably due to the fact that the electrocoagulation performance also depends on the final pH of the solution. Indeed, in the present study and in the available literature [4-7], the maximum removal was observed when the final pH was around 7.0, regardless of the initial pH. This was attributed to the nature of the hydrolysed species of the Al^{3+} and Fe^{3+} ions which are present in solution. According to Cañizares *et al.* [8] and Jiménez *et al.* [9], at this neutral pH the main Al^{3+} and Fe^{3+} species are the hydroxide precipitates. On increasing the pH, the aluminium precipitate dissolves to form monomeric anionic hydroxyaluminium species, which are soluble and negatively charged. Although the iron precipitate is still the main hydrolysis species at alkaline pH values [9], the large quantity of hydroxyl ions competes with the phosphate ions for adsorption on the iron precipitates.

The performance of the Al-2Mg electrode was not greatly affected by the variation of the concentration of chloride ions or the solution conductivity. A 10-fold increase in the chloride concentration, from 4.2×10^{-3} to 44.0×10^{-3} M, resulted in a slight increase of the removal efficiency from 85.2% to 88.8%. On the other hand, the performance of the AISI 420 electrode was reduced in low chloride-containing solutions. Indeed, as the concentration of chloride varied from 2.8×10^{-3} to 44.0×10^{-3} M, the removal efficiency increased from 76.5% to 89.3%. This was ascribed to the high potentials exhibited by the AISI 420 anode during the process. Potential values as high as 4.7 V vs. SCE, were recorded during the electrocoagulation test with a concentration of chloride of 2.8×10^{-3} M.

At these potentials concurrent reactions occur at the anode, which compete with the dissolution of iron, reducing the current efficiency and, consequently, the amount of Fe^{2+} generated. Low potential values were observed with the Al-2Mg electrode, consistent with the literature [10].

Using rotating disk voltammetry, RDV, it was shown that Fe(II) ions were generated at a pH of 5.0 and at a current density of 11.0 mA cm^{-2} on oxidation of the AISI 420 electrode.

The kinetics of the phosphate removal were studied and it was found that the rate law followed a pseudo first-order model, with the observed rate constant, k_{obs}, values of 0.0525 and 0.0263 min^{-1} for the Al-2Mg and the AISI 420 electrodes, respectively. The k_{obs} was dependent on the concentration of phosphates, ranging from 0.1531 to 0.0525 min^{-1} for the Al-2Mg electrode and 0.0600 and 0.0263 min^{-1} for the AISI 420 electrode with initial concentrations of phosphates of 20 and 150 mg L^{-1}, respectively. The k_{obs} values were computed at different current densities and it was concluded that they increased on increasing the current density, in good agreement with the data reported by Mameri *et al.* [11]. The dependence of k_{obs} on the concentration of phosphates was attributed to the degree of destabilisation attained in solution. A small degree of destabilisation, which occurs in solutions with high initial concentrations of phosphates, results in less efficient collisions and aggregations of the destabilised particles. This step was identified from the literature as the rate-determining step and is in good agreement with the kinetic analyses.

Adsorption isotherm studies were carried out to determine whether adsorption was the primary mechanism for the removal of phosphates under the conditions used in the present study. It was found that the Freundlich model gave a better fit for both aluminium and iron alloys, in agreement with a removal mechanism involving processes other than simple adsorption [12]. However, the Al-2Mg electrode showed a greater affinity for the adsorption of phosphates compared to the AISI 420 electrode. Indeed, the values of K_F and n were computed as 146 and 17 (mg g^{-1}) (L mg^{-1}), and 2.2 and 3.1 for the Al-2Mg and the AISI 420 electrodes, respectively.

The electrocoagulation tests were performed on real samples containing phosphates. Although the Al-2Mg electrode exhibited good removal efficiencies, the performance of the AISI 420 electrode was low in removing phosphates from a sample with a low conductivity. This was related to the passive nature of the material. It was concluded that the removal efficiency was dependent on the electrochemistry of the electrode and the physico-chemical properties of the solution. In the light of these findings, an extensive study on the electrochemical properties of various electrode materials was carried out, using classical corrosion techniques, such as polarisation and cyclic polarisation tests.

Pure iron, two stainless steel grades, AISI 310 and AISI 420, and two aluminium alloys, Al-2Mg and Al-3Zn-0.02In, were used as the anode materials in the corrosion studies. In order to obtain more realistic results, these studies were performed in simple chloride, sulfate and phosphate solutions and in synthetic wastewaters containing a mixture of the most common ions and with different conductivity levels. Pitting attack was observed for the pure iron electrode in simple chloride solutions. The pits ranged in size from 2 to 25 μm depending on the concentration of the chloride anions. However, this passive behaviour was reduced in the presence of phosphate anions and no passive behaviour, and more general-like dissolution or corrosion, was observed in the synthetic wastewaters. The AISI 310 and AISI 420 electrodes remained passive in the synthetic wastewaters, however at a sufficiently high applied potential, breakdown of the passive film occurred and the alloys suffered severe localised corrosion in the form of pits. Very different results were obtained with the aluminium alloys. In the presence of chloride anions, activation of the surface of the Al-2Mg electrode was observed, giving rise to dissolution. In the multicomponent wastewater solution, the corrosion behaviour of Al-2Mg was affected mainly by the presence of chloride ions, facilitating the dissolution of the alloy with no evidence of any passive region. Similar results were obtained with the Al-3Zn-0.02In alloy. Activation of the electrode, manifest by low corrosion potentials and the absence of a passive region, was observed in the chloride-containing solutions. In general, it was concluded that an efficient electrode material corrodes uniformly, has a low corrosion potential and exhibits a small or no passive region, making the pure iron, Al-2Mg and Al-3Zn-0.02In electrodes attractive in the electrocoagulation experiments.

The corrosion properties of the materials were then correlated to their efficiencies for the removal of three pollutants, phosphates, an azo dye and zinc ions. For the iron system, the pure iron electrode was the most efficient in terms of the removal of the three pollutants and energy consumption. An efficiency of 92.6%, 99.0% and 100% was observed for the removal of phosphates, azo dye and zinc ions, respectively, while 0.52 Wh was required for the process. These results are consistent with the general-like dissolution of iron in low and high conductivity solutions.

The AISI 420 electrode exhibited similar removal efficiencies and energy demand to those observed for the pure iron, with 86.4%, 98.6% and 100% for the removal of phosphates, azo dye and zinc ions, respectively and an energy consumption of 0.62 Wh. However, a lower efficiency was achieved for the removal of phosphates compared to the pure iron electrode, which was 92.6%. This was attributed to the fact that phosphate ions are removed mainly through a mechanism of adsorption on hydrolysed iron species. The high potential values exhibited by the anode during the electrocoagulation process, which facilitated the occurrence of concurrent reactions, reduced the dissolution of the iron and, consequently, decreased the concentration of the hydrolysed species in solution. However, the AISI 420 electrode was characterised by a severe form of localised corrosion in terms of large, deep pits growing on its surface. This form of corrosion is considered detrimental in electrocoagulation applications [13].

Poor energy and removal performance was observed using the AISI 310 stainless steel as the anode material. This is in good agreement with the passive characteristics of this anode. Good efficiencies, 98.2%, were achieved only for the removal of zinc ions, since their removal is related to the pH of the solution and the formation and precipitation of the corresponding hydroxide species. At the end of the electrocoagulation tests Cr(VI) was detected in the solutions. Accordingly the AISI 310 stainless steel is not suitable in the treatment of water by electrocoagulation.

As regards the aluminium system, both alloys showed excellent removal efficiencies for the removal of phosphates and zinc ions, with the Al-2Mg showing efficiencies of 93.0% and 99.1%, and the Al-3Zn-0.02In giving equally high efficiencies of 95.2% and 100% for the removal of phosphates and zinc ions, respectively. In addition, the Al-3Zn-0.02In electrode showed a consistent low corrosion potential, E_{corr}. As a

consequence, it also exhibited low energy consumption, 0.26 Wh compared to 0.51 Wh for the Al-2Mg electrode, making this alloy interesting in electrocoagulation applications. However, due to a complex mechanism of removing dyes, involving a combination of adsorption and degradation, the azo dye was not removed in an efficient way.

Some operating conditions of the electrocoagulation experiments were investigated to identify the most relevant factors affecting the performance of the process. A screening design of experiment, DoE, was used for this purpose and the current density and the ratio of the surface area of the electrode to the volume of the solution, SA/V, were determined as the most influencing factors for the electrocoagulation process.

6.2 Future works

The findings and the conclusions of this work provide basis for future research in several areas.

- A study on the parameters affecting the electrocoagulation performance of the aluminium-zinc-indium electrode would be valuable, since this electrode material showed excellent properties in terms of both removal and energy efficiencies. The effect of some other parameters in addition to those presented in this research, such as the temperature and the type of supporting electrolyte should also be evaluated.
- An investigation of the parasitic reactions occurring at the anode during electrocoagulation. In particular, the study would examine the negative difference effect, NDE, at the surface of the aluminium electrode and its effect at different current densities.
- An understanding of the buffer capacity observed during the electrocoagulation reactions and an estimation of the final pH value using Faraday's law of electrolysis. This would help on evaluating the final pH of the treated solution, which is generally regulated by law.
- An economic comparison of electrocoagulation and chemical coagulation costs. The comparison would also evaluate power demands, bulk chemical costs and the costs related to the electrode manufacturing and its lifecycle.

- Following the screening chemometric study, a complete design of experiment would be applied in order to optimise the electrocoagulation process in terms of removal efficiency and energy consumption.
- An application of the technique to the treatment of real samples and a possible scale-up of the system.

6.3 Conference presentations

- Adelaide Dura and Carmel B. Breslin, "A low carbon footprint wastewater treatment technology: electrocoagulation", ENVIRON 2011, 21st Irish Environmental Researchers Colloquium, UCC, Cork, Ireland, 6 - 8 April 2011 [Poster presentation].

- Adelaide Dura and Carmel B. Breslin, "Electrocoagulation for the Treatment of Wastewaters: Minimisation of Electrode Passivation", ENVIRON 2011, 8th IWA Leading-Edge Conference on Water and Wastewater Technologies, Amsterdam, The Netherlands, 6 - 10 June 2011 [Poster presentation].

- Adelaide Dura and Carmel B. Breslin, "Electrocoagulation for the effective Removal of Pollutants", 221st ECS Meeting, Seattle, WA, 6 - 10 May 2012 [Poster presentation].

- Adelaide Dura and Carmel B. Breslin, "Electrochemical Behaviour of Iron and Aluminium Alloys in a Synthetic Wastewater for Electrocoagulation Application", 221st ECS Meeting, Seattle, WA, 6 - 10 May 2012 [Oral presentation].

6.4 References

[1] Canizares, P., Jimenez, C., Martinez, F., Rodrigo, M.A., Saez, C., *J. Hazard. Mater.*, **163** (2009) 158-164.
[2] Chen, G.H., *Sep. Purif. Technol.*, **38** (2004) 11-41.
[3] Mouedhen, G., Feki, M., Wery, M.D.P., Ayedi, H.F., *J. Hazard. Mater.*, **150** (2008) 124-135.
[4] Irdemez, S., Demircioglu, N., Yildiz, Y.S., *J. Hazard. Mater.*, **137** (2006) 1231-1235.
[5] Irdemez, S., Yildiz, Y.S., Tosunoglu, V., *Sep. Purif. Technol.*, **52** (2006) 394-401.

[6] Bektas, N., Akbulut, H., Inan, H., Dimoglo, A., *J. Hazard. Mater.*, **106** (2004) 101-105.
[7] Vasudevan, S., Lakshmi, J., Jayaraj, J., Sozhan, G., *J. Hazard. Mater.*, **164** (2009) 1480-1486.
[8] Canizares, P., Martinez, F., Jimenez, C., Lobato, J., Rodrigo, M.A., *Ind. Eng. Chem. Res.*, **45** (2006) 8749-8756.
[9] Jimenez, C., Saez, C., Martinez, F., Canizares, P., Rodrigo, M.A., *Sep. Purif. Technol.*, **98** (2012).
[10] Jimenez Izquierdo, C., Canizares, P., Rodrigo, M.A., Leclerc, J.P., Valentin, G., Lapicque, F., *Desalination*, **255** (2010) 15-20.
[11] Mameri, N., Yeddou, A.R., Lounici, H., Belhocine, D., Grib, H., Bariou, B., *Water Res.*, **32** (1998) 1604-1612.
[12] Del Bubba, M., Arias, C.A., Brix, H., *Water Res.*, **37** (2003) 3390-3400.
[13] Gadd, A., Ryan, D., Kavanagh, J., Beaurain, A.-L., Luxem, S., Barton, G., *J. Appl. Electrochem.*, **40** (2010) 1511-1517.

Appendix

In this appendix some corrosion parameters are presented for pure iron, stainless steel 310, stainless steel 420, pure aluminium, aluminium-magnesium and aluminium-zinc-indium electrodes in several electrolytes. The parameters were evaluated from the potentiodynamic polarisation scans shown in Chapter 4 under the assumptions listed in Section 2.3.1.3 and were: (i) the corrosion potential, E_{corr}; (ii) the corrosion current density, j_{corr}; (iii) the breakdown potential, E_{br}; (iv) the extent of the passive range, ΔE_{pass}; (v) the anodic Tafel slope, β_a; (vi) and the cathodic Tafel slope, β_c.

Table 1: Corrosion parameters for the pure iron electrode.

Pure iron (Fe 99.99%)						
Solution	**Parameter**					
	E_{corr} **V vs. SCE**	j_{corr} **A cm^{-2}**	E_{br} **V vs. SCE**	ΔE_{pass} **V**	β_a **mV dec^{-1}**	β_c **mV dec^{-1}**
0.017 M NaCl	-0.359	9.29×10^{-7}	-0.091	0.267	270.4	-123.5
0.170 M NaCl	-0.463	3.04×10^{-6}	-0.288	0.179	210.3	-120.8
0.017 M NaCl + 8.1×10^{-4} M Na_2SO_4	-0.319	1.90×10^{-6}	-0.162	0.157	139.7	-121.2
0.016 M KH_2PO_4	-0.722	3.07×10^{-5}	-	-	94.2	-118.2
sww 1	-0.704	3.18×10^{-5}	-	-	67.2	-117.5
sww 2	-0.724	2.91×10^{-5}	-	-	64.1	-122.1

Table 2: Corrosion parameters for the stainless steel 310 electrode.

AISI 310 (Fe/Cr25/Ni20)						
Solution	**Parameter**					
	E_{corr} **V vs. SCE**	j_{corr} **A cm^{-2}**	E_{br} **V vs. SCE**	ΔE_{pass} **V**	β_a **mV dec^{-1}**	β_c **mV dec^{-1}**
0.017 M NaCl	-0.382	2.23×10^{-6}	0.102	0.484	921.8	-134.9
0.170 M NaCl	-0.421	2.03×10^{-6}	0.054	0.475	964.7	-127.8
0.017 M NaCl + 8.1×10^{-4} M Na_2SO_4	-0.370	2.62×10^{-6}	0.131	0.501	1358.4	-135.6
0.016 M KH_2PO_4	-0.384	2.28×10^{-6}	-	-	834.5	-173.7
sww 1	-0.448	1.09×10^{-6}	-	-	648.7	-143.2
sww 2	-0.525	1.41×10^{-6}	0.145	0.671	634.0	-139.9

Table 3: Corrosion parameters for the stainless steel 420 electrode.

AISI 420 (Fe86.7/Cr13.0/C0.3)						
Solution	**Parameter**					
	E_{corr} **V vs. SCE**	j_{corr} **A cm^{-2}**	E_{br} **V vs. SCE**	ΔE_{pass} **V**	β_a **mV dec^{-1}**	β_c **mV dec^{-1}**
0.017 M NaCl	-0.339	6.25×10^{-7}	-0.005	0.333	153.3	-120.0
0.170 M NaCl	-0.343	6.63×10^{-7}	-0.180	0.163	478.1	-115.1
0.017 M NaCl + 8.1×10^{-4} M Na_2SO_4	-0.277	8.39×10^{-7}	0.172	0.449	453.49	-183.8
0.016 M KH_2PO_4	-0.648	6.82×10^{-6}	-	-	221.49	-116.6
sww 1	-0.641	7.17×10^{-6}	0.112	0.753	227.38	-132.3
sww 2	-0.659	1.01×10^{-5}	-0.088	0.571	228.88	-126.1

Table 4: Corrosion parameters for the pure aluminium electrode.

Pure aluminium (Al 99.999%)						
Solution	**Parameter**					
	E_{corr} **V vs. SCE**	j_{corr} **A cm^{-2}**	E_{br} **V vs. SCE**	ΔE_{pass} **V**	β_a **mV dec^{-1}**	β_c **mV dec^{-1}**
0.10 M NaCl	-0.828	2.21×10^{-7}	-0.744	0.084	111.3	-111.9
0.10 M NaCl	-0.950	3.79×10^{-7}	-0.775	0.176	96.0	-209.3
0.10 M NaCl	-1.153	2.43×10^{-7}	-0.657	0.895	116.4	-73.1
0.10 M NaCl	-0.935	2.61×10^{-7}	-0.734	0.200	167.3	-211.4
0.10 M NaCl (chemical pre-treatment)	-1.378	2.95×10^{-6}	-0.794	0.584	122.3	-125.2
0.10 M NaCl (chemical pre-treatment)	-1.347	2.68×10^{-6}	-0.811	0.536	126.2	-127.4
0.10 M NaCl (chemical pre-treatment)	-1.306	1.98×10^{-6}	-0.785	0.521	128.3	-126.3
0.10 M NaCl (chemical pre-treatment)	-1.343	2.77×10^{-6}	-0.821	0.522	128.5	-128.0
0.005 M NaCl (chemical pre-treatment)	-1.209	2.53×10^{-6}	-0.557	0.652	121.4	-130.6
0.01 M NaCl (chemical pre-treatment)	-1.272	3.52×10^{-6}	-0.620	0.652	139.9	-127.6
0.10 M NaCl (chemical pre-treatment)	-1.364	2.28×10^{-6}	-0.829	0.535	121.6	-124.4
0.25 M NaCl (chemical pre-treatment)	-1.333	3.90×10^{-6}	-0.906	0.427	129.3	-138.2
0.50 M NaCl (chemical pre-treatment)	-1.290	3.34×10^{-6}	-0.961	0.330	132.1	-126.8
6.5×10^{-3} M KH_2PO_4 + 5.0×10^{-4} M NaCl	-0.864	1.04×10^{-7}	0.276	1.140	262.7	-
6.5×10^{-3} M KH_2PO_4	-0.869	1.40×10^{-7}	-	-	314.6	-

Table 5: Corrosion parameters for the aluminium-magnesium electrode.

Al-2Mg						
Solution	**Parameter**					
	E_{corr} V vs. SCE	j_{corr} A cm^{-2}	E_{br} V vs. SCE	ΔE_{pass} V	β_a mV dec^{-1}	β_c mV dec^{-1}
0.017 M NaCl	-0.554	1.09×10^{-6}	-0.530	0.024	20.0	-398.9
0.170 M NaCl	-0.664	1.27×10^{-6}	-0.636	0.028	26.1	-382.0
0.017 M NaCl + 8.1×10^{-4} M Na_2SO_4	-0.508	7.13×10^{-7}	-0.464	0.044	24.3	-389.1
0.016 M KH_2PO_4	-0.484	8.54×10^{-7}	0.103	0.587	241.9	-168.7
sww 1	-0.598	5.61×10^{-6}	-0.587	0.011	40.4	-406.2
sww 2	-0.670	7.21×10^{-6}	-0.661	0.009	21.3	-349.5

Table 6: Corrosion parameters for the aluminium-zinc-indium electrode.

Al-3Zn-0.02In						
Solution	**Parameter**					
	E_{corr} V vs. SCE	j_{corr} A cm^{-2}	E_{br} V vs. SCE	ΔE_{pass} V	β_a mV dec^{-1}	β_c mV dec^{-1}
0.017 M NaCl	-0.912	8.96×10^{-7}	-0.879	0.034	30.5	-292.3
0.170 M NaCl	-1.075	2.40×10^{-6}	-1.055	0.020	27.2	-318.9
0.017 M NaCl + 8.1×10^{-4} M Na_2SO_4	-1.015	1.40×10^{-6}	-0.858	0.156	80.1	-399.2
0.016 M KH_2PO_4	-0.680	1.41×10^{-6}	-0.233	0.447	477.8	-165.7
sww 1	-0.798	1.48×10^{-5}	-0.784	0.014	59.1	-453.2
sww 2	-0.857	1.11×10^{-5}	-0.848	0.009	13.6	-484.5